Theoretical studies of the geodynamics of accretion boundaries in the plate tectonics

N. J. Kusznir

THEORETICAL STUDIES OF THE GEODYNAMICS OF ACCRETION BOUNDARIES IN PLATE TECTONICS

by

N.J. Kusznir

A thesis presented for the degree of
Doctor of Philosophy in the
University of Durham

April, 1976.

ABSTRACT

Various aspects of the physical processes occurring at the accretion plate boundary in plate tectonics have been investigated.

Regional stresses have been investigated, arising from lateral density contrasts in the ocean lithosphere. Elastic, visco-elastic and elastic/visco-elastic models predict regional stresses in the ocean basin of the order of 0.25 kb..

Investigation of the thermal stresses created in the oceanic lithosphere as a consequence of the cooling of the ocean lithosphere as it moves away from the ridge axis, shows that tensional stresses occur in the upper lithosphere and compressional stresses in the lower lithosphere. An elastic/viscous model of the lithosphere predicts deviatoric stresses of the order of 3 kb. in the upper crust.

The temperature distribution beneath the ocean ridge with magma solidifying to form crustal layer 3 has been investigated. Numerical models show that the width of the magma chamber and the thickness of the dyke complex depends on half spreading rate. If there is significant crystal settling, the width of the chamber is predicted to be considerably reduced. A critical half spreading rate of 0.45 cm/yr is predicted, below which the intruded material solidifies instantaneously. Computations support Cann's

petrological model.

Investigation of the magnitude of the stresses caused by the buoyancy of a magma chamber in the lower crust at the ridge axis suggest that the magma chamber is unable to cause crustal fracture and is, alone, a dynamically stable structure. The additional stresses due to the upthrust of molten upper mantle material is required to cause crustal fracture and a zone of fracture of less than 5 km wide is predicted.

The stress field created in the oceanic lithosphere by a mantle plume has been calculated analytically. Estimates of the plume dimensions and velocity suggested by Morgan are predicted to be just sufficient to cause fracture of the lithosphere above the plume axis.

ACKNOWLEDGEMENTS

May I thank all members of the Department of Geological Sciences at Durham who, during my period of research for this thesis, have provided advice and stimulating discussion. In particular I should like to thank Professor M.H.P. Bott for his encouragement and direction over the last three years, Mr. D.J. Woodward for many interesting discussions, and Professor G.M. Brown in allowing me to carry out research in the Department of Geological Sciences at Durham while I have been a member of staff. Also may I thank all members of the Department of Computing, particularly Mr. B.R. Lander and Mr. R. Sheehan, who have provided assistance and advice on computing.

Part of this work was financed by a grant from the Natural Environment Research Council.

CONTENTS

CHAPTER 1

OCEANIC STRUCTURE, COMPOSITION AND ACCRETION PROCESS STUDIES

1.1 Introduction

In this thesis, models of the oceanic lithosphere structure and the processes occurring at the accretion boundary in plate tectonics are investigated quantitatively. These models investigate the stress fields in the oceanic lithosphere which arise from the laterally varying lithosphere density distribution, lithosphere thermal contraction, lithosphere intrusion by upwelling asthenosphere, and asthenosphere flow. The thermal evolution and solidification of the oceanic crust in the vicinity of the ridge axis has also been determined.

The structure and composition of the oceanic lithosphere are described with evidence in this chapter, providing the geological foundation for the lithosphere models. Major theoretical studies of the accretion processes are also summarized.

1.2 Oceanic structure

The ocean floor is dominated by the topographical feature known as the ocean ridge, which is typically about 2 to 3 km higher than the flanking ocean basins. The relief of the ocean ridges decays gently to the level of the ocean basins over a distance varying between approximately 500 to 4,000 km, and the ridges extend for a total length of 80,000 km throughout the world's oceans. In the theory of plate tectonics (McKenzie and Parker, 1967; Le Pichon, 1968), the ridge crest corresponds to the accretion boundary where new oceanic lithosphere is created. Ocean ridges are offset at intervals by transform faults (Wilson, 1965).

Seismic refraction and reflection have shown the oceanic crust to be approximately 8 km thick and divided into 3 layers, classified as oceanic layers 1, 2 and 3. The refraction and reflection work and techniques have been summarized by Ludwig, Nafe and Drake (1970) and Ewing and Ewing (1970) respectively. Shor, Menard and Raitt (1970) have presented a statistical analysis of a considerable quantity of data for velocity and thickness of the oceanic layers. Layer 1 forms a sediment cover above the igneous lower crust (layers 2 and 3) and increases in thickness with age and distance from the ridge axis in accordance with the predictions of the theory of sea floor spreading. Layer 2 is of approximate constant thickness over the ocean basins and ridges (Goslin et al., 1972).

Layer 3 appears to increase in thickness away from the ridge crest towards the ocean basins (Dehlinger, 1970; Talwani et al., 1971). Goslin et al. (1972), from statistical analysis of existing data, suggested a layer 3 thickening from 3.5 km to 5 km with increasing distance from the ridge axis. Maynard (1970) has presented evidence for a layer of velocity 7.3 km/sec. existing at the base of layer 3 in the Pacific.

The structure at the ridge crest has been investigated extensively by seismic refraction methods (Talwani et al., 1971; Aumento et al., 1971; Fowler and Matthews, 1974; Whitmarsh, 1975). Results are inconclusive with oceanic layer 3 absent in the interpretation of some researchers, yet present in those of others. Whitmarsh (1975) has suggested, from seismic evidence, the existence of a narrow zone, width approximately 2.5 km, of low velocity in the crust at the ridge crest in the FAMOUS region of the North Atlantic, which probably corresponds to the intrusion zone. The velocity of the upper mantle at the ridge crest is in some places less than the usual upper mantle velocity of 8.15 km/sec. (Talwani et al., 1971; Aumento et al., 1971; Fowler and Matthews, 1974; Tryggvason, 1964).

Surface wave dispersion analysis of teleseismic data indicates an ocean lithosphere thickness of approximately 70 km (Kanomori and Press, 1970) which is considerably thinner

than that of the continental lithosphere. Forsyth (1975), using similar techniques has shown the ocean lithosphere thickens away from the ridge axis.

Gravity surveys carried out across the ocean ridges show that they are in approximately isostatic equilibrium (Vening Meinesz, 1948; Talwani et al., 1971). The ocean ridges, which rise up to 3 km above the ocean basins, must therefore be compensated by a low density region below, yet from the seismic refraction evidence (Shor et al., 1970; Ludwig et al., 1970; Talwani et al., 1971) it can be seen that this is not achieved by crustal thickening. Talwani et al. (1965) from gravity and seismic evidence produced a model, later verified by Dehlinger (1970), which shows an anomalous low density upper mantle centred about the ridge axis with a density contrast of approximately -0.25 gm/cc extending down to depths of 40 km.

Interpretation of the magnetic anomalies of the ocean floor (Mason and Raff, 1961; Vacquier, 1969; Heirtzler, 1970) has provided a major contribution in evidence for sea floor spreading and plate tectonics (Vine and Mathews, 1963; Vine and Wilson, 1965; Vine, 1966). The magnetized layer responsible for the anomalies coincides with the oceanic basement, layer 2 (Vine and Wilson, 1965). Talwani (1971) has suggested that the magnetization is restricted to the top 400 metres although recent drilling of layer 2 (DSDP - Leg 37, 1974) indicates that material magnetized strongly yet randomly may

extend throughout layer 2.

The correlations between topographic roughness of the ocean floor, the presence of rift valleys, and spreading rates were noted by Menard (1967). For spreading rates smaller than 3 cm/yr the large scale oceanic topography is uneven and rift valleys exist (Laughton et al., 1970). Faster spreading rates, for example the East Pacific rise (Talwani et al., 1965) correspond to smoother topography with the absence of rift valleys. The rift valleys or median valleys of the ridge crests are typically 10 to 20 km wide and up to 3 km deep relative to the flanking crest mountains. The valley is bounded by steep scarps which dip towards the ridge axis (Le Pichon et al., 1971). The intrusion zone is restricted to a narrow zone only a few kilometres wide according to the analysis of the magnetic anomalies of the ocean floor (Matthews and Bath, 1967; Larson and Spiess, 1968) and seismicity (Francis and Porter, 1973). To the flanks tectonic activity is restricted to the upfaulting of the large blocks (Laughton et al., 1970) which form the sides of the rift valley structure.

1.3 Composition of the oceanic crust and upper mantle

The composition of the oceanic crust and upper mantle

must be inferred from geochemical analysis of samples collected by dredging and drilling on the ocean floor and from the seismic velocities and densities obtained from geophysical studies.

Dredging and photography of oceanic layer 2, where it outcrops on the ocean floor, reveal that its upper surface is composed of tholeiitic pillow lavas (Aumento et al., 1971; Talwani et al., 1971; Engel and Engel, 1970; Udintsev and Dmi triev, 1970). Drilling has confirmed the basaltic composition of layer 2 (Maxwell et al., 1970) and the seismic velocities obtained from the drill cores agree well with the refraction velocities of the layer (DSDP - Leg 37, 1974). Collection of rock samples from the fault scarps of the ridge crest and fracture zones indicate the presence of basalts and gabbros, and their metamorphic forms together with peridotite and serpentinite (Engel and Engel, 1970).

Relevant to any discussion of the structure and composition of the oceanic crust is the study of ophiolites which are interpreted as upthrusted ancient ocean floor. The sections deduced from these studies have been summarized for several ophiolite complexes (Jackson, Green and Moores, 1975; Gass, Smith and Vine, 1975). Interpretation of the ophiolite sequence in terms of oceanic crust and upper mantle is shown in figure 1.1 and is adapted from Gass et al. (1975). This interpretation assumes a considerable thinning of the ophiolite sequence during emplacement from their original oceanic environment.

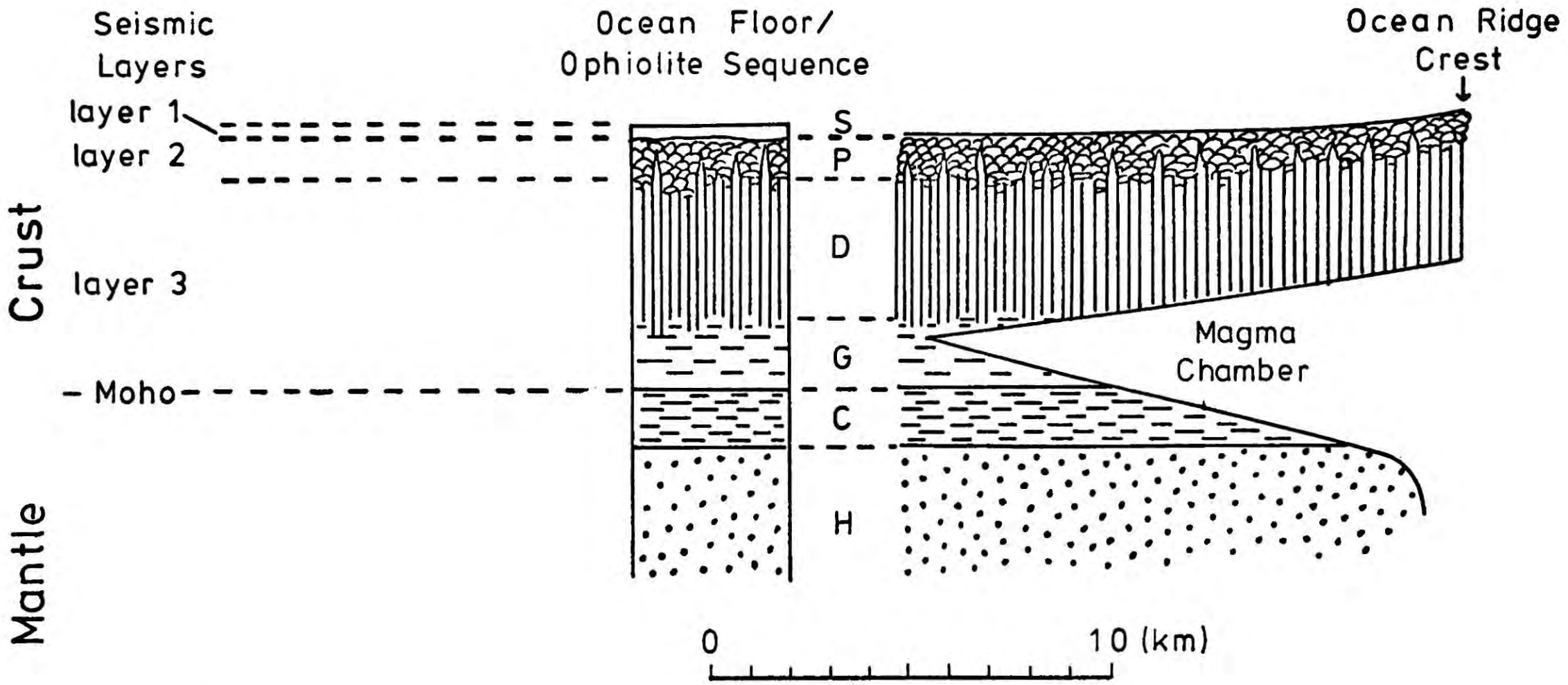

Fig. 1.1 Summary and comparison of postulated ocean crust and upper mantle structure, ophiolite structure and the oceanic seismic layers. (after Gass et al., 1975).

Key - S, sediments; P, pillow lavas; D, sheeted dyke complex; G, Gabbros; C, ultramafic cumulates; H, Harzburgite (depleted upper mantle).

Oceanic layer 2 is now widely accepted as being composed of basaltic pillow lavas lying above basalts metamorphosed to varying extent, this interpretation being consistent with collected samples seismic velocities and the origin of the magnetic anomalies.

The composition of layer 3 is however the subject of considerable argument (Matthews, 1971). Hess (1962) proposed that this layer was composed of partially serpentinized peridotite, while Cann (1970, 1974) believed that it consists of a metagabbroic layered complex. The arguments against the serpentinized peridotite composition are as follows:

(1) The high temperature of the crust at the ridge crest would prevent the serpentinization of peridotite which can only occur for temperatures less than 500^{o}C or possibly 300^{o}C (Coleman, 1971).

(2) The range of velocities for serpentinized peridotite is from 5 to 8 km/sec (Coleman, 1971) yet layer 3 has a very consistent velocity of about 6.8 km/sec. (Shor et al., 1970), suggesting a remarkably uniform degree of hydration.

(3) Gabbros and metagabbros dredged and drilled at the ridge crest have a velocity too high for layer 2 and so most probably belong to layer 3.

The metagabbro composition for layer 3, however, fails

to explain the thickening of layer 3 with increasing distance from the ridge (Talwani et al., 1971; Dehlinger, 1970; Goslin et al., 1972). However, this effect is not proved conclusively (Whitmarsh, 1975).

An hybrid composition, overcoming some of these objections, is a layer 3 consisting of approximately 2-3 km of gabbro below which lies a partially serpentinized peridotite (Le Pichon et al., 1971). All of these arguments are of course subject to the accuracy of the geophysical methods which investigate the oceanic crust and upper mantle.

Green and Ringwood (1969) have suggested that the tholeiitic basalts of the ocean crust are the product of fractionation of a mantle of pyrolitic composition at about 30 km depth. Extensive partial melting in the upper mantle at these depths are indicated (Green and Ringwood, 1969; Kay, Hubbard and Gast, 1970). A mechanism has been suggested by Bott (1965) for the generation of a partial melt in an upwelling mantle convection limb and this convection or advection mechanism is thought to be responsible (Green and Ringwood, 1969) for the partial melts under ocean ridges.

1.4 Models of the accretion process

The creation of new oceanic lithosphere involves the diapirism of partially molten asthenosphere into the

lithosphere at the ocean ridges. Cann (1970, 1974) has proposed a model where partially molten pyrolitic mantle ascends from depths of 100-150 km and fractionates at a depth of about 20-30 km producing a basalt liquid and an ultramafic residual. Prior to fractionation the pyrolitic partial melt behaves as a relatively fluid material but after separation of the basaltic liquid, the residual is left below its solidus temperature and solidifies (Presnall, 1969; Cann, 1974). The basaltic liquid being less dense than the surrounding upper mantle then rises, collecting into diapiric blobs (Weertman, 1972) and is intruded into the base of the crust forming a reservoir from which basaltic dykes penetrate upwards through the upper crust and extrude on the ocean floor, forming layer 2. With time, the basalt magma in the lower crust solidifies forming a layered gabbroic complex corresponding to layer 3. The Moho represents, in this model, the compositional boundary between basaltic fractionates and ultramafic residuals. This composition and structure for the oceanic crust and upper mantle is consistent with ophiolite studies (Gass et al., 1975; Jackson et al., 1974) and the geophysical interpretation of the ocean basins (Shor et al., 1970).

The alternative model (Hess, 1962) where layer 3 is composed of serpentinized peridotite is not as well supported as the model above.

Lachenbruch (1973) has developed the theory of mantle fractionation mathematically and has pointed out the possibility of enrichment of the lithosphere in crustal component with respect to the asthenosphere. Bottinga (1973) presented a combined chemical and thermal model which however used an all peridotite composition for layer 3, which is probably unrealistic.

1.5 The thermal evolution of the lithosphere

A model for the thermal evolution of the lithosphere has been suggested by McKenzie (1967) in which a continuous thickness of lithosphere is produced on a vertical boundary at a ridge axis. As the lithosphere moves away at a constant velocity, new hot lithosphere forms in the space between the diverging plates. McKenzie calculated the temperature throughout the lithosphere, assuming that the temperature of the newly formed lithosphere at the ridge axis coincided with that of the lithosphere - asthenosphere boundary. The amount of cooling of the lithosphere increases with distance from ridge axis and decreases with depth producing thermal contraction which gives the typical ocean rise topography (Le Pichon et al., 1971). McKenzie used this temperature distribution to produce heat flow profiles in approximate agreement with observed heat anomalies at ocean ridges,

which show a maximum above the ridge crests (Langseth and Von Herzen, 1970; Talwani et al., 1971). The temperature McKenzie used however for the lithosphere-asthenosphere boundary was too low.

In any model of the oceanic lithosphere the density distribution due to petrological zonation and thermal contraction must compensate the oceanic topography since oceanic regions are in isostatic equilibrium (Talwani et al., 1965). Refinement of the McKenzie model made by including the density variations of the mineral assemblage changes due to the lithosphere's varying pressure and temperature field, produces a much better agreement with the observed data for the ocean topography, (Sclater and Francheteau, 1970; Haigh, 1973; Forsyth and Press, 1971). Comparison of calculated and observed gravity anomalies enabled Haigh (1973) to estimate the temperature and depth of the base of the oceanic lithosphere. Typical thicknesses and temperatures were 70 to 80 km and 1000 to 1200^{o}C respectively. The density distributions produced by these models, especially those due to the plagioclase to pyroxene pyrolite mineral assemblage change, show a resemblance to the density model for the lithosphere obtained by Talwani et al. (1965) from geophysical data.

An alternative model for examining the temperature distributions in the upper mantle and crust was suggested by Oxburgh and Turcotte (1968) which consisted of a vertically

rising limb of a convection cell turning over to flow horizontally in the upper mantle. Their model differs from that presented by McKenzie which assumes rigid lithosphere to exist at the ridge axis.

The thermal model of McKenzie (1967) has been further developed by Oldenburg (1975) and Sleep (1975) allowing the solidification of the lithosphere to be investigated in addition to its cooling. Oldenburg (1975) has investigated the formation of the lithosphere from the asthenosphere by solidification of a partial melt and has suggested that the lithosphere thickens away from the ridge axis. Sleep (1975) has examined the formation and solidification of a magma chamber at the ocean ridges. In Chapter 5 the solidification of the ocean crust is further investigated with consideration taken for crystal settling and convection of the magma.

1.6 The stresses in the lithosphere

The stresses of the oceanic lithosphere may be categorized according to their origins and are as follows:

(1) Stresses resulting from lithospheric density distributions.

(2) Cooling stresses of the lithosphere.

(3) Stresses caused by the formation of new lithosphere from upwelling asthenosphere.

(4) Stresses exerted on the lithosphere base by asthenosphere flow.

(5) Membrane stresses (Turcotte and Oxburgh, 1973).

The geodynamical implications of the oceanic topography and the lithospheric density variations have been investigated by several workers. Jacoby (1970) calculated the horizontal forces due to gravity sliding of the ocean lithosphere along the top of the asthenosphere and concluded that this could be an effective driving force contribution for sea floor spreading. Stephansson and Berner (1970) used the finite element method to evaluate the fluid behaviour and stress fields of the oceanic lithosphere. They suggested that regional tension occurs at the ridge crest and compression in the ocean basins. Artyushkov (1973) showed by analytical calculations that the oceanic lithosphere topography and density distribution create a compressive horizontal stress in the ocean basins. In Chapter 3, the regional load stresses due to the topographic feature and density distribution are calculated for an elastic and visco-elastic model of the lithosphere by the method of finite elements.

Movement of the lithosphere away from the hot axis of its creation at the ridges enables the lithosphere to cool (McKenzie, 1967) and this cooling results in thermal stresses throughout the lithosphere. Turcotte (1974) deduced the stresses and the bending of the lithosphere and the results suggest a possible mechanism for the formation of fracture zones. His analytical derivation, however, used the simplifying assumption that the vertical thermal stresses throughout the lithosphere are zero which is unrealistic. The stresses caused by lithospheric cooling are examined in 3 dimensions in Chapter 4 by use of the finite element method of stress analysis.

The emplacement mechanism of new lithosphere must, without doubt, exert considerable force on the surrounding lithosphere. Diapirism of the mobile mantle material will produce outward pressure into the lithosphere. Piper and Gibson (1972) calculated the stress field resulting from a circular cross-sectioned cavity of negative density contrast situated in the crust and upper mantle. Their model represents a magma chamber of intruding body and their calculations showed that a region of horizontal tension is created above the body with horizontal compression at each side and, from this, dyke and sill distributions were predicted. In Chapter 6, the stress field created by the diapirism of upwelling asthenosphere material and the magma chamber are calculated.

The numerical technique of solution of the problem allows a more realistic shape for the intruding body and magma chamber to be used.

The stress field resulting from a mantle plume rising and dispersing under a lithospheric plate is examined in Chapter 7.

CHAPTER 2

NUMERICAL SOLUTIONS IN GEODYNAMIC STUDIES

2.1 Introduction

The investigation of geodynamic or geostatic models in geological science usually involves the solution of differential equations applying to the continuum mechanics of the region. The geometry of a region is often complex with noncontinuity of both material properties and boundary conditions. Consequently, analytical solutions are either impossible or involve unrealistic simplifying assumptions. To overcome these problems and to preserve the detail of the model, numerical solutions are used. The two most useful and versatile techniques for the solution of continuum mechanics problems are the methods of finite element, described below, and finite difference, described in Chapter 5. Use of these methods involves the construction of algorithms from the differential equations and numerical analysis, and subsequent solution by the use of electronic computers.

2.2 Finite element analysis of an elastic continuum

The finite element method is used in this thesis for determining the stress and displacement fields of elastic

continua and it is this application of the method which is outlined in this chapter. Fundamental properties of the elastic continuum are described in many books (Fung, 1965; Sokolnikoff, 1956; Jaeger and Cook, 1969) and are not discussed here. The deformation of the continuum is expressed in terms of the strain tensor, $\{\varepsilon\}$, which is related to the vector displacement, $\begin{Bmatrix} u \\ v \\ w \end{Bmatrix}$, of a point in the continuum by the relationship

$$\left\{\varepsilon\right\} = \begin{Bmatrix} \varepsilon_x \\ \varepsilon_y \\ \varepsilon_z \\ \varepsilon_{xy} \\ \varepsilon_{yz} \\ \varepsilon_{zx} \end{Bmatrix} = \begin{Bmatrix} \partial u/\partial x \\ \partial v/\partial y \\ \partial w/\partial z \\ \partial w/\partial y + \partial v/\partial x \\ \partial v/\partial z + \partial w/\partial y \\ \partial w/\partial x + \partial u/\partial z \end{Bmatrix} \qquad 2.1$$

Strain is related to stress, $\{\sigma\}$, by

$$\left\{\sigma\right\} = \begin{Bmatrix} \sigma_x \\ \sigma_y \\ \sigma_z \\ \sigma_{xy} \\ \sigma_{yz} \\ \sigma_{zx} \end{Bmatrix} = \left[D\right]\left(\left\{\varepsilon\right\} - \left\{\varepsilon_0\right\}\right) + \left\{\sigma_0\right\} \qquad 2.2$$

where $\{\sigma_0\}$ is the initial stress tensor, $\{\varepsilon_0\}$ is the initial strain tensor and $[D]$ the elasticity matrix. For plane strain ($\varepsilon_z = \varepsilon_{xz} = \varepsilon_{yz} = 0$) and $\{\varepsilon_0\} = 0$, $\{\sigma_0\} = 0$, this gives

$$\begin{Bmatrix} \sigma_x \\ \sigma_y \\ \sigma_{xy} \end{Bmatrix} = \frac{E(1-\nu)}{(1+\nu)(1-2\nu)} \begin{bmatrix} 1 & \frac{\nu}{1-\nu} & 0 \\ \frac{\nu}{1-\nu} & 1 & 0 \\ 0 & 0 & \frac{1-2\nu}{2(1-\nu)} \end{bmatrix} \begin{Bmatrix} \varepsilon_x \\ \varepsilon_y \\ \varepsilon_{xy} \end{Bmatrix} \qquad 2.3$$

$$\sigma_z = \nu\left(\sigma_x + \sigma_y\right)$$

where E is Young's modulus and ν is Poisson's ratio.

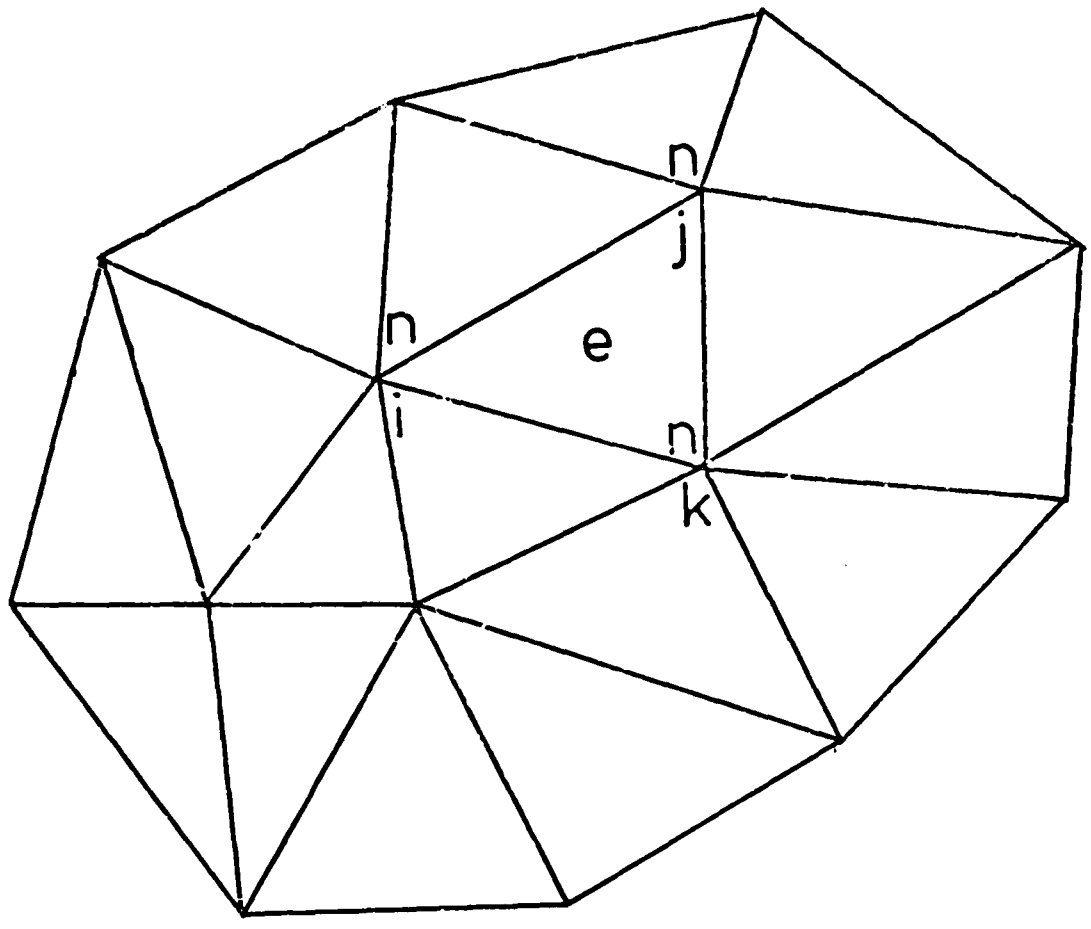

Figure 2.1 Finite element subdivision of a region showing elements (e) and nodes (n).

The finite element method is described in detail by Zienkiewicz (1971) who discusses its formulation and many uses and it is this formulation by Zienkiewicz which is followed in this chapter. The region over which the differential equation of an elastic continuum is to be solved is divided into a set of subdomains or elements, which in 2 dimensions, for the most simple case, are triangular (figure 2.1). The differential equation of the region is the minimization of the total energy of the continuum with respect to the elastic displacement of the continuum such that

$$\frac{\partial \Psi}{\partial \{f\}} = 0 \qquad 2.4$$

where Ψ is the total elastic energy and $\{f\}$ is the displacement vector, a spatially dependent function. Elastic energy, Ψ, is the sum of the strain energy and the work done by external loads on the continuum. This is given by the relationship.

$$\begin{aligned}\Psi = \tfrac{1}{2}\int \{\varepsilon\}^T [D] \{\varepsilon\} \, d(vol) - \int \{\varepsilon\}^T [D] \{\varepsilon_o\} \, d(vol) \\ + \int \{\varepsilon\}^T \{\sigma_o\} \, d(vol) + \int \{f\}^T \{p\} \, d(vol) \\ + \int \{f\}^T \{g\} \, d(area)\end{aligned} \qquad 2.5$$

where $\{g\}$ is the vector of distributed boundary forces and $\{p\}$ is the vector of distributed internal forces. Behaviour

of the continuum is approximated to that of the system of elements which are interconnected at their corners or nodes and the continuum behaviour is represented by the elastic displacements at these nodes. Formulation of a set of simultaneous equations yielding the equilibrium nodal displacement is achieved by expressing the energy in terms of nodal displacements and then minimizing the energy according to equation 2.4.

In order to express the energy of the elements in such a way it is necessary to obtain the element stress and strain tensors in terms of nodal displacements. If $\{\delta\}$ is the vector of nodal displacements for the whole body and $[N]$ is a mapping matrix known as the shape function, the displacement at any point in the body is given by

$$\{f\} = \begin{Bmatrix} u \\ v \end{Bmatrix} = [N]\{\delta\} . \qquad 2.6$$

The shape function $[N]$ is composed of individual shape functions, $[N]^e$, from each element, which take the form for an element with nodes i, j, k

$$[N] = \begin{bmatrix} N_i & 0 & N_j & 0 & N_k & 0 \\ 0 & N_i & 0 & N_j & 0 & N_k \end{bmatrix} \qquad 2.7$$

where

$$N_i = (a_i + b_i x + c_i y)/2\Delta$$

$$a_i = x_j y_k - x_k y_j$$

$$b_i = y_j - y_k \qquad 2.8$$

$$c_i = x_k - x_j$$

$$2\Delta = \begin{vmatrix} 1 & x_i & y_i \\ 1 & x_j & y_j \\ 1 & x_k & y_k \end{vmatrix}$$

and N_j and N_k are given by cyclic permutation. The strain at any point in the region may be obtained by the expression

$$\{\varepsilon\} = \begin{bmatrix} \partial/\partial x & 0 \\ 0 & \partial/\partial y \\ \partial/\partial y & \partial/\partial x \end{bmatrix} \{f\} \qquad 2.9$$

or

$$\{\varepsilon\} = [B]\{\delta\} \qquad 2.10$$

where $[B]$ is a matrix mapping nodal displacement into strain. Stress is then given by the constitutive equation such that

$$\{\sigma\} = [D](\,[B]\{\delta\} - \{\varepsilon_0\}\,) + \{\varepsilon_0\}\ . \qquad 2.11$$

From equation 2.5 the energy, Ψ, becomes in terms of nodal displacement

$$\begin{aligned}\Psi = \tfrac{1}{2}\int & (\,[B]\{\delta\}^T)\,[D][B]\{\delta\}\,d(\text{vol}) \\ & - \int (\,[B]\{\delta\}\,)\,[D]\{\varepsilon_0\}\,d(\text{vol}) + \int ([B]\{\delta\}\,)^T\{\sigma_0\}\,d(\text{vol}) \\ & + \int (\,[N]\{\delta\}\,)^T\{p\}\,d(\text{vol}) + \int ([N]\{\delta\}\,)^T\{g\}\,d(\text{area})\end{aligned} \qquad 2.12$$

The energy minimization for equilibrium is given by differentiating the energy with respect to nodal displacement and results in the fundamental equation of elastic finite element analysis,

$$\begin{aligned}&\int [B]^T[D][B]\{\delta\}\,d(\text{vol}) - \int [B]^T[D]\{\varepsilon_0\}\,d(\text{vol}) \\ &+ \int [B]^T\{\sigma_0\}\,d(\text{vol}) + \int [N]^T\{p\}\,d(\text{vol}) \\ &+ \int [N]^T\{g\}\,d(\text{area}) = 0\ .\end{aligned} \qquad 2.13$$

Using a simplifying notation the nature of the simultaneous equation may be seen which gives the nodal displacements,

$$[K]\{\delta\} = -\{F\}_p - \{F\}_g - \{F\}_{\varepsilon_o} - \{F\}_{\sigma_o} \qquad 2.14$$

where

$$[K] = \int [B]^T [D] [B] \, d(vol) \qquad 2.15$$

$$\{F\}_p = \int [N]^T \{p\} \, d(vol) \qquad 2.16$$

$$\{F\}_g = \int [N]^T \{g\} \, d(vol) \qquad 2.17$$

$$\{F\}_{\varepsilon_o} = -\int [B]^T [D] \{\varepsilon_o\} \, d(vol) \qquad 2.18$$

$$\{F\}_{\sigma_o} = \int [B]^T \{\sigma_o\} \, d(vol) \qquad 2.19$$

The matrix $[K]$ is known as the stiffness matrix.

Distributed loads usually take the form of the gravitational body forces and for triangular elements the loads may be applied as concentrated nodal forces $\{R\}$ by equally partitioning the weight of the element and applying one third of the weight to each node, such that

$$\{R\}_i = \{R\}_j = \{R\}_k = \Delta\rho g/3. \qquad 2.20$$

The finite element equation becomes for the situation of no initial stress, initial strains, distributed internal loads nor distributed surface loads

$$[K]\{\delta\} = \{R\} . \qquad 2.21$$

Displacement boundary conditions are applied by multiplying the diagonal element of the matrix $[K]$, corresponding to the boundary condition nodal displacement, by a very large number (10^{12}) and replacing the corresponding force vector by the nodal displacement times the new diagonal element. This has the effect of making the $[K]$ matrix extremely stiff

about the prescribed displacement.

Once the matrix $[K]$ and vector $\{R\}$ of equation 2.21 have been formulated numerically all that remains is the solution for $\{\delta\}$. The solution may be carried out by a number of numerical procedures which solve equation 2.21 directly, without matrix inversion. Inversion of matrices for solution is avoided since this operation introduces large numerical errors and consumes much computing time. Suitable solutions may be obtained by using the Gauss-Seidel, Cholesky or Gaussian elimination methods and these numerical techniques are all available in numerical analysis program libraries (Hopper, 1973: NAG, 1974). The mathematical basis of the methods are described by Forsyth and Moler (1967) and Fox (1964). The Gaussian elimination method is most suitable for the situations where many repeated solutions from the same matrix are required, while Seidel-Gauss and Cholesky methods are useful when the matrix is extremely large. The numerical values of $\{\delta\}$ from the solution are used to compute the element strain and stress according to equations 2.10 and 2.11. Results may conveniently be presented graphically using computers, displaying elastic displacement vectors, the principal stresses at their corresponding orientations, and deviatoric stresses.

The finite element mesh or grid is drawn subdividing the region into elements in such a way that physical constant

variations correspond to element boundaries. Nodes of the subdivided region are numbered in such a way that the maximum difference of nodal numbers for each element is as small as possible. This operation produces a banded matrix which allows more efficient storage of the matrix elements in the computing method.

This formulation of finite element for elastic stress analysis is followed in Chapter 6 where the stresses in the lithosphere caused by the upwelling and intruding asthenosphere at the ocean ridges are calculated. The computer program used is listed and explained in appendix 4.

2.3 Viscoelastic finite element analysis

A viscoelastic substance possesses properties which incorporate both elastic and viscous material behaviour. These physical properties correspond to those of many rocks, especially those of the mantle (Stocker and Ashby, 1973) whose behaviour appears to change from elastic to viscoelastic with increasing time. For example, the asthenosphere transmits seismic waves (an elastic process) yet over geological time appears to behave as a viscous fluid (Heiskanen and Vening Meinesz, 1958). Strain and stress are a function of time in a viscoelastic material and the rate of change of strain, the creep rate, is stress dependent. Creep rates may be obtained from experimental work on rock samples or from a

rheological model. The viscoelastic work of this thesis uses a Maxwell rheological model and the microscopic behaviour of this material corresponds to that of elastic and viscous materials in series. Jaeger and Cook (1969) described the properties of this and other rheological models together with experimentally determined creep rates.

The strain rate for a Maxwell substance is given by

$$\{\dot{\varepsilon}\} = [D]^{-1}\{\dot{\sigma}\} + [S]\{\sigma\} \qquad 2.22$$

where matrix $[S]$ is a function of viscosity. Dividing the strain rate into elastic and viscous components, the viscous creep is

$$\{\dot{\varepsilon}\}_v = [S]\{\sigma\} \qquad 2.23$$

and in detail the creep components are

$$\begin{aligned}
\{\dot{\varepsilon}_x\}_v &= \tfrac{1}{2}\eta\ (\sigma_x - \sigma_s)\\
\{\dot{\varepsilon}_y\}_v &= \tfrac{1}{2}\eta\ (\sigma_y - \sigma_s)\\
\{\dot{\varepsilon}_{xy}\}_v &= 1/\eta\ (\sigma_{xy})\\
\{\dot{\varepsilon}_z\}_v &= \tfrac{1}{2}\eta\ (\sigma_z - \sigma_s)
\end{aligned} \qquad 2.24$$

where $\sigma_s = 1/3\ (\sigma_x + \sigma_y + \sigma_z)$ (Jaeger and Cook, 1969; YIH,1969).

The finite element formulation for elastic continuum analysis may be extended for viscoelastic analysis by using the concept of initial strain (Zienkiewicz, 1971). The fundamental equilibrium equation for the viscoelastic finite element formulation is obtained from equation 2.14 and 2.21

and is

$$[K]\{\delta\} = \{R\} - \{F\}_{\varepsilon_0} \qquad 2.25$$

where

$$-\{F\}_{\varepsilon_0} = \int [B]^T [D] \{\varepsilon_0\} \, d(vol) \qquad 2.26$$

Creep is incorporated in the calculation as an initial strain and the stress at any time is given by

$$\{\sigma\} = [D]\left(\{\varepsilon\} - \{\varepsilon_0\}\right) \qquad 2.27$$

The usual objective of viscoelastic analysis is to study the behaviour of the stress, strain and displacement of a model with time. Analysis is initiated by an ordinary elastic solution which gives the elastic stress, strain and displacement at zero time. The viscoelastic behaviour of the model is then propagated through time by a series of time steps in each of which occurs the following sequence of calculations.

(1) The creep rate for the time step is calculated from the stress at the end of the previous time increment.

(2) The creep rate is integrated over the time increment to give the incremental creep which is then added to the creep of previous increments.

(3) The total creep is incorporated in the initial strain vector.

(4) Solution is obtained for the displacement, strain and stress at the end of the time increment.

(5) The stress at the end of the time increment is used to obtain a better estimate of the mean stress of the time increment and this new estimate is used to produce a new creep rate for the increment.

(6) The sequence is repeated from step (2) until constant values are obtained for the stress at the end of the time increment.

(7) Return to step (1) for start of next time increment.

This numerical process has been found to be stable provided the creep of an increment does not exceed the elastic strain. This corresponds to a maximum time increment of

$$\Delta t = 2\eta/E \qquad 2.28$$

Although the viscoelastic analysis is to be formulated for plain strain, the creep $\{\varepsilon_z\}_v$ is not zero. Since the total strain $\{\varepsilon_z\}$ is zero, the elastic strain $\{\varepsilon_z\}_e$ must be equal and opposite to the creep $\{\varepsilon_z\}_v$, i.e.

$$\{\varepsilon_z\} = \{\varepsilon_z\}_e + \{\varepsilon_z\}_v = 0 \qquad 2.29$$

In calculating the $[K]$ matrix for viscoelastic analysis, the elasticity matrix, $[D]$ given by equation 2.3 may be used since the total strain $\{\varepsilon_z\}$ is zero. However, the matrix $[D]$, for the calculation of the initial strain vector and for the constitutive equation 2.27, must be modified to accommodate the effects of the strains $\{\varepsilon_z\}_c$ and $\{\varepsilon_z\}_v$. The initial force vector is given by

$$\{F\}_{\varepsilon_o} = -\int [B]^T [D]' \{\varepsilon_o\} \, .d(vol) \qquad 2.30$$

where

$$\{\varepsilon_o\} = \begin{Bmatrix} \varepsilon_x \\ \varepsilon_y \\ \varepsilon_z \\ \varepsilon_{xy} \end{Bmatrix}_v \qquad 2.31$$

and

$$[D] = \frac{E(1-\nu)}{(1+\nu)(1-2\nu)} \begin{bmatrix} 1 & \nu/1-\nu & \nu/1-\nu & 0 \\ \nu/1-\nu & 1 & \nu/1-\nu & 0 \\ 0 & 0 & 0 & \frac{1-2\nu}{2(1-\nu)} \end{bmatrix} \qquad 2.32$$

The constitutive equation is given by

$$\begin{Bmatrix} \sigma_x \\ \sigma_y \\ \sigma_z \\ \sigma_{xy} \end{Bmatrix} = \frac{E(1-\nu)}{(1+\nu)(1-2\nu)} \begin{bmatrix} 1 & \nu/1-\nu & \nu/1-\nu & 0 \\ \nu/1-\nu & 1 & \nu/1-\nu & 0 \\ \nu/1-\nu & \nu/1-\nu & 1 & 0 \\ 0 & 0 & 0 & \frac{1-2\nu}{2(1-\nu)} \end{bmatrix} \left(\{\varepsilon\} - \{\varepsilon_o\} \right)$$

2.33

Incremental creep is calculated from the creep rates by the simple integration

$$\{\varepsilon\}_v = \Delta t \, \{\dot{\varepsilon}\}_v \qquad 2.34$$

Viscoelastic finite element analysis is used in Chapter 3 for calculating the body force stresses of the oceanic lithosphere. The computer program is listed and described in appendix 1.

2.4 Finite element calculation of cooling stresses

The finite element may easily be used for the calculation of stresses resulting from thermal contraction. Again use is made of the initial strain concept. For an element undergoing a temperature change ΔT, the initial strain is given by

$$\{\varepsilon_o\} = \begin{Bmatrix} \alpha \Delta T \\ \alpha \Delta T \\ 0 \end{Bmatrix} \qquad 2.35$$

where α is the coefficient of expansion. For plane strain the initial strain tensor becomes (Zienkiewisz, 1971)

$$\{\varepsilon_o\} = (1+\nu) \begin{Bmatrix} \alpha \Delta T \\ \alpha \Delta T \\ 0 \end{Bmatrix} \qquad 2.36$$

The initial strain vector is given by equation 2.18 and the nodal displacement by

$$[K]\{\delta\} = -\{F\}_{\varepsilon_o} \qquad 2.37$$

Thermal stresses are then obtained from the relationship

$$\begin{Bmatrix} \sigma_x \\ \sigma_y \\ \sigma_{xy} \end{Bmatrix} = [D]\left(\{\varepsilon\} - \{\varepsilon_o\}\right) \qquad 2.38$$

where $[D]$ is given by equation 2.3 and

$$\{\sigma_z\} = \nu(\sigma_x + \sigma_y) - \alpha \Delta T \qquad 2.39$$

In Chapter 4 this method is used to calculate the cooling stresses of the oceanic lithosphere. The computer program used for the calculation is listed and described in appendix 2.

CHAPTER 3

LOAD STRESSES IN THE OCEAN LITHOSPHERE

3.1 Introduction

The topographic high of the ocean ridge and the associated low density upper mantle which maintains the isostatic equilibrium (Talwani et al., 1965) gives rise to lateral density contrasts in the oceanic lithosphere. Artyushkov (1973) has shown that lateral changes in density in the lithosphere may lead to regional stress relative to the expected hydrostatic load stresses. For the oceanic lithosphere Artyushkov predicted, by analytical calculation, relative horizontal compressive stresses in the upper lithosphere which increase from zero at the ridge axis to about 0.25 kb in the ocean basins. Stephansson and Berner (1970), using finite element analysis to calculate the load stresses of a viscous model of the lithosphere, suggested that the oceanic crust was in horizontal tension at the ridge axis relative to the hydrostatic and in compression in the basins. The different conclusions of these two works is a consequence of the use of different boundary conditions at the ridge axis in the two models. While Artyushkov applied a hydrostatic stress boundary condition to the vertical ridge axis boundary, Stephansson and Berner used the lateral symmetry of the ridge axis.

In the following work, the state of stress in the oceanic lithosphere arising from the density distribution is investigated by the finite element method of stress analysis for both types of ridge axis boundary condition. Both elastic and viscoelastic models of the lithosphere are examined.

3.2 The lithospheric model

The lithospheric model, selected for the investigation of lithosphere load stresses, corresponds to the structure suggested by Talwani et al. (1965) for the mid-Atlantic ridge at 35^{o}N where the half spreading rate is 1.5 cm/yr. The density distribution of the model is shown in figure 3.1. Theoretical lithosphere density distributions (Forsyth and Press, 1970; Sclater and Francheteau, 1971; Haigh, 1973) have not been used since they are dependent on assumed mantle composition. The upper surface of the model, representing the ocean rise topography, uses the smoothed topography produced for the N. Atlantic ocean at 35^{o}N by Haigh (1973b). Densities of the lithospheric model are consistent with the observed existence of isostatic equilibrium at the ocean ridges.

The model dimensions are 1400km by 80km. Only one half of the ocean rise structure is included in the model

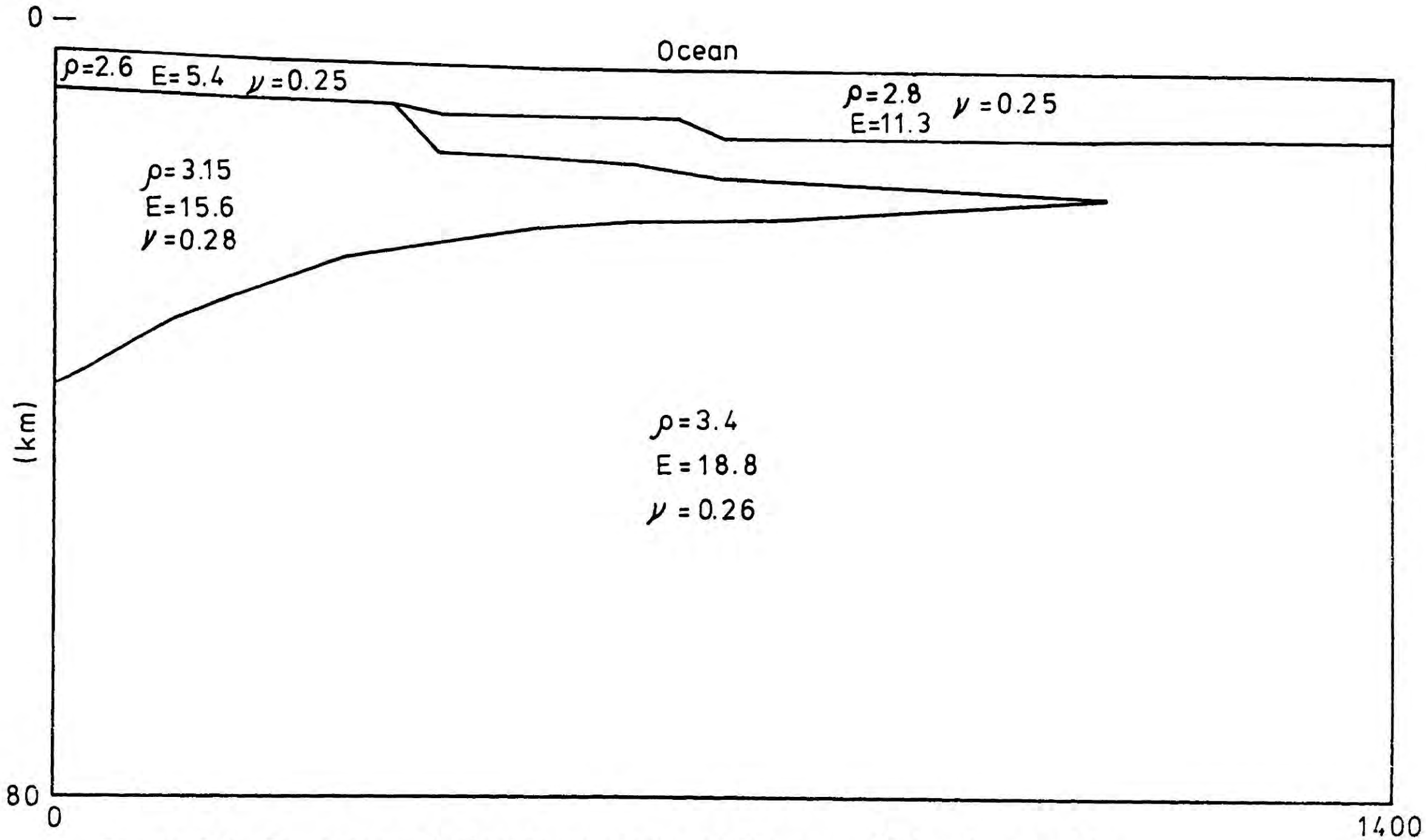

Figure 3.1 Densities and elastic constants of the ocean lithosphere model. (ρ in gm/cm^3, E in 10^{11} dynes cm^2)

by the assumption of symmetry. For a half spreading rate of 1.5 cm/yr, the ocean ridge topography decays to that of the level of the ocean basins at a distance of about 1200 km from the ridge axis (Haigh, 1973) and the model length of 1400 km is therefore adequate to incorporate the whole ocean rise structure. The model depth of 80 km is consistent with the values suggested by Kanamori and Press (1970) and Haigh (1973). The model assumes a level datum for the lithosphere-asthenosphere boundary.

Boundary conditions may be applied to the lithosphere model in the form of prescribed boundary displacements or stresses. The asthenosphere-lithosphere boundary is assumed to be a boundary of uniform stress and strain since it is below the level of lateral density variations and the lithosphere is in isostatic equilibrium. Consequently the boundary is constrained for zero vertical displacement. No displacement constraint is imposed horizontally since the asthenosphere behaves as a fluid body over geological time scales (Haskell, 1935; Heiskanen and Vening Meinesz, 1958; Crittenden, 1963). The vertical boundary of the model at the ocean basin is constrained for zero horizontal displacement, because of the lateral uniformity in this region. For the vertical boundary of the model at the ridge axis, two possibilities for a boundary condition exist

(a) hydrostatic stress

(b) zero horizontal displacement

The boundary condition of hydrostatic stress at the ridge axis was used by Artyushkov (1973) and assumes that the lithosphere at the ridge axis is fluid. This is substantiated by geochemical evidence for partial melts and fractionation in the mantle below the ridge crests (e.g. Kay, Hubbard and Gast, 1970) and seismic evidence, if the low velocities below the ridge crest (e.g. Talwani et al., 1965, 1971) are interpreted as indicative of partial melts. Further evidence exists which suggests that the asthenosphere may be very close to the ocean floor at the ridge crests (Forsyth, 1975; Oldenburg, 1975). The alternative boundary condition (b), used by Stephansson and Berner (1970), is suggested by the existence of horizontal symmetry about the ridge axis.

The hydrostatic stress boundary condition applied at the ridge axis may be modified by the effects of the vertical flow of the viscous intruding material at the ridge axis. Such flow would exert shear stresses on the vertical ridge axis boundary, in addition to the hydrostatic stresses already described. The effects of the shear stresses are not, however, considered quantitatively in the following work.

The values of elastic constants used for the different

regions of the lithosphere are shown in figure 3.1 and are those used in crustal tilt studies by Beaumont and Lambert (1972). The stresses in the oceanic lithosphere, due to density loading, are investigated for both elastic and viscoelastic models of the oceanic lithosphere. Although the lithosphere is usually considered as behaving as an elastic layer, evidence from lithosphere flexure (Walcott, 1970) indicates that it may behave, at least in part, as a viscoelastic material. Walcott has suggested that the purely elastic part of the lithosphere may be of the order of 20 km thick. The strong temperature dependence of the viscosity of mantle like material (Stocker and Ashby, 1973) together with the high temperature of the lower lithosphere and the lithosphere adjacent to the ridge axis (McKenzie, 1967; Haigh, 1973) gives further support to the possibility of a viscoelastic lower lithosphere. The Maxwell viscoelastic element, described in Chapter 2, is assumed to represent the viscoelastic behaviour of the oceanic lithosphere. A stress independent viscosity is used for simplicity. The viscoelastic lithosphere model is investigated for uniform viscosity and viscosity contrast between the upper and lower lithosphere.

The approximation is made in all analyses that the oceanic lithosphere is a stationary body.

3.3 The calculation of load stresses

The load stresses of the oceanic lithosphere may be calculated for the elastic model by considering the elastic loading of the lithosphere due to the ocean density and lithosphere density in addition to a hydrostatic stress boundary condition applied at the vertical ridge axis boundary. In calculating the load stresses of the ocean lithosphere it is hoped to be able to separate from the approximately hydrostatic load stresses of the lithosphere, the small stress component which departs from the hydrostatic and constitutes the regional stress of interest. However, this small perturbation of the hydrostatic load stresses, arising from the lateral density changes in the lithosphere, is very small compared to the magnitude of the total load stresses. In order to prevent these stresses of interest being hidden by numerical error, as would be the case if total stress were calculated, it is necessary to divide the calculation of the stresses into two parts. While the stress due to a uniform density throughout the ocean lithosphere may be calculated analytically, the stresses due to the density contrast are calculated separately, in this case by the method of finite element (e.g. Bott and Dean,1972). The stress field arising from the uniform density is hydrostatic and is given by

$$\sigma_x = \sigma_y = \sigma_z = g\rho z \qquad 3.1$$

where z is the depth below the surface, ρ is the uniform density and g is the gravitational acceleration.

The total stress field, if required, may be calculated from the two part stress field by the principle of stress superposition. One uniform density may be taken off the whole body or different uniform densities may be selected for regions between different horizontal datums.

In the following calculation two uniform densities are subtracted; a density of 1 gm/cc is taken off above the datum of the top of the ridge crest allowing the loading due to the ocean above the ridge crest datum to be omitted from the finite element calculation. A second uniform density of 3.2 gm/cc (the average lithosphere density) is subtracted below the ridge crest datum. A negative load of the ocean must therefore be applied at the upper surface of the lithosphere in the finite element analysis.

It should be noted that this division of the stress calculation into two parts, as above, is not applicable to an elastic model of the lithosphere with a zero displacement boundary condition at the vertical ridge axis boundary. An elastic model with these boundary conditions would not give uniform load stresses as given by equation 3.1, but rather a situation where the horizontal stress was a third of the overburden pressure (for $\nu = 0.25$). Such an elastic model leads to very high deviatoric stresses in the base of the

lithosphere which are felt to be unrealistic. Consequently an elastic lithosphere model, with the zero horizontal displacement ridge axis boundary condition is not investigated.

In the case of the viscoelastic models of the lithosphere, the load stresses of the lithosphere are assumed to be given by the steady state stress equilibrium of a viscoelastic body and are approximately hydrostatic. The viscoelastic model of the lithosphere allows both types of ridge axis boundary condition to be examined. The uniform densities subtracted from the actual lithosphere densities to give the density used in the finite element model are the same as for the elastic lithosphere model.

The subtraction of the uniform densities does not invalidate the viscoelastic analysis since the viscoelastic deformation used is only dependent on the deviatoric stress and not total stress.

The densities used in the finite element analysis of the lithosphere load stresses are shown in figure 3.2.

3.4 The finite element formulation and application

The finite element method of stress analysis for elastic and viscoelastic continua has been described in Chapter 2, where the formulation follows that suggested by Zienkiewicz (1971). The equilibrium equation giving total deformation

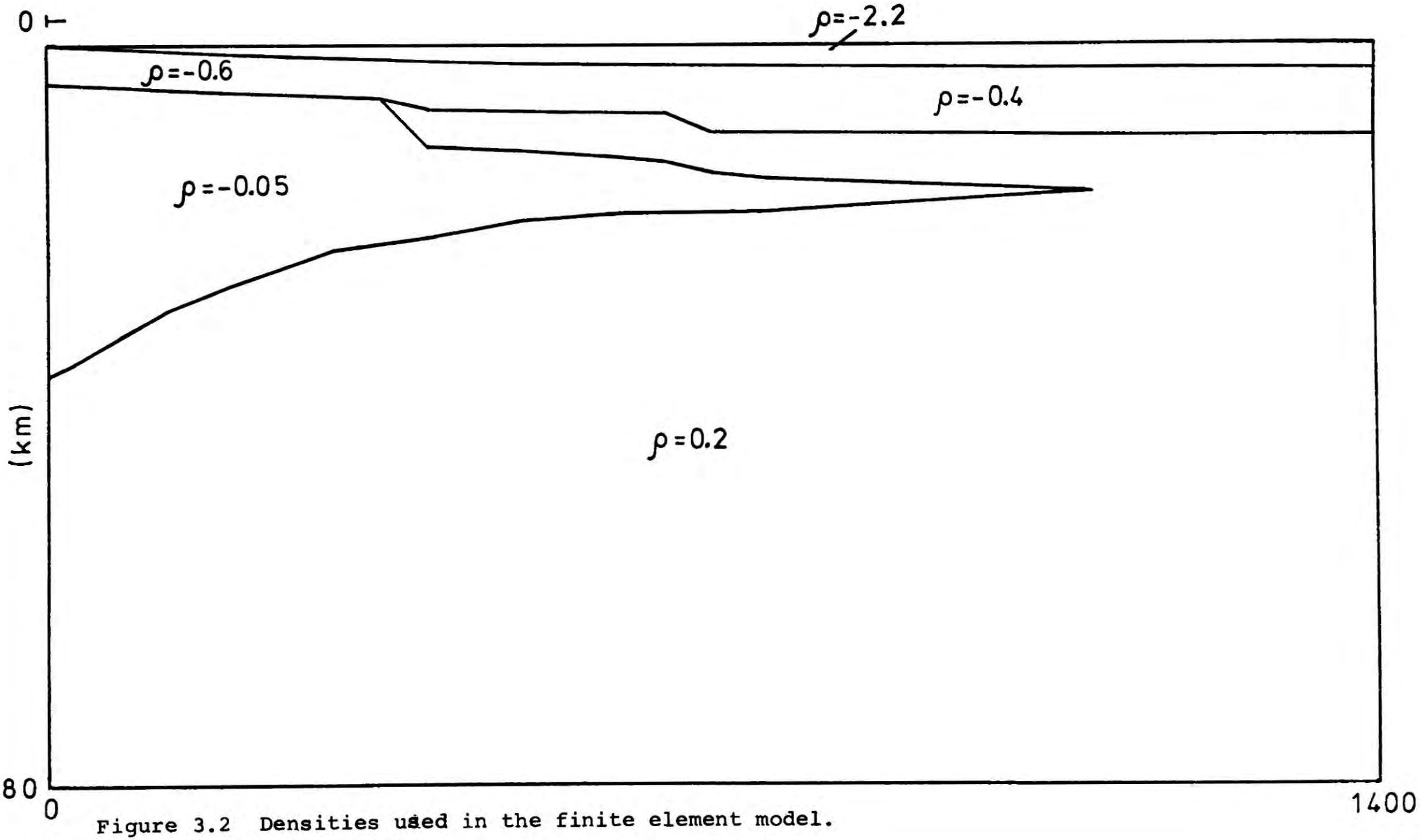

Figure 3.2 Densities used in the finite element model.

of the viscoelastic continuum is

$$[K]\{\delta\} = \{R\} - \{F\}_{\varepsilon_o} \qquad 3.2$$

where $[K]$ is the stiffness matrix of the continuum, $\{\delta\}$ is the vector of nodal displacement, $\{R\}$ is the vector of applied nodal forces and $\{F\}_{\varepsilon_o}$ is the initial strain vector. Construction of the initial strain vector for a Maxwell substance is given by equation 2.24 and 2.26.

While the finite element formulation of Chapter 2 described the propagation of viscoelastic deformation through time, in this work the deformation is propagated with respect to the variable t/η where η is viscosity. This enables the viscoelastic model to be studied for a range of viscosities.

Displacement boundary conditions are applied to equation 3.2. Numerical solution of equation 3.2 was carried out by Gaussian elimination.

The computer program used for the finite element analysis is listed and described in appendix 1.

The finite element subdivision of the lithosphere model is shown in figure 3.3. Elements are so arranged as to accommodate the density contrast boundaries of the model. The body forces of the thin low density upper mantle in the ocean basins, unrepresented by elements, are included

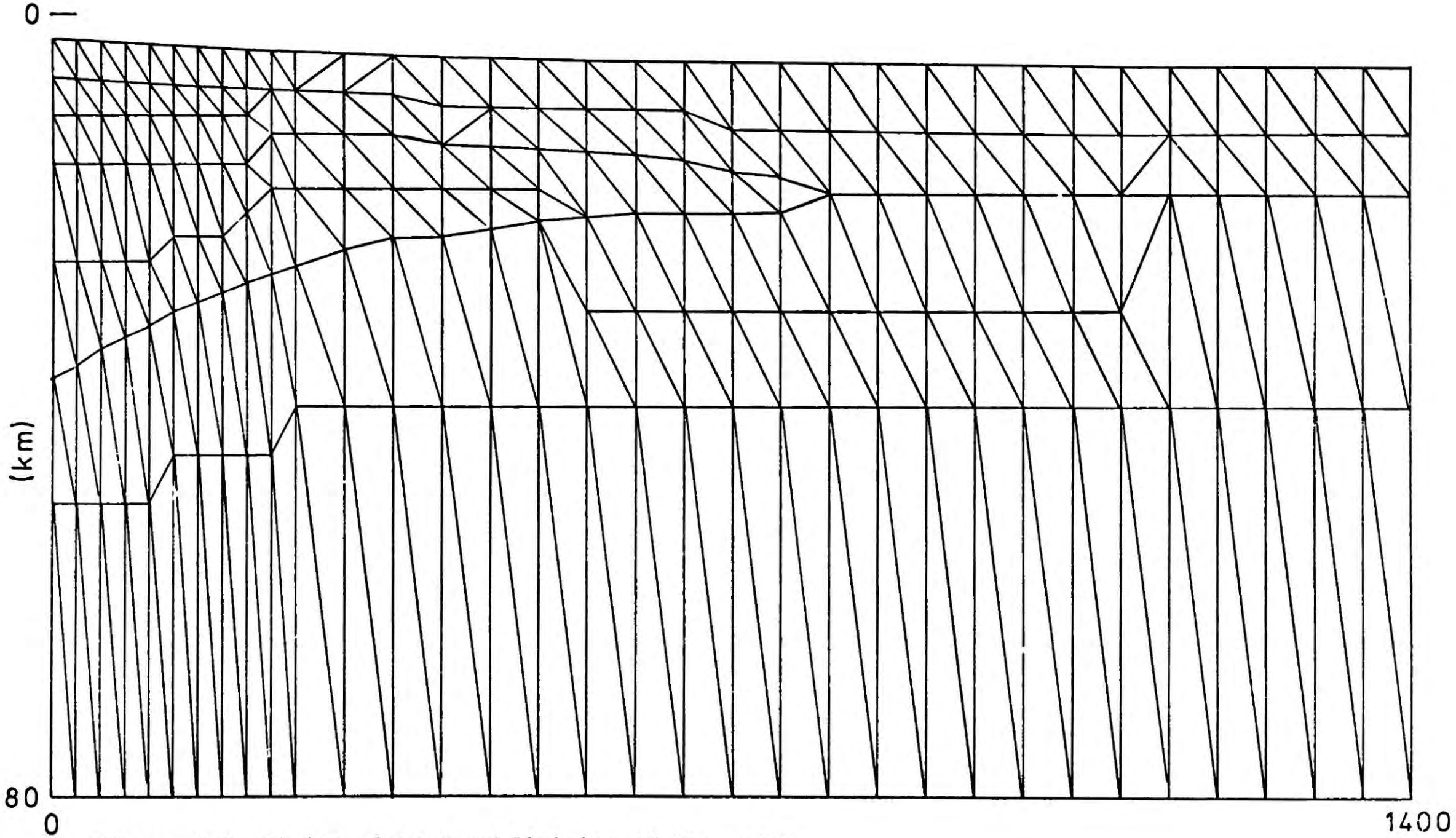

Figure 3.3 Finite element subdivision of the model

as nodal forces. The ridge axis stress boundary condition and the load of the ocean on the lithosphere are also expressed as equivalent nodal forces and applied at the appropriate nodes.

The viscoelastic analysis described above may be used for elastic analysis by setting t = 0, or using an infinite viscosity.

3.5 Elastic model load stresses

The load stresses due to the density contrast with respect to the uniform density are shown in fig. 3.4 for the elastic lithosphere model with hydrostatic stress boundary conditions applied at the vertical ridge axis boundary. Stresses are presented as principal stresses plotted at their principal orientations. Tensional stresses are denoted by a dot at the extremities of the principal stress. The plot shows that the load stresses in the lithosphere caused by the density contrast with respect to the uniform density of 3.2 gm/cc are tensional as expected. In the upper lithosphere, the stresses under the ridge are more compressive than the stresses at the same level in the ocean basins. This is a direct consequence of the lateral variation in density of the

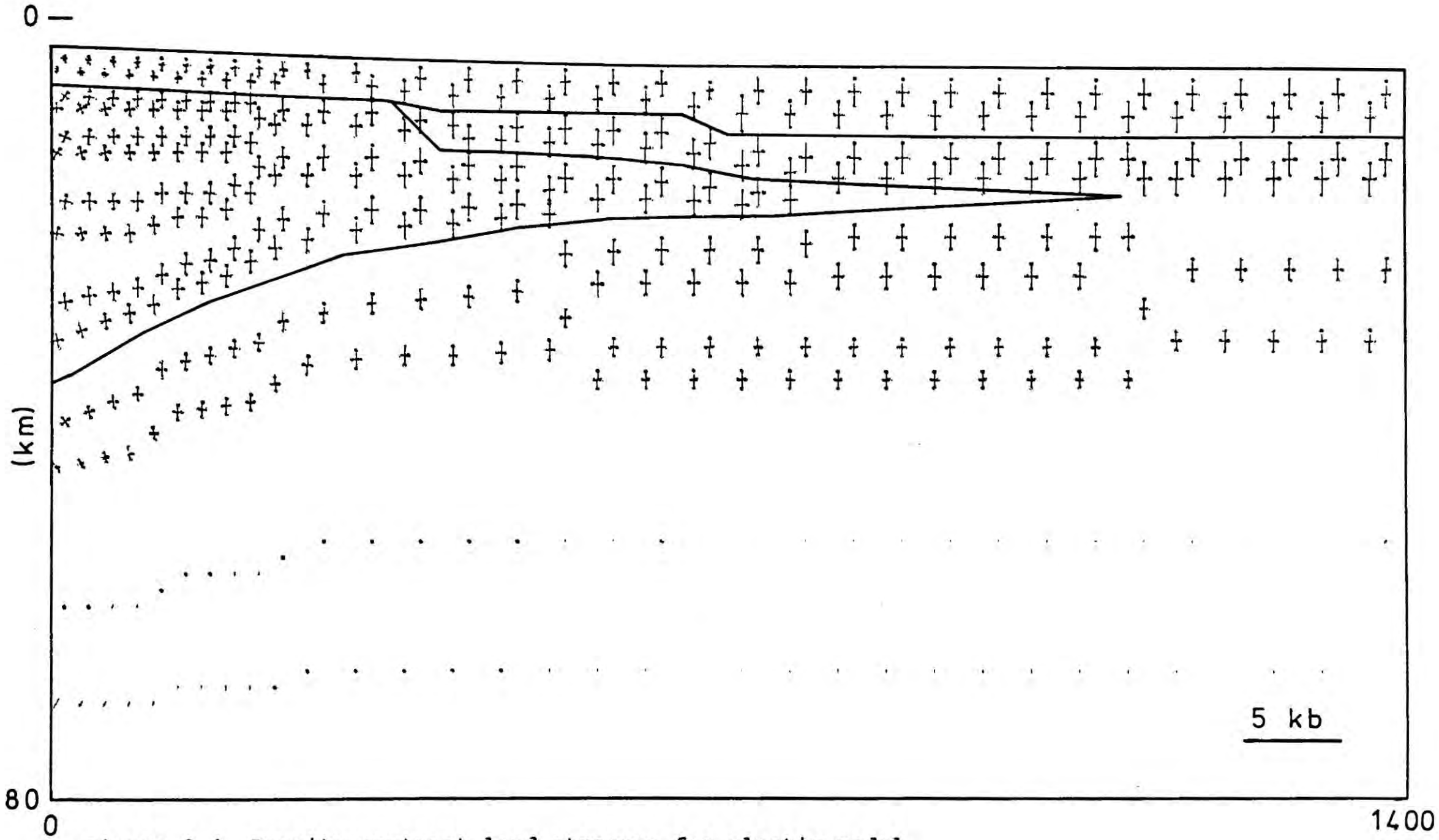

Figure 3.4 Density contrast load stresses for elastic model.

lithosphere model. While the lithosphere stresses of the ocean ridge in figure 3.4 are approximately hydrostatic, the stresses in the ocean basin show a relative horizontal compression. This is consistent with the predictions of Artyushkov (1973). The departure of the load stresses from the hydrostatic is best shown by the plot of the deviatoric stresses shown in figure 3.5. It can be seen that the deviatoric stresses increase in magnitude away from the ridge axis towards the ocean basin.

The influence of sea floor spreading rate on these regional stresses has been investigated by scaling the lithosphere model horizontally by a factor of two, corresponding to a model with a half spreading rate of 3 cm/yr. This is a valid approximation since the lithosphere away from the ridge axis cools largely by vertical heat flow (Haigh, 1973). The effect of an increase in spreading rate is to a good approximation simply to scale proportionately the horizontal extent of the region of compressive stress.

The effect of the upward acting shear stress exerted on the vertical ridge axis boundary by viscous intruding magma would be to exert a moment on the lithosphere. The magnitude of the moment is dependent on the velocity of upwelling of the magma and its viscosity, for which values of both are not known. Consequently an estimate of the

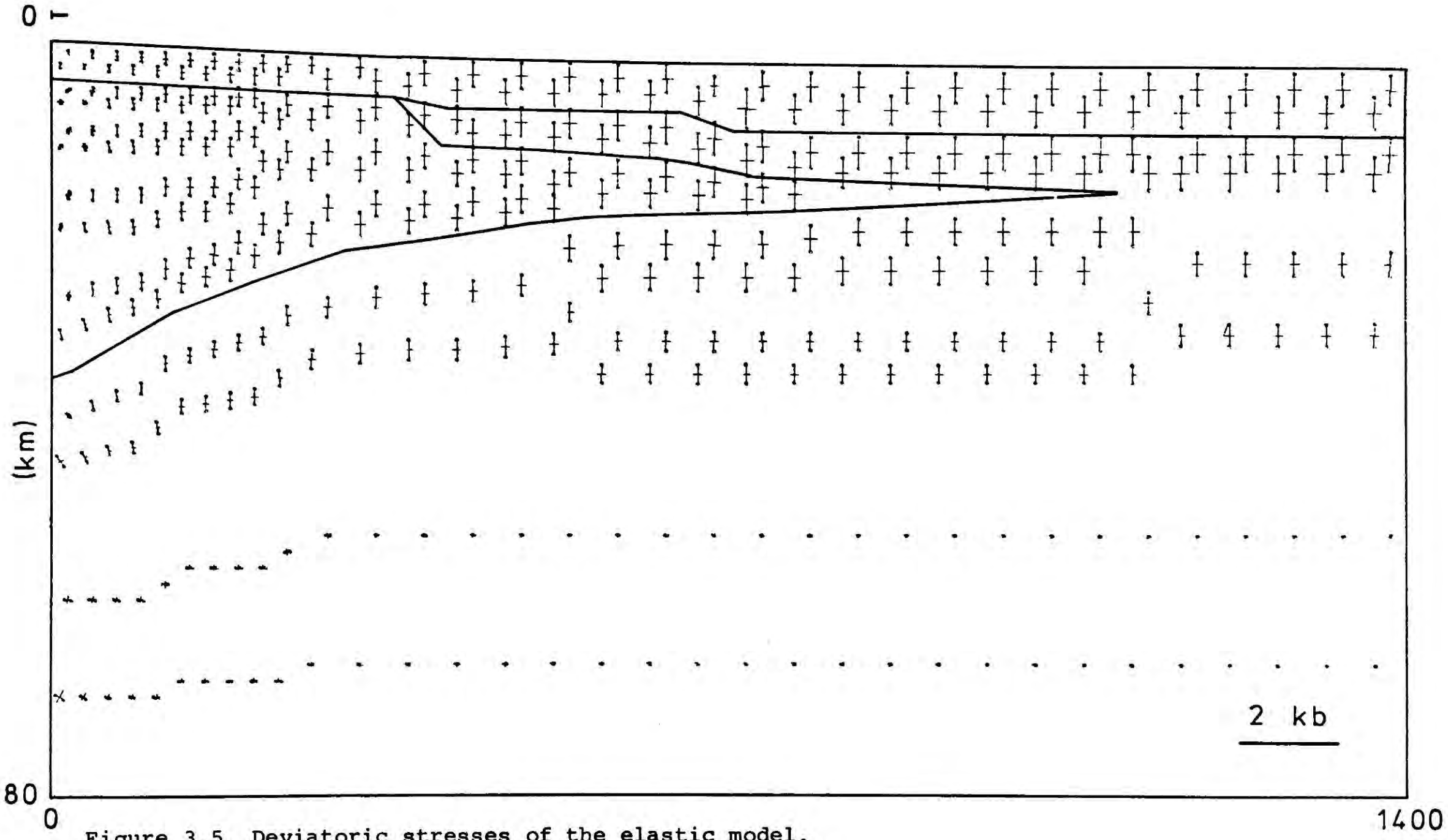

Figure 3.5 Deviatoric stresses of the elastic model.

magnitude of the moment is not made. The effect of the moment caused by the viscous drag on the lithosphere by the upwelling magma is however expected to cause tension at the ridge crest and compression in the ocean basin.

3.6 Viscoelastic model load stresses

The load stresses in a viscoelastic model of the lithosphere have been investigated for both the hydrostatic stress ridge axis boundary condition and the zero horizontal displacement boundary condition. Stresses for the two models are shown in figures 3.6 and 3.7, arising from the density contrast with respect to the uniform density. The plots show the stresses in both cases to be approximately hydrostatic with stress under the ridge axis more compressive than the stresses at the same level in the basins. For the stresses of the model with the zero horizontal displacement boundary condition small relative horizontal tension exists at the ridge axis. The departure of the stresses from the hydrostatic is best shown by the plot of the deviatoric stresses (figure 3.8 and 3.9). The lithosphere model with hydrostatic boundary condition shows hydrostatic stresses at the ridge axis and relative horizontal compression in the ocean basins. The lithospheric model with zero horizontal displacement boundary condition

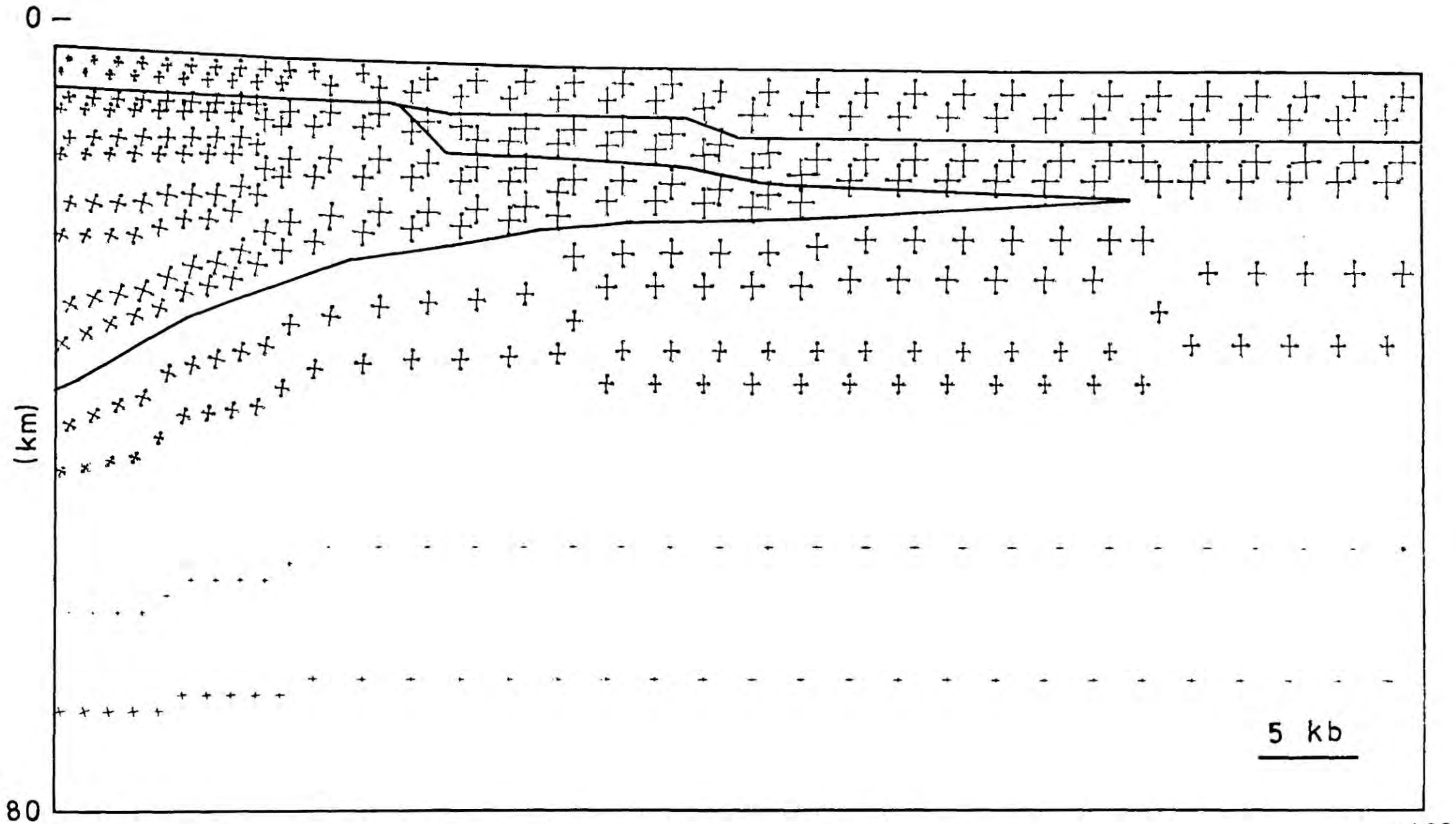

Figure 3.6 Density contrast load stresses for viscoelastic model with hydrostatic stress boundary condition.

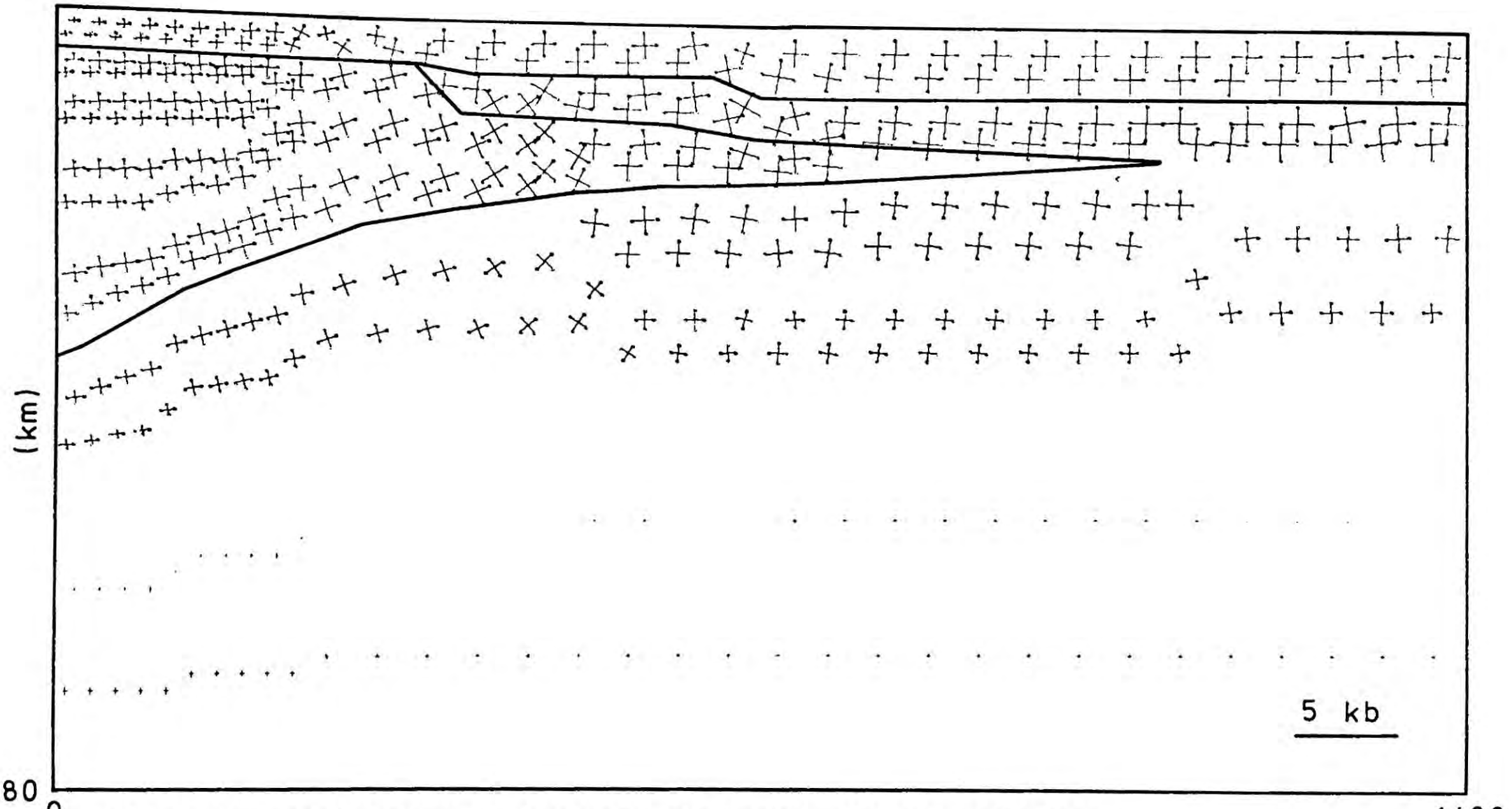

Figure 3.7 Density contrast load stresses for viscoelastic model with zero displacement boundary condition.

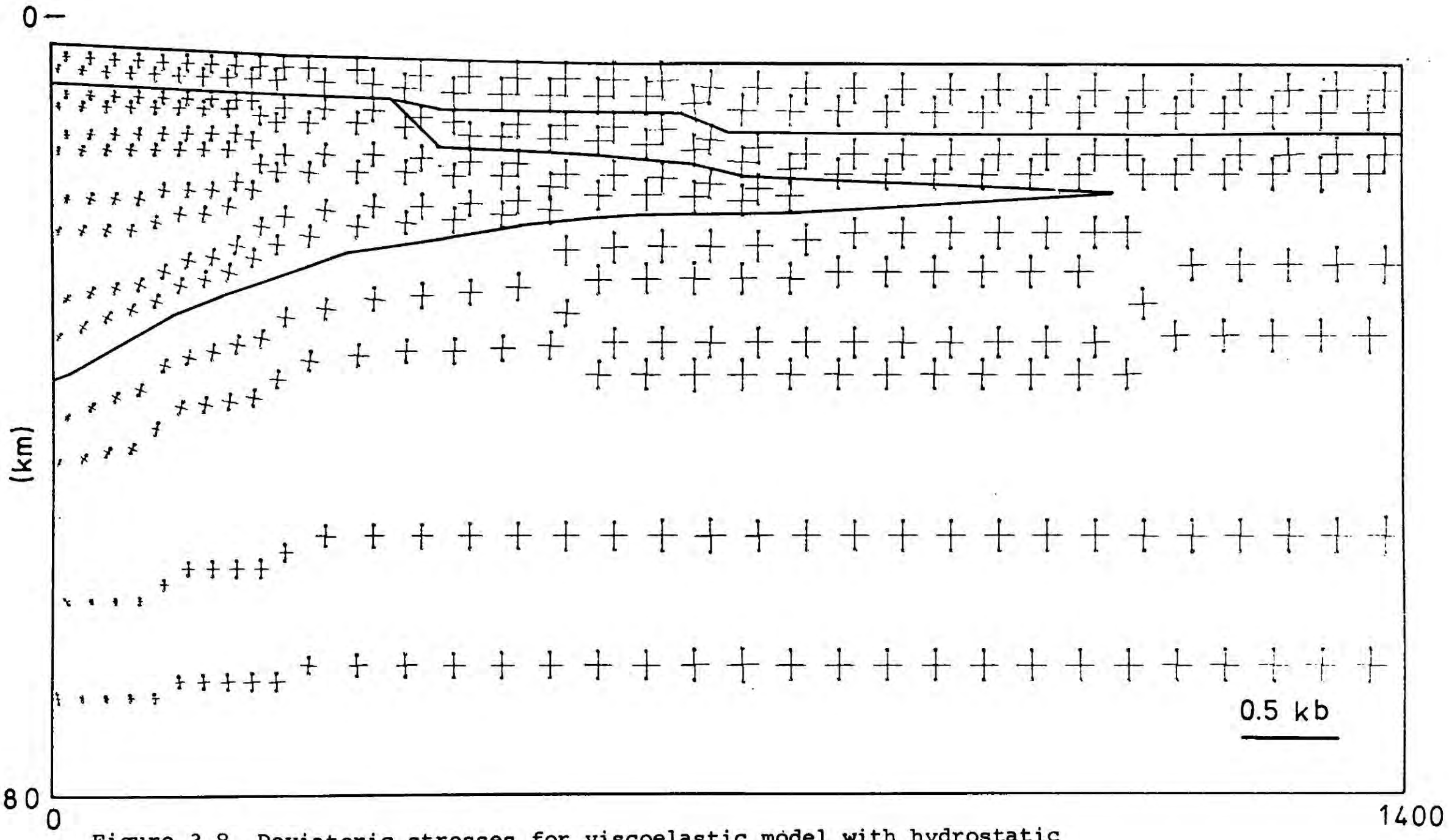

Figure 3.8 Deviatoric stresses for viscoelastic model with hydrostatic stress boundary condition.

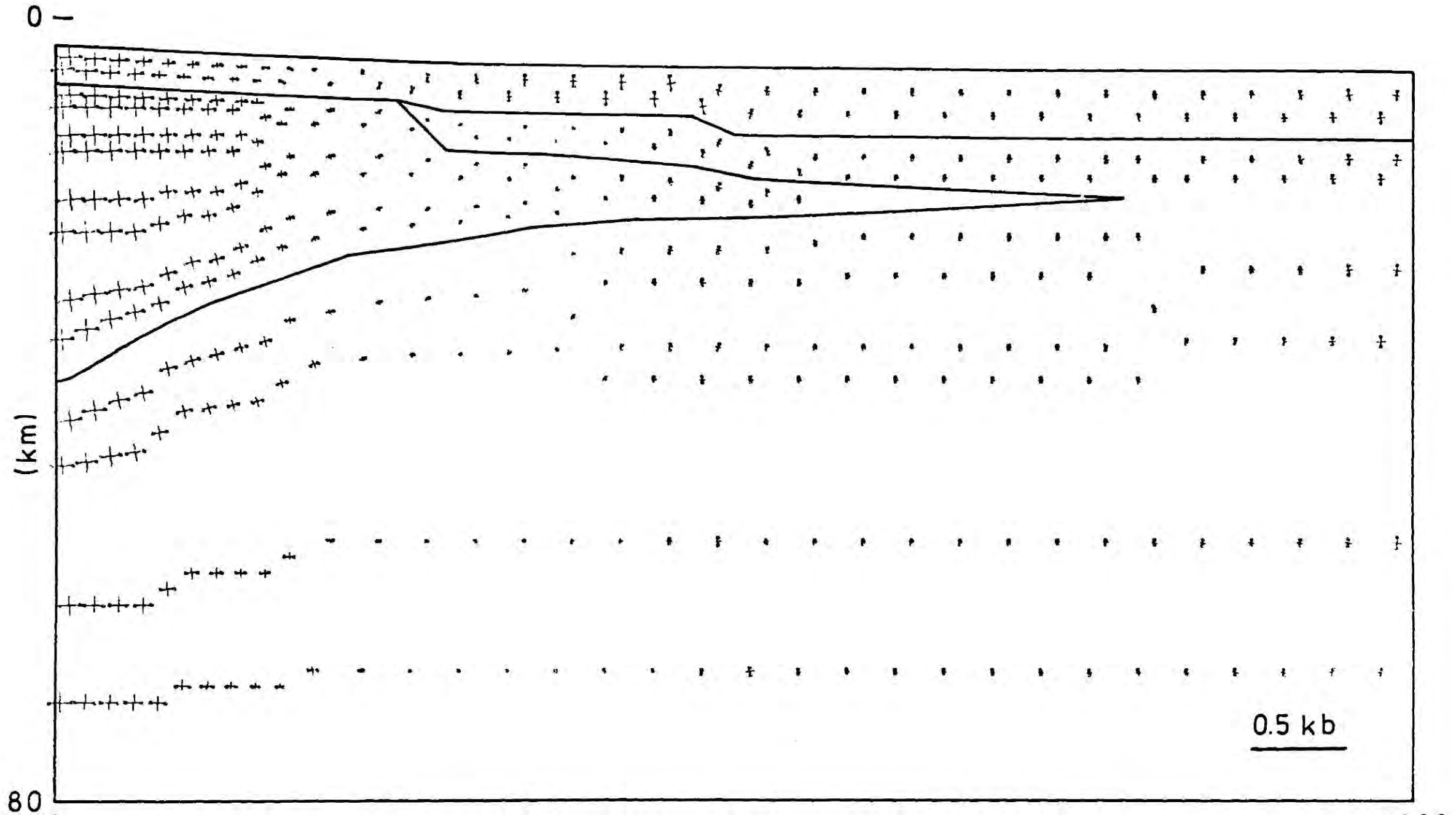

Figure 3.9 Deviatoric stresses for viscoelastic model with zero displacement boundary condition.

shows relative horizontal tension at the ridge axis and small relative horizontal compression in the ocean basins. In both cases regional stresses extend down throughout the lithosphere in contrast to the elastic model of the previous section whose regional stresses are concentrated in the upper lithosphere.

The value of t/η required for obtaining the steady state stress was found to be of the order of 2×10^{-11} sec/poise. Walcott (1970) from lithospheric flexure studies suggests a lithosphere viscosity of 10^{24} poise which gives a time required to reach the steady state stress of approximately 1 m.yr. Comparing this time with the 80 m.yr time span of the ocean ridge crest to basin section, it is suggested that the stress in the oceanic lithosphere could correspond to the steady state equilibrium of a viscoelastic body.

While the above analysis used a uniform viscosity for the ocean lithosphere, it is more probable that viscosity is greatest in the upper lithosphere away from the ridge axis and smallest in the lower lithosphere adjacent to the ridge axis. Walcott (1970), who suggested from lithosphere flexure studies that the lithosphere may behave as a visco-elastic body, has suggested that the top 20 km or so of the lithosphere may behave elastically. The load stresses of a lithosphere model, which is elastic in the upper 20 km

(except within 50 km of the ridge axis) and viscoelastic below, have been calculated.

The load stresses arising from the density contrast with respect to the uniform density are shown in figures 3.10 and 3.11 for the lithosphere models with different ridge axis boundary conditions. The model with the hydrostatic stress boundary condition shows relative horizontal compression in the ocean basin, as with the uniform viscosity model, but of greater magnitude. Figure 3.12 shows that the horizontal compression is concentrated in the elastic part of the lithosphere. The model with the zero horizontal displacement boundary condition shows the relative horizontal tension at the ridge axis, as does the uniform viscosity model, but with additional horizontal compression in the ocean basin. Figure 3.13 shows the deviatoric stress and displays a region, 250 km in extent at the ridge axis, of horizontal tension. The horizontal tension appears to be greatest in the upper mantle in contrast to the horizontal compressions which are greatest in the crust.

3.7 Conclusion

It has been shown that the lateral density contrast in the oceanic lithosphere gives rise to regional stress. The dependence of the lithosphere stress field on the boundary

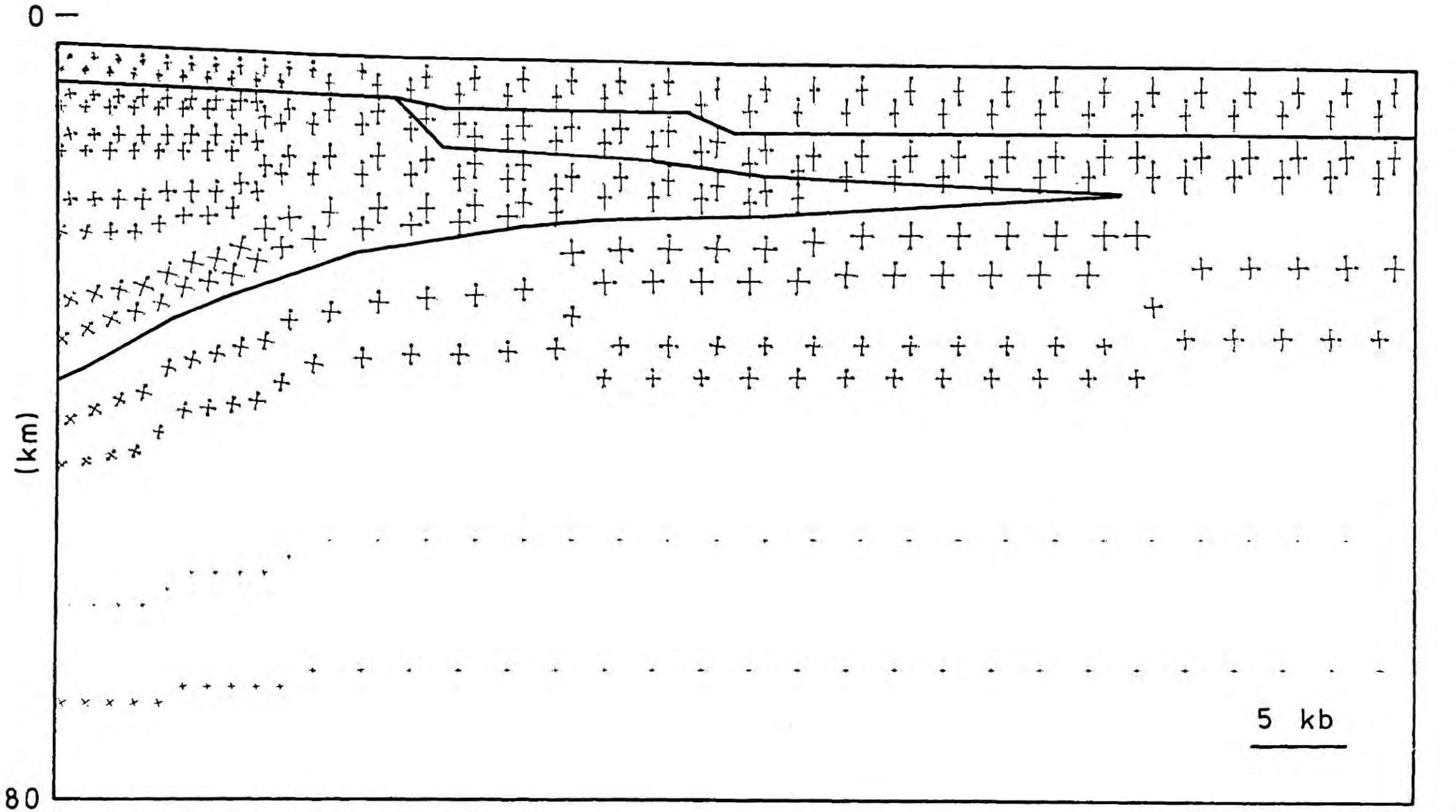

Figure 3.10 Density contrast load stresses for elastic/viscoelastic model of lithosphere and hydrostatic stress boundary condition.

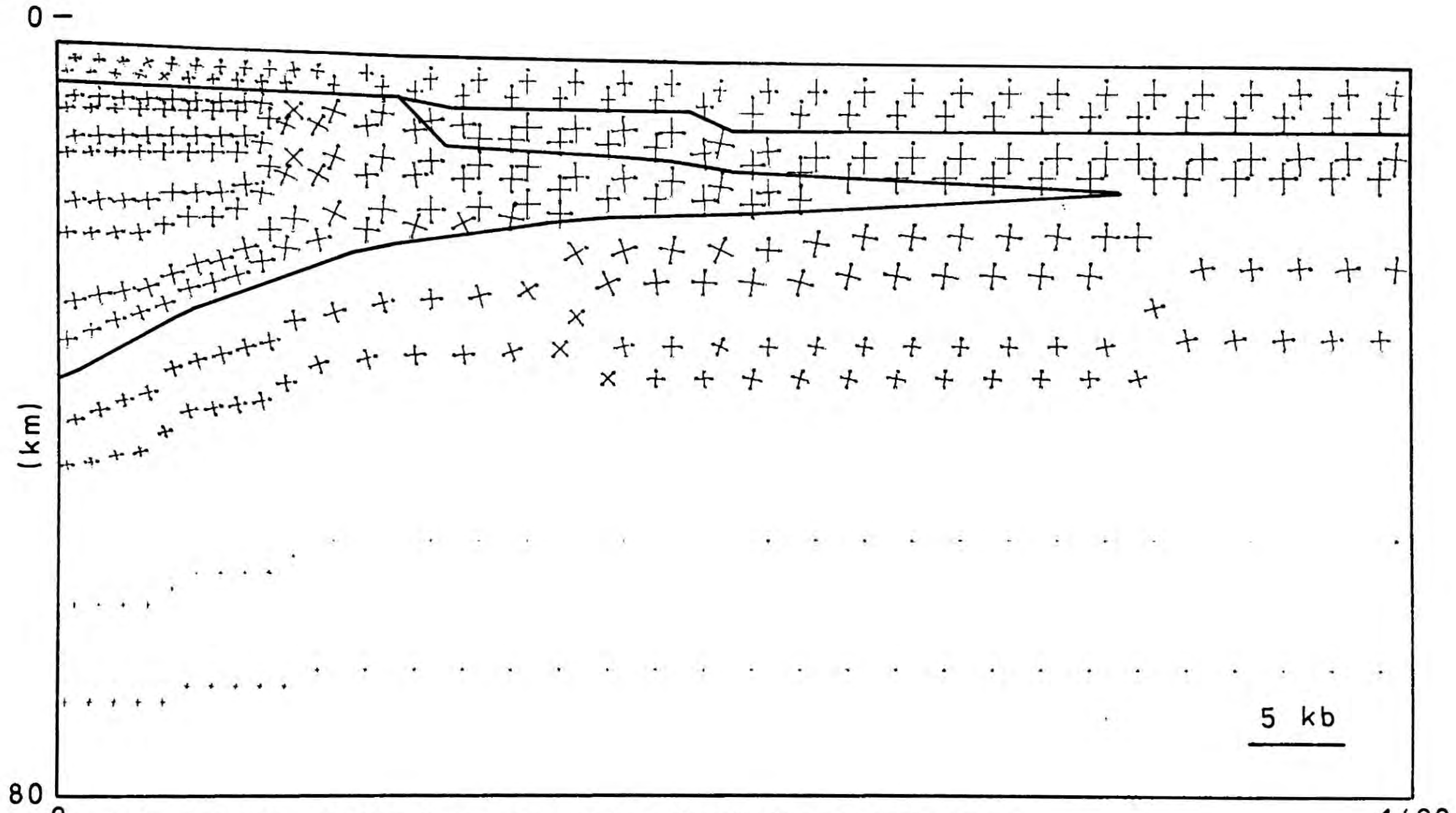

Figure 3.11 Density contrast load stresses for elastic/viscoelastic model of lithosphere and zero displacement boundary condition.

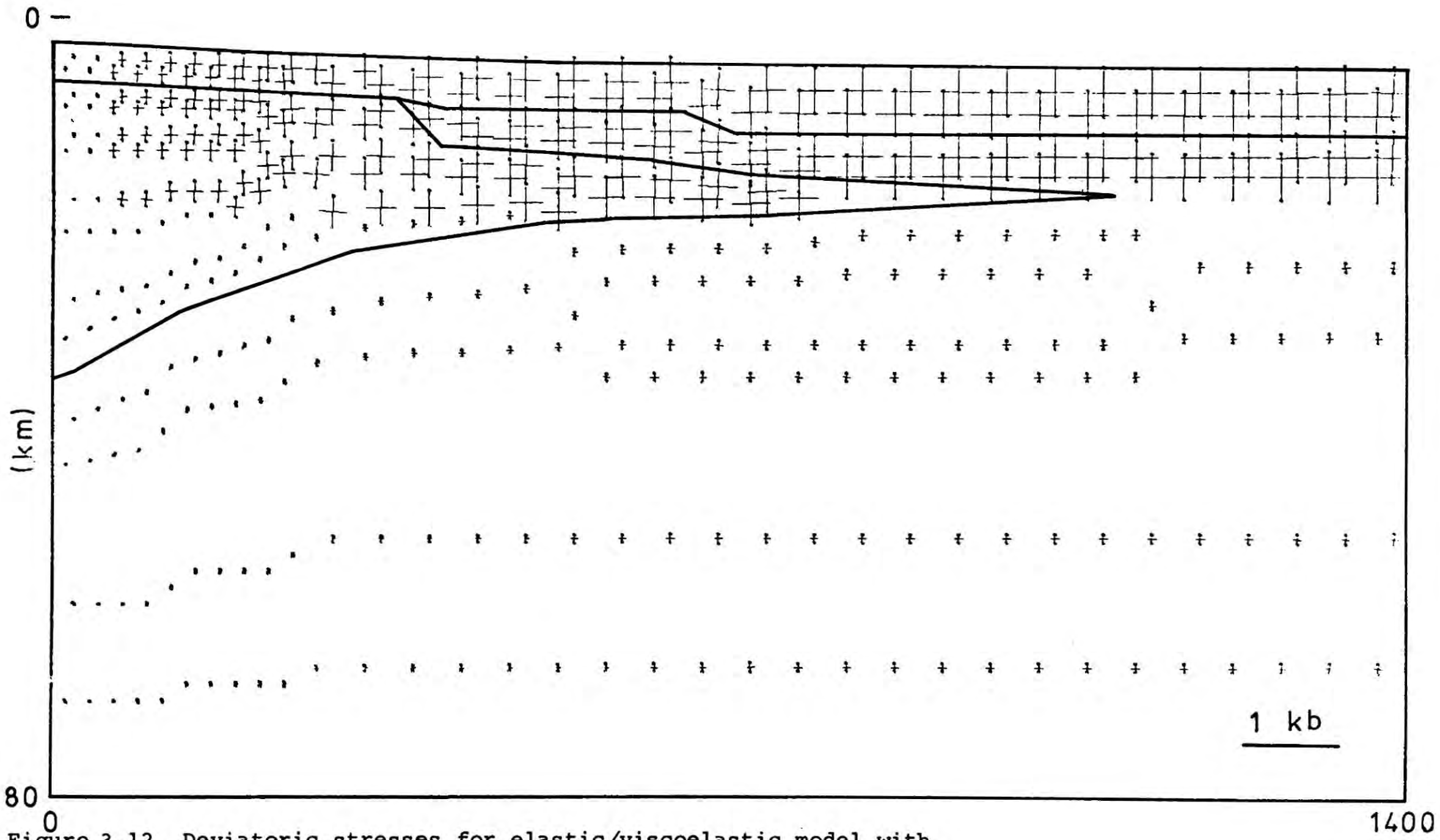

Figure 3.12 Deviatoric stresses for elastic/viscoelastic model with hydrostatic stress boundary condition.

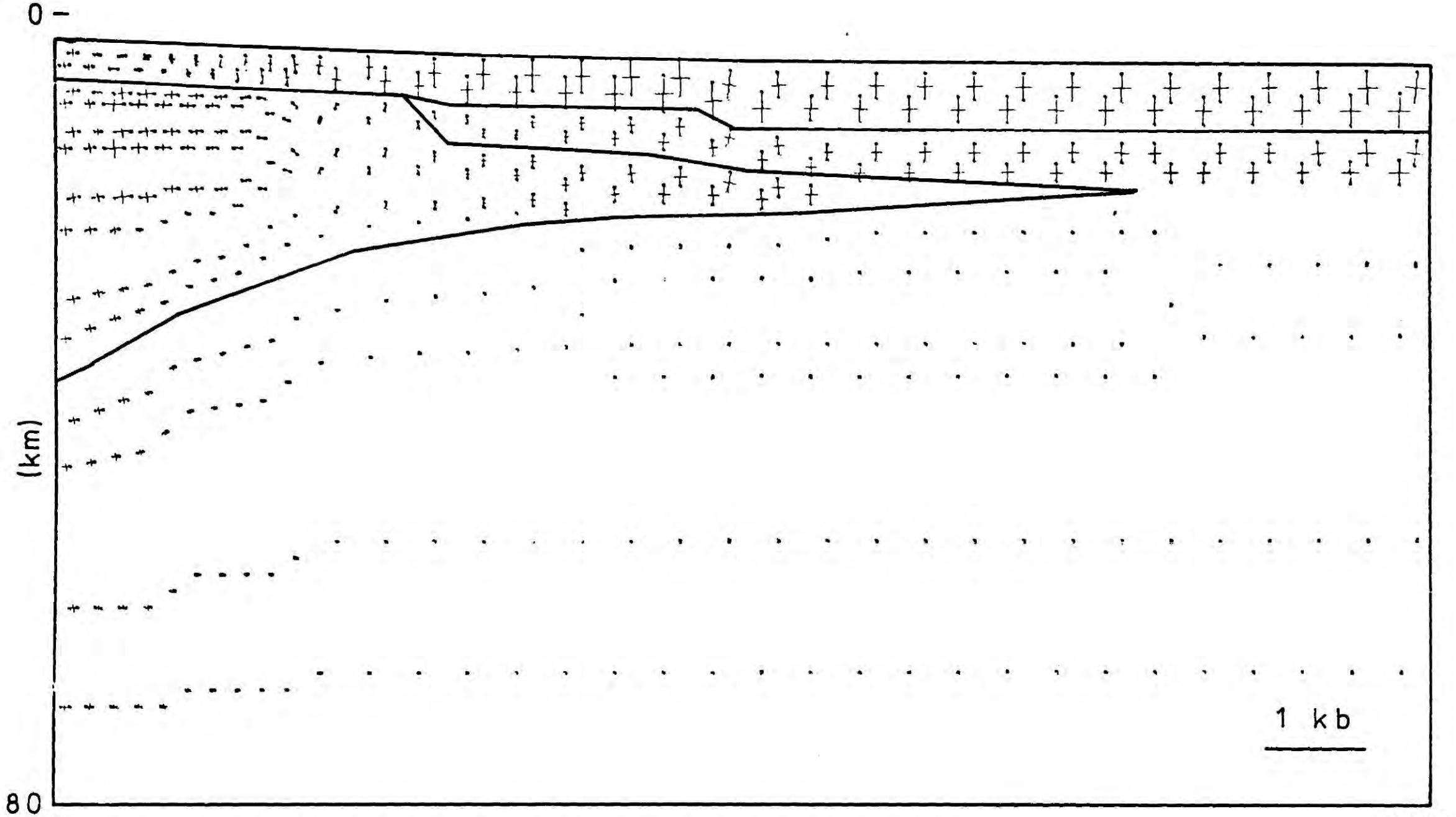

Figure 3.13 Deviatoric stresses for elastic/viscoelastic model with zero displacement boundary condition.

conditions applied at the ridge axis and lithosphere material properties is also evident from the above investigation.

The elastic and viscoelastic models of the lithosphere with the hydrostatic stress boundary condition supports Artyushkov (1973) in his suggestion that the regional stress of the ocean lithosphere is compressive and increases from zero at the ridge axis to the maximum value in the ocean basin. Artyushkov estimated a horizontal compression in the ocean basin of the order of 0.25 kb; a value midway between the estimate of the elastic model (0.5 kb) and the viscoelastic model (0.15 kb). While in the elastic model the regional stresses are largest in the upper lithosphere; in the viscoelastic model a uniform regional stress exists throughout the lithosphere.

The viscoelastic model of the lithosphere, with the zero horizontal displacement boundary condition at the ridge axis, shows regional tension throughout the lithosphere at the ridge crest reaching a maximum value of 0.15 kb. Some horizontal compression also exists on the ridge flanks. These results are consistent with the conclusions of Stephansson and Berner (1970) from their viscous model of the ocean lithosphere.

The fundamental difference of the regional stresses, depending on the ridge axis boundary conditions, raises the

question as to which boundary condition corresponds most closely to the actual solution. The hydrostatic stress boundary condition assumes that the material at the ridge axis is in exact hydrostatic equilibrium, which can only occur if the mobility of this material is far greater than that of the material of the remaining lithosphere. The alternative displacement boundary condition assumes an identical ridge axis viscosity to that of the remaining lithosphere. Considerable evidence suggests that the lithosphere below the ocean ridge crest is partially molten and also that asthenosphere may extend to within a few kilometers of the ocean floor (Forsyth, 1975; Oldenburg, 1975). Consequently, the lithosphere model with the hydrostatic stress boundary condition is the preferred model.

The introduction of an elastic layer of 20 km thickness into the top of an otherwise viscoelastic lithosphere model is suggested from some lithosphere flexure studies (Walcott, 1970). The effect of the elastic layer is to increase the regional stress and to concentrate them within it. Results are similar to that of the uniform viscosity models with the exception that for the zero horizontal displacement boundary condition model more horizontal compression is predicted in the ocean basin.

CHAPTER 4

THERMAL STRESSES IN THE OCEAN LITHOSPHERE

4.1 Introduction

The cooling of the oceanic lithosphere as it moves away from the ocean ridge is accompanied by thermal contraction which gives rise to thermal stresses. Turcotte (1974) used a simple analytical approach to calculate the distribution and magnitude of the thermal stresses. In this chapter, these thermal stresses are calculated by the finite element method of stress analysis described in Chapter 2. The finite element method enables a two dimensional analysis of the stress field to be made, as compared to the essentially one dimensional analysis of Turcotte.

A thermal model of the oceanic lithosphere, subsequent to its creation at the ridge axis has been suggested by McKenzie (1967). The temperature distribution in the lithosphere is given by

$$T = T_o\left[\frac{z}{L} + \sum_{n=1}^{\infty} \frac{(-1)^n}{\frac{1}{2}n\pi} \exp\left\{\left(\tfrac{1}{2}P - \left(\tfrac{1}{4}P^2 + n^2\pi^2\right)^{1/2}\right)\frac{x}{L}\right\} \sin\left(\frac{n\pi z}{L}\right)\right] \qquad 4.1$$

where $P = \rho\sigma v L / k$, k is thermal conductivity, V is half spreading rate, L is lithospheric thickness, ρ is density, σ is specific heat and T_o is the temperature at the ridge axis and the asthenosphere-lithosphere boundary. For a point in the oceanic lithosphere moving away from the ridge axis by sea floor spreading, the cooling is given by

$$\Delta T = T - T_o$$

$$= T_o\left[\frac{z}{L} - 1 + \sum_{n=1}^{\infty} \frac{1}{\frac{1}{2}n\pi} \exp\left\{\left(\tfrac{1}{2}P - \left[\tfrac{1}{4}P^2 + n^2\pi^2\right]^{1/2}\right)\right\} \sin(n\pi z/L)\right]$$

4.2

Contours of T and ΔT are shown in figure 4.1 and it is evident that the greatest temperature change occurs in the top of the lithosphere and away from the ridge axis.

Cooling of the lithosphere results in thermal contraction which varies in magnitude in accordance with the value of such that the volume change per unit volume, ΔV, is given by

$$\Delta V = 3 \alpha \Delta T \qquad 4.3$$

where α is the linear coefficient expansion. Any body subjected to non uniform thermal contraction has produced in it thermal stress and so the ocean lithosphere will be stressed as a consequence of its cooling. Assuming that a state of zero thermal stress exists at the ridge axis, from

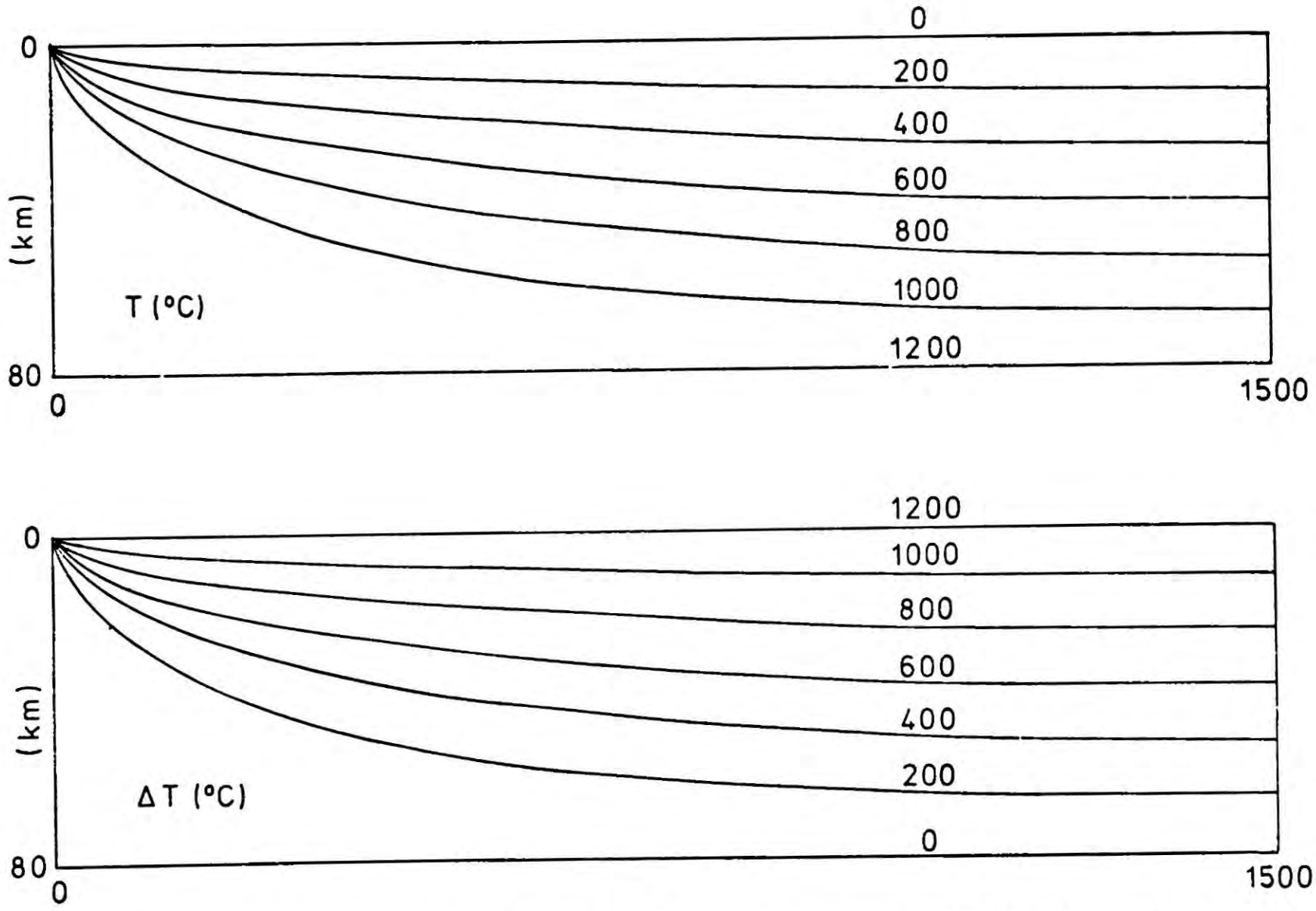

Figure 4.1 Isotherm of T and ΔT in the oceanic lithosphere for a spreading rate of 1.5 cm/yr.
$T_o = 1200^{o}C$.

the contours of ΔT (figure 4.1) it can be seen that the top of the lithosphere will contract more than the bottom. Consequently, for the stresses in the plane of the model, horizontal tension is expected in the upper lithosphere with horizontal compression in the lower lithosphere. The stress in the third direction, parallel to the ridge axis, will be dependent on the constraints imposed against contraction in this direction. The two extreme possibilities for the condition of constraint in this direction are plane strain and plane stress. Plane strain will result in large tensional stresses in the direction parallel to the ridge axis, while plane stress gives zero stress in this direction. In the following work the assumption of plane strain in the direction parallel to the ridge axis is made. However this may be an oversimplification since fracture zones may allow contraction in the ridge axis direction.

4.2 The lithospheric model

The model used for the thermal stress analysis represents oceanic lithosphere of uniform thickness, 80 km (Haigh, 1973) which extends from the ocean ridge to the ocean basin and has a half spreading rate of 1.5 cm/year. The length of the model, 1500 km, corresponds to the distance over which the lithosphere attains thermal equilibrium (Haigh, 1973).

The model is divided into crust and mantle. A crustal thickness of 7 km has been used throughout the calculations, corresponding to the thickness of the igneous crust formed at the ridge axis. Layer 1, composed of sediments is omitted from the model. Composition of crust and mantle are assumed to be basaltic and pyrolitic respectively (Cann, 1974; Green and Ringwood, 1969). The parts of the model have been assigned elastic constants and expansion coefficients according to their composition. For crustal material, the thermal expansion coefficient, $\alpha = 0.7 \times 10^{-5}\ ^{o}C^{-1}$ and Young's modulus, $E = 1.0 \times 10^{12}$ dynes / cm^2, while for the mantle, $\alpha = 1.0 \times 10^{-5}\ ^{o}C^{-1}$ and $E = 1.7 \times 10^{12}$ dynes/cm^2 (Clark, 1966). A Poisson ratio of 0.25 is used throughout the lithosphere.

The choice of parameters controlling the temperature in the oceanic lithosphere follow the work of Haigh (1973). A value of T_o equal to $1200^{o}C$ is used, while thermal conductivity, $k = 0.006$ cal $gm^{-1}\ ^{o}C^{-1}\ sec^{-1}$ and specific heat, $\sigma = 0.26$ cal $^{o}C^{-1}$. A uniform density of 3 gm/cc has been used over the whole lithosphere.

In the following calculations, the stress field resulting from cooling is separated from the body force stresses. Since the density of the lithosphere is assumed to be uniform, the stress at any point in the lithosphere due to body forces, may be derived analytically (Hafner,1951)

and are assumed to be hydrostatic (Chapter 3). The hydrostatic stress, σ_H , used is given by the following expression

$$\sigma_H(z) = \int -\rho_L(z)\, g\, dz \quad - \quad D g \rho_w \qquad 4.4$$

where D is the mean depth of the ocean, taken as 4 km; ρ_w is the density of the ocean taken as 1.0 gm/cc; and g is the gravitational acceleration, 981.0 cm/sec^2. The lithosphere density, ρ_L is 2.8 gm/cc in the crust and approximately 3.3 gm/cc in the mantle (Talwani et al.,1965).

Calculation of the thermal stresses is reduced to a two dimensional problem by the assumption of plane strain (section 4.1), with zero strain in the direction parallel to the ridge axis.

Bending of the lithosphere, as a result of thermal contraction, results in vertical movement of the lithosphere which is opposed by isostatic restoring forces (Walcott, 1970). Isostatic restoring forces will occur throughout the lithosphere and at the lithosphere-asthenosphere boundary, wherever vertical density contrasts occur. However these density contrasts within the lithosphere are small compared with that between ocean and lithosphere (approximately 2.0 gm/cc). Consequently only the isostatic restoring forces occurring at the upper surface of the lithosphere are considered. The restoring forces are included in the finite element formulation, which is described in the next section.

4.3 Finite element formulation

The method by which thermal contraction is incorporated in the finite element analysis has been described in chapter 2 and follows the formulation suggested by Zienkiewicz (1971). The equation of finite elements giving the elastic nodal displacements of the continuum is from equation 2.37

$$[K]\{\delta\} = -\{F\}_{\varepsilon_o} \qquad 4.5$$

where $\{F\}_{\varepsilon_o}$, the initial strain vector is

$$\{F\}_{\varepsilon_o} = -\int [B]^T [D] \{\varepsilon_o\} \, d(vol) \qquad 4.6$$

from equation 2.26 and $\{\varepsilon_o\}$, the initial strain tensor is from equation 2.36

$$\{\varepsilon_o\} = \begin{Bmatrix} \varepsilon_x \\ \varepsilon_y \\ \varepsilon_{xy} \end{Bmatrix} = (1 + \nu) \alpha \Delta T \begin{Bmatrix} 1 \\ 1 \\ 0 \end{Bmatrix} \qquad 4.7$$

The initial strain of equation 4.7 is calculated for each element of the model using the centroid coordinate of the element in equation 4.2. Strain and stress are obtained from the displacement vector $\{\delta\}$ according to equations 2.10, 2.38 and 2.39.

The isostatic restoring force of the lithosphere's upper surface may be easily incorporated into the finite element formulation itself (Dean, 1973). For a displacement, δ, on the surface of the lithosphere, the isostatic

restoring force/unit area is given by

$$f_z = -\delta_z \Delta\rho g \qquad 4.8$$

where $\Delta\rho$ is the density contrast across the surface, and g is the gravitational acceleration. In figure 4.2 are shown a series of surface nodes. The restoring force applied to the surface nodes must represent together the total restoring force of the whole surface. Thus the nodal force applied to the ith node is

$$R_z^i = - g \Delta\rho_i \Delta x_i \delta_z^i \qquad 4.9$$

where Δx_i is shown in figure 4.2 and is given by

$$\Delta x_i = \frac{x_{i+1} - x_{i-1}}{2} \qquad 4.10$$

The equilibrium finite element equation becomes from equation 4.5

$$[K]\{\delta\} = -\{F\}_{\epsilon_o} + \{R_z\} \qquad 4.11$$

where $\{R_z\}$ is the vector of nodal restoring forces such that

$$\{R_z\} = - g \{\Delta\rho \Delta x \delta_z\} \qquad 4.12$$

Equation 4.11 becomes on rearranging

$$[K]\{\delta\} + [S]\{\delta\} = - \{F_{\epsilon_o}\} \qquad 4.13$$

where $[S]$ is a diagonal matrix such that

$$\begin{aligned} S_{ii} &= g \Delta\rho_i \Delta x_i \quad \text{(for z element)} \\ S_{ii} &= 0 \quad \text{(for x element)} \end{aligned} \qquad 4.14$$

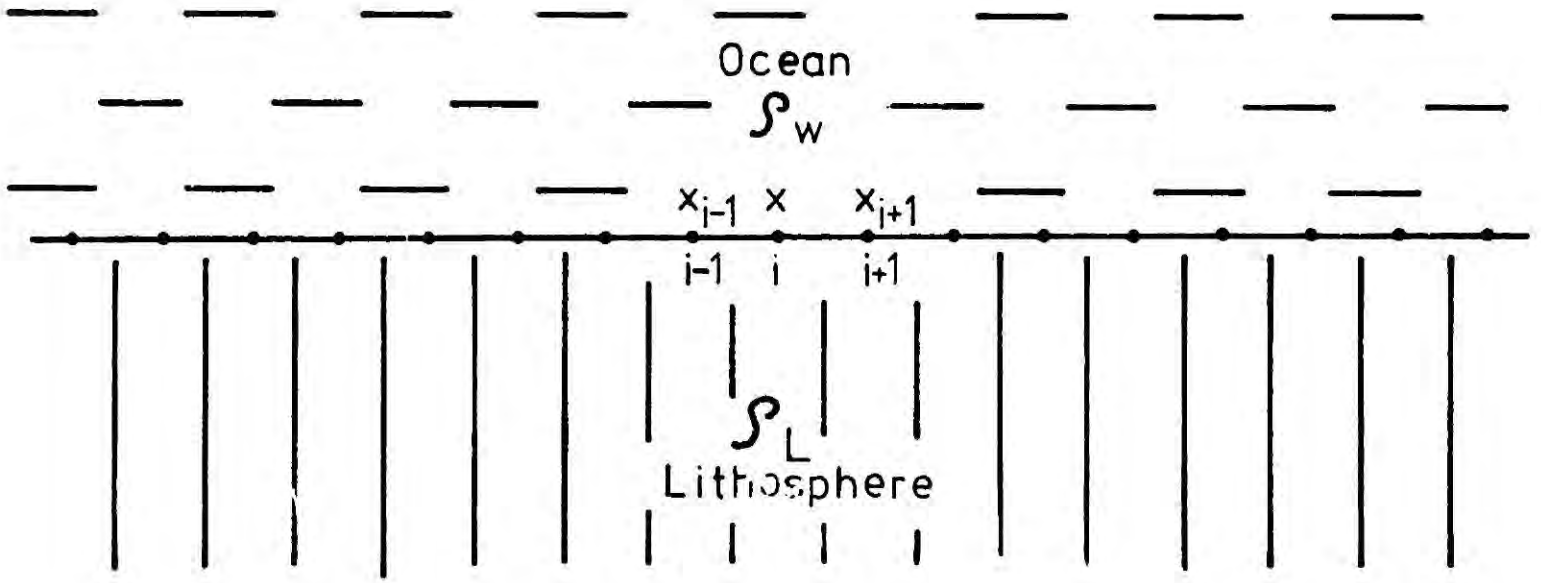

Figure 4.2 Group of adjacent surface nodes used in application of isostatic restoring forces.

Adding the two matrices $[K]$ and $[S]$, the equation of finite elements becomes

$$[K]'\{\delta\} = -\{F\}_{\varepsilon_0} \qquad 4.15$$

where

$$[K]' = [K] + [S] \qquad 4.16$$

It is to equation 4.16 that the displacement boundary conditions are applied. The value of $\Delta\rho$ used is calculated from the density difference between sea water and the upper lithosphere and is taken to be 2.0 gm/cc. Solution of equation 4.16 was carried out by Gaussian elimination. A computer program listing and description for the calculation of thermal stresses by finite elements is given in Appendix 2.

4.4 Application of the finite element method

The finite element subdivision of the lithospheric model is shown in figure 4.3 and is such as to allow the lithosphere to be divided into crust and mantle. Finer finite element subdivision in the region adjacent to the ridge crest is made because of the large lateral temperature gradients in this region.

At the ocean ridges, the lithosphere is at high temperature (McKenzie, 1967; Haigh, 1973) and is partially

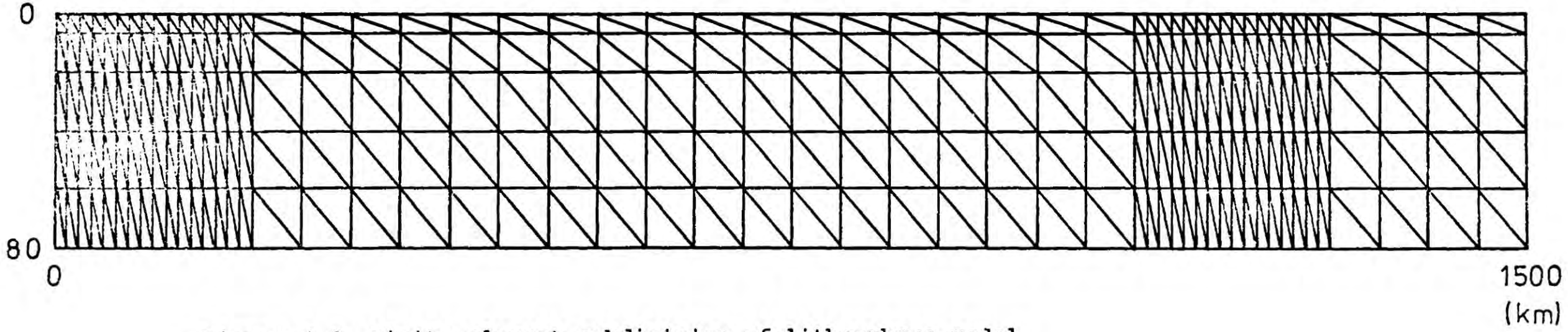

Figure 4.3 Finite element subdivision of lithosphere model.

molten (Trygvasson, 1964; Cann, 1974). As a consequence of near fluid properties due to the high temperatures, compressional or tensional stresses may not be transmitted through the lithosphere at the ridge axis. The near molten material can only support its own hydrostatic stresses due to body forces. Thus, since the body force stresses are removed from the calculations, the stresses due to thermal effects must be zero at the ridge axis of the model. Consequently, the lithosphere model boundary at the ridge axis is free to move and no displacement or stress boundary conditions are applied.

The boundary of the model corresponding to the asthenosphere-lithosphere interface is left unconstrained also, since it is assumed that the asthenosphere behaves as a viscous material over geological time scales (Heiskanen and Vening Meinesz, 1958).

In order to prevent whole body rotation and translation of the lithosphere model during analysis, the model boundary at the ocean basin is constrained in the horizontal direction and at one point in the vertical direction.

4.5 The thermal stresses

The thermal stresses of the oceanic lithosphere have been calculated by the finite element method previously described. Calculated thermal stresses are displayed

diagramatically as principal stresses. Principal stresses in the plane of the model are plotted to scale at their principal orientations. The principal stress perpendicular to the plane of the model is represented by a circle whose radius gives it magnitude. Tension is signified by a dot on the principal stress for plane stresses and by a dotted circle for the perpendicular stress.

In figure 4.4 the thermal stresses for the model discussed in section 4.2 are shown. The physical constants are summarized on the figure. Thermal stresses are tensional in the upper lithosphere becoming compressional with depth. The region of maximum tension occurs just below the Moho, not in the crust as might intuitively be expected. This is a consequence of the different physical constants (E and α) of the crust and mantle.

The thermal stresses for a model with physical constants uniform throughout the lithosphere is shown in figure 4.5 and for this model the maximum tensions do occur in the upper crust.

For both models in the zone of tension the maximum stress occurs in the direction perpendicular to the model with the vertical stress the smaller of the two principal stresses in the plane of the model.

In order to analyse the thermal stresses further for fracture of the lithosphere, the hydrostatic stresses due to the weight of the lithosphere and ocean must be added

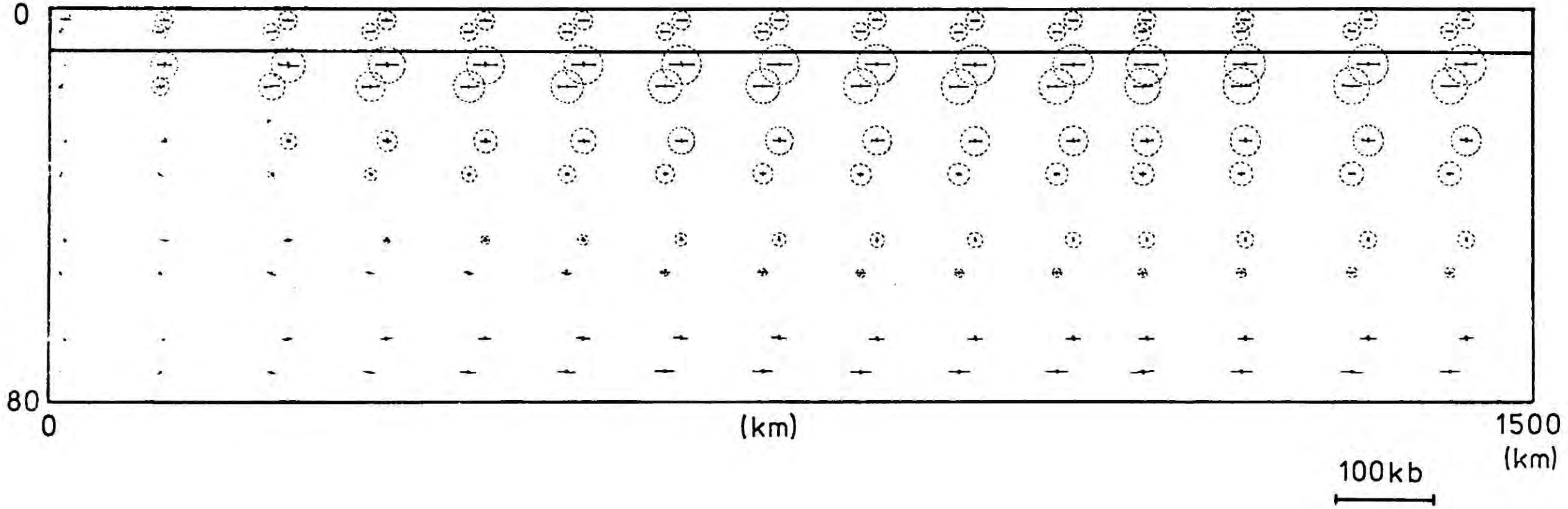

Figure 4.4 Thermal stresses of ocean lithosphere for half spreading rate of 1.5 cm/yr. Crustal and mantle constants not equal.

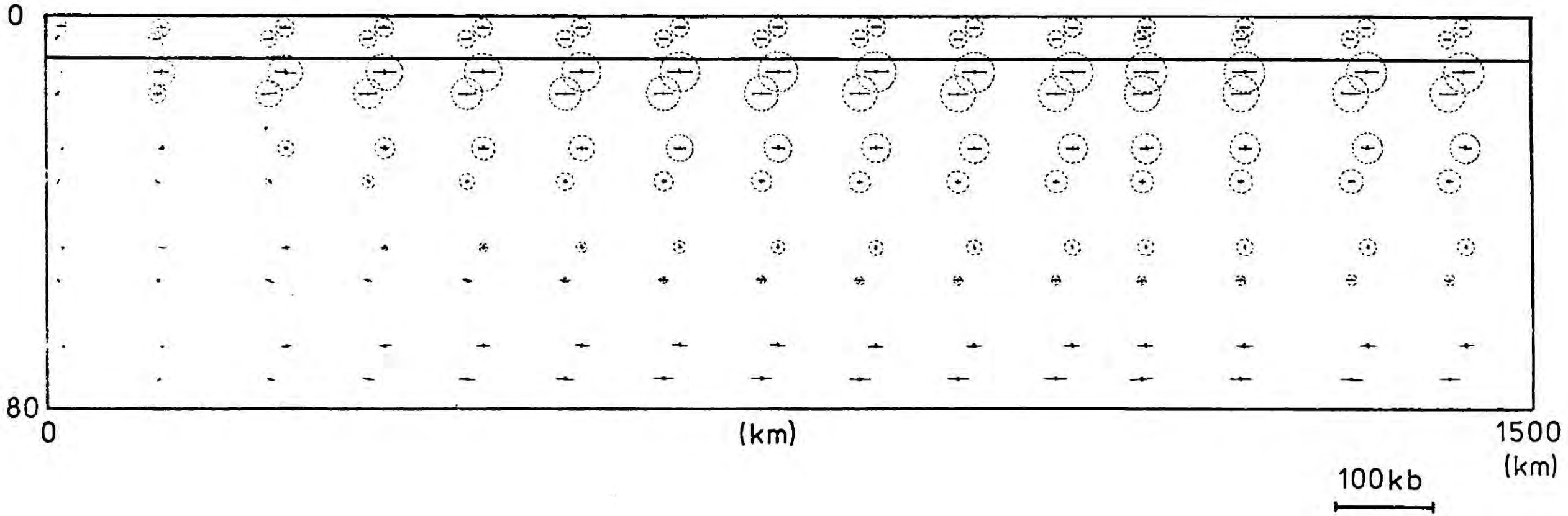

Figure 4.4 Thermal stresses of ocean lithosphere for half spreading rate of 1.5 cm/yr. Crustal and mantle constants not equal.

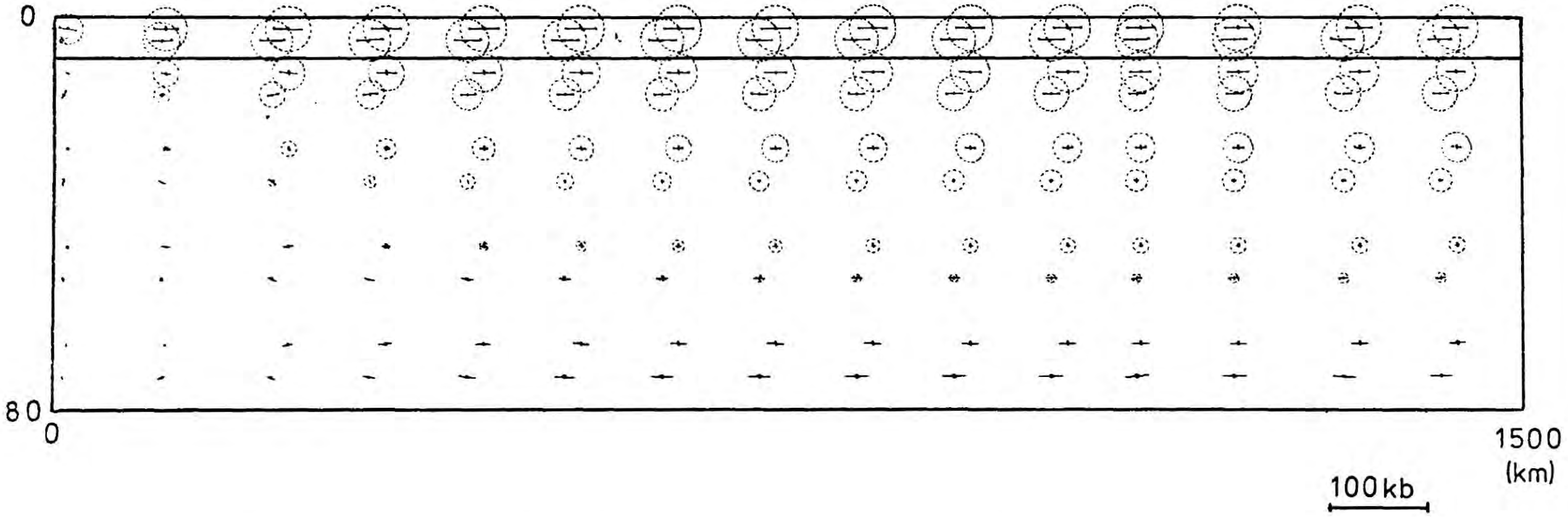

Figure 4.5 Thermal stresses of lithosphere for half spreading rate of 1.5 cm/yr. Crustal and mantle constants identical.

to the thermal stresses. Thermal stresses plus hydrostatic stresses are shown in figure 4.6 and 4.7 for the models with non-uniform and uniform physical constants respectively. In both models, absolute tension still occurs in the crust and upper mantle. The magnitude of the largest tensional stress, which lies in the direction perpendicular to the plane of the model, is of the order of 10 kilobars or more. The tensile strength of lithosphere material is of the order of 0.5 kb (Brace, 1961) and so tensional stresses of the magnitude calculated would, without doubt, lead to tensional fracture of the lithosphere. The plane of fracture would be vertical and perpendicular to the direction of the ridge axis.

4.6 Thermal stresses in a non elastic lithosphere

The thermal stresses will be modified from those shown in figure 4.4, 4.5, 4.6 or 4.7 by stress release due to creep or plasticity. Lithosphere bending studies (Walcott, 1970) have shown that over geological time, the lithosphere behaves as an elastic body of approximately 20 km thickness. Below this depth stresses are relieved by plastic or viscoelastic deformation. The creep rate of mantle like material (Stocker and Ashby, 1973) shows a strong temperature dependence and consequently, the isotherm at 20 km depth is taken as representing the plastic or viscoelastic limit for

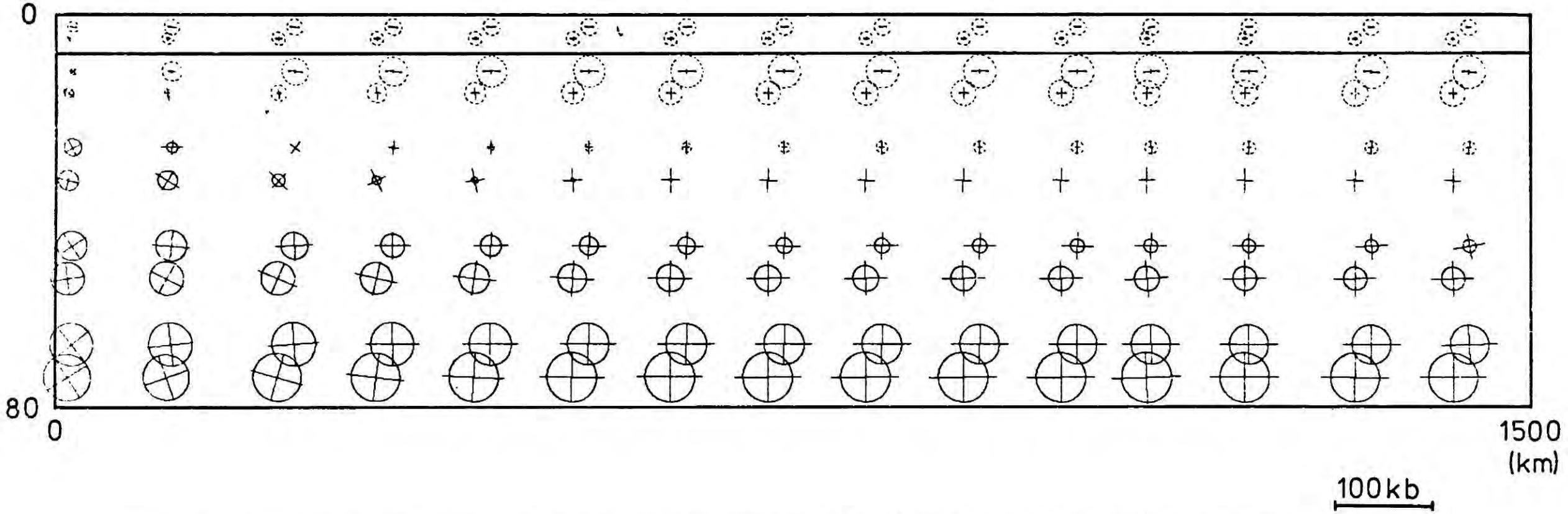

Figure 4.6 Thermal and hydrostatic load stresses of lithosphere for half spreading rate of 1.5 cm/yr. Crustal and mantle constants not equal.

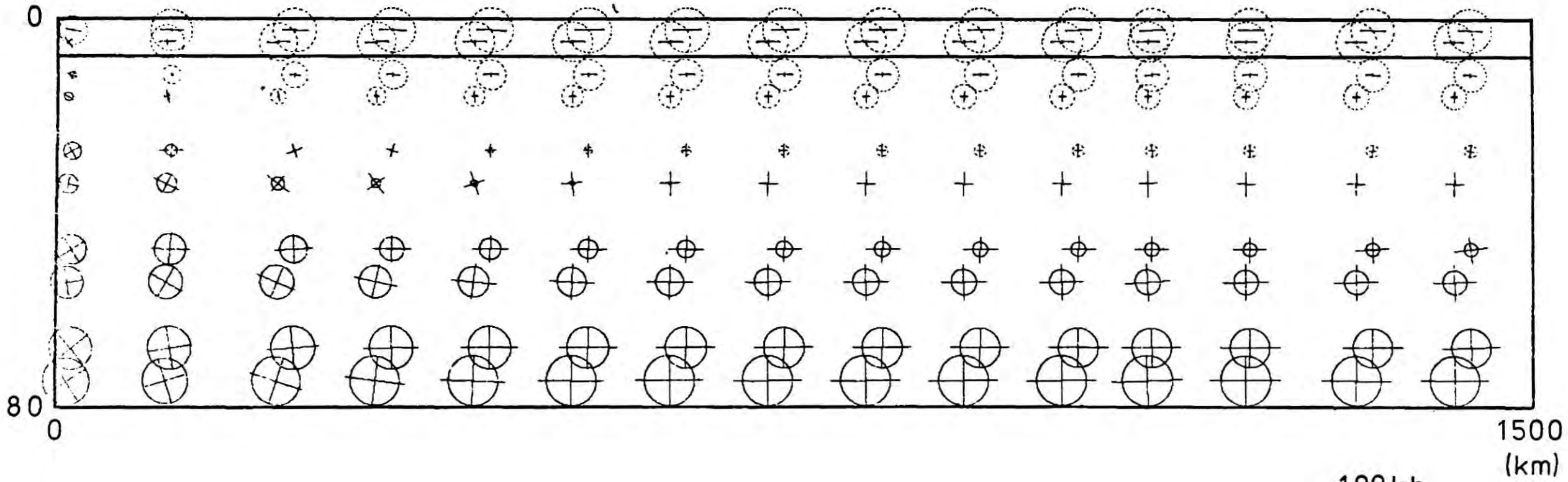

Figure 4.7 Thermal and hydrostatic load stresses of lithosphere for half spreading rate of 1.5 cm/yr. Crustal and mantle constants identical.

the non elastic lithosphere. For the temperature distribution of the lithosphere model used this critical isotherm has a value of 300°C. If the lithosphere is assumed not to be able to support deviatoric stresses above this isotherm, the thermal stresses of the lithosphere will only be caused by the cooling with respect to this critical isotherm, T_c , hence

$$\Delta' T = T - T_c \qquad \text{for } T < T_c$$
$$= 0 \qquad \text{for } T > T_c$$

where $\Delta' T$ is the temperature change due to cooling which gives rise to thermal stresses.

These arguments for incorporating stress release in the lithosphere model are identical to those presented by Turcotte (1974) in his analytical calculation of thermal stresses.

The finite element grid used for this new model need only consider the top 2.0 km of the lithosphere. The grid is shown in figure 4.8. Weak material in the finite element calculation (material with temperature above 300°C) is represented by an extremely low Young's modulus of 1 dyne/cm^2.

Thermal stresses of this model are shown in figures 4.9 and 4.10 without and with the hydrostatic body force stresses. The plot of thermal stresses alone shows that large tensions occur in the crust and upper mantle. Higher

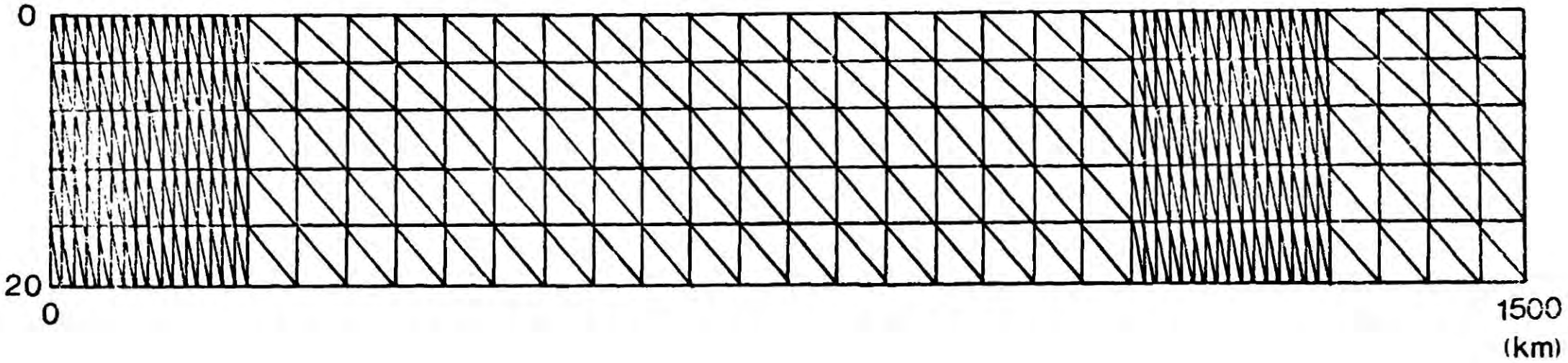

Fig. 4.8 Finite element subdivision of lithosphere model allowing viscous relaxation of the thermal stresses.

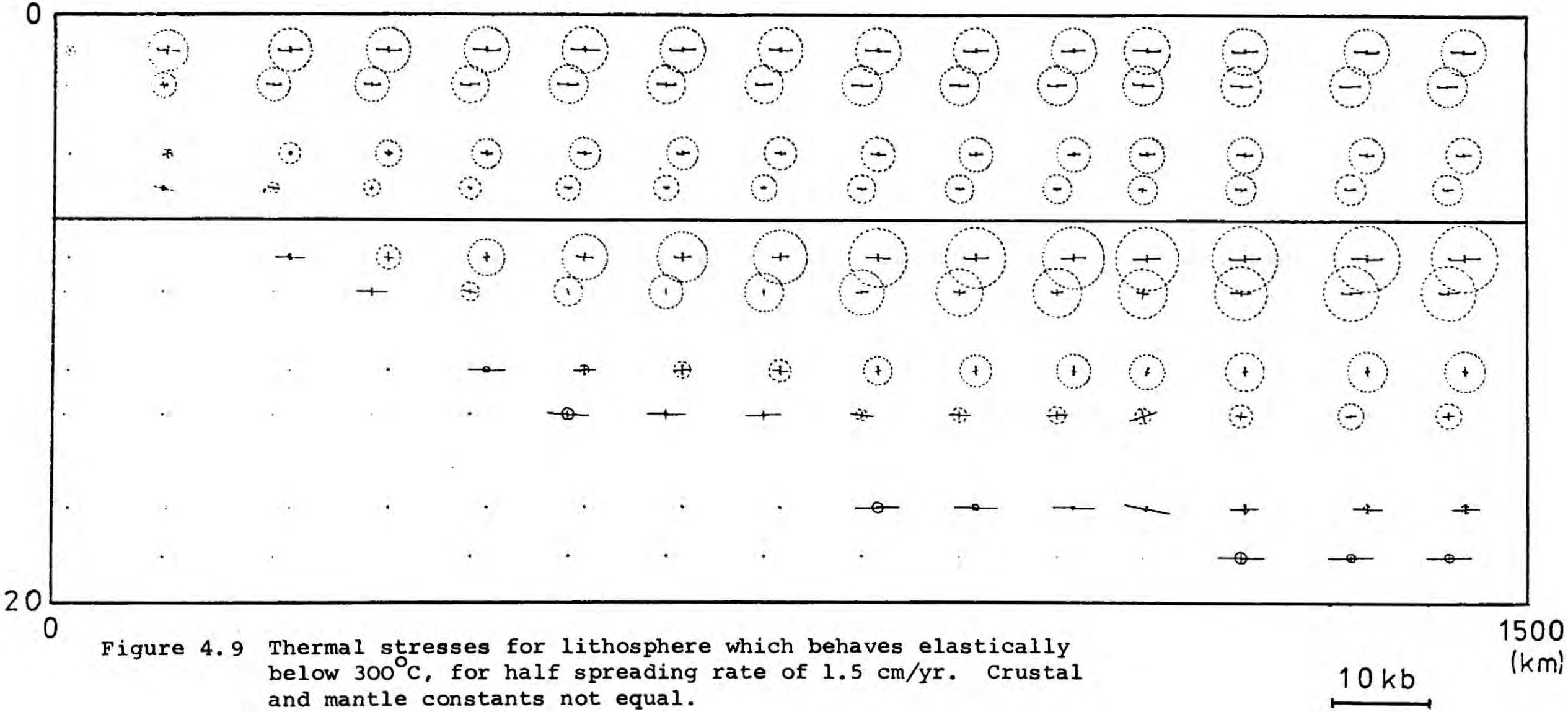

Figure 4.9 Thermal stresses for lithosphere which behaves elastically below 300°C, for half spreading rate of 1.5 cm/yr. Crustal and mantle constants not equal.

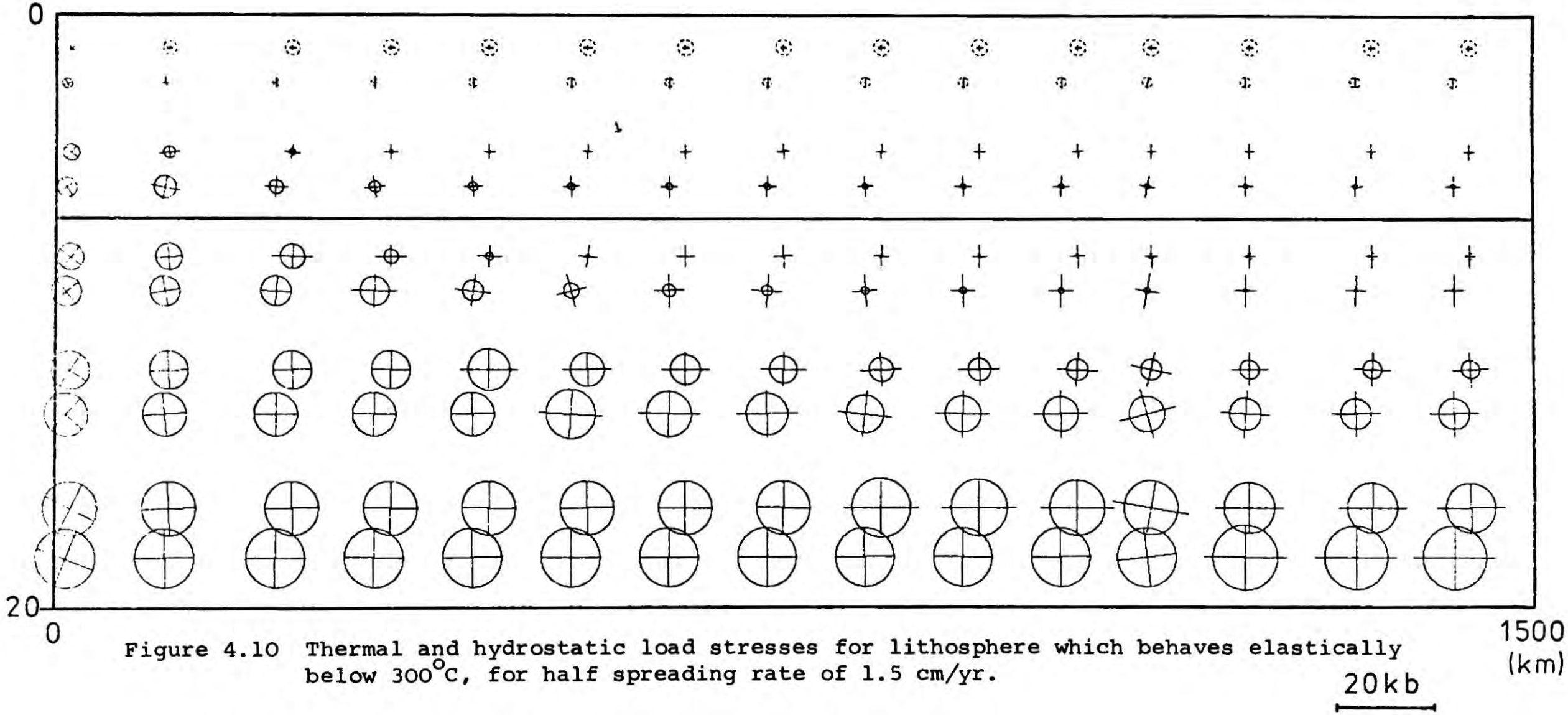

Figure 4.10 Thermal and hydrostatic load stresses for lithosphere which behaves elastically below 300°C, for half spreading rate of 1.5 cm/yr.

resolution of the finite element grid used for this model allows two maxima of stress to be recognized - one in the upper crust and the other in the upper mantle. Thermal stresses are absent at the ridge axis.

The plot of the hydrostatic body force stresses superimposed on the thermal stress field shows absolute tension existing in the upper oceanic crust. Deviatoric stresses are largest in the upper crust and upper mantle.

The possibility of failure in the lithosphere as a consequence of these stresses has been evaluated by the use of the Griffith's theory of brittle failure (Murrell, 1958; Service and Douglas, 1973) which is described in Chapter 6. Application of the theory predicts tensional failure in the upper crust with the plane of fracture corresponding to the plane of the model. This result is consistent with the suggestion made by Turcotte that thermal stresses caused by cooling of the oceanic lithosphere play an important part in the formation of fracture zones.

It is important to note that fracture in the plane of the model as predicted violates the assumption of plane strain made initially.

A further modification of the above stress field may occur as a consequence of the fractures in the upper crust. If the fractures in the upper crust become filled with

sediment, subsequent contraction of the material below could produce a compressive stress field in the topmost part of the crust. This mechanism has been suggested by Woodward (personal communication).

4.7 Thermal stresses and spreading rates

The temperature distribution of the oceanic lithosphere is controlled by the spreading rate (McKenzie, 1967). For the lithosphere not immediately adjacent to the ridge axis, the temperature distribution becomes a function of depth and age only (Le Pichon et al., 1971). Consequently, for increasing spreading rates the lithosphere cools less with increasing distance from the ridge axis. Thus, the cooling of the lithosphere, ΔT (x,z) from equation 4.2, and consequently the thermal stress field also, are a function of spreading rate.

Thermal stress fields for half spreading rates of 0.5 cm/yr and 3.0 cm/yr are shown in figures 4.11 and 4.12 and may be compared with those of the model with a spreading rate of 1.5 cm/yr shown in figure 4.9. The models assume the plastic or viscoelastic deformation of the lithosphere at temperatures higher than 300^{o}C.

As expected the thermal stresses are large nearer the ridge axis for smaller spreading rates. The calculations

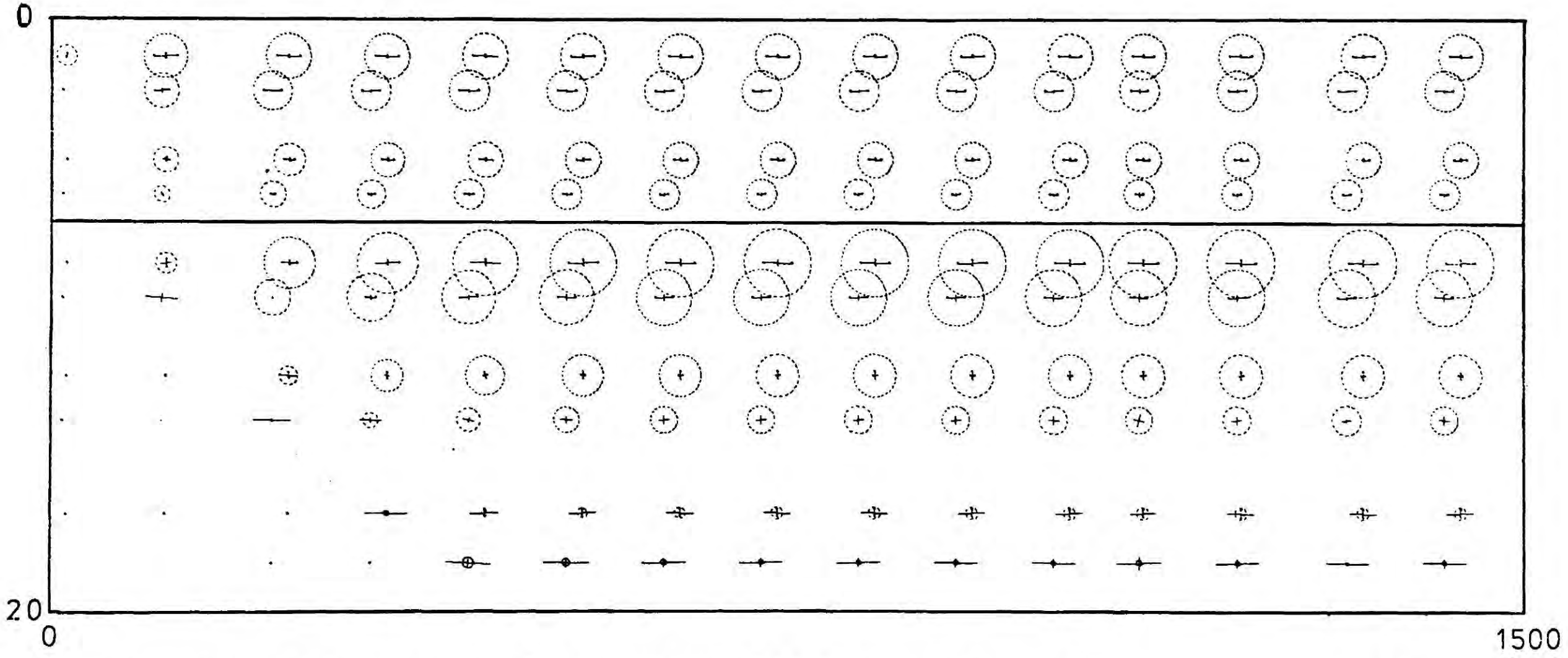

Figure 4.11 Thermal stresses for lithosphere which behaves elastically below 300°C for a half spreading rate of 0.5 cm/yr.

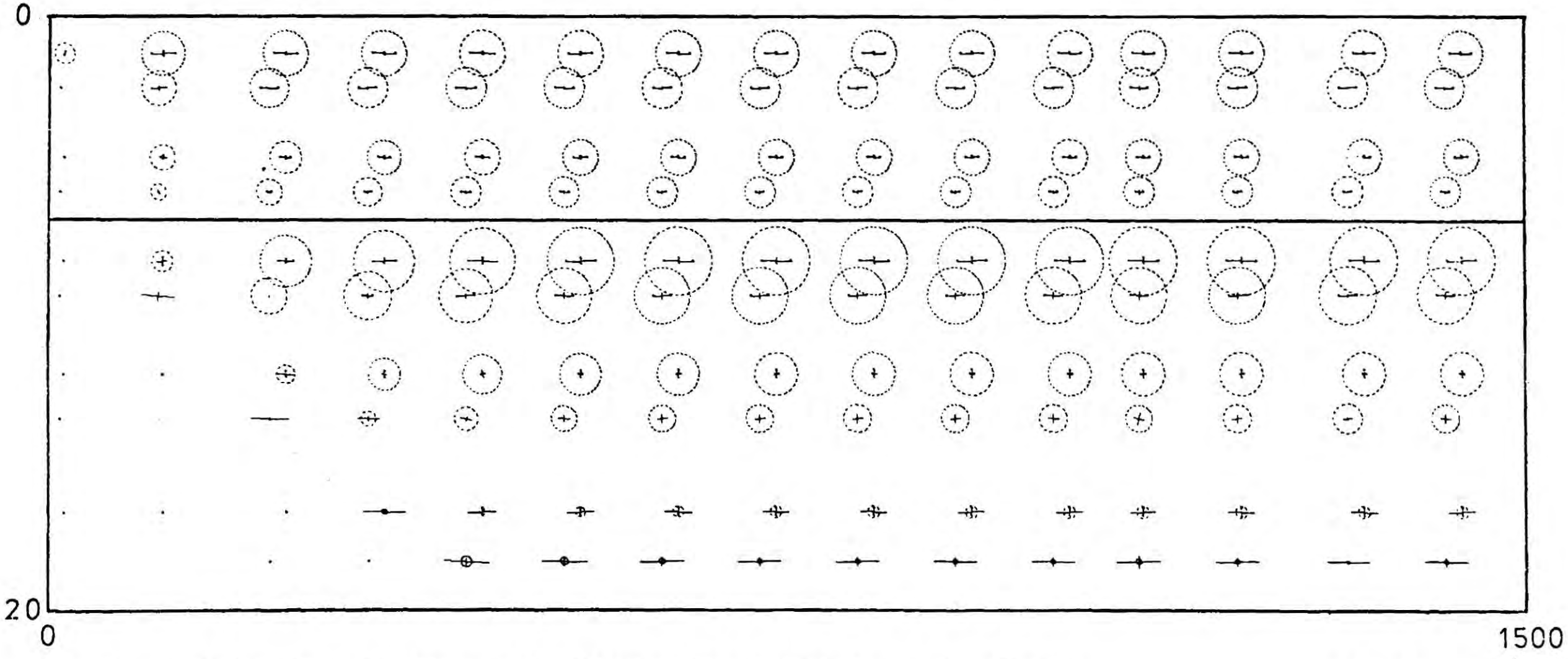

Figure 4.11 Thermal stresses for lithosphere which behaves elastically below 300°C for a half spreading rate of 0.5 cm/yr.

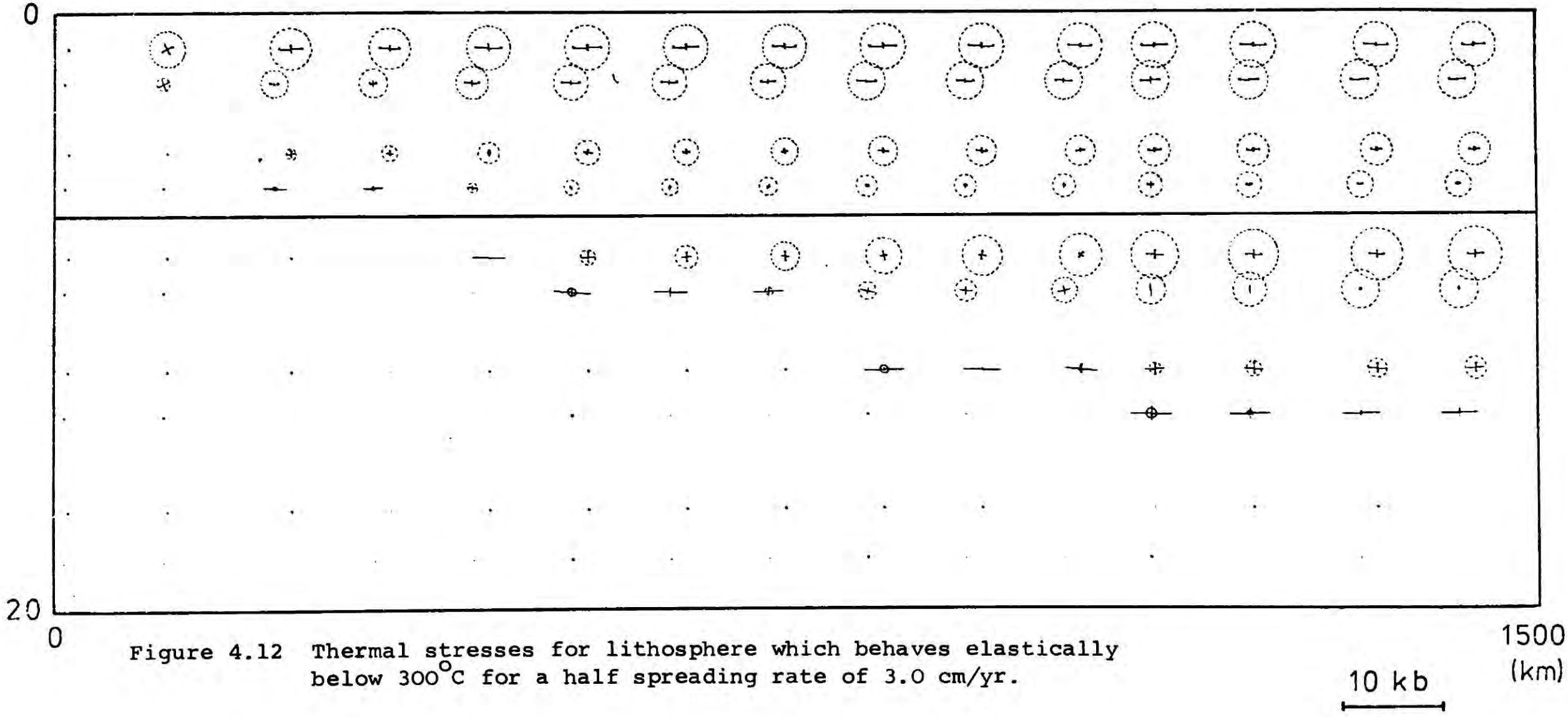

Figure 4.12 Thermal stresses for lithosphere which behaves elastically below 300°C for a half spreading rate of 3.0 cm/yr.

confirm that thermal stresses are a function of lithosphere age only and are otherwise independent of spreading rate.

4.8 Flexure of the lithosphere

Non uniform contraction of the lithosphere, in addition to causing thermal stresses, gives rise to flexure of the lithosphere. In figure 4.13 the vertical displacement of the lithosphere's upper surface is plotted as a function of distance from the ridge axis for the three models with half spreading rate 1.5 cm/yr. The lithosphere flexure is much greater for the elastic lithosphere models than the one allowing for stress release by plasticity or viscoelasticity. This is presumably a consequence of the much thinner elastic lithosphere of that model. The flexure of the lithosphere is greatest for the one with uniform physical constants as would intuitively be expected. For the elastic models the flexure is comparable in shape and magnitude with the oceanic topography except for the minimum occurring on the ridge flanks. However, this similarity is probably coincidental.

The negligible flexure of the model with stress release by viscous deformation is consistent with the observation that the oceanic lithosphere is in isostatic equilibrium (Talwani et al., 1965).

Figure 4.13 Flexure of the lithosphere caused by thermal stresses as a function of distance from ridge axis with spreading rate of 1.5 cm/yr.

(a) Elastic model with uniform physical constants

(b) Elastic model with different crustal and mantle physical constants

(c) Model with elastic properties only when lithosphere temperature less than 300°C. Physical constants as in (b).

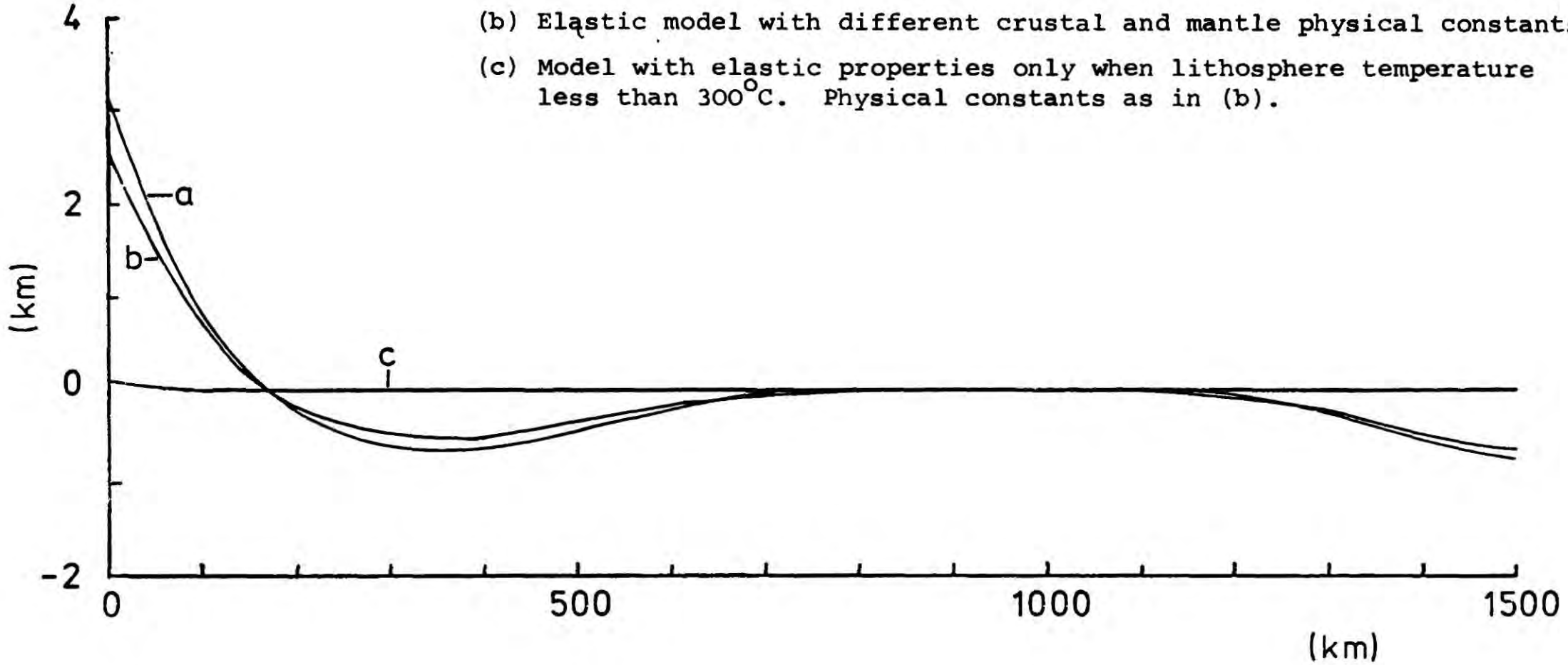

4.9 Conclusion

The finite element method has been used to calculate the thermal stresses induced in the lithosphere according to the cooling predicted by a "McKenzie" type of thermal model (McKenzie, 1967). Large tensional stresses are predicted to exist in the oceanic crust with the largest tension in the direction parallel to the ridge axis. Stresses are of sufficient magnitude to cause lithospheric fracture even after making the assumption that the lithosphere behaves as a fluid above the 300°C isotherm. The plane of fracture is in the vertical plane perpendicular to the ridge axis, consistent with a thermal stress origin for fracture zones. Calculation of the lithosphere flexure resulting from thermal stresses, suggests that elastic bending of the lithosphere of thermal cause is negligible.

CHAPTER 5

SOLIDIFICATION OF THE OCEAN CRUST

§.1 Introduction

A petrological model for the formation of ocean crust has been suggested by Cann (1970, 1974) and is described in Chapter 1. The structure of the crust predicted by the model agrees well with the geophysical evidence of marine seismic studies (e.g. Shor, Menard and Raitt, 1970) and the oceanic crust structure suggested by ophiolite studies (e.g. Gass, Smith and Vine, 1975; Jackson, Green and Moores, 1974). In this chapter, the solidification and cooling of the basaltic liquid which forms the ocean crust is investigated quantitatively.

The pillow lavas of oceanic layer 2 suggest quick cooling while oceanic layer 3, consisting of doleritic dykes above a gabbroic complex, indicates increasingly slower cooling with depth. Heat transfer in layer 2 is most probably by the circulation of convecting sea water (Bodvarson and Lowell, 1972; Pálmason, 1973; Lister, 1974) while it is assumed that layer 3 is cooled by conduction only. Convection is a far more efficient mechanism of heat transfer than conduction and consequently layer 2 solidifies and cools more quickly than layer 3.

Sleep (1975) has investigated quantitatively the solidification of a basalt melt in the ocean crust and predicts the existence of a magma chamber in the lower crust at the ridge axis. Cann (1970, 1974) has suggested from purely petrological arguments the existence of a magma chamber in this region. In the following work an estimate is made of the shape and extent of the molten body existing in the crust and the isotherm distribution in the adjacent lithosphere. The effects of sea floor spreading rate, magma convection and crystal settling are investigated also.

5.2 Formation of the thermal model

If there was no latent heat of solidification involved in the thermal history of the oceanic crust, the temperature of the lithosphere could be given by the relationship derived by McKenzie (1967) and discussed in Chapter 4. In the steady state temperature frame relative to the ridge axis, the differential equation of thermal equilibrium is given by

$$\nabla^2 T = \frac{\rho \sigma}{k} v_x \frac{\delta T}{\delta x} \qquad 5.1$$

where ρ is the density of the lithosphere, σ is specific heat, k is thermal conductivity, v_x is the half spreading rate and T is temperature. The analytical solution of

this equation (McKenzie, 1967) gives the temperature at any point in the lithosphere such that

$$T = T_0\left[\frac{z}{L} + \sum_{n=1}^{\infty} \frac{1}{\frac{1}{2}n\pi} \exp\left\{\left(\frac{1}{2}P - \left[\frac{1}{4}P^2 + n^2\pi^2\right]^{1/2}\right)\right\} \sin\left(n\pi z/L\right)\right. \qquad 5.2$$

where T_o is the temperature of the ridge axis and lithosphere-asthenosphere boundary, L is lithosphere thickness and $P = v_x L \rho \sigma / k$ Figure 5.1 shows McKenzie's thermal model with boundary conditions. The model assumes steady state accretion of the lithosphere at the ridge axis. Haigh (1973), from his comparison of gravity anomalies and ocean topography with the results of thermal models, suggests a value of of the order of 1050°C to 1200°C and a lithosphere thickness of 70 km to 80 km. In the following work, a lithosphere thickness of 80 km and a value of T_o of 1125°C have been used. This temperature, within the range suggested by Haigh, corresponds to the temperature measured for erupted ocean basalts (Thoranison et al., 1973).

The existence of liquid material at the ridge axis in the base of the crust requires inclusion of the latent heat of solidification in the thermal study of the oceanic crust. Molten material, for the purposes of the thermal model, is restricted to the crust since the upper mantle is left. below its solidus on fractionation of the basalt liquid (Presnell, 1969; Cann, 1974). The thickness of the molten

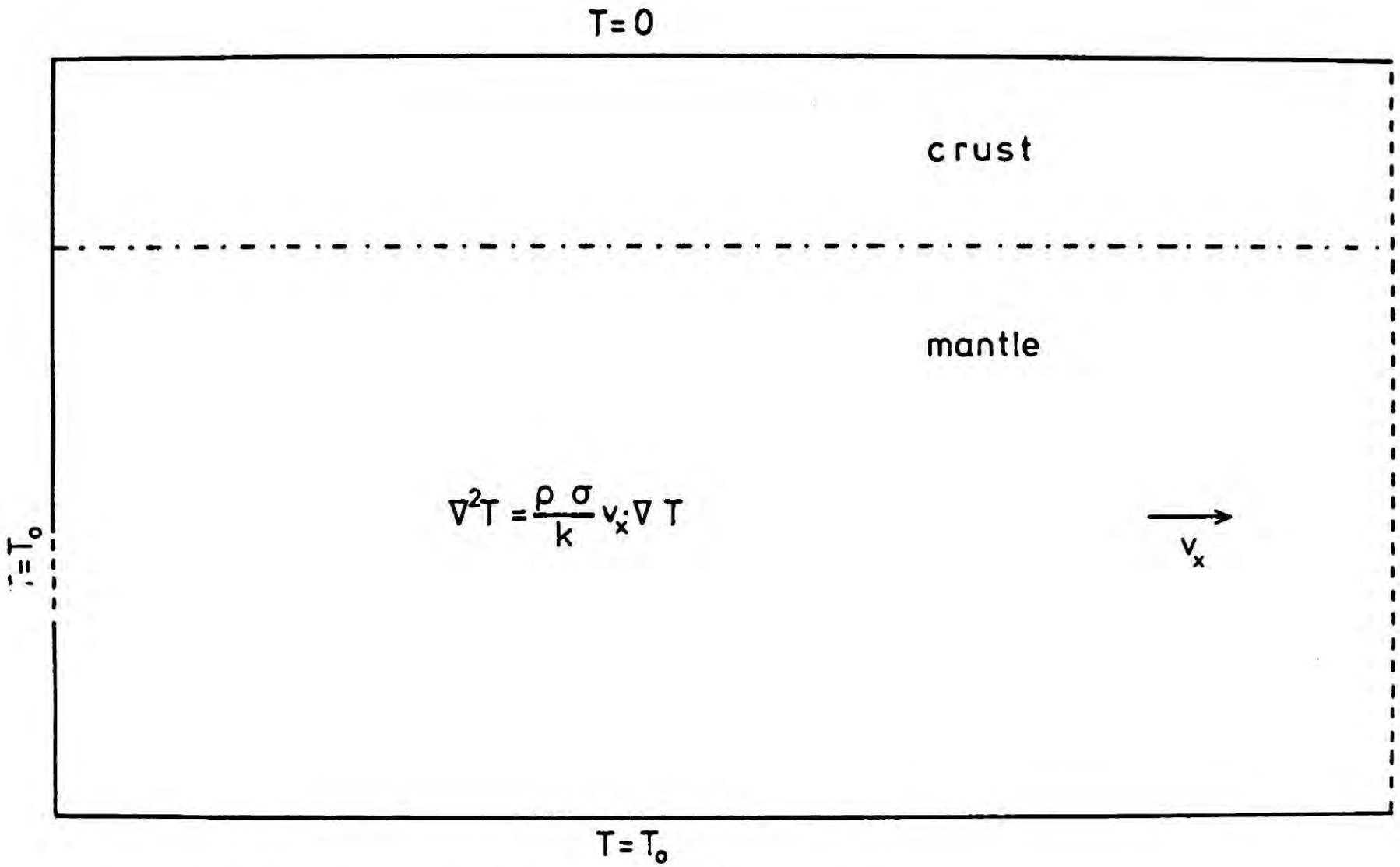

Figure 5.1 Thermal model of lithosphere neglecting latent heat (after McKenzie, 1967).

material at the ridge axis is assumed to be of the order of thickness of oceanic layer 3, since layer 2 is assumed to be cooled quickly by the circulation of convecting sea-water (Bodvarson and Lowell, 1972; Pálmason, 1973). The layer 2 - layer 3 boundary is assumed to correspond to the lower limit of the convecting sea-water system and the temperature of this boundary is assumed to be $0^{o}C$ for the thermal model.

The latent heat of solidification of the basalt melt may be introduced into the thermal model in two ways; (a) the latent heat may be considered to be distributed throughout the liquidus to solidus temperature interval and to form part of an apparent specific heat of the molten material, (b) the latent heat may be released at the solidus temperature of the molten material.

(a) Latent heat of solidification of a basalt melt is released throughout the temperature interval of liquidus to solidus (Hess, 1960; Jaeger, 1968). A convenient way of representing this in a thermal calculation is to introduce an effective specific heat, σ' , over the solidification temperature interval, which incorporates the distributed latent heat (Jaeger, 1968) such that

$$\sigma'(T) = \sigma + \frac{H}{(T_L - T_S)} \qquad 5.3$$

where σ is the actual specific heat, H is the latent heat and T_L and T_S are the liquidus and solidus temperatures respectively.

The introduction of the temperature dependent specific heat, $\sigma'(T)$, results in the differential equation

$$\nabla^2 T = \frac{\rho \sigma'(T)}{k} V_x \frac{\partial T}{\partial x} \qquad 5.4$$

which although not soluble analytically may be solved by the numerical method of finite difference discussed in the next section.

(b) If the latent heat is assumed to be released at the solidus temperature, T_S, the solidification may be represented in the thermal analysis by a differential equation applied to the solid-liquid boundary of the form

$$\frac{\partial n}{\partial t} \rho H = -k \frac{\partial T}{\partial n} \qquad 5.5$$

where $\hat{n}$ is the unit vector normal to the surface.

If α is the angle made by the liquid-solid interface with the horizontal, the differential equation becomes

$$u_x \frac{\rho H}{k} = -\left(\frac{\partial T}{\partial x} + \tan\alpha \frac{\partial T}{\partial z}\right) \qquad 5.6$$

where u_x is the horizontal velocity of the phase boundary. For a steady state position of the phase boundary with

respect to the ridge axis, the velocity u_x coincides with the half spreading rate. In figure 5.2 the lithosphere thermal model is shown for this formulation with its boundary differential equation in addition to its regional differential equation and boundary conditions.

The assumption that the latent heat is released at the solidus temperature implies that the molten crust has a high thermal mobility. The molten material of the crust would most probably convect and so this assumption is valid.

It is necessary to incorporate into the latent heat, a term which represents the heat liberated by the molten material in cooling from its liquidus to solidus temperature. Thus an apparent latent heat, H' , must be used in equation 5.6 such that

$$H' = H + (T_L - T_S)\sigma \qquad 5.7$$

The numerical method of finite difference is used for the solution of the problem as with the previous method, and the finite difference formulations are described in the next two sections. Both methods of incorporating the latent heat into the thermal model are used to investigate the solidification of the ocean crust. Sleep (1975), in a study of the solidification of the ocean crust, made the approximation that the latent heat was released at the ridge axis ($x = 0$). In the models proposed here, this approximation is not necessary.

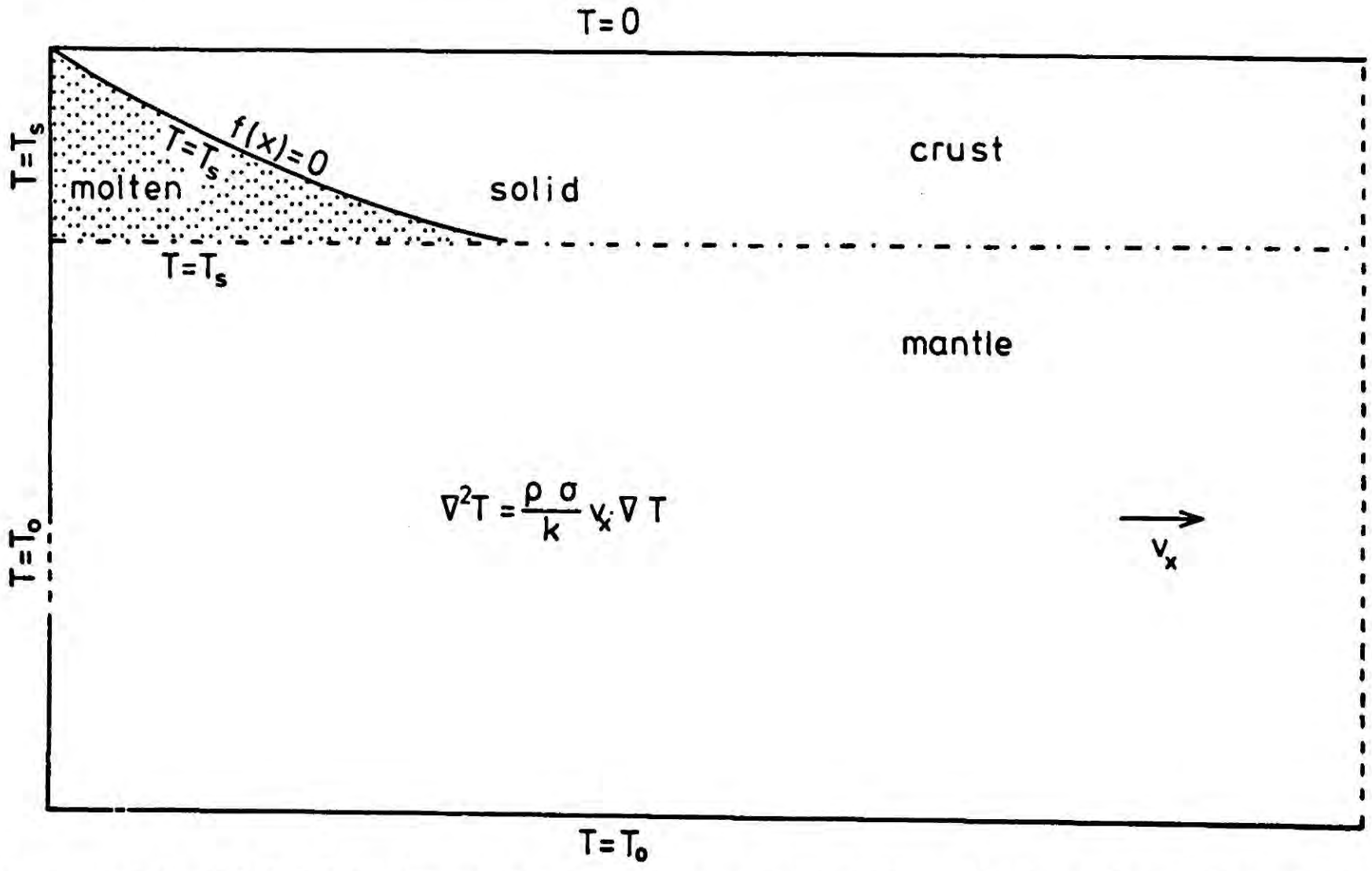

Figure 5.2 Thermal model of lithosphere including latent heat effect, with latent heat released at T_s.

5.3 Finite difference temperature analysis

The solution of a differential equation over a region by the method of finite differences involves satisfying the differential equation at a number of different points in the region. Carslaw and Jaeger (1959) describe the use of the method for the solution of the differential equations of transient heat flow which is

$$\frac{\partial^2 T}{\partial x^2} + \frac{\partial^2 T}{\partial z^2} = \frac{\rho \sigma}{k} \frac{\partial T}{\partial t} \qquad 5.8$$

for 2 dimensions where T is temperature, t is time, k is thermal conductivity, ρ is density and σ is specific heat.

As the first step towards obtaining a solution by this method, a network of regular spaced points is constructed throughout the region over which the differential equation applies (figure 5.3). It is at these points that the temperature solution is to be obtained and for the point shown the differential equation may be replaced by a difference equation which to a first approximation is

$$(T_1 + T_2 + T_3 + T_4 - 4T_0)/a^2 = \frac{\rho \sigma}{k} \frac{dT}{dt} \qquad 5.9$$

Replacing the time derivative by a difference expression it becomes

$$\frac{dT}{dt} = \frac{\Delta T}{\Delta t} \qquad 5.10$$

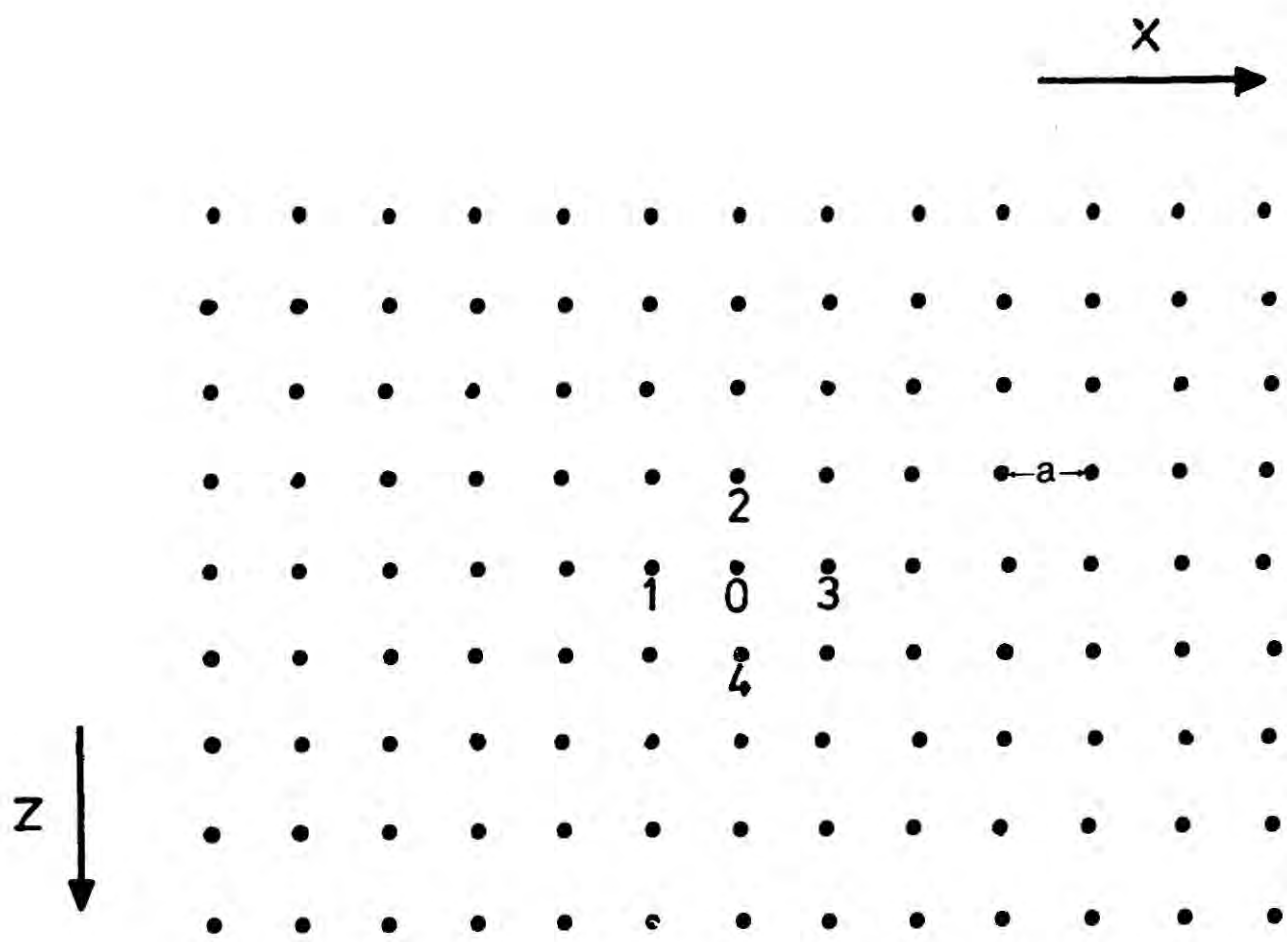

Figure 5.3 The finite difference representation of a region, with group of nodes used for finite difference approximation.

Hence for the time interval Δ t, the temperature change is at that point

$$\Delta T = \frac{k}{\rho\sigma} \Delta t (T_1 + T_2 + T_3 + T_4 - 4T_o)/a^2 \qquad 5.11$$

Similar expressions may be applied to each point of the region, in turn. The thermal constants may be a function of space or temperature and this dependency may easily be incorporated in the calculations. To propagate the thermal model through time the temperature change over a small time increment is applied to each point in turn and the process repeated for subsequent time increments. The points of the region possessing the boundary conditions have their values of temperature held at the prescribed values throughout the calculation.

The accuracy of the method is good provided that too large time steps are avoided. The critical value of time increment is given by (Carslaw and Jaeger, 1959).

$$\Delta t = \tfrac{1}{2} \frac{a^2 \rho\sigma}{k} \qquad 5.12$$

A non regular grid may be used, provided it allows the differential equation to be expressed by a difference equation to a reasonable accuracy.

Thermal equilibrium occurs when $\frac{\partial T}{\partial t} = 0$ and the differential equation becomes

$$\frac{\partial^2 T}{\partial x^2} + \frac{\partial^2 T}{\partial z^2} = 0 \qquad 5.13$$

In finite difference formulation this becomes

$$\frac{T_1 + T_2 + T_3 + T_4 - 4T_o}{a^2} = 0 \qquad 5.14$$

However, prior to solution, it is found that

$$\frac{T_1 + T_2 + T_3 + T_4 - 4T_o}{a^2} = R \qquad 5.15$$

and this residual R must be used to correct the value of T_o in such a way that R tends to zero. By comparison with the transient heat problem, the correction applied to T_o is

$$\Delta T_o = \tfrac{1}{2} Ra^2$$

This correction is applied to all grid points in turn and then the whole process repeated for the whole body. The iterations are continued until the equilibrium state is reached where R tends to zero.

The method described for the solution of $\nabla^2 T = 0$ may be extended for the solution of the differential equation

$$\nabla^2 T = \frac{\rho\sigma}{k} v_x \cdot \nabla T \qquad 5.16$$

The difference equation for this is

$$\frac{T_1 + T_2 + T_3 + T_4 - 4T_o}{a^2} - \frac{\rho\sigma v_x}{2ka}(T_3 - T_1) = 0 \qquad 5.17$$

and the temperature correction ΔT_o for each grid point

is given by

$$\Delta T_o = \tfrac{1}{2}\, a^2 \left[\frac{T_1 + T_2 + T_3 + T_4 - 4T_o}{a^2} - \frac{\rho\sigma}{k} V_x \frac{(T_3 - T_1)}{2a} \right] \qquad 5.18$$

For large values of V_x the solution of equation 5.16 may become unstable using this method. The instability may be overcome by multiplying ΔT_o of equation 5.18 by a relaxation factor of value of 0.1.

5.4 Application of the finite difference method to solidification

(a) The use of an equivalent specific heat σ', defined in equation 5.3, as a method of including the latent heat of solidification into the thermal calculations has been described in section 5.2. The specific heat σ' is temperature dependent and is given by

$$\sigma'(T) = \sigma \qquad T < T_S$$

$$\sigma'(T) = \sigma + \frac{L}{T_L - T_S} \qquad T_L > T > T_S \qquad 5.19$$

The differential equation for the temperature distribution of the lithosphere therefore becomes

$$\nabla^2 T = \frac{\rho\sigma'(T)}{k} V_x \cdot \nabla T \qquad 5.20$$

Solution may be carried out in the same way as for a temperature independent specific heat using the method of finite difference.

(b) The alternative method of including solidification in the thermal calculations involves the introduction of an auxiliary boundary, which represents the interface between solid and liquid crust, and must satisfy a boundary differential equation (equation 5.6). Since the latent heat is assumed to be released at the solidus temperature, the temperature of the auxiliary boundary is that of the solidus, T_s . Elsewhere in the solid lithosphere the regions differential equations (equation 5.1) and boundary conditions are identical to that of a thermal model without solidification.

The finite difference method may be extended to solve this problem by allowing the auxiliary boundary to be represented by a series of finite difference points or nodes. The nodes chosen are those nearest to the position of the boundary on the finite difference grid, and are moved from their regular position on the grid to correspond to the actual boundary position. In figure 5.4 the boundary is shown as represented by the finite difference grid.

The numerical solution of the problem is found by repeated iterations of the two part sequence. The two parts of the repeated sequence are:—

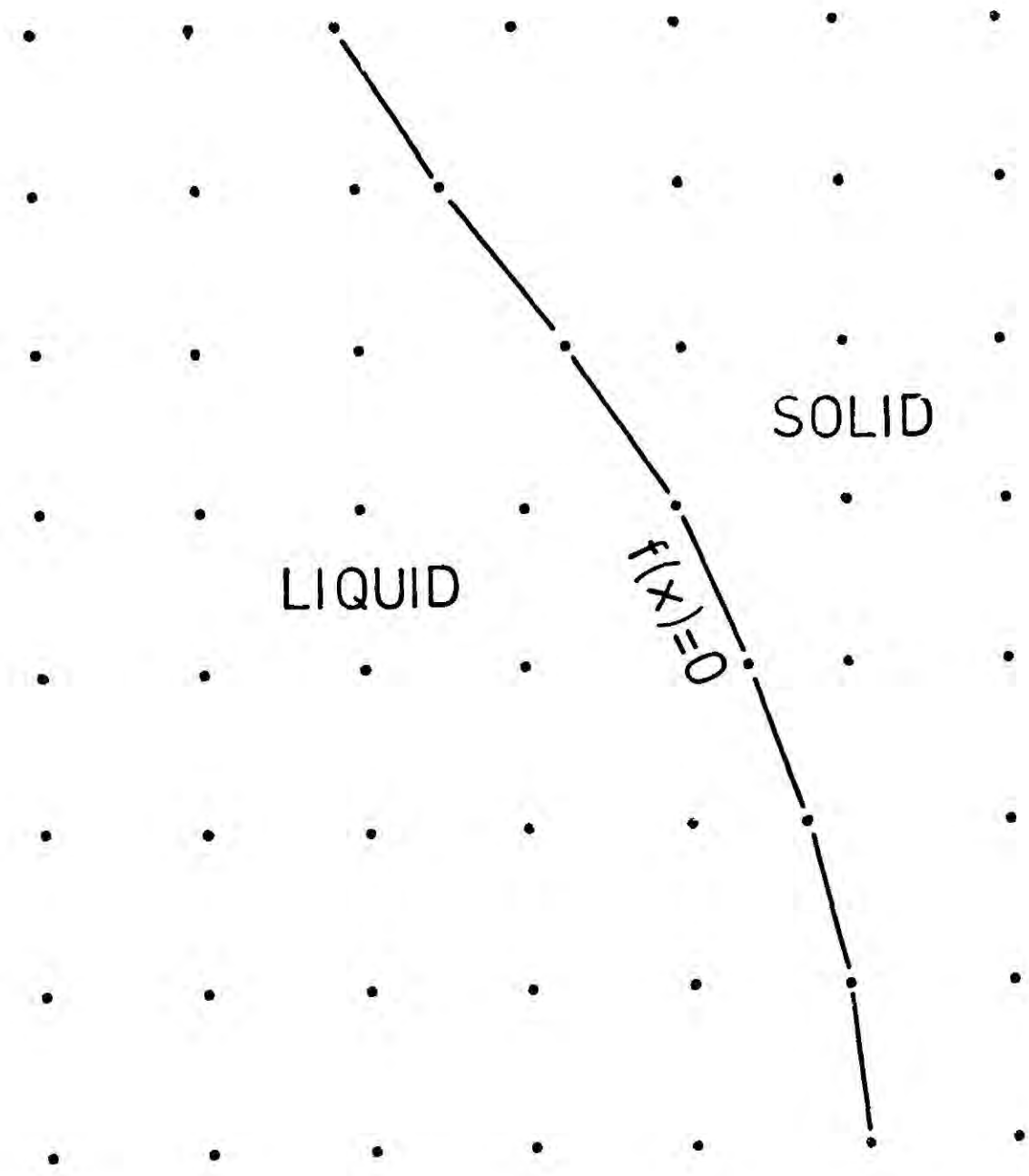

Figure 5.4 Finite difference representation of the liquid-solid interface.

(a) The temperature field of the solid lithosphere is calculated according to the method presented in the previous section using the method of finite difference. The auxiliary boundary is fixed during the solution.

(b) The vertical and horizontal gradients of the temperature field are calculated for the auxiliary boundary from the nodal temperature distribution obtained in part (a). The gradients are calculated for the position midway between two boundary nodes. Prior to solution the differential equation for the auxiliary boundary (expressed as finite differences) will not be satisfied exactly such that

$$\left(\frac{\Delta T_x}{\Delta X}\right) + \tan\alpha\left(\frac{\Delta T_z}{\Delta Z}\right) + \frac{v_x \rho H}{k} = R \qquad 5.21$$

The residue, R, is used to perturbate the position of the auxiliary boundary in the horizontal direction. Perturbations of the z coordinates of the boundary are not considered directly.

If $\left(\frac{\Delta T_x}{\Delta X}\right)'$ is the horizontal temperature gradient which would satisfy the auxiliary boundary differential equation then

$$\left(\frac{\Delta T_x}{\Delta X}\right) - \left(\frac{\Delta T_x}{\Delta X}\right)' = R \qquad 5.22$$

Putting $\Delta T_x = \Delta' T_x$ and rearranging this becomes

$$\Delta T_x \left(\frac{1}{\Delta X} - \frac{1}{\Delta X'}\right) = R \qquad 5.23$$

If $\Delta X' = \Delta X + \xi$, where ξ is the horizontal perturbation of the boundary required for the better solution, then

$$\xi = \frac{R\ \Delta X}{\left(\frac{\Delta T_x}{\Delta X}\right) - R} \qquad 5.24$$

This perturbation ξ is applied in turn to the boundary nodes for the whole of the auxiliary boundary. Each boundary node receives 2 perturbations: from the section of the boundary immediately below and above it.

Having applied the perturbation to the auxiliary boundary position, the temperature field of the solid lithosphere is readjusted, since the movement of the auxiliary boundary will slightly alter the temperature distribition in the solid lithosphere. The two part sequence of adjusting the temperatures of the lithosphere and perturbating the auxiliary boundary is continued until the boundary ceases to move signifying convergence. It is necessary to change the nodes representing the solidification boundary during solution since the boundary moves. The numerical calculations may be greatly speeded up by using a good initial estimate of boundary position. It has been found advantageous to multiply the perturbation of the boundary by a relaxation factor of value 0.1 which ensures convergence of the numerical process without large

oscillations about the solution values and the possible threat of divergence. Furthermore, the application of a small perturbation allows the solution of the solid lithosphere temperature field to be obtained with few finite difference iterations.

The solution of the temperature field of the lithosphere may be greatly speeded by using a good initial estimate of the temperature distribution. The estimate may be obtained by using equation 5.2.

The numerical calculations were carried out by computer and the programs written and used for the solutions of the two different thermal models are listed and described in Appendix 3.

5.5 Application of the finite difference method

The finite difference grid representing the region over which the two thermal models are to be solved is shown in figure 5.5. Node spacing is closest in the region adjacent to the ridge crest where the solidification of crust occurs. The coarser node spacing, away from the ridge axis is 10 km, while a selection of finer spacings of values 1 km, 0.5 km and 0.25 km have been used. This is the highest resolution computing resources would permit, but the agreement of solutions for different grid spacings

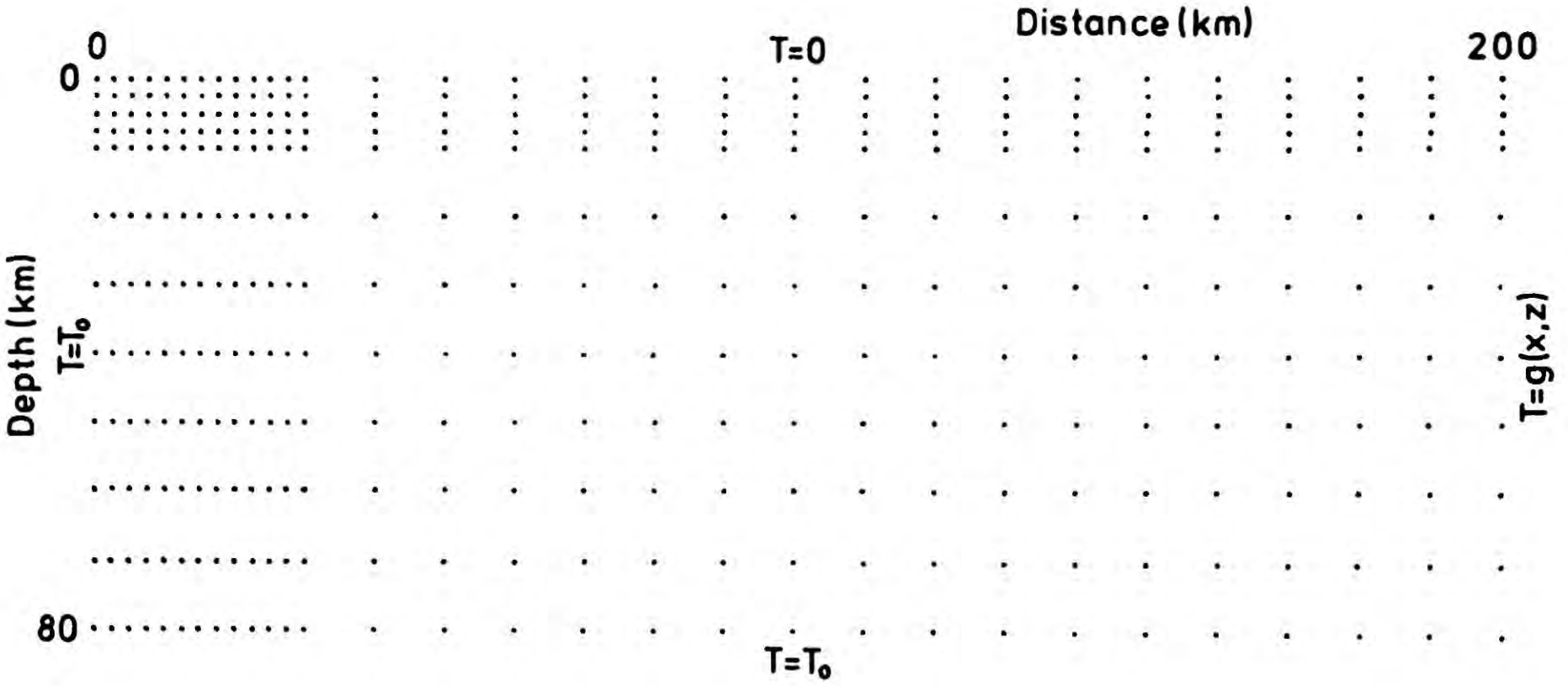

Figure 5.5 Diagrammatical representation of the finite difference grid used in the numerical calculations g(x) defined by equation 2.

suggests that the resolution is adequate.

Boundary conditions of temperature are applied to the peripheral nodes of the grid and are shown in figure 5.5. The vertical boundary remote from the ridge axis is assigned temperatures according to the analytical solution given by equation 5.2 because at this distance the perturbation effect on the temperature field of the latent heat is negligible.

For both thermal models, convergence and solution of the problem was achieved within 600 iterations of the finite difference correction for the whole body. This reduced the maximum ΔT_o (equation 5.18) to less than $0.1^{\circ}C$, which is adequate convergence. For the method using the auxiliary boundary representing the liquid-solid interface the perturbations of the boundary on solution were less than 10 metres.

The values of the thermal constants used in the calculation were:

latent heat, H 100 cal/gm (Jaeger, 1968; Bottinga, 1974)

thermal conductivity, k 0.006 cal/s $^{\circ}C$ cm^2 (Clark and Ringwood, 1964)

density, ρ 3.0 gm/cc

specific heat, σ 0.26 cal/gm $^{\circ}C$ (Birch, 1952; Haigh, 1973)

A liquidus temperature of $1125^{\circ}C$ (c.f. $1140^{\circ}C$ of Hess (1960) and $1180^{\circ}C$ of Sleep (1975)) has been chosen since

this value corresponds to that of T_o, the intrusive temperature selected for the model. Adiabatic temperature effects in the intruding magma have been neglected together with the radioactive heating of the lithosphere. The value of the solidus temperature used in the calculations is 1000°C, the value suggested by Hess (1960) and used by Jaeger (1968).

5.6 Crustal temperatures and the shape of the molten regions

The temperature distribution in the lithosphere at the ridge axis have been calculated using the numerical techniques described in the previous sections.

The isotherms of the thermal model using distributed latent heat (method (a)) are shown in figure 5.6 for a lithosphere with a spreading rate of 3 cm/yr. Isotherms for the same spreading rate but with no latent heat are also shown on the diagram for comparison and the difference between the two sets of isotherms is seen to be greatest in the base of the crust at the ridge axis. At large distances from the ridge axis the two isotherm distributions become identical. For a spreading rate of 3 cm/yr this is achieved at a distance of 30 km from the ridge axis.

Latent heat is effectively an extra heat source in the crust in the vicinity of the ridge axis and consequently the temperatures are somewhat higher in this region when

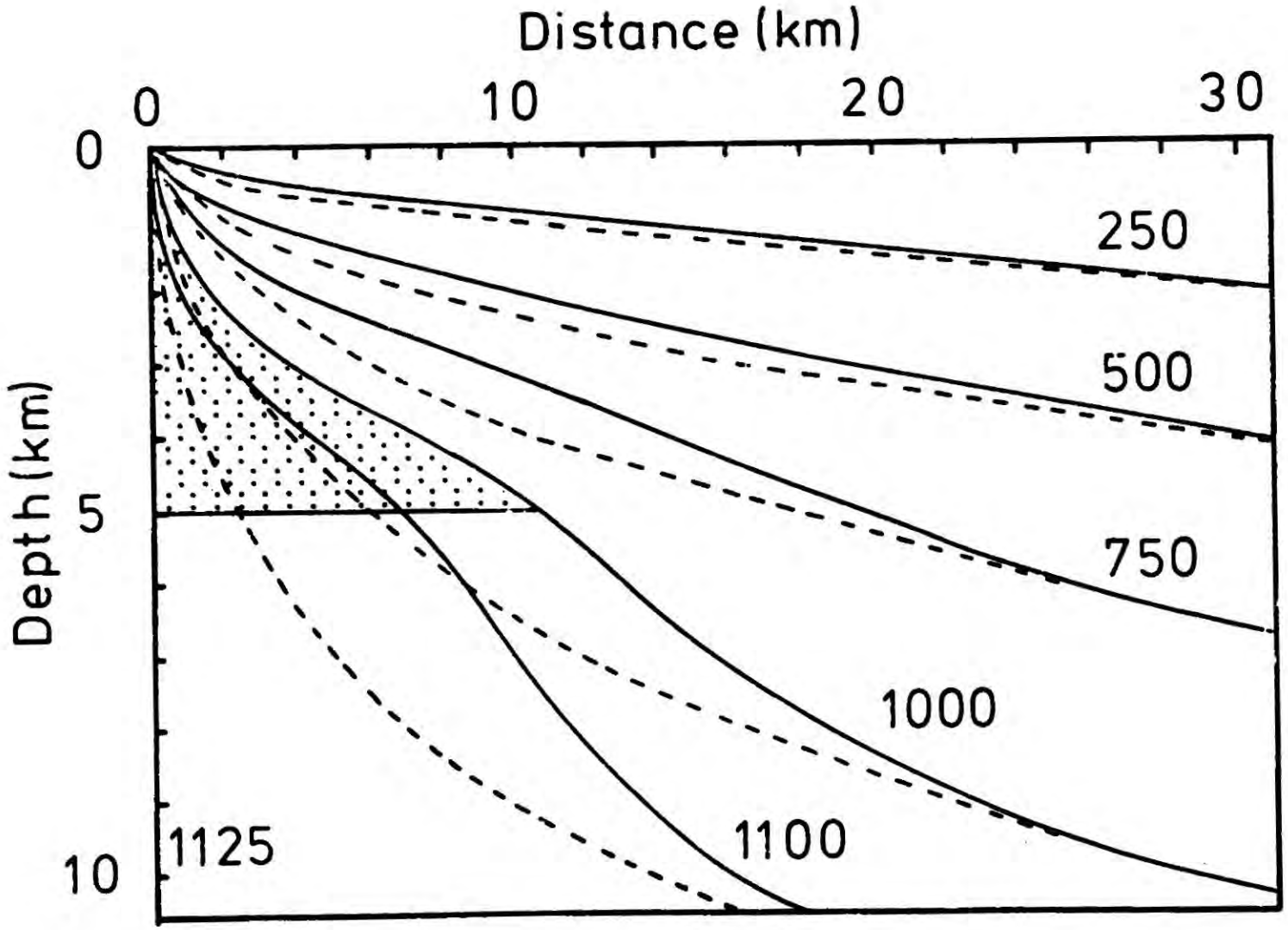

Figure 5.6 Isotherm distribution (^{o}C) in oceanic crustal layer 3 and upper mantle at ridge crest with distributed latent heat, for a spreading rate of 3 cm yr^{-1}. Isotherms for model neglecting latent heat are shown as dashed curves.

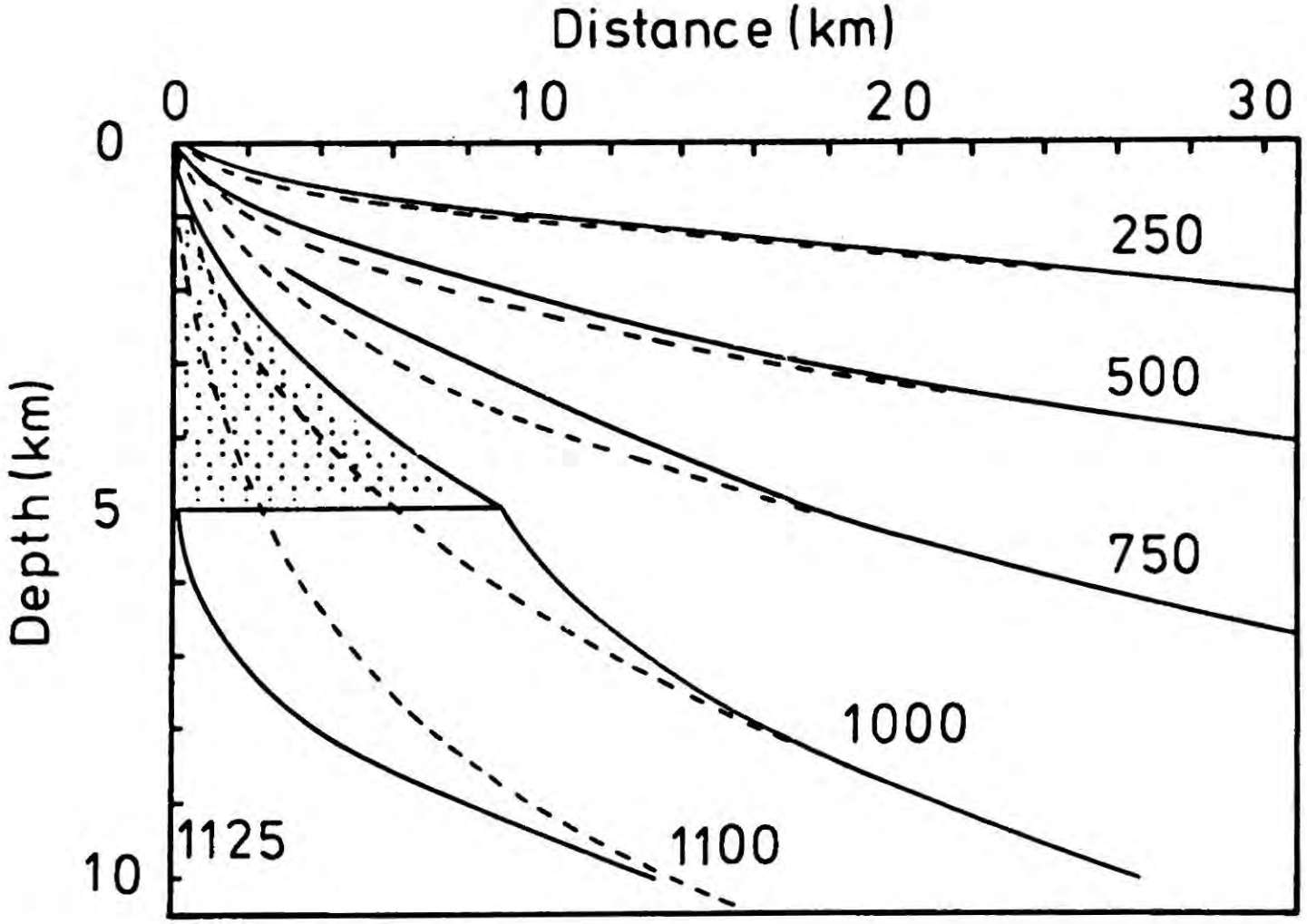

Figure 5.7 Isotherm distribution (^{o}C) in oceanic crustal layer 3 and upper mantle at ridge crest with latent heat released at solidus, for a spreading rate of 3 cm yr^{-1}. Isotherms for model neglecting latent heat are shown as dashed curves.

this effect is included, than for models neglecting latent heat (McKenzie, 1967; Sclater and Francheteau, 1970; Haigh, 1973).

In figure 5.7 the isotherms are shown for the thermal model where the latent heat is released entirely at the solidus temperature. The effect of the convection in the molten region reduces the temperature in the upper mantle with respect to the simple model (dashed line). In the crust, the temperature is raised with respect to the simple model because of the release of the latent heat.

For both types of model of the solidification, the solidus isotherm corresponds to the limits of the molten body in the crust. In figure 5.8 the position of the solidus isotherm is shown for both models as a function of spreading rate. It can be seen that to a good approximation the width of the molten body is directly proportional to the spreading rate. The width of the molten body produced by the model releasing all latent heat at solidus is considerably less than that for the model with latent heat distributed throughout the liquidus to solidus interval. It is felt that the two models represent extremes with the true situation lying somewhere in between.

The effect of reducing the thickness of the molten material intruded at the ridge axis from 5 km to 3 km has been investigated and it is found that the shape of the

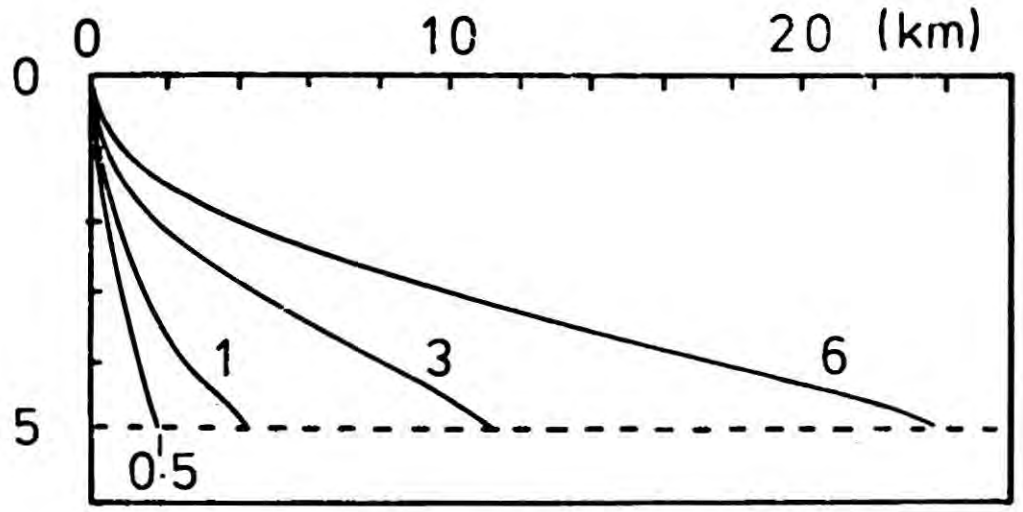

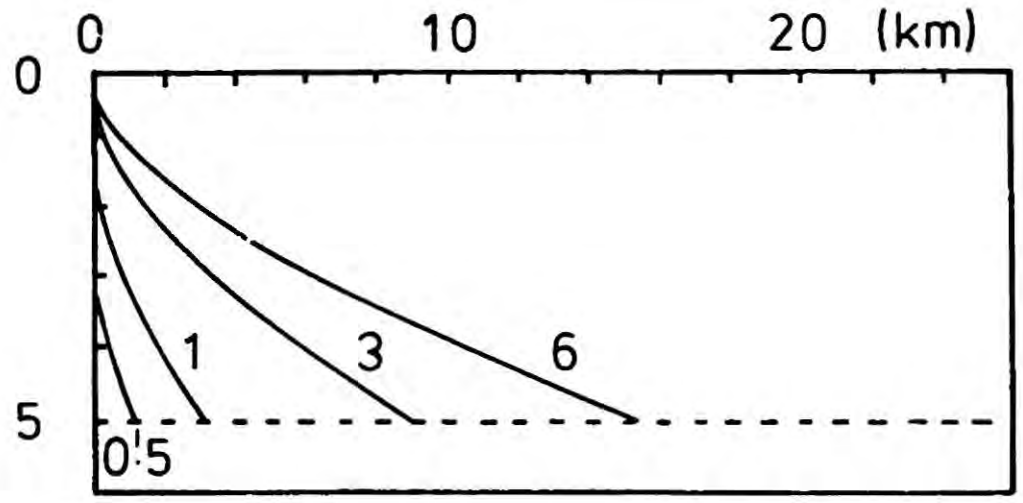

Figure 5.8

Position of solidus isotherm in the oceanic crust as a function of half spreading rate (cm yr^{-1})

(a) Latent heat distributed over liquidus to solidus temperature interval.

(b) Latent heat released entirely at solidus.

molten region does not change significantly except for being truncated at 3 km depth below the top of layer 3.

The models predict the existence of a molten body or magma chamber in the base of the crust. Geophysical research consisting of shallow seismic refraction studies in the median valley (Whitmarsh, 1975) have possibly detected a narrow zone of very low velocity material while small earthquakes in the crust at the ridge axis (Francis and Porter, 1973) have been used to suggest a shallow velocity conversion in the crust consistent with a magma chamber. Evidence, however, has not positively confirmed the existence of magma chambers. For the model where latent heat is distributed throughout the liquidus to solidus interval, it is possible to analyse the temperature distribution within the solidifying material. In figure 5.9 temperature is plotted against age as a function of spreading rate and depth. From the plot is is evident that molten material solidifies more slowly with increasing depth, suggesting that the solidified basaltic crust will be of coarser grained texture with increasing depth. Hence the model predicts a layer 3 of basalt graduating into dolerite and gabbro with increasing depth; a structure identical with that of Cann's model and compatible with that suggested by ophiolite studies. The extrusion process which probably creates a large part or all of layer 2 is not accounted for

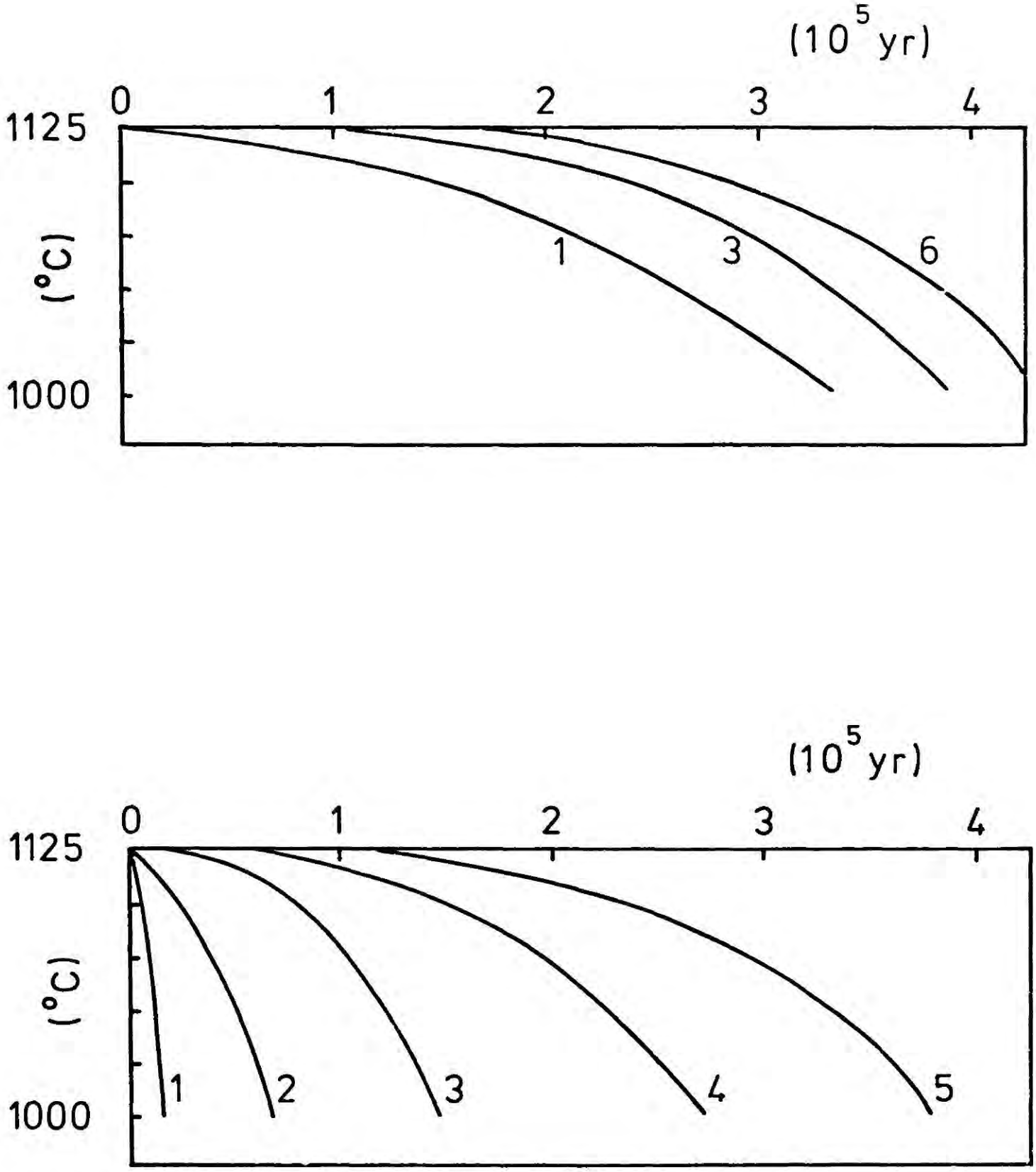

Figure 5.9 Temperature distribution in the ocean crust as a function of crustal age showing dependence on

(a) half spreading rate (cm/yr) at depth 5 km .

(b) depth (km) at half spreading rate of 3 cm/yr .

in the thermal models and the texture sequence derived above requires an additional layer of basalt extrusives on top of it.

The rate of cooling of the molten material decreases with increasing spreading rate (figure 5.9). In the temperature interval just below the liquidus, the cooling is considerably more rapid for slower spreading rates. The result of this numerical model (distributed latent heat) may signify that a finer crystalline texture occurs in the ocean crust for slower spreading rates.

5.7 Refinements to the distributed latent heat model - non-linear distribution of latent heat and crystal settling

Hess (1960) suggested that the latent heat of solidification is distributed throughout the liquidus to solidus interval in a non linear proportion. In the temperature interval, T_L to 1100°C, 60.0 cal/gm are liberated and from 1100°C to T_S, the remaining 40.0 cal/gm. An effective specific heat, σ', has been used in the finite difference calculations where the latent heat is distributed throughout the liquidus to solidus temperature interval according to the above proportions.

In figure 5.10 the position of the solidus isotherm is shown as a function of depth and spreading rate. Comparison with the linearly distributed latent heat model, shows that

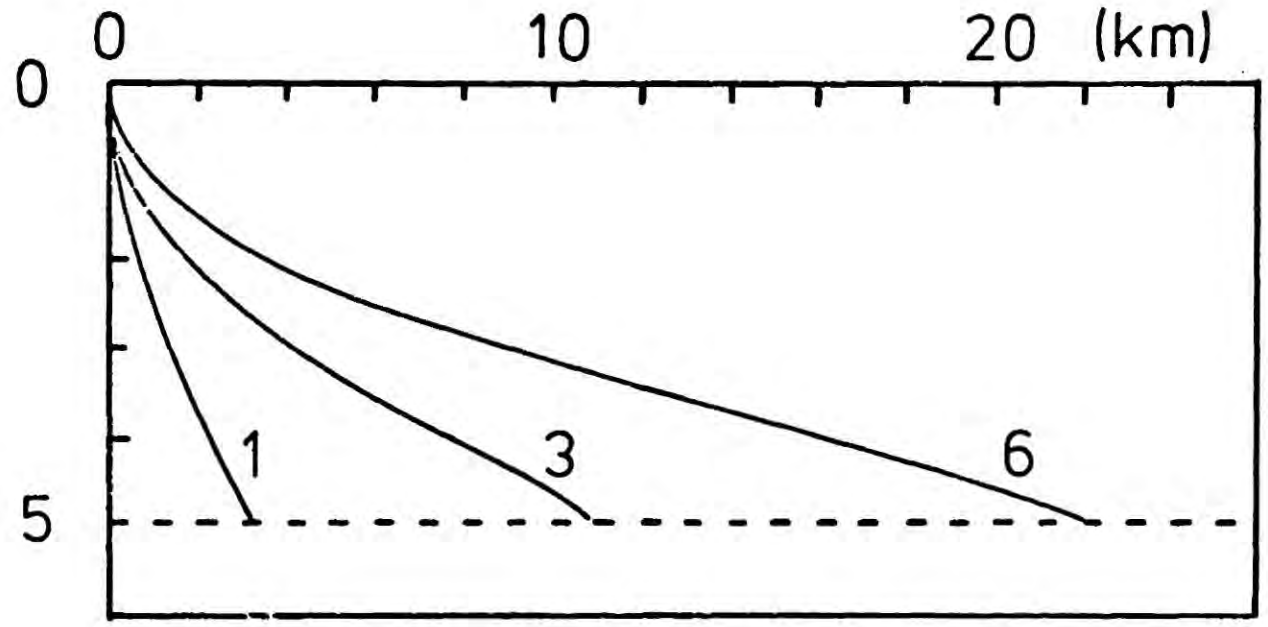

Figure 5.10 Position of the solidus isotherm in the ocean crust as a function of half spreading rate (cm/yr) for distributed latent heat, with 60% liberated above 1100°C.

the effect of releasing 60% of the latent heat above 1100°C decreases the magma chamber width for all spreading rates. The decrease is however, quite small being of the order of 10% to 20%.

The shape of the magma chamber in the oceanic crust will be further modified by the accumulation of crystals falling to the magma chamber bottom, together with pieces broken off the chamber roof. The transfer of solid material downwards will cause hot liquid to move upwards. Thus the process of crystal settling brings about convection in the magma chamber which would lead to more rapid solidification.

The distributed latent heat solidification model permits an estimate of the effect of crystal settling and roof slumping to be made. The assumption is made that the ratio of solidified material forming the roof of the chamber to that falling to the bottom is 1:f. Thus, if the thickness of the settled material is implicit from the thickness of solid crust above the chamber, the latent heat of the molten material must be adjusted to account for the latent heat of the settled material. Thus, a corrected latent heat, must be used, such that,

$$H' = H(1 + f)$$

The apparent specific heat σ' used in the finite difference calculation is therefore

$$\sigma' = \sigma + \frac{H(1+f)}{T_L - T_S} \qquad 5.25$$

The further assumption must be made that the solidified material does not remelt. The shape of the magma chamber have been computed for values of f equal to ½, 1 and 2 as a function of spreading rate and are shown in figure 5.11. The width of the magma chamber is strongly dependent on the intensity of crystal settling and roof collapse and for increasing f becomes narrower.

5.8 Analytical models

The approximate relationship that the width of the molten region is linearly dependent upon spreading rate suggests that the cooling of the ocean lithosphere, in the region just away from the ridge axis, is controlled predominantly by heat conduction in the vertical direction. If the approximation is made that the latent heat is released at a single temperature corresponding to that of the solidus, the rate of movement of the solidification in the vertical direction, z , is given by the differential equation

$$H \rho \frac{\partial z}{\partial t} = k \left. \frac{\partial T}{\partial z} \right|_{T_s} \qquad 5.26$$

Replacing $\frac{\partial T}{\partial z}$ by the approximation T_o/z, the differential equation becomes

$$H \rho \frac{dz}{dt} = k \frac{T_o}{z} \qquad 5.27$$

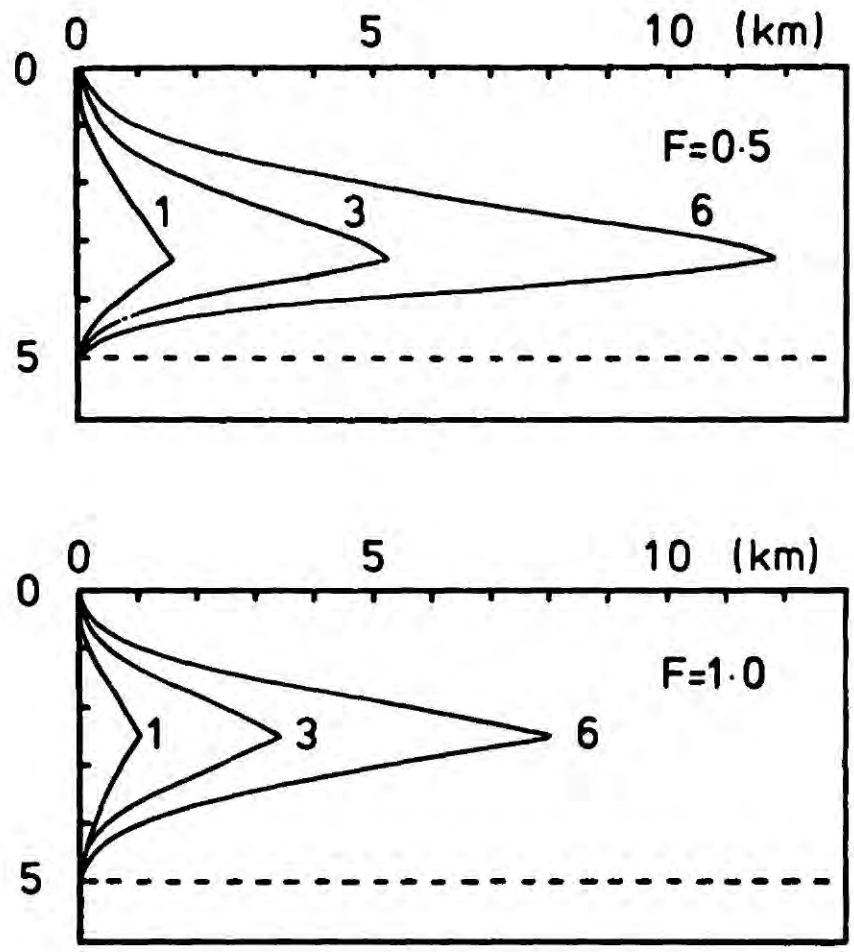

5.11 Position of the solidus isotherm in oceanic layer 3 as a function of half-spreading rate (cm/yr) and crystal settling factor F.

where z is the depth of the liquid-solid interface, and after integration this gives

$$z^2 = \frac{2 k T_s t}{H \rho} \qquad 5.28$$

For a half spreading rate of v , the time t may be replaced by x/v, where in the horizontal distance of the phase boundary point from the ridge axis and substituting this in equation 5.28 gives

$$x = \frac{v H z^2}{2 k T_s} \qquad 5.29$$

In figure 5.12 the phase boundary produced by this analytical expression is plotted as a function of spreading rate. The magma chamber dimensions are comparable with those produced by the numerical model where the latent heat is released entirely at the solidus.

The results from the numerical calculations, suggesting that the ocean crust may solidify more quickly for slower spreading rates, if extrapolated for very small rates, may indicate a situation where the intruded magma solidifies almost immediately on intrusion at the ocean ridge axis. If the horizontal temperature gradient, $\frac{\partial T}{\partial x}$, at the idealized accretion boundary, x = 0, is sufficiently large to carry away the latent heat of solidification, the magma

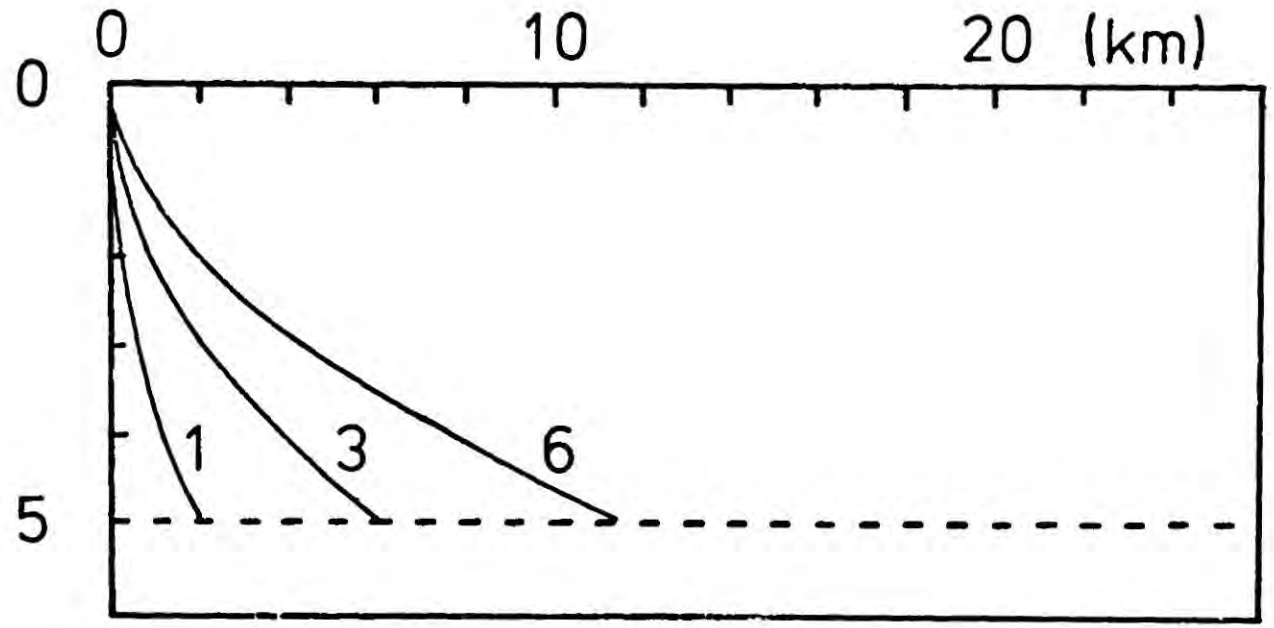

Figure 5.12 Position of the solidus isotherm in oceanic layer 3 as a function of spreading rate for a simple one-dimensional analytical approximation.

will solidify immediately at the accretion boundary. This phenomena is investigated by calculating the horizontal temperature gradient close to the ridge axis from equation 5.2 and comparing it with the rate of release of latent heat. A vertical solidification boundary is considered since this is the geometry of the molten material for slow spreading. The simplifying approximation is made again that the latent heat of solidification is released at the solidus temperature T_s.

The rate of release of latent heat is

$$Q_L = V_x H \rho \qquad 5.30$$

From equation 5.2 the thermal gradient $\frac{dT}{dx}$ is given by

$$\frac{dT}{dx} = 2T_0 \sum_{n=1}^{\infty} \frac{1}{n\pi} \left\{ \frac{P}{2} - \left(\frac{P^2}{4} + n^2\pi^2 \right)^{1/2} \right\} / L \cdot$$
$$\exp\left\{ \left(\frac{P}{2} - \left(\frac{P^2}{4} + n^2\pi^2 \right)^{1/2} \right) \frac{x}{L} \right\} \sin\left(n\pi z / L \right) \qquad 5.31$$

and the horizontal heat flow is given by

$$Q_H = k \frac{dT}{dx} \qquad 5.32$$

The solidification boundary will be stationary when

$Q_L = Q_H$ or $\Delta Q = 0$ where

$$\Delta Q = Q_H - Q_L \qquad 5.33$$

In figure 5.13 the quantity ΔQ is plotted as a function of distance from the ridge axis, for various half spreading rates, for a depth of 5 km. It can be seen from figure 5.13 that the critical velocity at which solidification is immediate on intrusion is approximately 0.45 cm/yr. Sleep (1975) has suggested a similar critical spreading rate effect with a critical velocity of 0.9 cm/yr. If the assumptions of this simple analytical model are valid, this critical velocity may represent a velocity at which the formation mechanism of the ocean crust is radically altered or even ceases. It suggests also that for low spreading velocity the gabbroic layer of ocean layer 3 may disappear, with layer 3 being composed of dykes intruding from below the crust.

5.9 Conclusion

The numerical model of the solidification of the ocean crust indicates the existence of a region of molten material existing at the ridge axis whose width is approximately directly proportional to the spreading rate of the ocean. Assuming that oceanic layer 2, composed of pillow lavas, is cooled by hydrothermal circulation, the molten region corresponds to ocean layer 3. The model predicts a decrease in the rate of cooling with depth, suggesting the upper layer

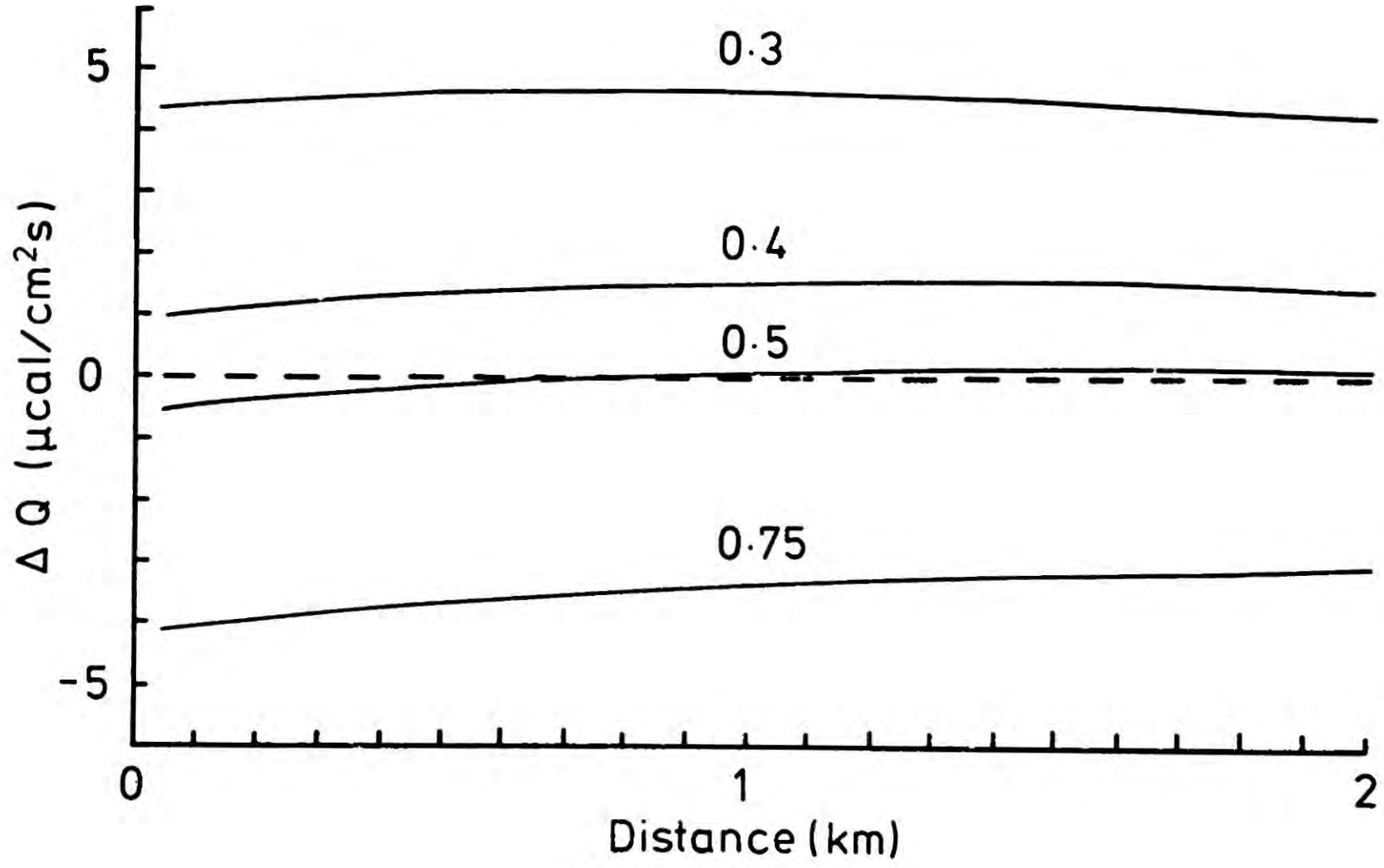

Figure 5.13 Q (see text) as a function of distance from ridge axis and half spreading rate, computed at a depth of 5 km within layer 3.

3 is doleritic becoming increasing gabbroic below; a structure compatable with that held by Cann (1974) and indicated from ophiolite studies.

For increasingly slower spreading rates, the model suggests that the molten region cools more quickly. This indicates the possibility of the ocean crust of slower spreading ridges having a more doleritic and less gabbroic composition than those of faster spreading ridges. In the case of very slow spreading centres, the possibility exists of the situation existing where material intruded into the crust solidifies immediately, not forming a magma chamber. In this situation the normal accretion process would be extensively modified or even cease. The critical velocity for instantaneous cooling appears to be approximately 0.5 cm/yr.

The inclusion of crystal settling in the thermal model shows the strong dependence of the magma chamber dimension and shape on settling. With increase in crystal settling, the magma chamber becomes less wide and increasingly flat topped.

The crustal structure at the ocean ridge indicated by the above calculations is summarized in figure 5.14 for a model with half spreading rate 3 cm/yr and a crystal settling factor of 0.5.

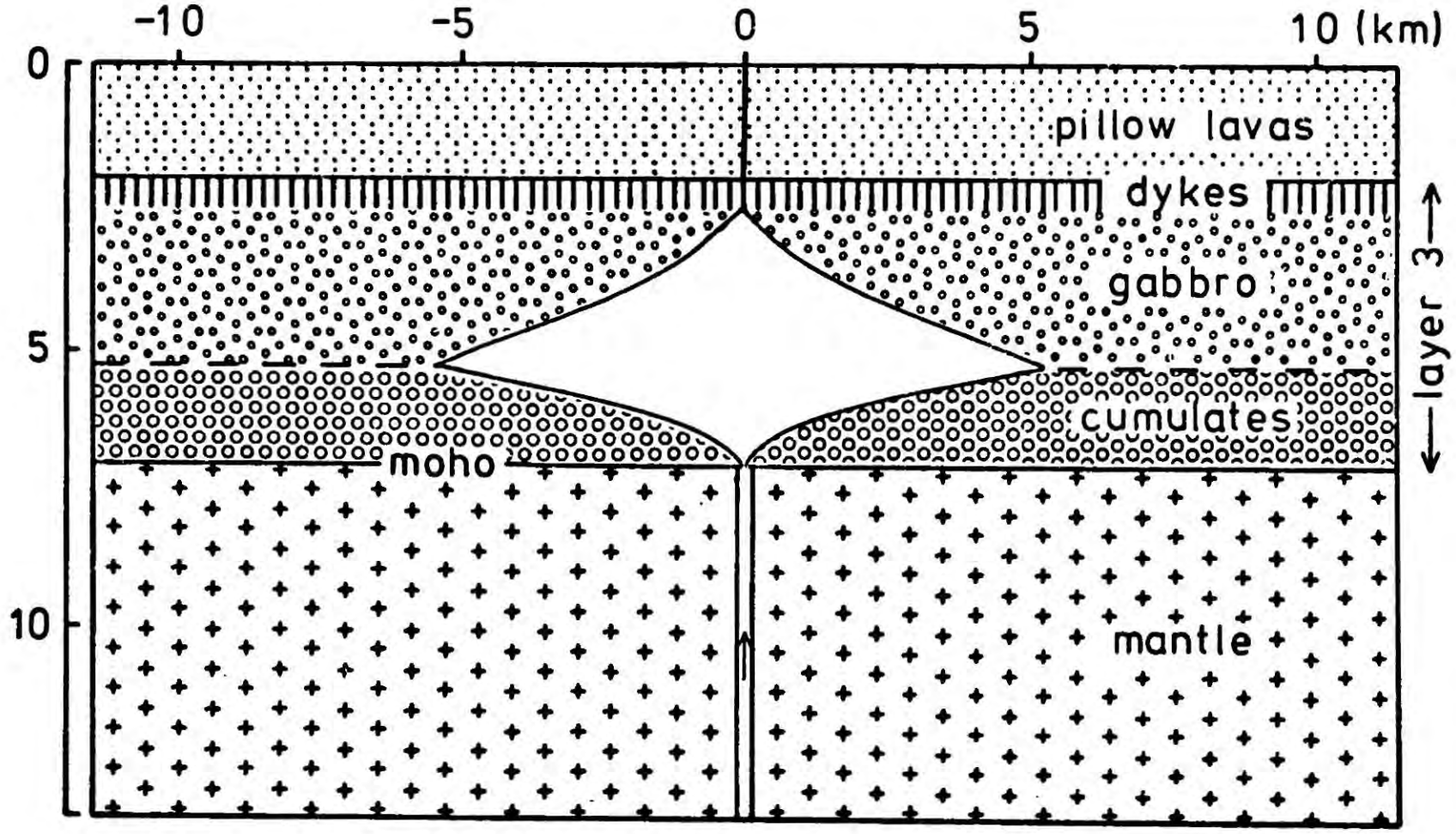

Figure 5.14 Model to show formation of oceanic crust.

CHAPTER 6

INTRUSION STRESSES IN THE OCEAN LITHOSPHERE AT THE RIDGE CREST

6.1 Introduction

In this chapter, the stresses in the oceanic lithosphere resulting from the existence of a magma chamber in the lower oceanic crust and the intrusion of asthenospheric material into the lithosphere at the ridge axis are investigated. The forces exerted by the intruding material are applied to an elastic lithosphere model and the method of finite element is used to calculate the stresses. Analytical studies of the stresses caused by intruding bodies (Piper and Gibson, 1972) require simplifying assumptions for the force distribution and geometry, while the numerical method of finite element allows a more realistic model of the intrusion to be investigated.

6.2 Forces exerted on the lithosphere by the asthenosphere in the accretion process

The petrological model of the accretion process proposed by Cann (1970, 1974) suggests that the nature of the material intruding into the lithosphere is dependent on depth. In the lower crust the intruding material takes the

form of a basaltic liquid/crystal mush which may form a magma chamber. In the upper mantle, the intruding material consists of a mush of basalt liquid and ultramafic crystals. The mush contains an increasingly higher proportion of the basalt melt with decreasing depth (Lachenbruch, 1973) such that at the Moho it is entirely basalt liquid. At the level of fractionation of the upwelling asthenosphere the composition of the mush should correspond approximately to that of the primitive asthenosphere. Following Green and Ringwood (1969) a depth of 30 km is taken for the level of fractionation. Below the level of fractionation, the intrusive material takes the form of a partial melt of the mantle.

The intruding material exerts a force on the lithosphere because of its excess pressure with respect to the surrounding lithosphere. The excess pressure originates from the negative density contrast of the intruding material with respect to the lithosphere. For the following calculation of the intrusion stresses the simplifying assumption is made that the lithosphere behaves as an elastic solid, while the asthenosphere and intruding material behaves as a fluid.

Stresses in the lithosphere, neglecting those due to the intrusion forces are assumed to be hydrostatic (Chapter 3) and consequently the pressure at any point in

the lithosphere due to the body forces is given by

$$P_L(z) = \int_0^z \rho_L(z)\, g\, dz \qquad 6.1$$

where z is the depth (positive downwards), g is the gravitational acceleration, and $\rho_L(z)$ is the density of the lithosphere as a function of depth in the vicinity of the ridge axis. If P_o is the pressure at the base of the lithosphere adjacent to the ridge axis and ρ_I is the density of the intruding material, then the pressure in the intruding liquid is given by

$$P_I(z) = P_o - \int_z^T \rho_I(z)\, g\, dz \qquad 6.2$$

where T is the lithosphere thckness.

It is assumed that the pressure in the asthenosphere at the asthenosphere-lithosphere boundary is uniform in the immediate vicinity of the ridge axis. Hence the pressure at the base of the lithosphere is simply

$$P_o = \int_0^T \rho_L(z)\, g\, dz \qquad 6.3$$

Therefore the lateral difference in pressure between lithosphere and intruding fluid is given by the expression

$$\Delta P(z) = P_I(z) - P_L(z) \qquad 6.4$$

$$= \int_z^T \Delta\rho(z)\, g\, dz$$

where $\Delta\rho(z) = \rho_L(z) - \rho_I(z)$ 6.5

Thus, if $\Delta\rho(z)$ is everywhere positive, there is higher pressure in the intruding material than the lithosphere. This excess pressure is zero at the asthenosphere-lithosphere boundary and increases upwards becoming a maximum in the upper crust.

The density contrast $\Delta\rho(z)$ of equation 6.4 is a function of depth. In the lower crust the density contrast, $\Delta\rho(z)$, is the difference in density between basalt liquid and the solid lithosphere laterally adjacent. In the upper mantle above 30 km depth $\Delta\rho(z)$ is given by the density contrast of the ultramafic crystal/basalt liquid mush with the surrounding upper mantle. Below the level of basalt liquid fractionation, the density contrast, $\Delta\rho(z)$, is taken as the density difference between the partial melt and the solid lithosphere. An estimate of a 10% melt in this region (30 km to 80 km depth) is used.

Consequently, the density contrast as a function of depth below the ocean floor is as follows.

(a) 2 km to 7 km (oceanic layer 3) $\Delta\rho$ = 0.3 gm/cc

(b) 7 km to 30 km (upper mantle) $\Delta\rho$ = 0.5 gm/cc at Moho

$\Delta\rho$= 0.2 gm/cc at 30 km

(c) 30 km to 80 km (lower lithosphere) $\Delta\rho$= 0.03 gm/cc

The force applied to the lithosphere by the intruding asthenosphere not only depends on its excess pressure given by equation 6.4, but also on the shape of the intruding material. The shape of the intruding material present in the magma chamber of the lower oceanic crust has been discussed in detail in Chapter 5. Little is known of the shape of the intruding material in the mantle. Theoretical studies (Oldenburg, 1975) and analysis of surface wave dispersion data (Forsyth, 1975) suggest that the lithosphere thickens only very slowly away from the ridge axis. However, the extent of the intrusion at the ridge axis is very narrow, a few kilometers wide (Matthews and Bath, 1967; Francis and Porter, 1973) which suggests a relatively narrow zone of fractionation and partial melting in the mantle at the ridge axis. The width of the mobile zone in the lithosphere at the ocean ridges has been discussed in greater detail by Cann (1974).

6.3 The lithosphere model and finite element subdivision

The lithosphere model, used for the calculation of the intrusion stresses, is 80 km thick (Haigh, 1973; Kanomori and Press, 1970) and extends 1500 km from the ridge axis. Only one half of the ocean rise structure is considered in the calculation by the assumption of symmetry about the

ridge axis.

Uniform elastic constants are assumed throughout the model; values of Young's modulus of 10^{12} dynes/cm^2 and Poisson ratio 0.25 are used. These values correspond approximately to those of the ocean crust (Beaumont and Lambert, 1972). Uniform lithospheric elastic constants are used, simplifying the construction of the finite element grid, since no crustal-mantle interface need be included in the model.

Plane strain in the direction parallel to the ridge axis is assumed, thus reducing the calculations to one of two dimensions only. It is felt that this is a valid assumption, provided the length of the ocean ridge is large in comparison to the lithospheric thickness and ocean width.

Stresses due to the density load of the lithosphere have been assumed to be hydrostatic and have not been included in the calculation, but may easily be added to the intrusion stresses by the principle of stress superposition (Hafner, 1951). The hydrostatic body force stresses are calculated assuming a 7 km thick oceanic crust of density 2.8 gm/cc, an upper mantle density of 3.15 gm/cc and an ocean depth of 3 km at the ridge axis. These densities correspond to those suggested by Talwani et al. (1965) for the oceanic lithosphere at ocean rises.

In figures 6.1 and 6.2 the finite element representation of the lithosphere is shown. Elements are smaller in the region adjacent to the ridge crest allowing greater resolution in this region where intrusion stresses are of greatest magnitude. The magma chamber dimensions are those predicted by the solidification studies of the ocean crust for a half spreading rate of 1cm/yr. Elements corresponding to the magma chamber are given a Young's modulus of 1.0 dyne/cm^2, representing the weak molten magma chamber material.

Vertical displacement of the upper surface of the lithosphere, in response to the application of intrusion forces on the lithosphere, will be opposed by isostatic restoring forces (Walcott, 1970) which have been described in Chapter 4. The isostatic restoring forces are incorporated in the finite element formulation discussed in the next section.

The asthenosphere-lithosphere boundary of the model is allowed to undergo free elastic displacement since the asthenosphere is assumed to behave as a fluid (Heiskanen and Vening Meinesz, 1958). The model is constrained horizontally and vertically at the end of the model remote from the ridge axis, in order to prevent free rotation and translation of the model as a whole. The ridge axis of the lithosphere is constrained for zero horizontal displacement

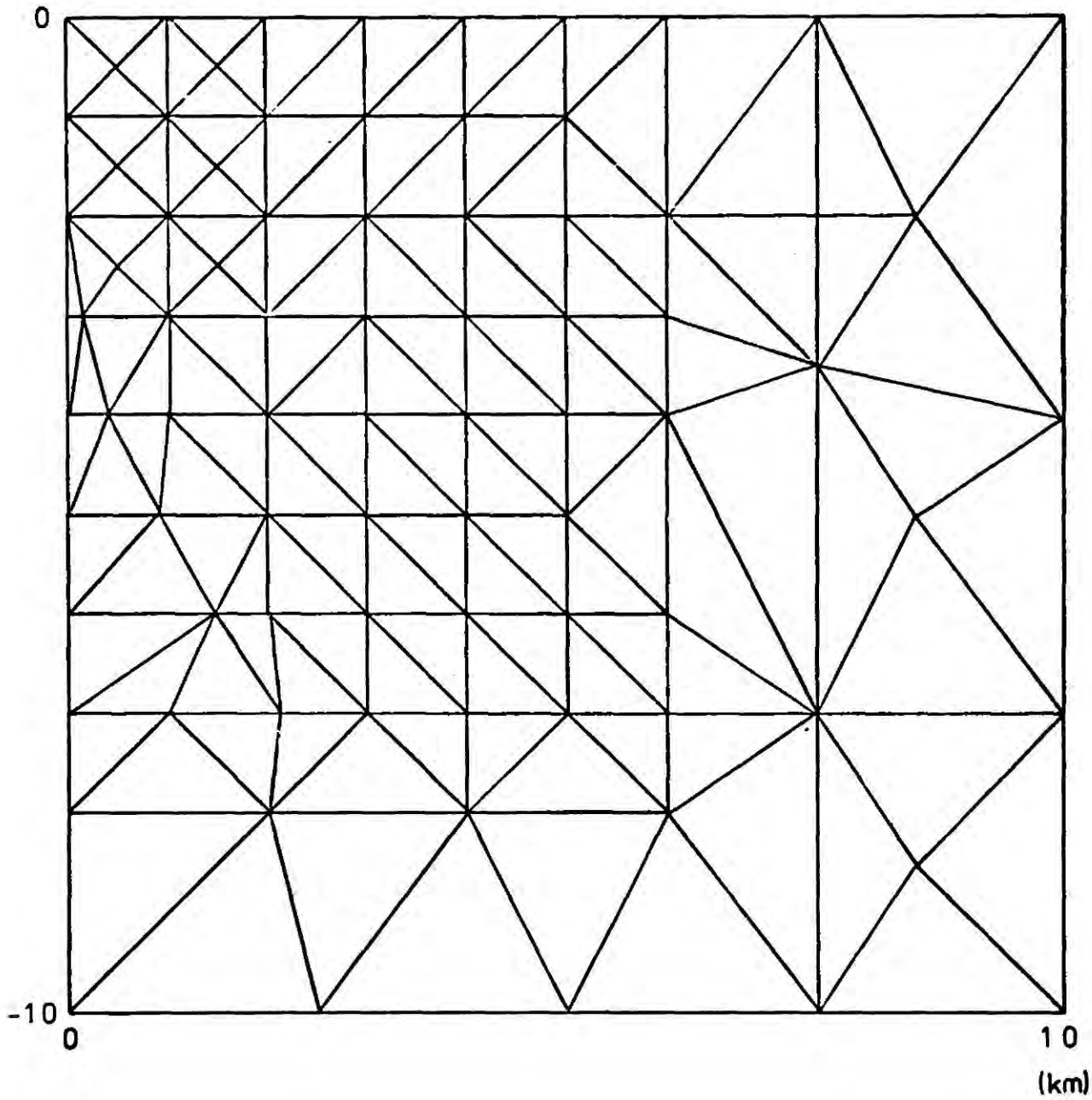

Figure 6.1 Finite element subdivision of lithosphere model adjacent to ridge axis.

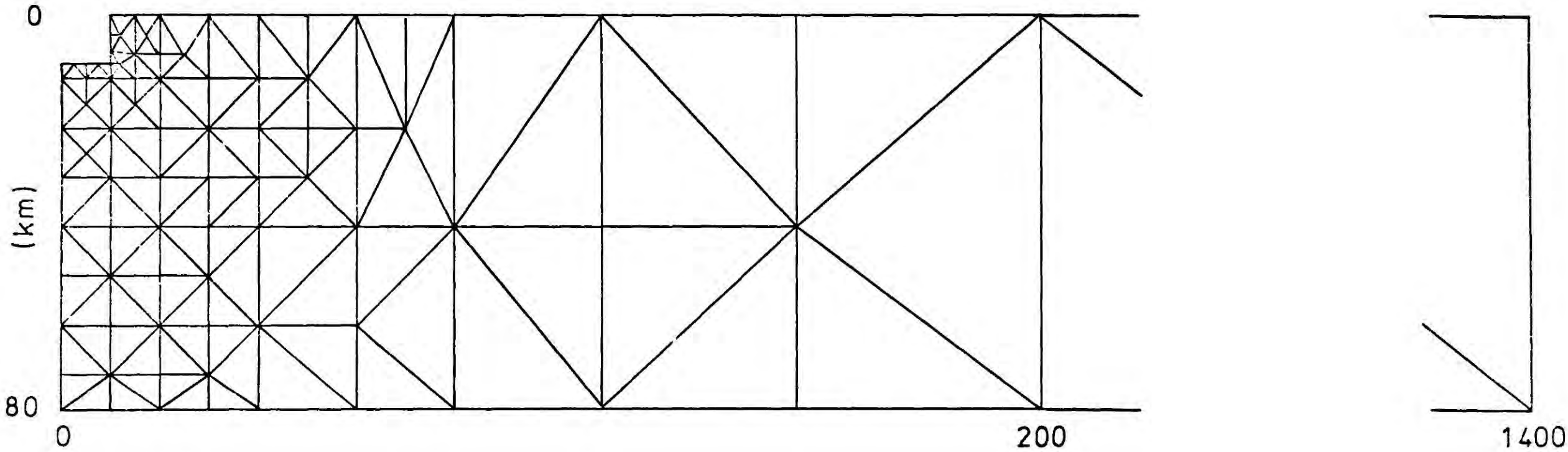

Figure 6.2 Finite element subdivision of the remaining lithosphere model.

above the level of intrusion, since the material corresponds to unfractured lithosphere.

6.4 Finite element formulation and application

The finite element method of stress analysis has already been described in Chapter 2 and used in Chapters 3 and 4. In this chapter, the methods is used to evaluate the elastic response of the lithosphere to applied forces. The finite element equation of equilibrium for an elastic continuum is given by equation 2.21 and is

$$[K]\{\delta\} = \{R\} \qquad 6.6$$

where $[K]$ is the stiffness matrix, $\{\delta\}$ is the vector of nodal elastic displacements and $\{R\}$ is the vector of applied nodal forces.

The isostatic restoring forces along the upper boundary are applied in the same way as in Chapter 4, for the calculation of thermal stresses. The equation of equilibrium, incorporating the effect of restoring forces is from equation 4.13

$$[K]\{\delta\} + [S]\{\delta\} = \{R\} \qquad 6.7$$

where $[S]$ is a matrix representing the effect of the isostatic restoring forces. As in Chapter 4 a new matrix

is constructed such that

$$[K]'\{d\} = \{R\} \qquad 6.8$$

where

$$[K]' = [K] + [S] \qquad 6.9$$

The matrix $[S]$ is constructed according to equation 4.14. A density contrast of 2.0 gm/cc is used between ocean and lithosphere. It is to equation 6.8 that the displacement boundary conditions are applied.

Intrusion forces are exerted along the whole of the boundary between solid lithosphere and intruding asthenosphere. The approximation is made that this interface is vertical in the mantle. Forces are integrated along the intrusion boundary and applied to the boundary nodes of the finite element model as components of the applied nodal force vector $\{R\}$. The force exerted on the solid lithosphere by the intruding asthenosphere is normal to the boundary separating the two regions, and it is necessary to resolve the force into horizontal and vertical components when constructing the force vector $\{R\}$. The force applied to a boundary node is calculated by integrating the forces along the boundary nearest to that boundary node.

Solution of equation 6.8 for elastic displacement was carried out by the Seidel-Gauss method. Strain and stress

were calculated from the elastic displacement vector according to equations 2.10 and 2.11.

The stresses calculated by the finite element method have been interpreted in terms of fracture of the lithosphere by application of the Griffith's theory of brittle failure (Murrell, 1958). This theory of brittle failure will only apply for material which is cool and therefore brittle. Consequently its use is restricted to the upper oceanic crust which is cooled by water circulation (Lister, 1974). Service and Douglas (1973) have described the application of this failure criterion to the stresses produced by a finite element analysis. The failure theory assumes the existence of microcracks in the rock material, which by concentrating stress at their tips, cause failure.

Three regions of brittle failure are postulated;

(a) a tensional region of failure,

(b) a compressional open crack region, and

(c) a compressional closed crack region.

The failure criterion is expressed in terms of the minimum principal stress, R, the maximum principal

stress P (compressional negative) and the tensile strength of the material, T. Brace (1961) has suggested a value of T of approximately 0.5 kb for igneous rocks.

Failure criterions for the three regions are as follows:

(a) Tensional failure occurs in the stress region defined by $3P + R \geqslant 0$ when $P - T \geqslant 0$. The plane of fracture is perpendicular to the direction of the largest tensional stress.

(b) Open crack compressional failure occurs in the region defined by $3P + R \leq 0$ when

$$-\frac{(P-R)^2}{8(P+R)} - T \geqslant 0 \qquad 6.10$$

The plane of failure is orthogonal to the plane containing P and R and has an angle θ with the direction of the stress R where

$$\cos 2\theta = -\frac{(P-R)}{2(P+R)} \qquad 6.11$$

(c) If the stress is large enough to close the cracks, the failure region becomes that of closed crack compressional failure with failure occurring when

$$(P + R) + \alpha (P - R) - 4T\left(1 - \frac{\sigma_c}{T}\right)^{1/2}/\mu - 2\sigma_c \geq 0 \qquad 6\text{-}12$$

where σ_c is the stress required to close cracks, μ is the coefficient of friction and $\alpha = (1 - \mu^2)^{1/2}/\mu$

The angle of failure ϑ is given by

$$\tan 2\vartheta = \frac{1}{\mu} \qquad 6\text{-}13$$

Murrell (1965) suggested a value of 1.09 for μ and $-4.19\,T$ for σ_c .

The above failure criteria assume that the effect of the intermediate principal stress may be neglected. Murrell and Digby (1965) have shown that the intermediate stress has a negligible effect on the onset of fracture. Pore pressure has not been included in the above fracture analysis, although it is very important, since the pore pressure distribution is not known.

6.5 The lithosphere stress field resulting from the magma chamber

The buoyancy of the magma chamber in the lower crust will give rise to tensional stresses in the oceanic crust above the magma chamber, the upthrust arising from the density contrast of about -0.3 gm/cc between basaltic magma and the largely doleritic and gabbroic oceanic layer 3.

In figure 6.3 the stresses in the upper lithosphere at the ridge axis resulting from the presence of the magma chamber, for a half spreading rate of 1 cm/yr, are shown. The convention of representation is that defined in Chapter 4. Above the chamber, in the upper crust, horizontal tensions occur. The stresses produced by the magma chamber together with the hydrostatic load stresses, are shown in figure 6.4. It can be seen that the departure of the total stress field from hydrostatic is very small. Application of the modified Griffiths' criterion of brittle failure suggests that the total stress field does not cause fracture of the oceanic crust. The contoured maximum deviatoric stresses are shown in figure 6.5.

The results of the finite element stress analysis therefore suggest that the magma chamber in the lower crust is stable and cannot, without additional stress fields, fracture the crust allowing the basaltic liquid to escape from the chamber.

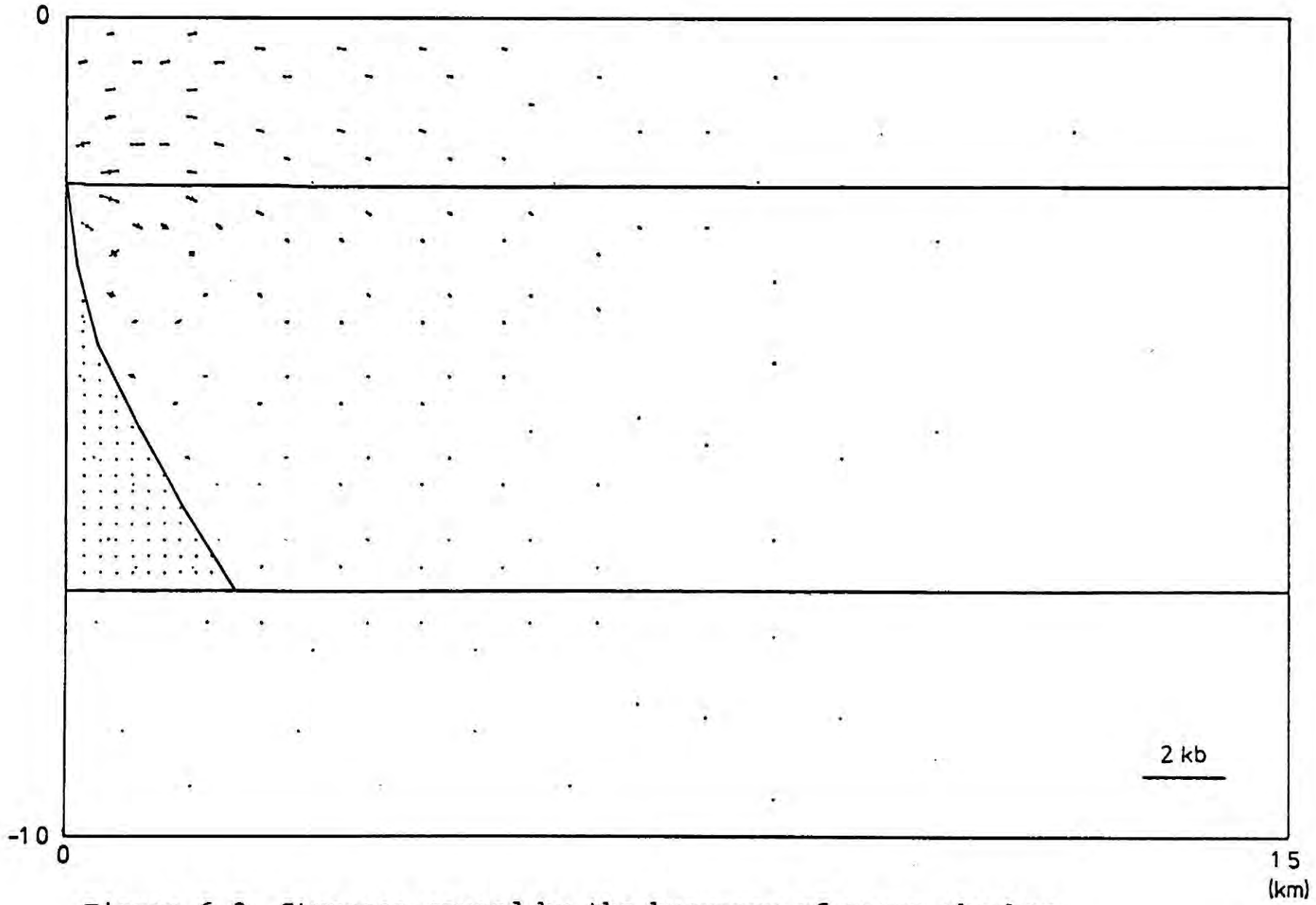

Figure 6.3 Stresses caused by the buoyancy of magma chamber. Magma chamber is signified by stippled region.

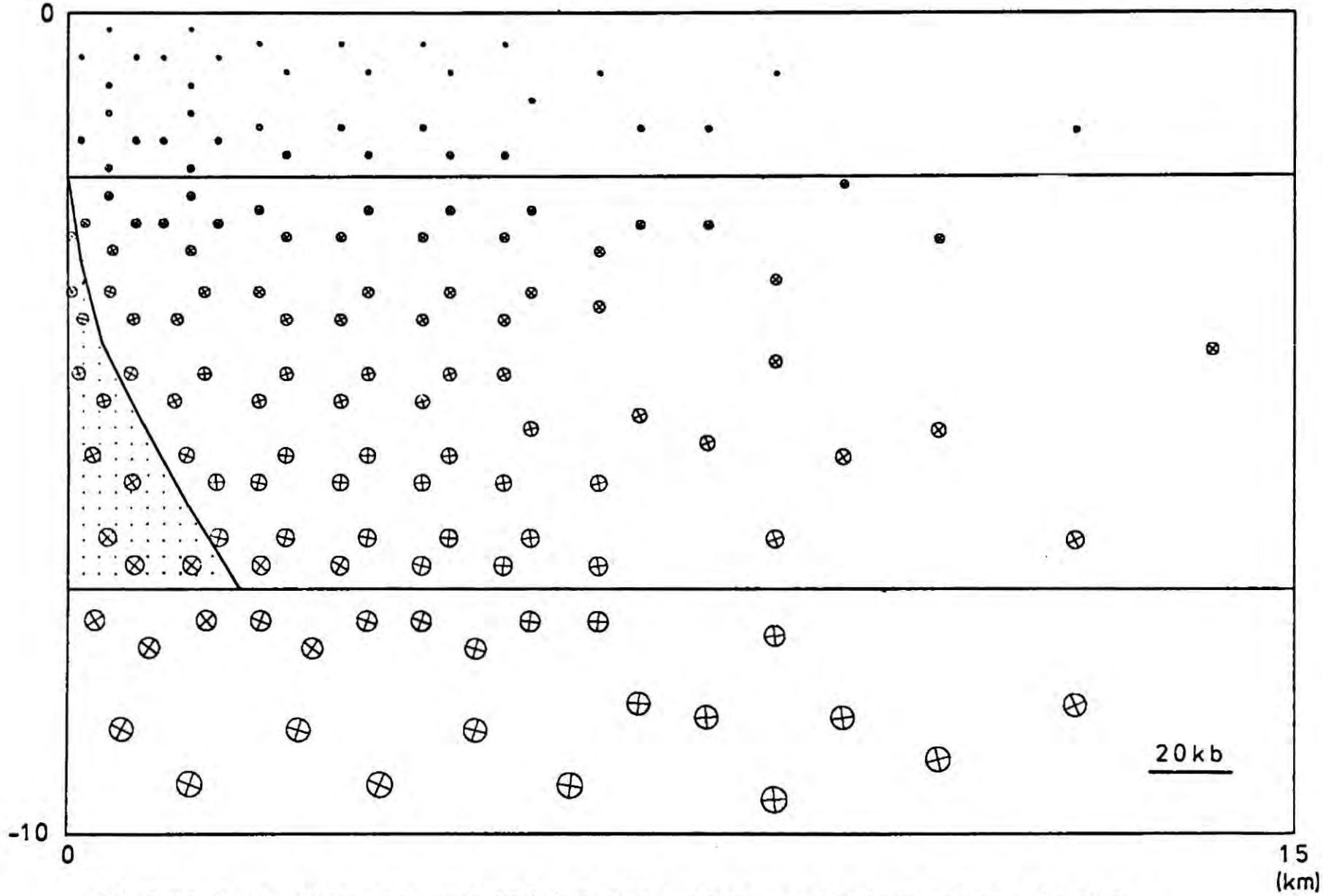

Figure 6.4 Stresses caused by the buoyancy of the magma chamber together with hydrostatic load stresses.

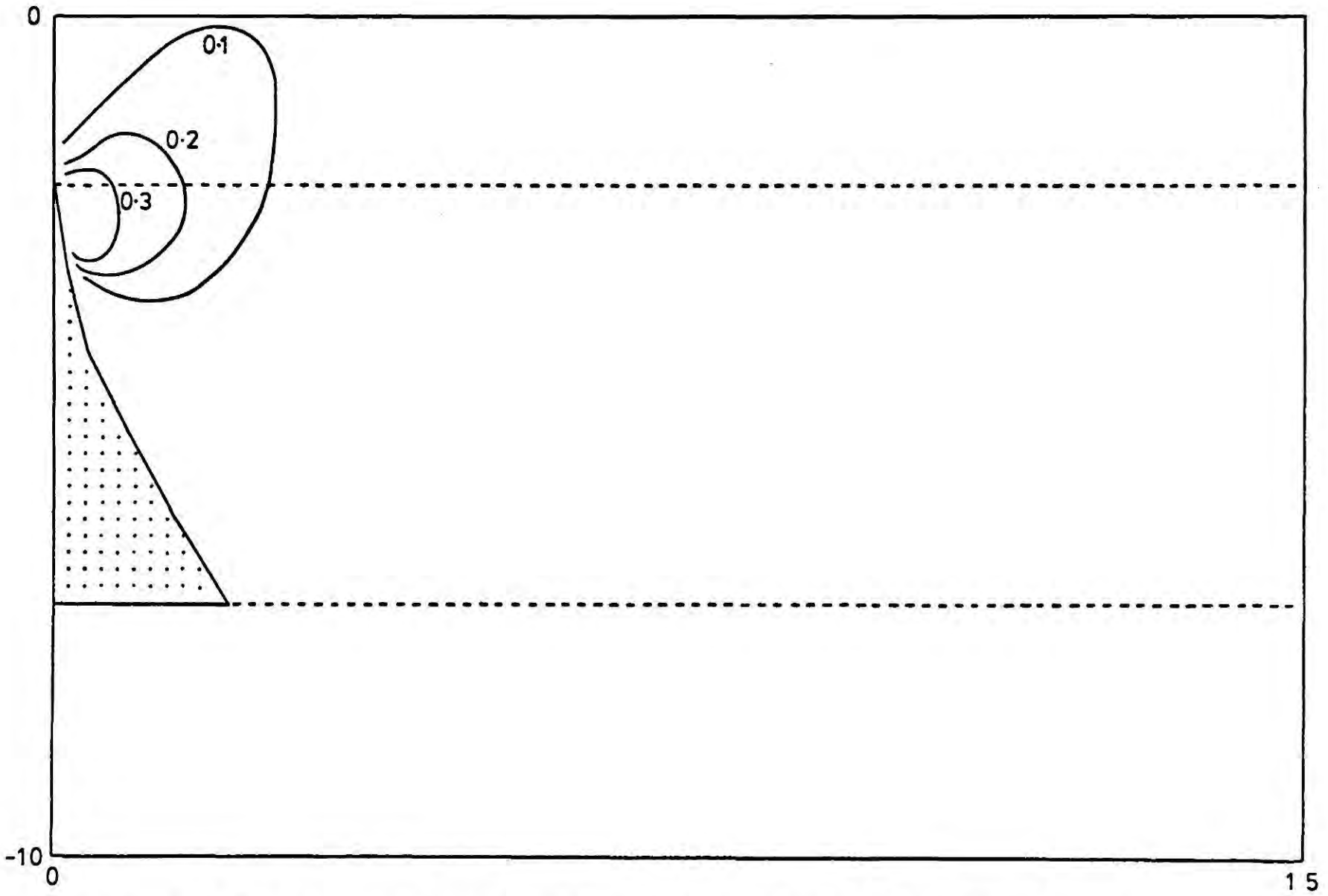

Figure 6.5 Maximum deviatoric stress contours (kb) for stress field arising from buoyancy of magma chamber.

6.6 The stress field resulting from the intrusion of asthenospheric material

In this section the stress field caused by intruding asthenosphere, extending from the bottom of the lithosphere up into the magma chamber of the lower crust is investigated.

The stresses, calculated by the finite element method, are shown in figure 6.6 for the upper lithosphere adjacent to the ridge axis. Large tensions exist in the upper crust, with the largest tensional stress horizontal. Greatest stresses occur immediately above the top of the magma chamber. The total stresses, intrusion stresses together with hydrostatic load stresses, are shown in figure 6.7. With increasing depth, the stresses become compressional as the hydrostatic load stresses exceed the largely tensional intrusion stresses.

The zone of failure predicted by application of the modified Griffiths' theory of brittle fracture is shown in figure 6.8, together with contoured maximum deviatoric stress. Application of the failure criterion is probably only valid for the upper two kilometers or so of the oceanic crust, which is sufficiently cool to be brittle. The orientations of the stresses in the predicted failure zone suggest vertical fissures with their plane parallel to the ridge axis. Those fissures connecting with the magma chamber would most probably form dykes carrying the basalt

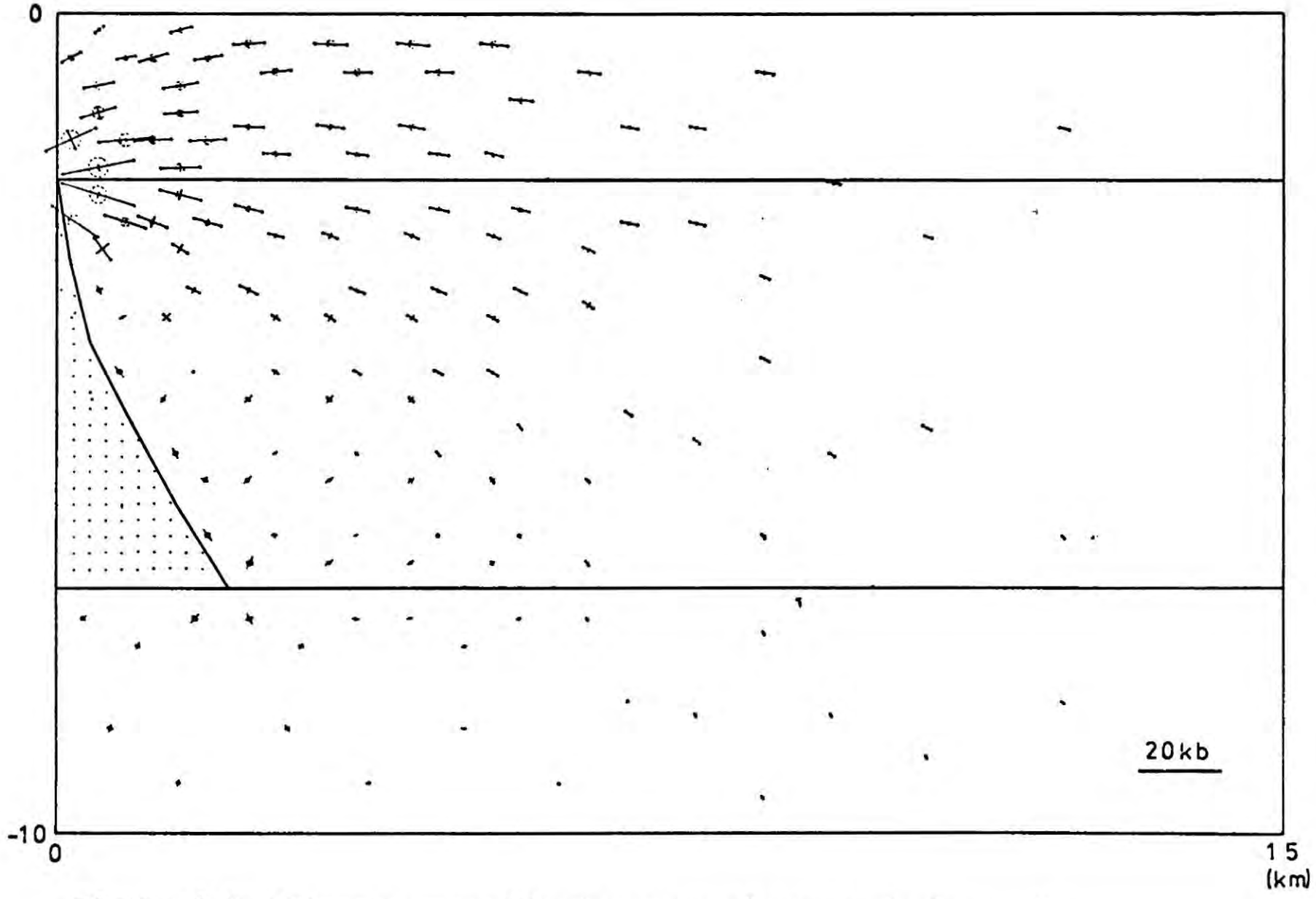

Figure 6.6 Stresses caused by buoyancy of magma chamber and molten material in upper mantle.

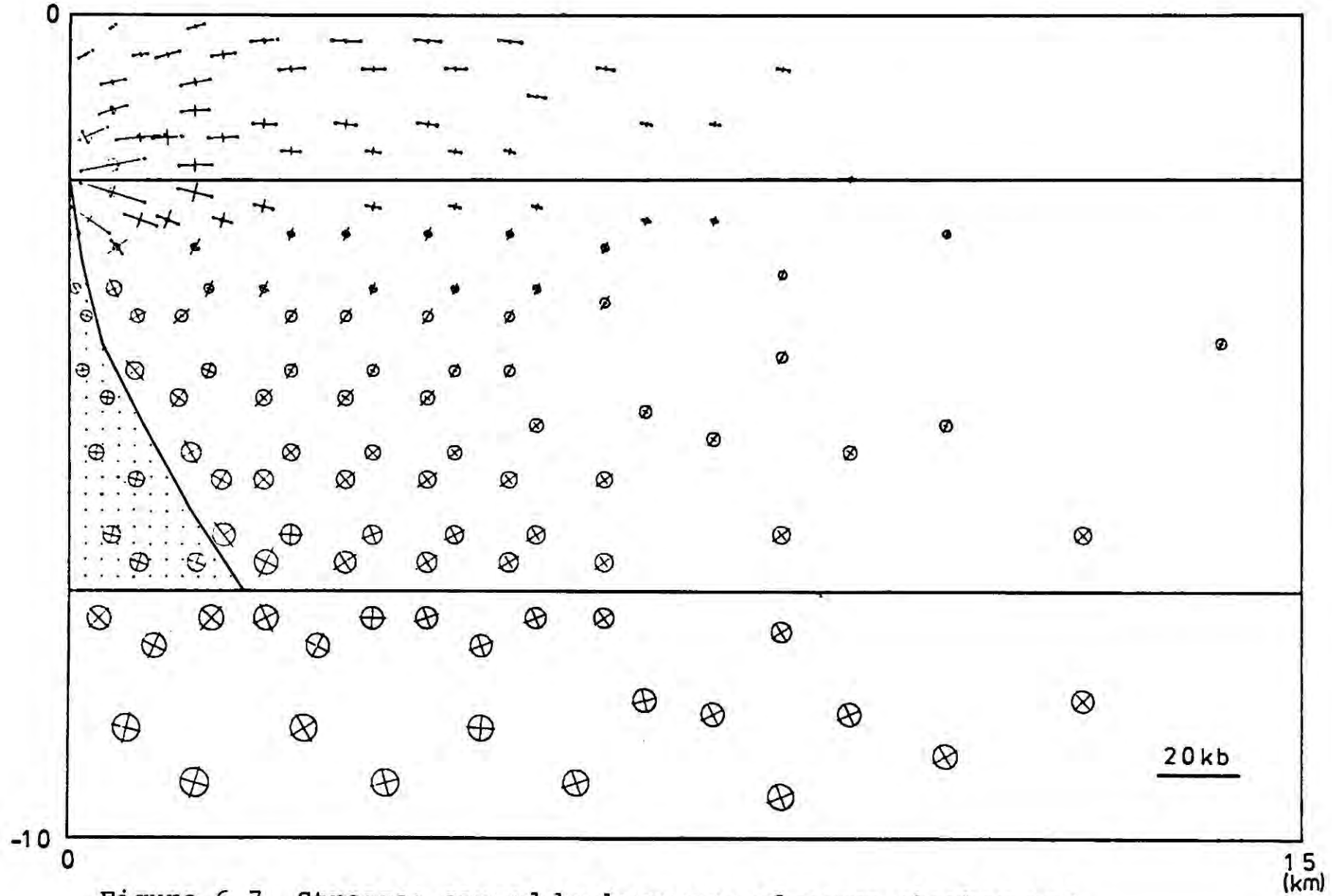

Figure 6.7 Stresses caused by buoyancy of magma chamber and molten material in upper mantle together with hydrostatic load stresses.

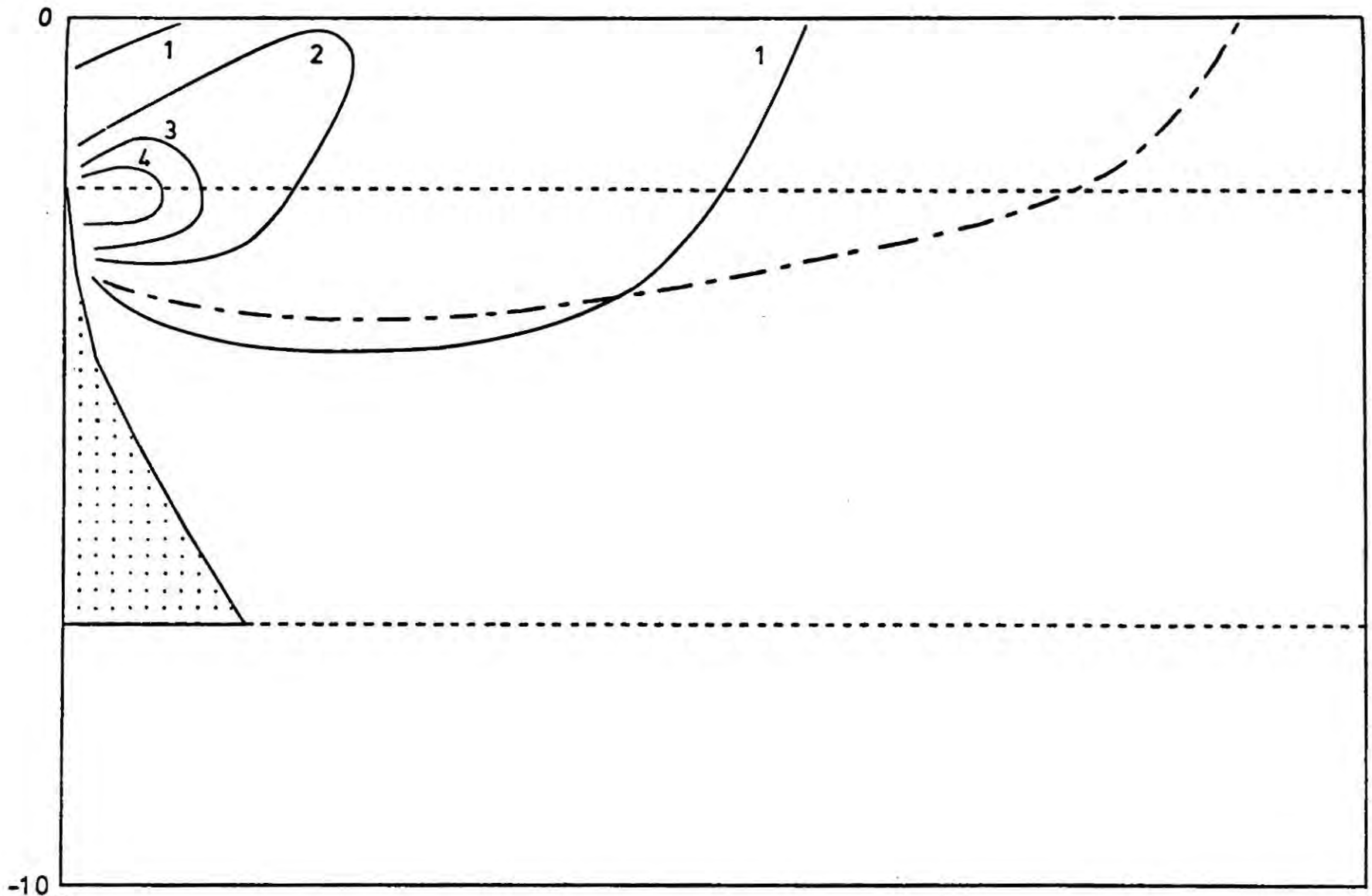

Figure 6.8 Maximum deviatoric stress contours (kb) for stress field arising from buoyancy of magma chamber and molten material in upper mantle. Extent of predicted failure is shown by dash/dot line.

liquid to the surface.

Figure 6.8, displaying the maximum deviatoric stress, shows a zone of high deviatoric stress extending upwards at approximately 45° to the vertical. At the ocean floor the two zones of high deviatoric stress, one either side of the ridge axis, would enclose a region of about 5 km width. It is expected that the crustal fracture would be restricted to this zone. Fracture extending through the crust would allow the dissipation of the intrusion pressures of the upwelling asthenosphere and so relieve the lithosphere intrusion stresses.

The shape of the magma chamber controls the distribution of the intrusion forces in the ocean crust. Furthermore, the shape of the magma chamber was shown in Chapter 5 to be critically controlled by crystal settling and the sea floor spreading rate. In figure 6.9 the intrusion stresses, together with the hydrostatic load stresses, are shown for a magma chamber with crystal settling. The deviatoric stresses are shown together with the region of predicted fracture in figure 6.10. The calculations suggest that the stress field is not affected by crystal settling to any great extent.

In figure 6.11 the maximum deviatoric stresses and the predicted failure regions are compared for the three half spreading rates of 0.5 cm/yr, 1.0 cm/yr and 3.0 cm/yr. It

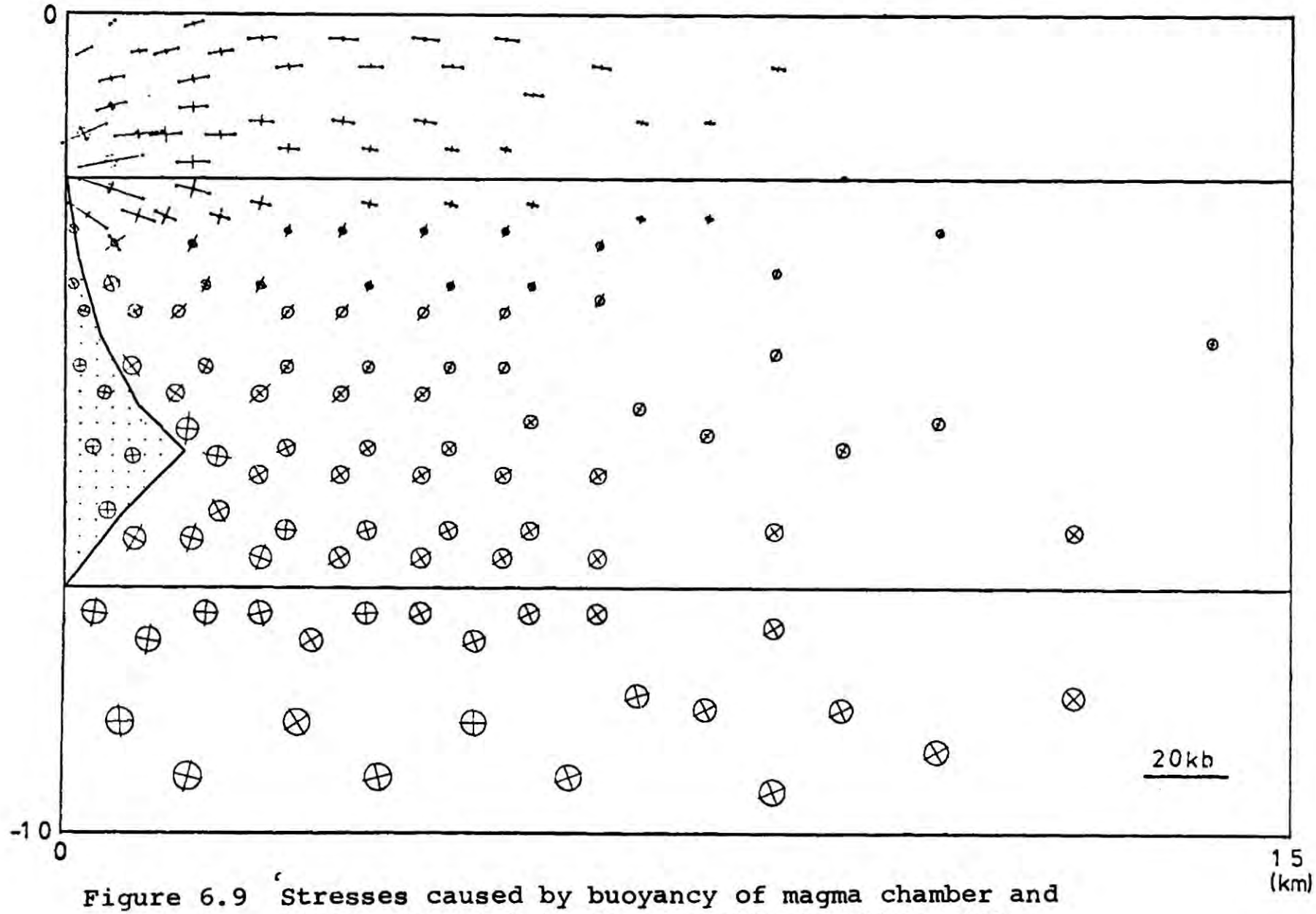

Figure 6.9 Stresses caused by buoyancy of magma chamber and molten material in upper mantle together with hydrostatic load stresses for magma chamber with crystal settling.

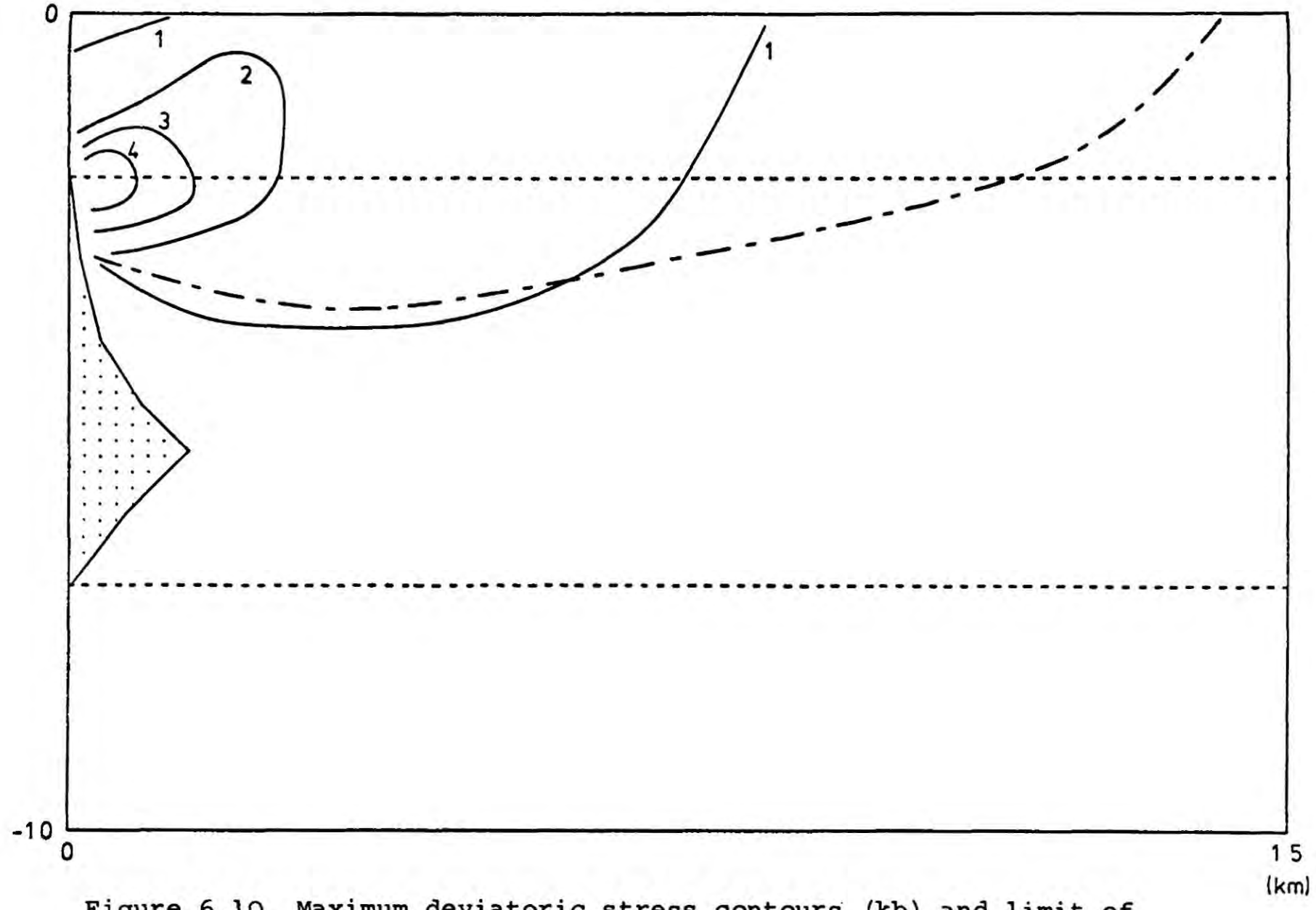

Figure 6.10 Maximum deviatoric stress contours (kb) and limit of failure for buoyancy of molten material in upper mantle and magma chamber with crystal settling.

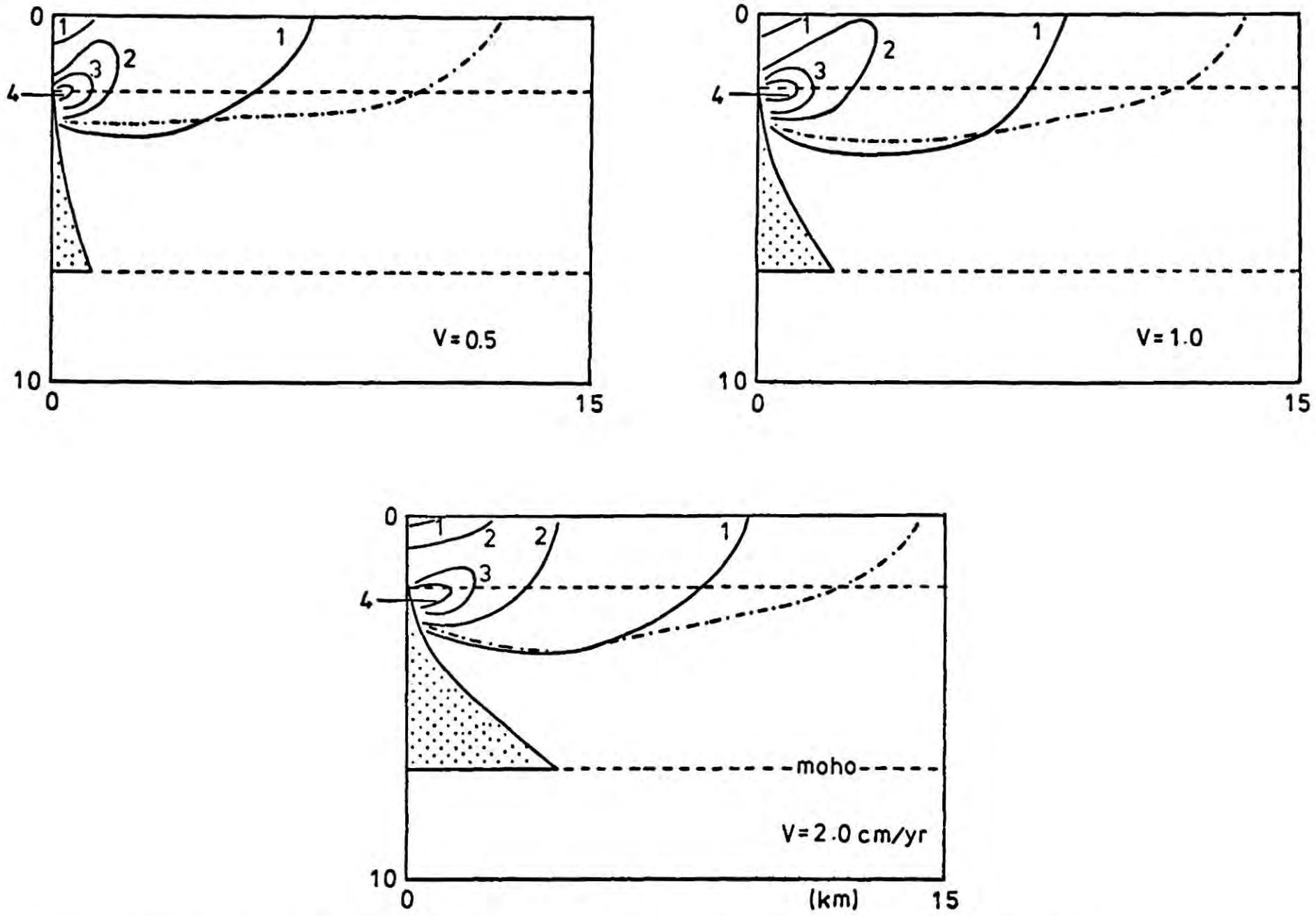

Figure 6.11 Maximum deviatoric stress contours (kb) and limit of failure as function of half spreading rate (cm/yr).

is suggested, from the calculations that an increase in spreading rate causes a slight increase in the magnitude of the tensional intrusion stresses. A slight increase in the width of the zones of maximum deviatoric stress and predicted fracture are also noted.

6.7 Conclusion

The stress fields in the oceanic lithosphere at the ridge axis arising from the presence of a magma chamber in the oceanic crust and the intrusion of asthenospheric material into the ocean lithosphere have been calculated by elastic finite element analysis. The magnitude of the calculated stresses arising from the magma chamber in the oceanic crust is insufficient to cause fracture of the oceanic crust. It is suggested that the magma chamber is not able, alone, to cause the intrusion of its contents into the upper crust and out onto the ocean floor and consequently is a stable structure.

The calculated stresses in the lithosphere at the ridge axis arising from the intrusion of asthenosphere material in addition to those due the magma chamber are of sufficient magnitude to cause absolute tension in the upper crust. Application of the Griffith's theory of brittle failure predicts that fracture occurs in the upper crust. The orientation of the stresses suggests that fracture of the

ocean crust is of the form of vertical fissures parallel to the ridge axis. Consideration of the zones of maximum deviatoric stress suggest that the width of the region of fracture is of the order of 5 km.

The stress field does not appear to be strongly dependent on the half spreading rate or the proportion of crystal settling in the magma chamber.

CHAPTER 7

THE LITHOSPHERIC STRESS FIELD CAUSED BY A MANTLE PLUME

7.1 Introduction

The existence of mantle plumes and their associated hot spots (Vogt, 1971, 1972, 1974; Morgan, 1971, 1972) is at present more speculative than proven. Movement of lithospheric plates over mantle hot spots has been suggested as an explanation for the origin of some island chains and aseismic ridges (Morgan, 1972) while asthenosphere flow, resulting from mantle plumes, has been put forward as an explanation for the echelon topographic features of the Reykjanes ridge (Vogt, 1971, 1974). Geochemical evidence for plumes has also been offered (Schilling, 1973). It is proposed that plumes transport mantle material and heat up from the lower mantle and then disperse by lateral flow in the asthenosphere (Vogt, 1971, 1974). The dimensions and velocities of mantle plumes, assuming that they exist, is unknown. Morgan (1972) suggested a diameter of 150 km with an upward flow of about 2 m/yr.

Flow in the asthenosphere away from the plume axis would produce stresses in the overlying lithosphere as a consequence of drag exerted on the lower boundary of the

lithosphere (Morgan, 1972). It has been suggested that these stresses may play an important part in plate tectonics (Morgan, 1972). Previous calculations of the stresses exerted on the lithosphere by this cause have assumed a fluid model of the lithosphere (Tryggvason, 1974). In the following work the stresses in an elastic lithosphere are calculated. Radial flow of the dispersing plume material in the asthenosphere is assumed. The vertical forces exerted on the overlying lithosphere by the plume motion are neglected since they may be shown to be small.

7.2 Asthenospheric velocity distribution

In order to calculate the stresses exerted on the overlying oceanic lithosphere by moving asthenosphere material it is necessary to obtain an expression for the horizontal velocity distribution in the asthenosphere. The plume model assumes that the vertically rising plume material disperses radially into the asthenosphere on encountering the overlying lithosphere. Below the asthenosphere, the plume is represented by vertical flow of material in a circular pipe. A steady state velocity distribution is assumed throughout. The flow model is shown diagrammatically in figure 7.1.

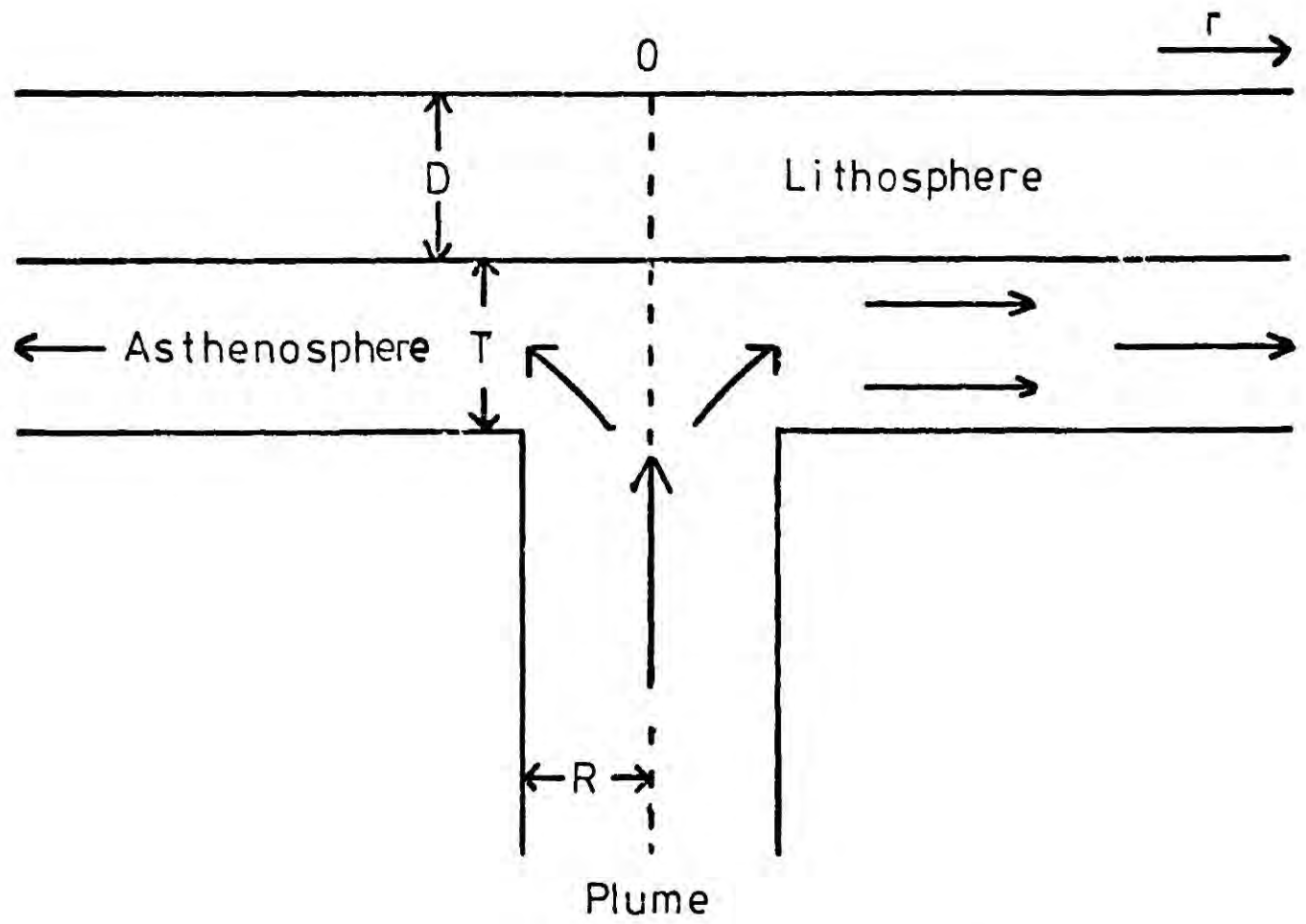

Figure 7.1 The mantle plume model showing material rising vertically at plume axis and flowing radially away in the asthenosphere.

For the plume material rising vertically at the plume axis, the steady state velocity is that of a circular pipe and is given as a function of radius r by

$$v(r) = \frac{V_{max}}{R^2} \left(R^2 - r^2 \right) \qquad 7.1$$

where Vmax is the velocity of the flow at the pipe centre and R is the pipe radius.

The radial dispersion of the plume on encountering the lithosphere may be treated as a jet of viscous fluid encountering a flat infinite plate and then spreading radially outwards between two plates; the gap between the two plates representing the asthenosphere. For this situation, the radial flow $u(r)$, at large distances from the plume axis is given by

$$u(r) = -\frac{K}{r\, 2\pi\eta} \left(z^2 - z\,T \right) \qquad 7.2$$

where K is a constant related to the driving force of the flow, T is the asthenosphere thickness and z is measured positive downwards.

Equating the total flux of material rising in the plume and dispersing radially in the asthenosphere, the radial velocity may be rewritten,

$$u(r) = -\frac{6\, R^2\, V_{max}}{4\, r\, T^3} \left(z^2 - z\,T \right) \qquad 7.3$$

The drag exerted on the lithosphere's lower surface by

the asthenosphere motion is proportion to $\frac{du}{dz}$ which is from equation 7.3,

$$\frac{du}{dz} = \frac{6R^2 V_{max}}{4 r T^2} \qquad 7.4$$

at the asthenosphere-lithosphere boundary for large distance from the plume axis.

The analysis of a jet of viscous fluid impinging on a flat infinite plate has been carried out by Homann (1936). It is found that the value of $\frac{du}{dz}$ at the plate surface is directly proportional to the radius, r . No estimate of the proportional constant may be made since the analysis assumes a plate and jet of infinite radial extent. Thus, $\frac{du}{dz}$ at the asthenosphere-lithosphere boundary above the rising plume is given by

$$\frac{du}{dz} = J \cdot r \qquad 7.5$$

where J is an unknown constant.

Thus, summarizing, the vertical gradient of radial velocity is given by

$$\frac{du}{dz} = J \cdot r \qquad \text{for small } r$$

$$\frac{du}{dz} = \frac{6 R^2 V_{max}}{4 r T^2} \qquad \text{for large } r \qquad 7.6$$

A single continuous function which satisfies both of these limits is,

$$\frac{du}{dz} = \frac{1}{ar + b/r} \qquad 7.7$$

where $a = \frac{4T^2}{6R^2 v_{max}}$

and $b = 1/J$

A value of the parameter J may be estimated by considering the location of the maximum of the function of equation 7.7 which occurs when

$$r = \sqrt{\frac{b}{a}} \qquad 7.8$$

Assuming that this maximum occurs at a distance corresponding to the radius of the plume pipe, R, this gives a value of J such that

$$\frac{du}{dz} = \frac{6R^2 v_{max}}{4T^2}\left(\frac{r}{r^2 + R^2}\right) \qquad 7.9$$

For large radius, the radial velocity of asthenosphere flow, according to equation 7.3 was of the form

$$u(r) = -\frac{6R^2 v_{max}}{4 r T^3}\left(z^2 - zT\right) \qquad 7.10$$

Although the velocity function tends to zero with increasing radius, the total flux of radially flowing material in the asthenosphere is a constant independent of radius. In reality, the radial flow in the asthenosphere would be expected to cease at a finite distance from the plume axis, possibly as a consequence of the asthenosphere material having cooled and become denser, returning to the mantle. If the radius at which the downflow of asthenosphere material occurs is S, then the radial velocity as a function of r

becomes for large r

$$u = 0 \qquad r > S$$

$$u = -\frac{G R^2 V_{max}}{4 r T^3}(z^2 - 2T) \qquad r < S \qquad 7.11$$

Consequently for radius larger than S

$$\frac{du}{dz} = 0 \qquad 7.12$$

7.3 Force exerted on lithosphere

The radial flow of the asthenosphere exerts a drag on the base of the lithosphere, by virtue of the shear stress in the flowing material at this boundary. Shear stress is given by the expression below for a viscous fluid.

$$\tau_{zr} = \eta \frac{du(r)}{dz} \qquad 7.13$$

where η is viscosity. From equation 7.9 and 7.12 this becomes

$$\tau_{zr} = \eta \frac{G R^2}{4 T^2} \left(\frac{r}{r^2 + R^2} \right) \qquad r < S$$

$$\tau_{zr} = 0 \qquad r > S \qquad 7.14$$

The shear stress acting at the base of the lithosphere will cause a stress field in the lithosphere as a whole. In the situation in which a shear stress is applied to the base of an infinite plate, the problem may be treated as a force applied to the bottom edge of the plate. If the plate

is assumed to be thin compared with its length, the force may be evenly distributed through the plate such that

$$\text{Radial force/unit area} = \frac{\tau_{rz}}{D}$$

where D is the lithosphere thickness. More explicitly, using equation 7.14 this becomes,

$$F(r) = \frac{G \eta R^2 v_{max}}{4 T^2 D} \left(\frac{r}{r^2 + R^2} \right) \qquad r<S \qquad 7.15$$

$$F(r) = 0 \qquad r>S$$

where $F(r)$ is the radial force/unit area.

7.4 The stress field of the lithosphere

A fundamental equation of the elastic continuum is the equilibrium equation which is

$$X_i = \rho \ddot{\omega}_i - \frac{\partial \sigma_{ji}}{\partial x_j} \qquad 7.16$$

where X_i is the force vector, ω the displacement vector, σ the stress tensor, and ρ the density. In this problem the inertial term may be neglected and in axisymmetric two dimensional polar coordinates the equation becomes

$$-F(r) = \frac{1}{r} \frac{d}{dr}(r \sigma_r) - \frac{\sigma_\theta}{r} \qquad 7.17$$

where $F(r)$ is the radial force component given by equation 7.15, σ_r , is the radial stress, and σ_θ , is the tangential stress. Fung (1965) has described in detail the mathematical properties of the elastic continuum. For the axisymmetric problem, the radial coordinate system is the principalized coordinate system of the stress field and so no shear stress, $\sigma_{r\theta}$, need be considered.

The relationship linking stress and strain for the axisymmetric case is as follows,

$$\begin{Bmatrix} \sigma_r \\ \sigma_\theta \end{Bmatrix} = \frac{E(1-\nu)}{(1+\nu)(1-2\nu)} \begin{bmatrix} 1 & \frac{\nu}{1-\nu} \\ \frac{\nu}{1-\nu} & 1 \end{bmatrix} \begin{Bmatrix} \varepsilon_r \\ \varepsilon_\theta \end{Bmatrix} \qquad 7.18$$

where

$$\begin{Bmatrix} \varepsilon_r \\ \varepsilon_\theta \end{Bmatrix} = \begin{Bmatrix} \frac{dw}{dr} \\ \frac{w}{r} \end{Bmatrix} \qquad 7.19$$

Then equation 7.17 becomes

$$-F(r) = \frac{E(1-\nu)}{(1+\nu)(1-2\nu)} \left[\frac{d^2w}{dr^2} + \frac{1}{r}\frac{dw}{dr} - \frac{w}{r^2} \right] \qquad 7.20$$

or more explicitly,

7.21

$$\frac{d^2w}{dr^2} + \frac{1}{r}\frac{dw}{dr} - \frac{w}{r^2} = -\frac{(1+\nu)(1-2\nu)}{E(1-\nu)} \cdot \frac{G\pi R^2 v_{max}}{4T^2 D} \left(\frac{r}{r^2+R^2} \right) \qquad r < S$$

$$\frac{d^2w}{dr^2} + \frac{1}{r}\frac{dw}{dr} - \frac{w}{r^2} = 0 \qquad r > S$$

Solution of the equations gives

$$\omega = -\frac{(1+\nu)(1-2\nu)}{E(1-\nu)} \quad \frac{6R^2 V_{max}}{16T^2 D}\left[\begin{array}{l} \log(R^2+r^2)\,r + Gr \\ + \frac{R^2}{r}\log(R^2+r^2) + \frac{H}{r} \end{array}\right] \qquad r<S \qquad 7.22$$

$$\omega = Ar + B/r \qquad r>S$$

where G, H, A, B are constants of integration.

At r = 0 and r = ∞ , the radial elastic displacement ω must be zero

Hence

$$H = -R^2 \log R^2$$

$$A = 0 \qquad 7.23$$

The two remaining constants of integration may be obtained from matching ω and $\frac{d\omega}{dr}$ for the two expressions at the point $r = S$. The matching of both of these functions is identical to matching the radial and tangential stress as well as displacement. The constants of integration have values as follows

$$G = -(1 + \log(S^2 + R^2))$$

$$B = Q\,(S^2 - R^2 \log(R^2+S^2)/R^2) \qquad 7.24$$

where

$$Q = \frac{(1+\nu)(1-2\nu)}{E(1-\nu)} \quad \frac{6R^2 V_{max}}{16T^2 D} \qquad 7.25$$

Hence the expressions for ω are

$$\omega = -Q\left(\log\frac{R^2+r^2}{R^2+S^2}\cdot r - r + \frac{R^2}{r}\log\frac{R^2+r^2}{R^2}\right) \qquad r<S$$

$$\omega = \frac{Q}{r}\left(S^2 - R^2\log\frac{R^2+S^2}{R^2}\right) \qquad r>S$$

7.26

Radial strain is given by

$$\frac{\partial\omega}{\partial r} = -Q\left(\log\frac{R^2+r^2}{R^2+S^2} + 1 - \frac{R^2}{r^2}\log\frac{R^2+r^2}{R^2}\right) \qquad r<S$$

7.27

$$\frac{\partial\omega}{\partial r} = -\frac{Q}{r^2}\left(S^2 - R^2\log\frac{R^2+r^2}{R^2}\right) \qquad r>S$$

and tangential strain by

$$\frac{u}{r} = -Q\left(\log\frac{R^2+r^2}{R^2+S^2} - 1 + \frac{R^2}{r^2}\log\frac{R^2+r^2}{R^2}\right) \qquad r<S$$

$$\frac{u}{r} = \frac{Q}{r^2}\left(S^2 - R^2\log\frac{R^2+S^2}{R^2}\right) \qquad r>S$$

7.28

From equation 7.18, the radial and tangential stresses are therefore

$$\begin{Bmatrix}\sigma_r\\ \sigma_\theta\end{Bmatrix} = -[D]\begin{Bmatrix}\log\frac{R^2+r^2}{R^2+S^2} + 1 - \frac{R^2}{r^2}\log\frac{R^2+r^2}{R^2}\\ \log\frac{R^2+r^2}{R^2+S^2} - 1 + \frac{R^2}{r^2}\log\frac{R^2+r^2}{R^2}\end{Bmatrix} \qquad r<S$$

$$\begin{Bmatrix}\sigma_r\\ \sigma_\theta\end{Bmatrix} = -[D]\begin{Bmatrix}\frac{1}{r^2}\left(S^2 - R^2\log\frac{R^2+S^2}{R^2}\right)\\ -\frac{1}{r^2}\left(S^2 - R^2\log\frac{R^2+S^2}{R^2}\right)\end{Bmatrix} \qquad r>S$$

7.29

where matrix $[D]$ is given by

$$[D] = \frac{6\eta R^2 V_{max}}{16\,T^2\,D}\begin{bmatrix}1 & \frac{\nu}{1-\nu}\\ \frac{\nu}{1-\nu} & 1\end{bmatrix}$$

7.30

At $r = 0$, the stresses are given by

$$\begin{Bmatrix} \sigma_r \\ \sigma_\theta \end{Bmatrix} = - \left[D \right] \begin{Bmatrix} \log \frac{R^2}{R^2+S^2} \\ \log \frac{R^2}{R^2+S^2} \end{Bmatrix} \qquad 7.31$$

where the radial and tangential stresses are equal resulting in zero deviatoric stress immediately above the plume.

For $r = S$, the stresses are

$$\begin{Bmatrix} \sigma_r \\ \sigma_\theta \end{Bmatrix} = - \left[D \right] \begin{Bmatrix} 1 - R^2/S^2 \log \frac{R^2+S^2}{R^2} \\ -1 + R^2/S^2 \log \frac{R^2+S^2}{R^2} \end{Bmatrix} \qquad 7.32$$

with the two principal stresses equal in magnitude but opposite in sign. Note that the radial stress has changed sign from being tensional (positive) to compressive (negative).

It can be seen from equation 7.29 that while the magnitude of the stresses are controlled by the parameters V_{max} R, η, T and D, the shape of the stress-radius relationship is controlled by parameters R and S only.

In figures 7.2, 7.3 and 7.4, the radial, tangential, and maximum deviatoric stresses, $\frac{\sigma_r - \sigma_\theta}{2}$, are plotted as a function of r for various values of the parameters R and S. Values for T and D of 100 km have been used (Haigh, 1973, Kanamore and Press, 1970). The units of the stress diagrams allow the stress fields to be obtained for any value of η or V_{max} (η being in units of poise and V_{max} in cm/year).

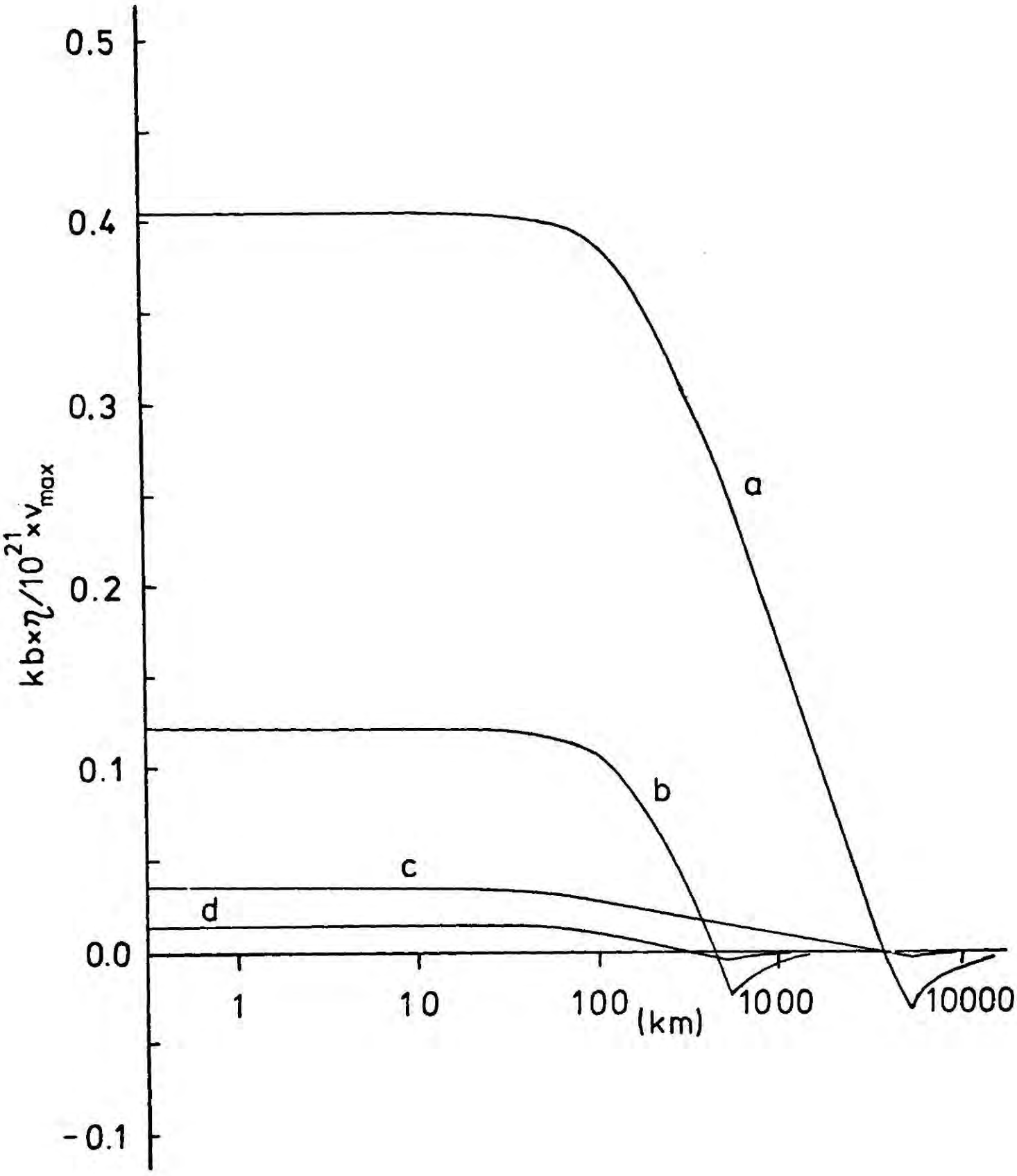

Figure 7.2 Radial stress as a function of radius

(a) R = 200 km, S = 5000 km

(b) R = 200 km, S = 500 km

(c) R = 50 km, S = 5000 km

(d) R = 50 km, S = 500 km

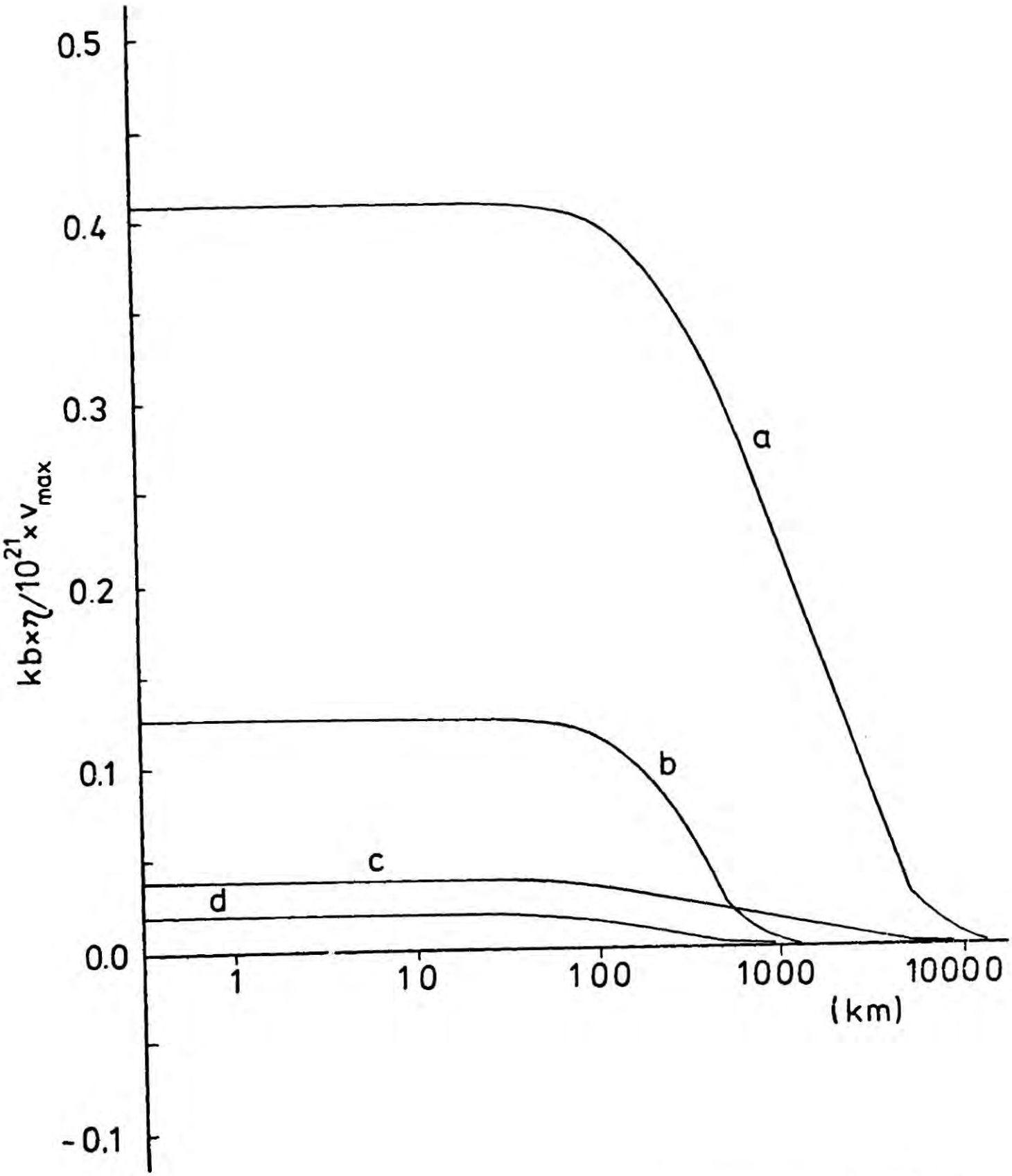

Figure 7.3 Tangential stress as a function of radius

(a) R = 200 km, S = 5000 km

(b) R = 200 km, S = 500 km

(c) R = 50 km, S = 5000 km

(d) R = 50 km, S = 500 km

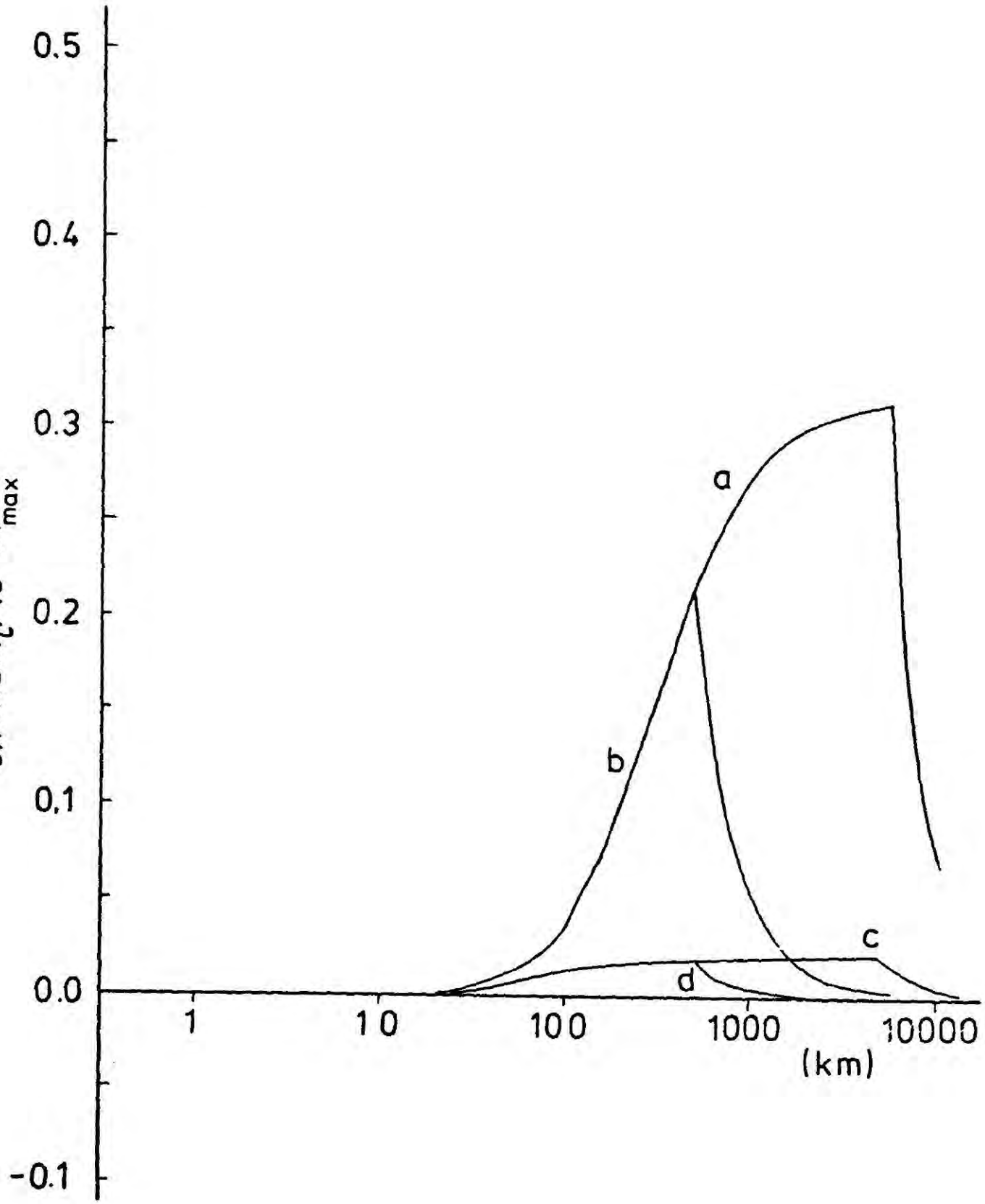

Figure 7.4 Deviatoric stress as a function of radius

(a) R = 200 km, S = 5000 km

(b) R = 200 km, S = 500 km

(c) R = 50 km, S = 5000 km

(d) R = 50 km, S = 500 km

7.5 Discussion

The radial, tangential and deviatoric stresses produced in the lithosphere and shown in figures 7.2, 7.3 and 7.4 display strong radial dependence. In the region above the plume, both the radial and the tangential stresses are tensional and achieve their maximum values. The deviatoric stress (in the horizontal plane) is zero here as a consequence of the equality of the two principal stresses. With increasing radial distance, both stresses decrease. While the tangential stress remains tensional throughout, the radial stress becomes compressive in the vicinity of $r = S$. At $r = S$, the deviatoric stress takes its maximum value. All stresses show a strong dependence on the parameters η, v_{max}, R and S.

In order to interpret the stresses in terms of lithospheric fracture the resulting stress field of plume stresses and lithosphere load stresses must be considered. If hydrostatic stresses are assumed for the load stresses, fracture will be most likely to occur in the upper lithosphere, where the plume stresses will cause the largest relative perturbation from the hydrostatic.

An estimate of the stresses in the lithosphere, due to the plume, may be made using Morgan's estimates (1972) of plume velocity and diameter (R = 75 km, v_{max} = 200 cm/yr)

provided additional estimates of viscosity, η , and S are made. Estimates of asthenosphere viscosity give values of the order of 10^{21} -$2x10^{22}$ poise (Haskell, 1935; Heiskanen and Vening Meinesz, 1958; Crittenden, 1962; McConnell, 1965) for continental regions. In oceanic regions a lower viscosity is expected as a consequence of the higher temperature at asthenosphere depths than continental regions (MacDonald, 1965) and the temperature dependence of viscosity in mantle like materials (Stocker and Ashby, 1973). An estimate of 10^{19} - 10^{20} poise may be made therefore for the viscosity of the oceanic asthenosphere. A value of S = 1500 km is obtained by considering Morgan's estimate (1972) of 3000 km for the distance between mantle plumes. These values together yield tensile radial and tangential plume stresses of the order of 1 kb, for η = 10^{20} poise, above the plume and a maximum deviatoric stress (in the horizontal plane) of 0.1 kb at radius, $r = S$.

The plume stresses, together with the load stresses, of the lithosphere give a total stress field above the plume whose horizontal stress is less than the vertical stress. Assuming a tensile strength of 0.5 kb (Brace, 1960) the stresses above the plume are sufficient (assuming η = 10^{20} poise for the asthenosphere) to cause brittle fracture in the upper lithosphere under normal ocean load conditions

provided stress relaxation by creep does not occur. The relationship of the stresses predicts vertical fissures becoming normal faults with depth. The equality of radial and tangential stresses above the plume suggest no preferred orientation for the strike of the fault. At the plume radius, the radial stresses become less tensional than the tangential stresses and in this region the faults may take on a radial orientation. With increasing radius the plume stresses become smaller and faulting will cease.

Morgan (1972) has suggested that the stress field of a plume may interact with the stresses at a plate boundary. In the case of a mantle plume situated at a ridge axis, the tensional stress field above the plume might extend the region of tensional tectonics occurring at the ridge axis. This may account for the diffuse spreading centre on Iceland which is thought to lie above a mantle plume (Morgan, 1971, 1972; Vogt, 1971, 1974; Schilling, 1973).

Further discussion of the geological effects of stresses created in the lithosphere by asthenosphere flow associated with a mantle plume should, however, await evidence for the existence of plume and details of their dimensions and velocities.

BIBLIOGRAPHY

Artyushkov, E.V., 1973. Stresses in the lithosphere caused by crustal thickness inhomogeneities, J. geophys. Res., 78, 7675-7708.

Aumento, F., Loncarevic, B.D. & Ross, D.I., 1971. Hudson geotraverse: geology of the Mid-Atlantic Ridge at 45°N, Phil. Trans. Roy. Soc. London, A., 268, 623-650.

Beaumont, C. & Lambert, A., 1972. Crustal structure from surface Load Tilts, using a Finite Element Model, Geophys. J. R. astr. Soc., 29, 203-226.

Bodvarsson, G. & Lowell, R.P., 1972. Ocean-floor heat flow and the circulation of interstitial waters, J. geophys. Res., 77, 4472-4475.

Bott, M.H.P., 1965. Formation of ocean ridges, Nature,Lond., 207, 840-844.

Bott, M.H.P. & Dean, D.S., 1972. Stress systems at young continental margins, Nature (Phys. Sci.), 235, 23-25.

Bottinga, Y., 1974. Thermal aspects of sea-floor spreading, and the nature of the suboceanic lithosphere, Tectonophysics, 21, 15-38.

Brace, W.F., 1961. Dependence of fracture strength on grain size, Bull. Miner. Inds. Stn. Penn. Univ., 76, 99-103.

Cann, J.R., 1968. Geological processes at mid-ocean ridge crests, Geophys. J. R. astr. Soc., 15, 331-341.

Cann, J.R., 1970. New model for the structure of the ocean crust, Nature, Lond., 226, 928-930.

Cann, J.R., 1974. A model for oceanic crustal structure developed, Geophys. J. R. astr. Soc., 39, 169-187.

Carslaw, H.S. & Jaeger, J.C., 1959. Conduction of heat in solids, 2nd edition, Oxford University Press, 510 pp.

Clark, S.P. & Ringwood, A.E., 1964. Density distribution and constitution of the mantle, Rev. Geophysics., 2, 35-88.

Clark, S.P., (ed) 1966. Handbook of Physical Constants, Mem. Geol. Soc. Am., 97, 583 pp.

Coleman, R.G., 1971. Petrologic and Geophysical nature of Serpentinites, Bull. geol. Soc. Am., 82, 897-918.

Crittenden, M.D., 1963. Effective viscosity of the Earth derived from isostatic loading of Pleistocene Lake Bonneville, J. geophys. Res., 68, 5517-5530.

Dean, D.S., 1973. Stress analysis of the Lithosphere, unpublished Ph.D. thesis, University of Durham.

Deep sea drilling project, 1974. Leg 37 - the volcanic layer, Geotimes, 19, 16-18.

Dehlinger, P., Gough, R.W., McManus, D.A. & Gemperle, M., 1970. Northeast Pacific Structure, The Sea, 4, pt. 2, 133-189, edited by Maxwell, A.E., Interscience, New York.

Engel, A.E.J. & Engel, C.G., 1970. Mafic and ultramafic rocks, The Sea, 4, pt.1, 465-519, edited by Maxwell, A.E., Interscience, New York.

Ewing, M. & Ewing, J., 1970. Seismic Reflection, The Sea, 4, pt.1, pp 1-51, edited by Maxwell, A.E., Interscience, New York.

Forsyth, D.W. & Press, F., 1971. Geophysical tests of petrological models of the spreading lithosphere, J. geophys. Res., 76, 7963-7979.

Forsyth, D.W., 1975. The early structural evolution and anisotropy of the oceanic upper mantle, Geophys. J.R. astr. Soc., 43, 103-162.

Forsythe, G. & Moler, C.B., 1967. Computer Solution of Linear Algebraic Systems, Prentice-Hall, 148 pp.

Fowler, C.M.R. & Matthews, D.H., 1974. Seismic refraction experiment on the Mid-Atlantic Ridge in the FAMOUS area, Nature, Lond., 249, 752-754.

Fox, L., 1964. An introduction to numerical linear algebra, Clarendon Press, Oxford, 328 pp.

Francis, T.J.G. & Porter, I.T., 1973. Median valley seismology: the Mid-Atlantic ridge near 45°N, Geophys. J. R. astr. Soc., 34, 279-311.

Fung, V.C., 1965. Foundation of solid mechanics, Prentice Hall, 525 pp.

Gass, I.G., Smith, A.G. & Vine, F.J., 1975. Origin and emplacement of ophiolites, in Geodynamics today, 54-64. The Royal Society, London.

Goslin, J. Beuzart, P., Francheteau, J. & Le Pichon, X., 1972. Thickening of the oceanic layer in the Pacific ocean, Marine geophys. Res., 69, 3895-3900.

Green, D.H. & Ringwood, A.E., 1969. The origin of basalt magmas, The Earth's crust and upper mantle, Mon. Am. geophys. Union., 13, 489-495.

Hafner, W., 1951. Stress distributions and faulting, Bull. geol. Soc. Am., 62, 373-398.

Haigh, B.I.R., 1973. North Atlantic oceanic topography and lateral variations in the upper mantle, Geophys. J. R. astr. Soc., 33, 405-420.

Haigh, B.I.R., 1973,b. Crustal and Upper mantle structures in oceanic regions, Unpublished Ph.D. thesis, University of Durham.

Haskell, N.A., 1935. The motion of a viscous fluid under a surface load, Physics, 6, 265-269.

Heirtzler, J.R., 1970. Magnetic anomalies measured at sea, The Sea, 4, pt. 1, 85-128, edited by Maxwell, A.E., Interscience, New York.

Heiskanen, W.A. & Vening Meinesz, F.A., 1958. The Earth and its Gravity Field, McGraw-Hill, New York, Toronto and London, 470 pp.

Hess, H.H., 1960. Stillwater igneous complex, Montana, Mem. Geol. Soc. Am., 80, 230 pp.

Hess, H.H., 1962. History of ocean basins, Petrological Studies - Buddington Memorial Volume, Geol. Soc. Am., 599-620.

Homann, F., 1936. Der Einfluss grösser zahig keit bei der Strömung um den Zylinder und um die Kugel, Ztshr. f. angew. Math. und Mech., 16, 153-164.

Hopper, M.J., 1973. Harwell subroutine library, H.M.S.O.

Jackson, E.D., Green, H.W. & Moores, E.M., 1975. The Vourinos ophiolite, Greece: cyclic units of lineated cumulates overlying harzburgite tectonite, Bull. geol Soc. Am., 86, 390-398.

Jacoby, W.R., 1970. Instability in the upper mantle and global plate movements, J. geophys. Res., 75, 5671-5679.

Jaeger, J.C., 1968. Cooling and solidification of igneous rocks, in Basalts, 2, 503-536, ed. H.H. Hess and A. Poldervaart, Interscience, New York.

Jaeger, J.C. & Cook, N.G.W., 1969. Fundamentals of Rock Mechanics, Science Paperbacks, 515 pp.

Kanamori, H. & Press, F., 1970. How thick is the lithosphere?, Nature, Lond., 226, 330-331.

Kay, R., Hubbard, N.J. & Gast, P.W., 1970. Chemical characteristics and origin of oceanic ridge volcanic rocks, J. geophys. Res., 75, 1585-1613.

Lachenbruch, A.H., 1973. Differentiation and the gravitational driving force for material rising at an ocean ridge, J. geophys. Res., 78, 825-831.

Langseth, M.G. & Von Herzen, R.R., 1970. Heat flow through the floor of the world oceans, The Sea, 4, pt. 1, 299-353, edited by Maxwell, A.E., Interscience, New York.

Larson, R.L. & Spiess, F.N., 1968. East Pacific Rise Crest: a near-bottom geophysical profile, Science, 163, 68-71.

Laughton, A.S., Whitmarsh, R.B. & Jones, M.T., 1970. The evolution of the Gulf of Aden, Phil. Trans. Roy. Soc. London, A, 267, 227-266.

Lee, E.H., Radok, J.R.M. & Woodward, W.B., 1959. Stress analysis for linear viscoelastic materials, Trans. Soc. Rheology, 3, 41-59.

Le Pichon, X., 1968. Sea floor spreading and continental drift, J. geophys. Res., 73, 3661-3697.

Le Pichon, X., Francheteau, J. & Bonnin, J., 1971. Developments in Geotectonics 6: Plate tectonics, Elsevier, 300 pp.

Lister, C.R.B., 1974. On the penetration of water into hot rock, Geophys. J. R. astr. Soc., 39, 465-509.

Ludwig, W.J., Nafe, J.E. & Drake, C.L., 1970. Seismic Refraction, The Sea, 4, pt. 1, 53-84, edited by Maxwell, A.E., Interscience, New York.

Mason, R.G. & Raff, A.D., 1961. Magnetic survey off the west coast of the United States, 32°N latitude to 42°N latitude, Bull. geol. Soc. Am., 72, 1259-1266.

Matthews, D.H. & Bath, J., 1967. Formation of magnetic anomaly pattern of mid-Atlantic ridge, Geophys. J. R. astr. Soc., 13, 349-357.

Matthews, D.H., 1971. An account of the meeting for informal discussion held on Friday 14 November 1969. Phil. Trans. Roy. Soc. London, A, 268, 733-736.

Maxwell, A.E., Von Herzen, R.P., Hsü, K.J., Andrews, J.E., Saito, T., Percival, S.F., Milow, E.D. & Boyce, R.E., 1970. Deep Sea drilling in the South Atlantic, Science, 168, 1047-1059.

Maynard, G.L., 1970. Crustal layer of seismic velocity 6.9 to 7.6 kilometers per second under the deep oceans, Science, 168, 120-121.

Menard, H.W., 1967. Sea floor spreading, topography and the second layer, Science, 157, 923-924.

Morgan, W.J., 1971. Convection plumes in the lower mantle, Nature, Lond., 230, 42-43.

Morgan, W.J., 1972. Deep mantle convection plumes and plate motion, Am. Assoc. Petrol. Geol. Bull., 56, 203-213.

Murrell, S.A.F., 1958. Mechanical properties of non-metallic brittle materials. 123-145, ed. W.H. Walton, Butterworths, London.

Murrell, S.A.F., 1965. The effect of triaxial stress systems on the strength of rocks at atmospheric temperatures, Geophys. J. R. astr. Soc., 10, 231-281.

Murrell, S.A.F. & Digby, P.J., 1970. The theory of brittle fracture initiation under triaxial stress conditions - 1, Geophys. J. R. astr. Soc., 19, 309-334.

McConnell, R.K., 1965. Isostatic adjustment in a layered earth, J. geophys. Res., 70, 5171-5188.

McKenzie, D.P., 1967. Some remarks on heat flow and gravity anomalies, J. Geophys. Res., 72, 6261-6273.

McKenzie, D.P. & Parker, R.L., 1967. The North Pacific: an example of tectonics on a sphere, Nature, Lond., 216, 1276-1280.

N.A.G., 1974, Numerical Algorithms Group Manual, N.A.G. Executive, Computing Laboratory, Oxford University.

Oldenburg, D.W., 1975. A physical model for the creation of the lithosphere, Geophys. J. R. astr. Soc., 43, 425-451.

Oxburgh, E.R. & Turcotte, D.L., 1968. Mid-ocean ridges and geotherm distribution during mantle convection, J. geophys. Res., 76, 1315-1327.

Pálmason, G., 1973. Kinematics and heat flow in a volcanic rift zone, with application to Iceland, Geophys. J. R. astr. Soc., 33, 451-481.

Parker, R.L. & Oldenburg, D.W., 1973. Thermal model of ocean ridges, Nature (Phys. Sci.), Lond., 242, 137-139.

Piper, J.D.A. & Gibson, I.L., 1972. Stress control of processes at extensional plate margins, Nature (Phys. Sci.), Lond.,238, 83-86.

Presnall, D.C., 1969. The geometrical analysis of partial fusion, Am. J. Sci., 267, 1178-1194.

Schilling, J.G., 1973. Iceland mantle plume; geochemical study of Reykjanes Ridge, Nature, Lond., 242, 565-571.

Sclater, J.G. & Francheteau, J., 1970. The implications of terrestrial heat flow observations on current tectonic and geochemical models of the crust and upper mantle of the earth, Geophys. J. R. astr. Soc., 20, 509-542.

Service, K.G. & Douglas, A., 1973. Boundaries and fractures in finite element models of geological structures, Geophys. J. R. astr. Soc., 32, 1-14.

Shor, G.G., Menard, H.W. & Raitt, R.W., 1970. Structure of the Pacific Basin, The Sea, 4, pt. 2, 3-27, edited by Maxwell, A.E., Interscience, New York.

Sleep, N.H., 1975. Formation of oceanic crust: some thermal constraints, J. geophys. Res., 80, 4037-4042.

Sokolnikoff, I.S., 1956. Mathematical theory of elasticity, McGraw Hill, New York.

Stephansson, O. & Berner, H., 1971. The finite element method in tectonic processes, Phys. Earth. Planet. Int., 4, 301-321.

Stocker, R.L. & Ashby, M.F., 1973. On the Rheology of the Upper Mantle, Rev. geophys. space phys., 11, 391-425.

Sykes, L.R. & Shar, M.L., 1972. Intraplate earthquakes, lithosphere stresses and the driving mechanism of plate tectonics, Nature, Lond., 245, 298-302.

Talwani, M., Le Pichon, X. & Ewing, M., 1965. Crustal structure of the Mid-Ocean Ridges, 2. Computed model from gravity and seismic refraction data, J. geophys. Res., 70, 341-352.

Talwani, M., Windisch, C.C. & Lanseth, M.G., 1971. Reykjanes ridge crest: a detailed study, J. geophys. Res., 76, 473-517.

Thorarinsson, S., Steinthórsson, S., Einarsson, T., Kristmannsdóttir, H. & Oskarsson, N., 1973. The eruption on Heimaey, Iceland, Nature, Lond., 241,372-375.

Tryggvason, E., 1964. Arrival times of P waves and upper mantle structure, Bull. seism. Soc. Am., 54, 727-736.

Turcotte, D.L. & Oxburgh, E.R., 1973. Mid-plate tectonics, Nature, Lond., 1973, 337-339.

Turcotte, D.L., 1974. Arc transform faults thermal contraction cracks?, J. geophys. Res., 79, 2573-2577.

Udintsev, G.B. & Dmi triev, L.V., 1970. Ultra basic rocks, The Sea, 4, pt. 1, 521-573, edited by Maxwell, A.E., Interscience, New York.

Vacquier, V., 1969. Magnetic intensity field in the Pacific, The Earth's crust and upper mantle, Mem. Am. geophys. Union, 13, 422-430.

Vening Meinesz, F.A., 1948. Gravity expeditions at sea, 1923-1938, Vol IV, Publ. Netherlands Geod. Comm. Delft.

Vine, F.J. & Matthews, D.H., 1963. Magnetic anomalies over oceanic ridges, Nature, Lond., 199, 947-949.

Vine, F.J. & Wilson, J.T., 1965. Magnetic anomalies over a young oceanic ridge off Vancouver Island, Science, 150, 485-489.

Vine, F.J., 1966. Spreading of the ocean floor: new evidence, Science, 154, 1405-1415.

Vogt, P.R., 1971. Asthenosphere motion recorded by the ocean floor south of Iceland, Earth Planet Sci. Lett., 13, 153-160.

Vogt, P.R., 1972. Evidence for global synchronism in mantle plume convection, and possible significance for geology, Nature, Lond., 240, 338-342.

Vogt, P.R., 1974. The Iceland Phenomena: Imprints of a hot spot on the ocean crust, and implications for flow beneath the plates, Geodynamics of Iceland and the North Atlantic area, 105-127, ed. L. Kristjansson, NATO Advanced Study Institute, Reykjavik, 1974, Reidel.

Walcott, R.I., 1970. Flexural rigidity, thickness, and viscosity of the lithosphere, J. geophys. Res., 75, 3941-3954.

Weertman, J., 1972. Coalescence of magma pockets into large pools in the upper mantle, Bull. geol. Soc. Am., 83, 3531-3532.

Whitmarsh, R.B., 1975. Axial intrusion zone beneath the median valley of the Mid-Atlantic ridge at 37°N detected by explosion seismology, Geophys. J. R. astr. Soc., 42, 189-215.

Wilson, J.T., 1965. A new class of faults and their bearing on continental drift, Nature, Lond., 207, 343-347.

Zienkewicz, O.C., 1971. The finite element method in Engineering Science, McGraw-Hill, London, 521 pp.

APPENDIX 1

The program described and listed in this appendix executes the numerical calculations of finite element visco-elastic stress analysis which are used in Chapter 3 and formulated in Chapter 2. The program is written in Fortran 4 G and consists of the main program together with four sub-routines. Double precision is used for all real characters.

Main Program. A flow diagram of the main program is shown in figure A1.1 and summarizes the main steps in carrying out the finite element calculation.

Subroutine Plots. This subroutine plots the calculated principal stresses (total and deviatoric), the finite element grid, the nodal displacements and the numerical values of the deviatoric stress. Options exist whereby all or some of these items may be plotted (see input data). The plotting routines called in this subroutine are local (NUMAC only).

Subroutine GMPRD. This subroutine multiplies two matrices together forming a third matrix. The subroutine is adapted from an I.B.M. scientific subroutine package.

Subroutine GMTRA. This subroutine takes the transpose of a matrix. The subroutine is adapted from an I.B.M. scientific subroutine package.

Subroutine MA07BD. This subroutine is used to solve the equilibrium equation of finite element, $[K]\{\delta\} = \{F\}$ for displacement $\{\delta\}$ where $[K]$ is the stiffness matrix and $\{F\}$ is the total force vector. The subroutine is available on the

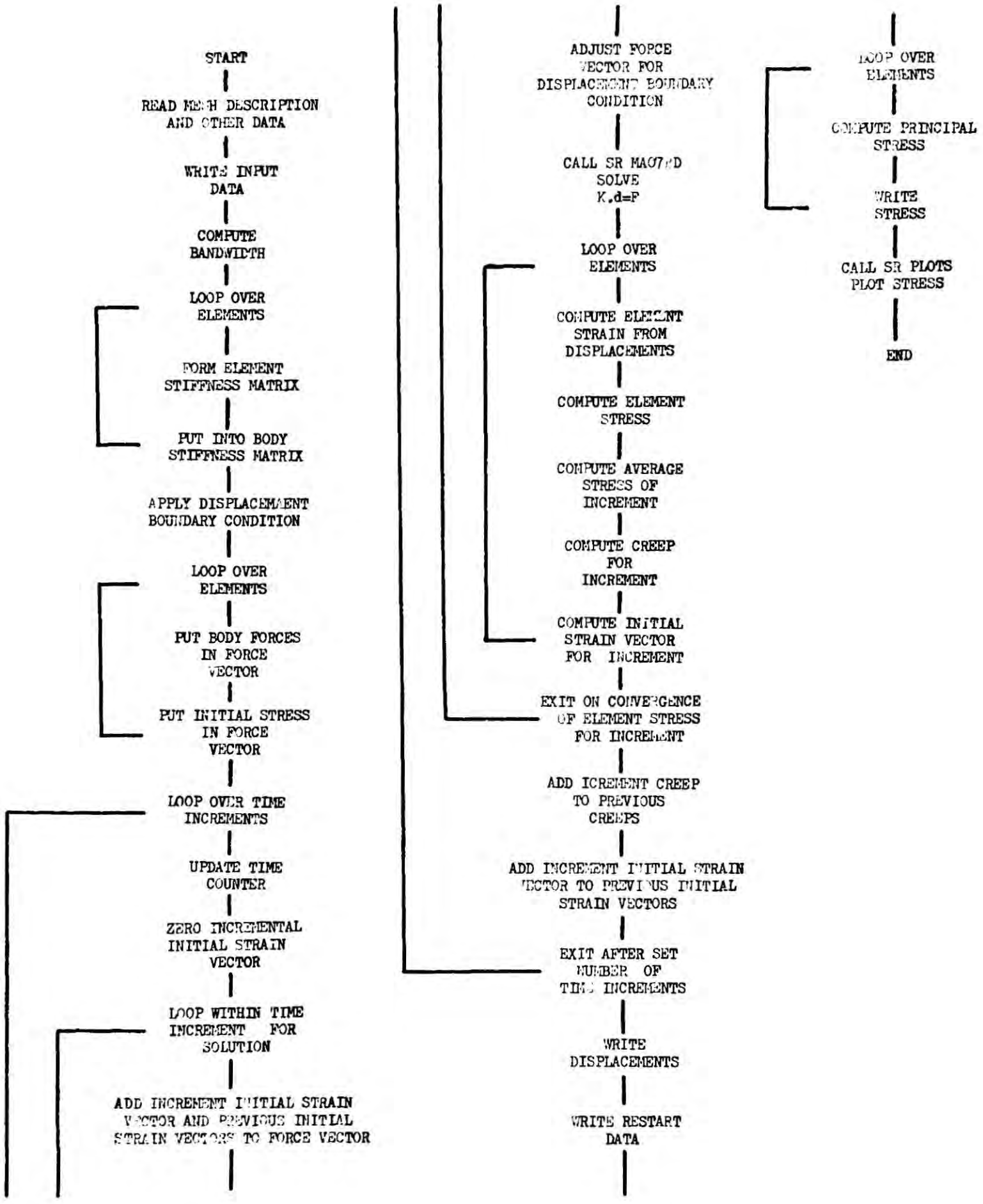

Figure A1.1 Flow Diagram

Harwell scientific subroutine package (Hopper, 1973) and uses Gaussian elimination.

A listing of the main program and the subroutines is given at the end of the appendix.

Program Input

The program input defines the geometry, physical constants and boundary conditions of the region under investigation, together with the time increment information. Additional input controls the form of output. Formats and device numbers for input are given in brackets.

1. NNOD,NEL,STMAX,DEV (2I10,E10.3,F10.3 device 5)

   NNOD, number of nodes of finite element grid.

   NEL, number of elements of finite element grid.

   STMAX, stress plot scaling factor (dynes/cm^2/inch).

   DEV, controls stress output form.

   DEV = 0 total stress printed and plotted.

   DEV = 1 deviatoric stress printed and plotted.

2. For all nodes

   K,X(K),Y(K) (I10,2F10.3 device 5)

   K node number.

   X(K),Y(K) , X and Y coordinate of node (cm)

3. For all elements

   K,(NODEL(K,J),J=1,3),E(K),P(K),DN(K),VISCOS(K) (4I10,E10.3, 2F10.3,E10.3 device 5)

   K, element number.

   NODEL(K,1,2,3), numbers of 3 nodes specifying element.

E(K), element Young's modulus (dynes/cm^2).

P(K), element Poisson ratio.

DN(K), element density (gm/cc).

VISCOS(K), element viscosity (poise).

4. NTIM,TIMQ (I10.3,E10.3 device 5).

NTIM, number of time increments for visco-elastic analysis.

TIMQ, length of time increment (sec).

5. NOYES (I10 device5).

NOYES, controls restart option; if NOYES equals 1 stresses and displacements of previous analysis are read. Stresses are then incorporated in force vector as initial stress vector and displacements are subtracted from original grid coordinates.

6. NBC (I10 device 5).

NBC, number of specified nodal forces.

7. I,FORST(2*I-1),FORST(2*I) (I10,2E10.3 device 5).

I, node number at which nodal forces specified.

FORST(2*I-1),FORST(2*I), X and Y components of nodal force vector.

8. ND (I10 device 5).

ND, number of nodes with specified displacements.

9. LD(I),(ISP(I,J),PDIS(I,J),J=1,2) (I10,2(I10,F10.3) device 5).

LD(I), node number at which displacements specified.

ISP(I,1),ISP(I,2), controls specification of displacement for X and Y directions. If equals 0 no displacement is specified: if equals 1 displacement is specified.

PDIS(I,1),PDIS(I,2), X and Y components of specified displacements.

10. KPLOT,KIK (2I10 device 5)

KPLOT,KIK, control stress plot output.

KPLOT = 0 no plot.

= 1 plot numerical value of deviatoric stress, principal stress, nodal displacements and finite element grid.

= 2 plot principal stresses only.

= 3 plot numerical value of deviatoric stress only.

if KIK = 1 no grid is plotted.

11. XSC,XSH,YSC,YSH (4F10.3 device 5)

These parameters control scale of plot

XSC X coordinate scale (cm/inch).

XSH X coordinate shift (cm).

YSC Y coordinate scale (cm/inch).

YSH Y coordinate shift (cm).

Program Output

1. All input data specifying grid, boundary conditions and time increment information is printed, (device 6).
2. Information is printed describing the maximum stress change between successive iterations for solution within the time increment, (device 4).
3. The number of iterations required to obtain solution for a time increment is printed, (device 4).

4. Final nodal displacements are printed, (device 6).
5. Final nodal displacements and element stresses are sent to device 2 for use in restart option.
6. Final element stresses are printed, (device 6).

Additional facilities exist to plot element principal stress, nodal displacement, the finite element grid and the numerical values of deviatoric stress.

Preset internal parameters

1. G, gravitational acceleration (cm/sec^2).
2. RNODEF, parameter controlling perturbation of the finite element grid after restart; if equal to 0 grid not changed - if equal to 1 grid changed.
3. OUT, stress convergence tolerance of iteration for solution within time increment.

Program Test

A test of the finite element visco-elastic stress analysis program has been made against an analytical solution for the time dependent visco-elastic deformation of a hollow cylinder of visco-elastic material, enclosed in an elastic ring, and subject to applied internal pressure. The analytical solution of the problem is given by Lee, Radok and Woodward (1959). The finite element representation of the cylinder is shown in figure A1.2; only one quarter need be considered owing to symmetry. The steel ring has elastic constants $E = 5 \times 10^7$ psi

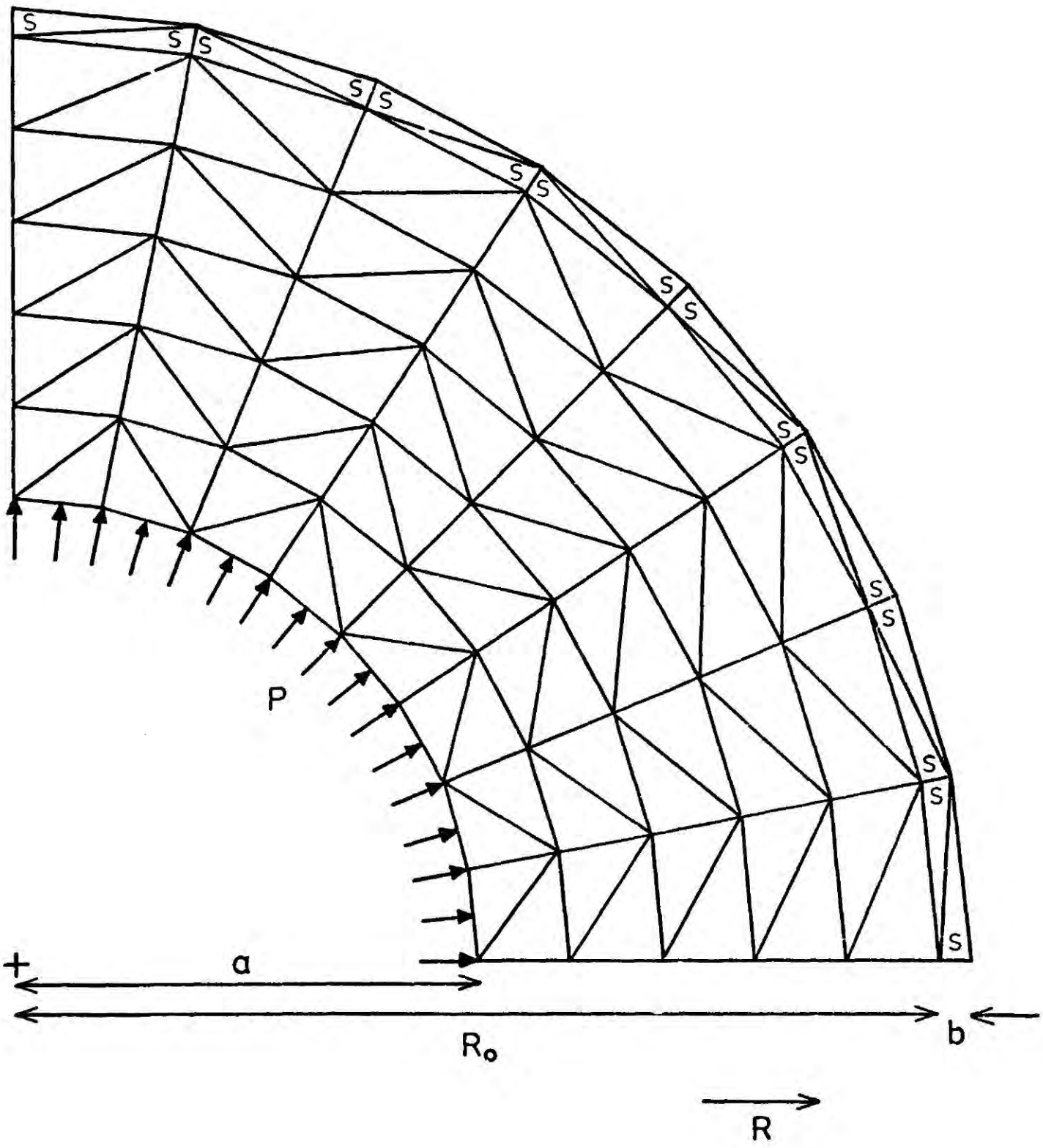

Figure A1.2 Finite element subdivision of anulus used for testing the viscoelastic finite element formulation.

and $\nu = 1/3$, while the hollow cylinder has $E = 10^5$ psi and $\nu = 1/\sqrt{11}$. The viscosity of the visco-elastic cylinder is $\frac{3}{8}\ 10^5$. Cylinder dimensions are as follows: a = 2", b = $\frac{3}{8}$" and R_o = 4". The free ends of the segment of anulus are constrained for zero tangential displacement. In figure A1.3 the values of tangential stress calculated by finite element analysis are compared with the analytical solution as a function of time (normalized with respect to the relaxation time constant). Figure A1.3 shows the good accuracy achieved by the numerical solution.

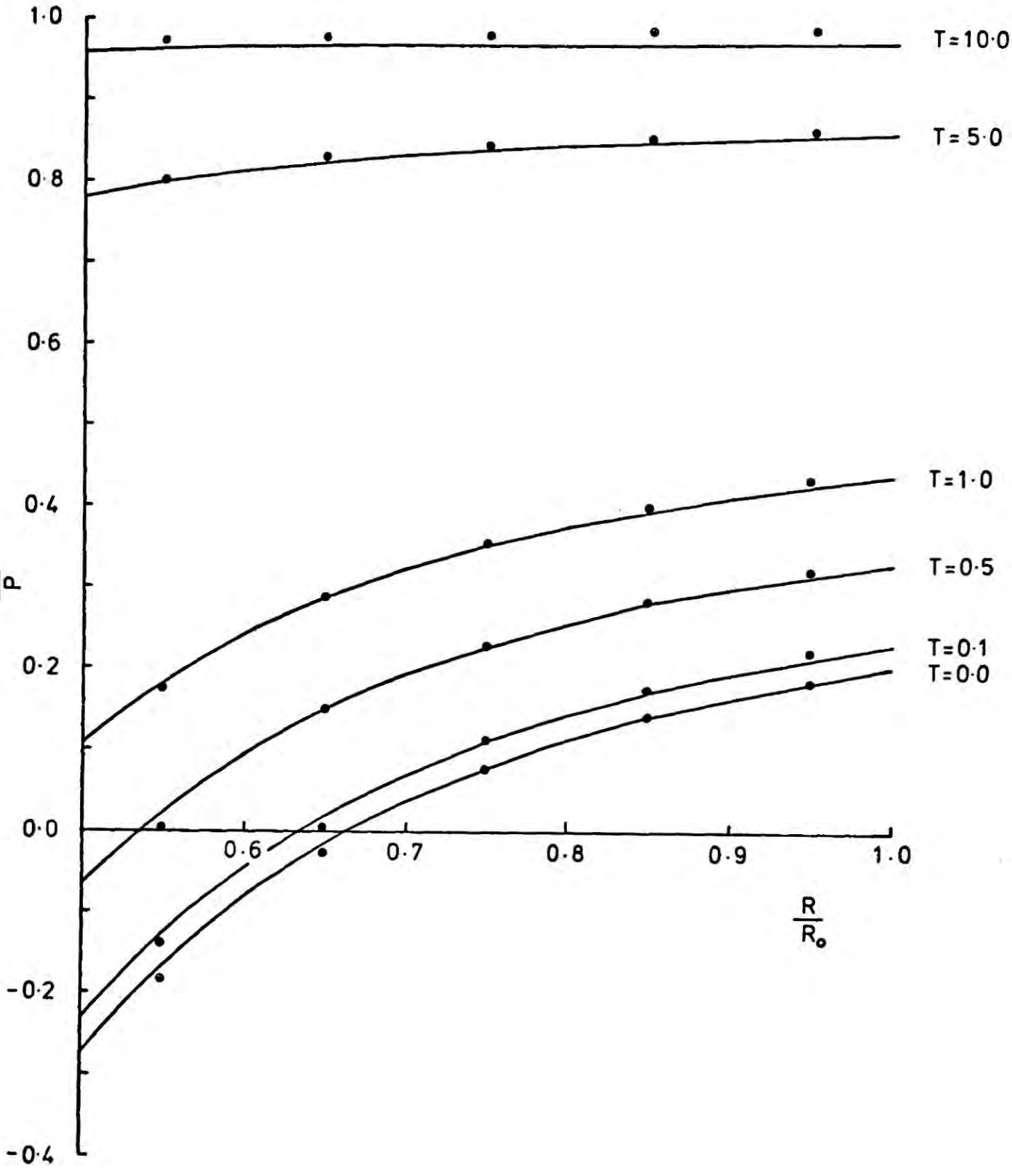

Figure A1.3 Tangential stress as a function of time and radius. Analytical solutions are given by curves, while dots are values predicted by viscoelastic finite element analysis.

```
C***** VISCO-ELASTIC F.E. PROGRAM*****
C******MAIN PROGRAM*****
      IMPLICIT REAL *8 (A-H,O-Z)
C*****DIMENSION STATEMENTS*****
      DIMENSION
     1 X(228),Y(228),NODEL(460,3),E(460),P(460),DN(460),
     2 NK(100),PRES(100),YFINC(100),
     3 LD(100),ISP(100,2),PDIS(100,2),
     4 FORST(456),FIST(456),
     5 CSTIN(460,4),STIN(460,4),
     6 T(36),D(9),B(18),V(6),F(18),H(18),VISCOS(460),
     7 W(3),QQ(3),CC(3),STRAY(460,4),
     8 CREEP(4),DISEL(6),STRESS(4),STRAIN(4),STEL(4),DISP(456)
     9 ,DF(9),EF(3),AT(126,50),DINIT(456),TRAY(460,4)
     1 ,DLIB(9,460),BLIB(18,460),DELIB(460)
     2 ,DFS(50),PREDIP(456),STREN(456,4)
C*****GRAV ACCELERATION*****
      G=-981.0
      RNODEF=0.0
C*****STRESS CONVERGENCE CONDITION*****
      OUT=1.0D6
      TIMTOT=0.0
C
C*****READ IN INPUT DATA*****
C*****READ NUMBER OF NODES AND ELEMENTS,STRESS SCALER AND OUTPUT MARKER*
      READ(5,800) NNOD,NEL,STMAX,DEV
      NNOD2=NNOD*2
  800 FORMAT(2I10,E10.3,F10.3)
      DO 850 I=1,NNOD
  850 READ(5,801) K,X(K),Y(K)
  801 FORMAT(I10,2F10.3)
      DO 851 I=1,NEL
  851 READ(5,802) K,(NODEL(K,J),J=1,3),E(K),P(K),DN(K),VISCOS(K)
  802 FORMAT(4I10,E10.3,2F10.3,E10.3)
C*****READ NUMBER OF TIME INCREMENTS AND STEP LENGTH*****
      READ(5,803) NTIM,TIMC
      DO 200 I=1,NNOD2
      FORST(I)=0.0
      STIN(I,1)=0.0
      STIN(I,2)=0.0
      STIN(I,3)=0.0
      STIN(I,4)=0.0
      STREN(I,1)=0.0
      STREN(I,2)=0.0
      STREN(I,3)=0.0
      STREN(I,4)=0.0
      PREDIP(I)=0.0
  200 CONTINUE
C*****RESTART OPTION*****
C*****READ INITIAL STRESS AND INITIAL DISPLACEMENT*****
      READ(5,806) NOYES
      IF(NOYES.EQ.0) GO TO 25
C***** READ INITIAL  DISPLACEMENT AND STRESS
      DO 257 I=1,NNOD2
  257 READ(1,256) PREDIP(I),(STREN(I,J),J=1,4)
  256 FORMAT(2X,5E15.7)
   25 CONTINUE
  803 FORMAT(I10,E10.3)
C***** TAKE PREDIP OFF X,Y TO PERT GRID POSITION*****
      DO 26 I=1,NNOD
```

```
      KY=2*I
      KX=KY-1
      X(I)=X(I)+PREDIP(KX)/1.0E5
      Y(I)=Y(I)+PREDIP(KY)/1.0E5
   26 CONTINUE
C***** READ BOUNDARY CONDITIONS*****************************************
C*****READ SPECIFIED NODAL FORCES*****************************************
      READ(5,806) NBC
  806 FORMAT(I10)
  804 FORMAT(E10.3)
      DO 853 J=1,NBC
  853 READ(5,805) I,FORST(2*I-1),FORST(2*I)
  805 FORMAT(I10,F10.5,E10.3)
C*****READ SPECIFIED DISPLACEMENTS*************************************
      READ(5,808) ND
  808 FORMAT(I10)
      DO 854 I=1,ND
  854 READ(5,807) LD(I),(ISP(I,J),PDIS(I,J),J=1,2)
  807 FORMAT(I10,2(I10,F10.3))
C
C*****WRITE OUT INPUT DATA*********************************************
      WRITE(4,150) NNOD,NEL,STMAX,DEV
  150 FORMAT(2X,'NUMBER OF NODES =',I4,10X,'NUMBER OF ELEMENTS =',I4,
     1 5X,E10.3,F4.1)
      WRITE(6,199)
  199 FORMAT('0')
      DO 100 I=1,NNOD
  100 WRITE(6,152) I,X(I),Y(I),FORST(2*I-1),FORST(2*I)
  152 FORMAT(13X,I5,24X,F10.3,12X,F10.3,10X,2E10.3)
      WRITE(6,199)
      DO 101 I=1,NEL
  101 WRITE(6,154) I,(NODEL(I,J),J=1,3),E(I),P(I),DN(I),VISCOS(I)
  154 FORMAT(14X,I4,18X,I4,12X,I4,12X,I4,D10.3,2F6.3,D10.3)
      WRITE(6,199)
      WRITE(6,155) NTIM
  155 FORMAT(2X,'NUMBER OF TIME ITERATIONS=',I4)
      WRITE(6,199)
      WRITE(6,156) TIMC
  156 FORMAT(2X,'TIMC=',E10.3)
      WRITE(6,199)
  158 FORMAT(18X,I5,24X,E12.5,12X,E12.5)
      WRITE(6,199)
      WRITE(6,199)
      DO 105 I=1,ND
  105 WRITE(6,169) LD(I),((ISP(I,J),PDIS(I,J)),J=1,2)
  169 FORMAT(20X,I10,12X,I10,10X,F10.3,10X,I10,10X,F10.3)
C*****TO CALC THE PARAM NBW*********************************************
      PT=1.0
      NBW=0
      DO 9182 I=1,NEL
      KB1=IABS(NODEL(I,1)-NODEL(I,2))
      KB2=IABS(NODEL(I,2)-NODEL(I,3))
      KB3=IABS(NODEL(I,3)-NODEL(I,1))
 9182 NBW=AMAX0(KB1,KB2,KB3,NBW)
      NBW=2*NBW+2
      NBW=2*NBW-1
      WRITE(6,9187) NBW
 9187 FORMAT(2X,'NBW=',I10)
C
C*****TO FORM ELEMENT STIFNESS MATRIX***********************************
```

```
      DO 6 I=1,NEL
C*****TO SET H AND T TO ZERO*************************************************
      DO 41 LIT=1,36
   41 T(LIT)=0.0
      DO 42 LIT=1,18
   42 H(LIT)=0.0
C*****FORM D MATRIX**********************************************************
      A=E(I)*(1.0-P(I))/((1.0+P(I))*(1.0-2*P(I)))
      Q=P(I)/(1.0-P(I))
      D(1)=A
      D(2)=A*Q
      D(3)=0.0
      D(4)=A*Q
      D(5)=A
      D(6)=0.0
      D(7)=0.0
      D(8)=0.0
      D(9)=A*(1.0-Q)/2.0
C*****FORM B MATRIX**********************************************************
      I1=NODEL(I,1)
      I2=NODEL(I,2)
      I3=NODEL(I,3)
      DELTA=Y(I3)*X(I2)
     1      -Y(I2)*X(I3)
     2      -X(I1)*Y(I3)
     3      +X(I1)*Y(I2)
     4      +Y(I1)*X(I3)
     5      -Y(I1)*X(I2)
      QQ(1)=(Y(I2)-Y(I3))/DELTA
      CC(1)=(X(I3)-X(I2))/DELTA
      QQ(2)=(Y(I3)-Y(I1))/DELTA
      CC(2)=(X(I1)-X(I3))/DELTA
      QQ(3)=(Y(I1)-Y(I2))/DELTA
      CC(3)=(X(I2)-X(I1))/DELTA
      B(1)=QC(1)
      B(2)=0.0
      B(3)=CC(1)
      B(4)=0.0
      B(5)=CC(1)
      B(6)=QQ(1)
      B(7)=QC(2)
      B(8)=0.0
      B(9)=CC(2)
      B(10)=C.0
      B(11)=CC(2)
      B(12)=CQ(2)
      B(13)=QQ(3)
      B(14)=0.0
      B(15)=CC(3)
      B(16)=C.0
      B(17)=CC(3)
      B(18)=CQ(3)
      DELTA=DABS(DELTA)
      DO 9401 KK=1,18
 9401 BLIB(KK,I)=B(KK)
      DELIB(I)=DELTA
      DO 9402 KK=1,9
 9402 DLIB(KK,I)=D(KK)
      N=3
      M=6
```

```
      CALL GMTRA(B,F,N,M)
C*****B IS TRANSPOSED TO F*************************************************
C*****MULTIPLY D BY B TO GIVE H******
      N=3
      M=3
      L=6
      CALL GMPRD(D,B,H,N,M,L)
C*****MULTIPLY F BY H TO GIVE T******
      N=6
      M=3
      L=6
      CALL GMPRD(F,H,T,N,M,L)
C*****TO MULTIPLY BY DELTA/2************************************************
      DO 38 NI=1,36
   38 T(NI)=T(NI)*DELTA/2.0
C*****WE NOW HAVE ELEMENT STIFFNESS MATRIX**********************************
C*****TO PUT T INTO BODY STIFFNESS MATRIX************************************
      K=1
      DO 10 MS=1,3
      DO 10 NS=1,2
      DO 10 KS=1,3
      DO 10 LS=1,2
      JX=NODEL(I,MS)
      JX=2*JX-2+NS
      IY=NODEL(I,KS)
      IY=2*IY-2+LS
      LOC=JX-IY+0.5*(NBW+1)
      IF(LOC.LT.1) GO TO 10
      IF(LOC.GT.NBW) GO TO 10
      AT(IY,LOC)=AT(IY,LOC)+T(K)
   10 K=K+1
    6 CONTINUE
      WRITE(6,922)
  922 FORMAT(2X,'TOTOL STIFFNESS FORMED')
C***** INTRODUCE PRESCRIBED DISPLACEMENTS*********************************
      DO 30 II=1,NC
      DO 31 J=1,2
      LIK=ISP(II,J)
      IF(LIK.EQ.0) GO TO 31
      I=LD(II)
      N=2*I+J-2
      FORST(N)=PDIS(II,J)*1.0D 24
      LOC=0.5*(NBW+1)
      AT(N,LOC)=1.0D 24
   31 CONTINUE
   30 CONTINUE
      WRITE(6,923)
  923 FORMAT(2X,'PRESCRIBED DISPLACEMENTS INTRODUCED')
C
C*****TO PUT BODY FORCES AND INITIAL STRESS INTO FORCE VECTOR***********
C*****TO INCORPORATE BODY FORCES******
      DO 4 I=1,NEL
      I1=NODEL(I,1)
      I2=NODEL(I,2)
      I3=NODEL(I,3)
      I11=2*I1-1
      I12=2*I1
      I21=2*I2-1
      I22=2*I2
      I31=2*I3-1
```

```
241           I32=2*I3
242           X(I1)=X(I1)-PREDIP(I11)
243           Y(I1)=Y(I1)-PREDIP(I12)
244           X(I2)=X(I2)-PREDIP(I21)
245           Y(I2)=Y(I2)-PREDIP(I22)
246           X(I3)=X(I3)-PREDIP(I31)
247           Y(I3)=Y(I3)-PREDIP(I32)
248           DELTA=Y(I3)*X(I2)
249          1      -Y(I2)*X(I3)
250          2      -X(I1)*Y(I3)
251          3      +X(I1)*Y(I2)
252          4      +Y(I1)*X(I3)
253          5      -Y(I1)*X(I2)
254           DELTA=DABS(DELTA)
255           X(I1)=X(I1)+PREDIP(I11)
256           Y(I1)=Y(I1)+PREDIP(I12)
257           X(I2)=X(I2)+PREDIP(I21)
258           Y(I2)=Y(I2)+PREDIP(I22)
259           X(I3)=X(I3)+PREDIP(I31)
260           Y(I3)=Y(I3)+PREDIP(I32)
261           A=DELTA/6.0*G*DN(I)
262           K1=2*I1
263           K2=2*I2
264           K3=2*I3
265           L1=K1-1
266           L2=K2-1
267           L3=K3-1
268           FORST(K1)=FORST(K1)+A
269           FORST(K2)=FORST(K2)+A
270           FORST(K3)=FORST(K3)+A
271       C*****TO INCORPORATE INITIAL STRESSES*****************************************
272           DO 411 KK=1,18
273         411 B(KK)=BLIB(KK,I)
274           DELTA=DELIB(I)
275           N=3
276           M=6
277           CALL GMTPA(B,F,N,M)
278           W(1)=STREN(I,1)
279           W(2)=STREN(I,2)
280           W(3)=STREN(I,3)
281           N=6
282           M=3
283           L=1
284           CALL GMPRD(F,W,V,N,M,L)
285           DO 412 KK=1,6
286         412 V(KK)=V(KK)*DELTA/2.0
287           FORST(L1)=FORST(L1)-V(1)
288           FORST(K1)=FORST(K1)-V(2)
289           FORST(L2)=FORST(L2)-V(3)
290           FORST(K2)=FORST(K2)-V(4)
291           FORST(L3)=FORST(L3)-V(5)
292           FORST(K3)=FORST(K3)-V(6)
293           4 CONTINUE
294       C*****START ITERATIONS FOR TIME INCREMENTS*********************************
295           DO 201 IN=1,NTIM
296           TIMTOT=TIMTOT+TIMC
297       C*****SET INCREMENTAL CREEP TO ZERO*****************************************
298           DO 24 J=1,NNOD2
299           FIST(J)=0.0
300           DO 24 IJ=1,4
```

```
      24 CSTIN(J,IJ)=0.0
C
C*****START SOLUTION ITERATIONS WITHIN TIME STEP**************************
      DO 204 J=1,10
      DIFSTR=0.0
C*****ADD FIST TO FORST TO GIVE FORCE VECTOR*******************************
      DO 205 K=1,NNOD2
  205 DISP(K)=FIST(K)+FORST(K)
C*****TO SET FORCE VECTOR TO ZERO FOR PRESCRIBED DISPLACEMENTS**********
      DO 35 KOD=1,ND
      DO 36 LOD=1,2
      MOD=ISP(KOD,LOD)
      IF(MOD.EQ.0) GO TO 36
      NID=LD(KOD)
      MID=2*NID+LOD-2
      KID=2*NNOD*(MID-1)+MID
      DISP(MID)=PDIS(KOD,LOD)*1.0D 24
   36 CONTINUE
   35 CONTINUE
C
C*****TO SOLVE THE EQUATION   AT*DISP=DISP*****************************
C*****CALL SOLUTION SUBROUTINE HARWELL LIBRARY GAUSSIAN ELIMINATION*****
      NUM=NNOD2
      CALL MA07BD(AT,DISP,NUM,NNOD2,NBW,PT)
      PT=0.0
C*****RESET FIST TO ZERO***************************************************
      DO 208 LI=1,NNOD2
  208 FIST(LI)=0.0
C*****WE NOW HAVE DISPLACEMENTS********************************************
C*****TO OBTAIN STRAINS FROM DISPLACEMENTS**********************************
      DO 20 I=1,NEL
      I1=NODEL(I,1)
      I2=NODEL(I,2)
      I3=NODEL(I,3)
      DO 9403 KK=1,18
 9403 B(KK)=BLIB(KK,I)
      DO 9404 KK=1,9
 9404 D(KK)=DLIB(KK,I)
      DELTA=DELIB(I)
      J1=2*I1
      K1=J1-1
      J2=2*I2
      K2=J2-1
      J3=2*I3
      K3=J3-1
      DISEL(1)=DISP(K1)
      DISEL(2)=DISP(J1)
      DISEL(3)=DISP(K2)
      DISEL(4)=DISP(J2)
      DISEL(5)=DISP(K3)
      DISEL(6)=DISP(J3)
C*****MULT B BY DISEL TO GIVE STRAINS IN STRAIN*****
      N=3
      M=6
      L=1
      CALL GMPRD(B,DISEL,STRAIN,N,M,L)
C*****TO OBTAIN STRESSES FROM STRAINS**************************************
C*****TO MULT D BY STRAINS TO GET STRESS ***********************************
      STRAIN(4)=0.0
C***** SUBTRACT INITIAL STRAIN TO GIVE ELASTIC STRAIN**********************
```

```
      DO 1007 IK=1,4
 1007 STEL(IK)=STRAIN(IK)-STIN(I,IK)-CSTIN(I,IK)
      N=3
      M=3
      L=1
      CALL GMPRD(D,STEL,STRESS,N,M,L)
C***** AMEND STRESS TO ALLOW FOR CREEP*************************************
      ELC=E(I)/((1.0+P(I))*(1.0-2.0*P(I)))
      STRESS(1)=STRESS(1)+ELC*P(I)*STEL(4)
      STRESS(2)=STRESS(2)+ELC*P(I)*STEL(4)
      STRESS(4)=ELC*P(I)*(STEL(1)+STEL(2))+ELC*(1.0-P(I))*STEL(4)
C***** ADD INITIAL STRESS TO CALC STRESS******************************
      DO 1019 IK=1,4
 1019 STRESS(IK)=STRESS(IK)+STREN(I,IK)
      IF(J.GT.1) GO TO 526
C PUT STRESSES INTO TRAY*************************************************
      DO 1000 IK=1,4
 1000 TRAY(I,IK)=STRESS(IK)
  526 CONTINUE
      AS=STRESS(1)-TRAY(I,1)
      BS=STRESS(2)-TRAY(I,2)
      CS=STRESS(3)-TRAY(I,3)
      DS=STRESS(4)-TRAY(I,4)
      ZAS=DABS(AS)
      ZBS=DABS(BS)
      ZCS=DABS(CS)
      DIFSTR=DMAX1(ZAS,ZBS,ZCS,DIFSTR)
      AS1=AS/2.0
      BS1=BS/2.0
      CS1=CS/2.0
      DS1=DS/2.0
      STRAY(I,1)=STRESS(1)
      STRAY(I,2)=STRESS(2)
      STRAY(I,3)=STRESS(3)
      STRAY(I,4)=STRESS(4)
      AS=TRAY(I,1)+AS/2.0
      BS=TRAY(I,2)+BS/2.0
      CS=TRAY(I,3)+CS/2.0
      DS=TRAY(I,4)+DS/2.0
C*****TO OBTAIN VALUE OF CREEP FROM STRESS AND STRAIN*********************
C*****FOR PLANE STRAIN*****************************************************
      STRM=(AS+BS+DS)/3.0
      S1=AS-STRM
      S2=BS-STRM
      S3=CS
      S4=DS-STRM
      CREEP(1)=S1*RTIMC/(VISCOS(I)*2.0)
      CREEP(2)=S2*RTIMC/(VISCOS(I)*2.0)
      CREEP(3)=S3*RTIMC/(VISCOS(I))
      CREEP(4)=S4*RTIMC/(VISCOS(I)*2.0)
C***** AMEND MATRIX W FOR CREEP*******************************************
      AW1=ELC*P(I)*CREEP(4)
C*****PUT ELEMENT CREEP INTO CSTIN****************************************
      DO 207 NIL=1,4
  207 CSTIN(I,NIL)=CREEP(NIL)
C*****TO INCORPERATE INITIAL  CREEP BY EXPRESSING AS INITIAL STRAIN*******
C*****TO MULTIPLY D BY CREEP**********************************************
      N=3
      M=3
      L=1
```

```
      CALL GMPRD(D,CREEP,W,N,M,L)
      W(1)=W(1)+AW1
      W(2)=W(2)+AW1
C*****TO TRANSPOSE B TO F**************************************************
      N=3
      M=6
      CALL GMTRA(B,F,N,M)
C*****TO MULTIPLY F BY W***************************************************
      N=6
      M=3
      L=1
      CALL GMPRD(F,W,V,N,M,L)
      DO 831 NERG=1,6
  831 V(NERG)=V(NERG)*DELTA/2.0
C*****TO MAKE FIST*********************************************************
      FIST(J1)=FIST(J1)+V(2)
      FIST(K1)=FIST(K1)+V(1)
      FIST(J2)=FIST(J2)+V(4)
      FIST(K2)=FIST(K2)+V(3)
      FIST(J3)=FIST(J3)+V(6)
      FIST(K3)=FIST(K3)+V(5)
   20 CONTINUE
C*****TO TEST FOR CONVERGENCE**********************************************
      WRITE(4,8520) DIFSTR
 8520 FORMAT(2X,'DIFSTR=',E10.3)
      DFS(J)=DIFSTR
      IF(J.EQ.1) GO TO 204
      JH=J-1
      DIFSTR=DFS(J)-DFS(JH)
      DIFSTR=DABS(DIFSTR)
      IF(J.LE.2) DIFSTR=1.0E10
      IF(DIFSTR.LE.OUT) GO TO 293
  204 CONTINUE
  293 CONTINUE
C***** ADD CSTIN TO STIN***************************************************
      DO 28 IJ=1,NEL
      DO 28 IK=1,4
      STIN(IJ,IK)=STIN(IJ,IK)+CSTIN(IJ,IK)
   28 CONTINUE
C***** ADD FIST TO FORST***************************************************
      DO 27 IJ=1,NNOD2
   27 FORST(IJ)=FORST(IJ)+FIST(IJ)
      WRITE(4,250) IN,J,TIMTOT
  250 FORMAT(2X,'TIME INCREMENT=',I10,2X,'NUMBER OF ITERATIONS=',I10
     1 ,5X,'TIME=',E10.3)
C*****WRITE INFORMATION ON CONVERGENCE*************************************
C
C*****WRITE RESULTS FOR FINAL STATE****************************************
  201 CONTINUE
      DO 209 I=1,NNOD
      IJ=2*I
      IK=IJ-1
      PREDIP(IK)=PREDIP(IK)+DISP(IK)*RNODEF
      PREDIP(IJ)=PREDIP(IJ)+DISP(IJ)*RNODEF
  209 WRITE(6,162) I,DISP(IK),DISP(IJ)
  162 FORMAT(13X,I5,17X,E10.3,16X,E10.3)
C***** WRITE PREDIP AND STRAY**********************************************
C*****SENT TO FILE (DEVICE 2) FOR RESTART OPTION***********
      DO 252 IC=1,NNOD2
  252 WRITE(2,253) PREDIP(IC),(STRAY(IC,JC),JC=1,4)
```

```
  253 FORMAT(2X,5E15.7)
      WRITE(6,199)
C
C***** TO CALCULATE THE PRINCIPAL SRESSES**********************************
      DO 210 I=1,NEL
      SC1=STRAY(I,1)
      SC2=STRAY(I,2)
      SC3=STRAY(I,3)
      SC4=STRAY(I,4)
      AVER=(SC1+SC2+SC4)/3.0
      AVER=AVER*DEV
      THET=2.0*SC3/(SC1-SC2)
      THET=DATAN(THET)
      THET=THET/2.0
      THET=57.29*THET
      IF(THET.GT.0.0) GO TO 192
      THET=THET+90.0
  192 CONTINUE
      ALPHA=THET/57.29
      ANZA=(SC1*(DCOS(ALPHA))**2)+
     1 (SC2*(DSIN(ALPHA))**2)+
     2 (SC3*(DSIN(2.0*ALPHA)))
      ANZB=SC1+SC2-ANZA
      BXB=X(NODEL(I,1))+X(NODEL(I,2))+X(NODEL(I,3))
      BYB=Y(NODEL(I,1))+Y(NODEL(I,2))+Y(NODEL(I,3))
      BXB=BXB/3.0*1.0E-5
      BYB=BYB/3.0*1.0E-5
      ANZA=ANZA-AVER
      ANZB=ANZB-AVER
      WRITE(6,164) I,ANZA,ANZB,THET,SC4,BXB,BYB
      STRAY(I,1)=ANZA
      STRAY(I,2)=ANZB
      STRAY(I,3)=THET
  210 CONTINUE
  164 FORMAT(13X,I5,16X,E10.3,15X,E10.3,6X,F8.3,2X,E10.3,3X,2(F10.3))
C***** TO PLOT THE STRESSES AND DISPLACEMENTS**************************
      READ(5,5005)KPLOT,KIK
 5005 FORMAT(2I10)
      IF(KPLOT.EQ.0) GO TO 5010
      READ(5,5011) XSC,XSH,YSC,YSH
 5011 FORMAT(4F10.3)
      CALL PLOTS(X,Y,NODEL,STRAY,DISP,NNOD,NEL,XSC,XSH,YSC,YSH,KPLOT
     1 ,DINIT,KIK,STMAX,TRAY)
 5010 CONTINUE
      STOP
      END
C
C***** SUBROUTINE PLOTS STRESSES AND DISPLACEMENTS*********************
      SUBROUTINE PLOTS(X,Y,NODEL,STRAY,DISP,NNOD,NEL,
     1 XSC,XSH,YSC,YSH,KPLOT,DINIT,KIK,STMAX,TRAY)
      IMPLICIT REAL *8(A-H,O-Z)
      DIMENSION
     1 X(1),Y(1),NODEL(460,3),STRAY(460,4)
     2 ,TRAY(460,4),DISP(1),DINIT(1)
      CALL PLTXMX(80.0)
C*****TO FIND MAXIMUM DISPLACEMENT*************************************
      DISMAX=0.0
      DO 5013 I=1,NNOD
      IRT2=I*2
      IRT1=IRT2-1
```

```
      CMAX=DISP(IRT1)
      EMAX=DISP(IRT2)
      CMAX=DABS(CMAX)
      EMAX=DABS(EMAX)
 5013 DISMAX=DMAX1(DISMAX,CMAX,EMAX)
C*****PLOT NUM VALUE OF DEV STRESS OR MEAN STRESS************************
      IF(KPLOT.EQ.2) GO TO 5018
      DO 200 I=1,NEL
      X1=X(NODEL(I,1))
      Y1=Y(NODEL(I,1))
      X2=X(NODEL(I,2))
      Y2=Y(NODEL(I,2))
      X3=X(NODEL(I,3))
      Y3=Y(NODEL(I,3))
      X1=(X1+XSH)*XSC
      X2=(X2+XSH)*XSC
      X3=(X3+XSH)*XSC
      Y1=(Y1+YSH)*YSC
      Y2=(Y2+YSH)*YSC
      Y3=(Y3+YSH)*YSC
      IF(X1.GE.20.0) GO TO 200
      IF(X2.GE.20.0) GO TO 200
      IF(X3.GE.20.0) GO TO 200
      IF(Y1.LT.0.0) GO TO 200
      IF(Y2.LT.0.0) GO TO 200
      IF(Y3.LT.0.0) GO TO 200
      IF(KIK.EQ.1) GO TO 9494
C*****DRAW GRID*********************************************************
      CALL PENUP(X1,Y1)
      CALL PENDN(X2,Y2)
      CALL PENDN(X3,Y3)
      CALL PENDN(X1,Y1)
 9494 CONTINUE
      XXC=(X1+X2+X3)/3.0
      YYC=(Y1+Y2+Y3)/3.0
      SDT1=STRAY(I,1)
      SDT2=STRAY(I,2)
      SDT4=STRAY(I,4)
      SDT1=DABS(SDT1)
      SDT2=DABS(SDT2)
      SDT4=DABS(SDT4)
      SDT=(SDT1+SDT2+SDT4)/3.0
      SDT=SDT/1.0E9
      RDT=STRAY(I,1)-STRAY(I,2)
      RDT=RDT/2.0
      RDT=DABS(RDT)
      RDT=RDT/1.0E9
C     RDT=SDT
      XXC=XXC-0.25
      IF(XXC.GE.20.0) GO TO 200
      IF(YYC.LT.0.0) GO TO 200
      CALL PNUMBR(XXC,YYC,0.07,RDT,0.C,'F2.3 *',0.0)
  200 CONTINUE
      IF(KPLOT.EQ.3) GO TO 5010
 5018 CONTINUE
C    PLOT PRINCIPLAL STRESSES OR DEV STRESSES*************************
      DO 501 I=1,NEL
      X1=X(NODEL(I,1))
      Y1=Y(NODEL(I,1))
      X2=X(NODEL(I,2))
```

```
      Y2=Y(NODEL(I,2))
      X3=X(NODEL(I,3))
      Y3=Y(NCDEL(I,3))
      X1=(X1+XSH)*XSC+20.0
      X2=(X2+XSH)*XSC+20.0
      X3=(X3+XSH)*XSC+20.0
      Y1=(Y1+YSH)*YSC
      Y2=(Y2+YSH)*YSC
      Y3=(Y3+YSH)*YSC
      IF(X1.GE.40.0) GO TO 501
      IF(X2.GE.40.0) GO TO 501
      IF(X3.GE.40.0) GO TC 501
      IF(Y1.LT.0.0) GO TO 501
      IF(Y2.LT.0.0) GC TC 501
      IF(Y3.LT.0.0) GO TO 501
      IF(KIK.EQ.1) GC TO 5017
C*****PLOT GRID**********************************************************
      CALL PENUP(X1,Y1)
      CALL PENDN(X2,Y2)
      CALL PENDN(X3,Y3)
      CALL PENDN(X1,Y1)
 5017 CONTINUE
      XXC=(X1+X2+X3)/3.0
      YYC=(Y1+Y2+Y3)/3.0
      IF(XXC.GE.40.0) GC TO 501
      IF(YYC.LT.0.0) GO TO 501
      TA=DCOS(STRAY(I,3)/57.29)*STRAY(I,1)/STMAX
      TB=DSIN(STRAY(I,3)/57.29)*STRAY(I,1)/STMAX
      TX=DCOS(STRAY(I,3)/57.29)*STRAY(I,2)/STMAX
      TY=DSIN(STRAY(I,3)/57.29)*STRAY(I,2)/STMAX
      XN1=XXC+TA
      XN2=XXC-TA
      YN1=YYC+TB
      YN2=YYC-TB
      XS1=XXC-TY
      XS2=XXC+TY
      YS1=YYC+TX
      YS2=YYC-TX
      CALL PENUP(XN1,YN1)
      CALL PENDN(XN2,YN2)
      CALL PENUP(XS1,YS1)
      CALL PENDN(XS2,YS2)
      TA=STRAY(I,1)
      TX=STRAY(I,2)
      IF(TA.LT.0.0) GO TO 9331
      CALL PSYMB(XN1,YN1,0.02,01,0.0,-1)
      CALL PSYMB(XN2,YN2,0.02,01,0.0,-1)
 9331 CONTINUE
      IF(TX.LT.0.0) GO TO 9332
      CALL PSYMB(XS1,YS1,0.02,01,0.0,-1)
      CALL PSYMB(XS2,YS2,0.02,01,0.0,-1)
 9332 CONTINUE
  501 CONTINUE
      IF(KPLOT.EQ.2) GO TO 5010
C***** PLOT NODAL DISPLACEMENTS*************************************
      DO 506 I=1,NNOD
      XXC=X(I)
      YYC=Y(I)
      XXC=(XXC+XSH)*XSC+40.0
      YYC=(YYC+YSH)*YSC
```

```
661           IF(XXC.GE.60.0) GO TO 506
662           IF(YYC.LT.0.0) GO TO 506
663           IRT2=2*I
664           IRT1=IRT2-1
665           XDINC=DISP(IRT1)
666           YDINC=DISP(IRT2)
667           XDINC=XDINC*0.5/DISMAX
668           YDINC=YDINC*0.5/DISMAX
669           XDINC=XXC+XDINC
670           YDINC=YYC+YDINC
671           CALL PSYMB(XXC,YYC,-0.02,0,0.0,-1)
672           CALL PENUP(XXC,YYC)
673           CALL PENDN(XDINC,YDINC)
674         506 CONTINUE
675        5010 CONTINUE
676           CALL PLTEND
677           RETURN
678           END
679        C
680        C***** SUBROUTINE MATRIX MULTIPLICATION**********************************
681           SUBROUTINE GMPRD(A,B,R,N,M,L)
682           IMPLICIT REAL*8 (A-H,O-Z)
683           DIMENSION A(1),B(1),R(1)
684           IR=0
685           IK=-M
686           DO 10 K=1,L
687           IK=IK+M
688           DO 10 J=1,N
689           IR=IR+1
690           JI=J-N
691           IB=IK
692           R(IR)=0
693           DO 10 I=1,M
694           JI=JI+N
695           IB=IB+1
696        10 R(IR)=R(IR)+A(JI)*B(IB)
697           RETURN
698           END
699        C
700        C*****  SUBROUTINE MATRIX TRANSPOSITION**********************************
701           SUBROUTINE GMTRA(A,R,N,M)
702           IMPLICIT REAL*8 (A-H,O-Z)
703           DIMENSION A(1),R(1)
704           IR=0
705           DO 10 I=1,N
706           IJ=I-N
707           DO 10 J=1,M
708           IJ=IJ+N
709           IR=IR+1
710        10 R(IR)=A(IJ)
711           RETURN
712           END
713        $ENDFILE
 OF FILE
```

APPENDIX 2

The program described in this appendix executes the numerical calculations of the finite element thermal stress analysis for the oceanic lithosphere used in Chapter 4 and formulated in Chapter 2. The program is written in Fortran 4 G and consists of the main program and five subroutines. Double precision is used for all real characters.

Main Program. A flow diagram of the main program is shown in figure A2.1 and summarizes the main steps carried out in the finite element calculation.

Subroutine Plots. This subroutine plots the calculated principal stresses. It is not the same subroutine as the one described in appendix 1 of similar name.

Subroutine Delts. This subroutine calculates the temperature at a point in the oceanic lithosphere and hence the cooling, according to equations 4.1 and 4.2. The initial strain is then calculated from the cooling at that point.

Subroutines GMPRD, GMTRA and MA07BD. These subroutines are idential to those of similar name in appendix 1.

A listing of the main program and the subroutines is given at the end of the appendix.

Program Input

The program input defines the geometry, physical constants and boundary conditions of the region under investigation together with information controlling output. Formats and device numbers are given in brackets.

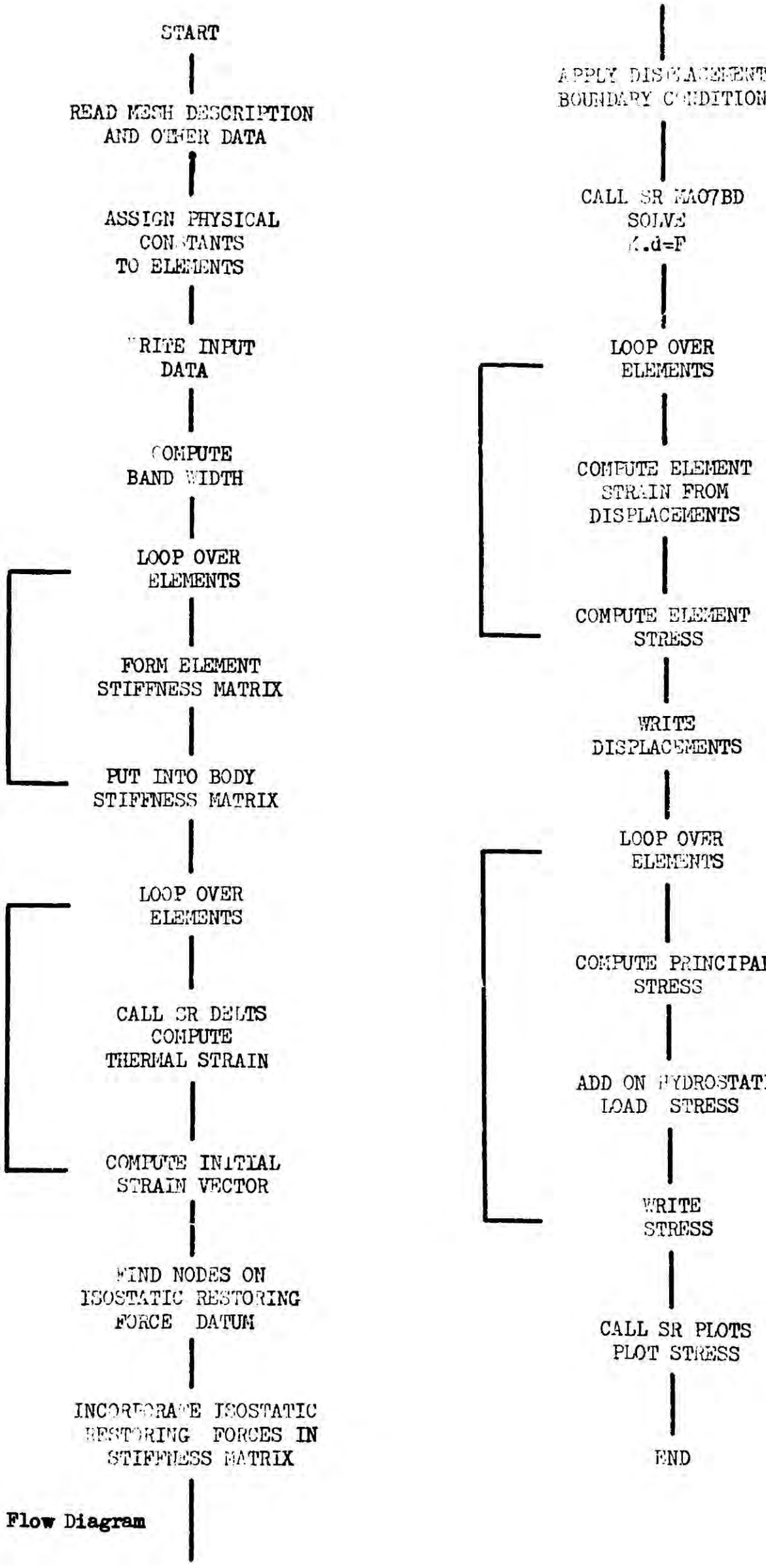

Figure A2.1 Flow Diagram

1. NNOD,NEL (2I10 device 5)

   NNOD, number of nodes of finite element grid.

   NEL, number of elements of finite element grid.

2. TLIM,DENLIT,VEL,STMAX (3F10.3, E10.3 device 5)

   TLIM, temperature above which lithosphere is assumed to be a viscous body as opposed to elastic.

   DENLIT, if equals 0.0 thermal stresses alone are printed and plotted; if equals 1.0 thermal and hydrostatic load stresses are printed and plotted.

   VEL, half spreading rate of the ocean ridge (cm/yr).

   STMAX, stress plot scaling factor (dynes/cm^2/inch).

3. For all nodes

   K,X(K),Y(K) (I10,2F10.3 device 5)

   K, node number

   X(K),Y(K), X and Y coordinate of node (cm).

4. For all elements

   K,(NODEL(K,J),J=1,3) (4I10 device 5)

   K, element number.

   NODEL(K,1,2,3), numbers of nodes specifying element.

5. ND (I10 device 5)

   ND, number of nodes with specified displacements.

6. LD(I),((ISP(I,J),PDIS(I,J),J=1,2) (I10,2(I10,F10.3) device 5)

   LD(I), node number at which displacement specified.

   ISP(I,1),ISP(I,2), controls specification of displacement for X and Y directions. If equal to 0 no displacement is specified; if equal to 1 displacement is specified.

   PDIS(I,1),PDIS(I,2), X and Y components of specified displacements.

7. KPLOT (I10 device 5)

KPLOT, controls stress plot output.

KPLOT = 0 no plot

KPLOT = 1 principal stresses are plotted.

Program Output

1. All input data specifying grid and boundary conditions and information of Input line 2 are printed, (device 4).
2. Temperature and initial thermal strain of elements are printed, (device 6).
3. Final nodal displacements are printed, (device 3).
4. Final element principal stresses are printed, (device 3). Additional facilities exist to plot element principal stresses. They are plotted with or without the hydrostatic load stress of the ocean crust and mantle according to the value input for DENLIT.

Preset internal parameters

1. DATSOS, the datum at which isostatic restoring forces are to be applied.
2. DMOHO, depth of Moho.
3. P(I), element Poisson's ratio.
4. E(I), element Young's modulus.
5. VEC(I), element coefficient of linear expansion.
6. HPW, hydrostatic load stress of the ocean.
   HPC, hydrostatic load stress of the crust.

7. L, (subroutine Delts), lithosphere thickness.

8. TS, temperature T_o of equation 4.1.

9. P, parameter p of equation 4.1.

Program Test

The program described in this appendix is adapted from the program described in appendix 1. The way in which the initial strain is calculated has been altered (thermal strain replacing creep) and the facilities for iterations within and over time steps, required for visco-elastic analysis are omitted. A test of this program has not been made explicitly, however, the tests made on the visco-elastic program apply to the program of this appendix. Stresses in the z direction (parallel to the ridge axis) calculated by the program agree well with simple analytical estimates as described by Turcotte (1974).

```
C***** F E PROGRAM FOR TEMPERATURE INDUCED STRESSES ********************
C***** MAIN PROGRAM*************************************************
      IMPLICIT REAL *8 (A-H,C-Z)
C*****DIMENSION STATEMENTS*****************************************
      DIMENSION
     1 X(330),Y(330),NCDEL(540,3),E(540),P(540),DN(540),
     3 ISP(100,2),PDIS(100,2),
     5 CSTIN(540,3),
     6 T(36),D(9),B(18),V(6),F(18),H(18),VEC(540),
     7 W(3),QQ(3),CC(3),STRAY(540,4),
     8 CREEP(3),DISEL(6),STRESS(3),STRAIN(3),STEL(3),DISP(660)
     9 ,LD(540),AT(660,50),FISOS(100),NK(100)
     1 ,DLIB(9,540),BLIB(18,540),DELIB(540)
C***** ISOSTATIC RESTORING FORCE DATUM IS*******************************
      DATSOS=0.0
C*****MOHO DEPTH IS*************************************
      DMOHO=-7.0
C
C*****READ IN INPUT DATA*******************************************
C*****READ NUMBER OF NODES AND ELEMENTS*****************************
      READ(5,800) NNOD,NEL
C*****READ ELASTIC TEMP LIMIT,LOAD STRESS MARKER SPREADING RATE AND STRF
      READ(5,9801) TLIM,DENLIT,VEL,STMAX
      WRITE(4,9801) TLIM,DENLIT,VEL,STMAX
 9801 FORMAT(3F10.3,E10.3)
      NNOD2=NNOD*2
  800 FORMAT(2I10)
      DO 850 I=1,NNOD
  850 READ(5,801) K,X(K),Y(K)
  801 FORMAT(I10,2F10.3)
      DO 851 I=1,NEL
  851 READ(5,802) K,(NODEL(K,J),J=1,3)
  802 FORMAT(4I10)
C*****READ SPECIFIED DISPLACEMENTS*********************************
      READ(5,808) ND
  808 FORMAT(I10)
      DO 854 I=1,ND
  854 READ(5,807) LD(I),(ISP(I,J),PDIS(I,J),J=1,2)
  807 FORMAT(I10,2(I10,F10.3))
C***** ASSIGN ELASTIC AND EXPANSION CONSTANTS***********************
      DO 7001 I=1,NEL
      XO=(X(NODEL(I,1))+X(NCDEL(I,2))+X(NCDEL(I,3)))/3.0
      YO=(Y(NODEL(I,1))+Y(NODEL(I,2))+Y(NODEL(I,3)))/3.0
      P(I)=0.25
      VEC(I)=1.0E-5
      E(I)=1.7E12
      IF(YO.GT.DMOHO) VEC(I)=0.7E-5
      IF(YO.GT.DMOHO) P(I)=0.25
      IF(YO.GT.DMOHO) E(I)=1.0E12
      PARY=P(I)
      CALL DELTS(XO,YO,CREEP,TO,A,TLIM,VEL,PARY)
      IF(TO.GT.TLIM) E(I)=1.0
 7001 CONTINUE
C
C*****WRITE OUT INPUT DATA*****************************************
      WRITE(4,150) NNOD,NEL
  150 FORMAT(2X,'NUMBER OF NODES =',I4,10X,'NUMBER OF ELEMENTS =',I4)
      WRITE(6,199)
  199 FORMAT('0')
      DO 100 I=1,NNOD
```

```
  100 WRITE(6,152) I,X(I),Y(I)
  152 FORMAT(13X,I5,24X,F10.3,12X,F10.3)
      WRITE(6,199)
      DO 101 I=1,NEL
  101 WRITE(6,154) I,(NODEL(I,J),J=1,3),E(I),P(I),VFC(I)
  154 FORMAT(14X,I4,18X,I4,12X,I4,12X,I4,D10.3,F6.3,D10.3)
      WRITE(6,199)
      WRITE(6,199)
      WRITE(6,199)
      DO 105 I=1,ND
  105 WRITE(6,169) LD(I),((ISP(I,J),PDIS(I,J)),J=1,2)
  169 FORMAT(20X,I10,12X,I10,10X,F10.3,10X,I10,10X,F10.3)
C*****TO CALC THE PARAM NBW*****************************************
      PT=1.0
      NBW=0
      DO 9182 I=1,NEL
      KB1=IABS(NODEL(I,1)-NODEL(I,2))
      KB2=IABS(NODEL(I,2)-NODEL(I,3))
      KB3=IABS(NODEL(I,3)-NODEL(I,1))
 9182 NBW=AMAX0(KB1,KB2,KB3,NBW)
      NBW=2*NBW+2
      NBW=2*NBW-1
      WRITE(4,9187) NBW
 9187 FORMAT(2X,'NBW=',I10)
C
C*****FORM STIFFNESS MATRIX*****************************************
C*****TO FORM ELEMENT STIFNESS MATRIX********************************
      DO 6 I=1,NEL
C*****TO SET H AND T TO ZERO****************************************
      DO 41 LIT=1,36
   41 T(LIT)=0.0
      DO 42 LIT=1,18
   42 H(LIT)=0.0
C*****FORM D MATRIX*************************************************
      A=E(I)*(1.0-P(I))/((1.0+P(I))*(1.0-2*P(I)))
      Q=P(I)/(1.0-P(I))
      D(1)=A
      D(2)=A*Q
      D(3)=0.0
      D(4)=A*Q
      D(5)=A
      D(6)=0.0
      D(7)=0.0
      D(8)=0.0
      D(9)=A*(1.0-Q)/2.0
C*****FORM B MATRIX*************************************************
      I1=NODEL(I,1)
      I2=NODEL(I,2)
      I3=NODEL(I,3)
      DELTA=Y(I3)*X(I2)
     1      -Y(I2)*X(I3)
     2      -X(I1)*Y(I3)
     3      +X(I1)*Y(I2)
     4      +Y(I1)*X(I3)
     5      -Y(I1)*X(I2)
      QQ(1)=(Y(I2)-Y(I3))/DELTA
      CC(1)=(X(I3)-X(I2))/DELTA
      QQ(2)=(Y(I3)-Y(I1))/DELTA
      CC(2)=(X(I1)-X(I3))/DELTA
      QQ(3)=(Y(I1)-Y(I2))/DELTA
```

```
      CC(3)=(X(I2)-X(I1))/DELTA
      B(1)=QQ(1)
      B(2)=0.0
      B(3)=CC(1)
      B(4)=0.0
      B(5)=CC(1)
      B(6)=QQ(1)
      B(7)=QQ(2)
      B(8)=0.0
      B(9)=CC(2)
      B(10)=0.0
      B(11)=CC(2)
      B(12)=QQ(2)
      B(13)=QQ(3)
      B(14)=0.0
      B(15)=CC(3)
      B(16)=0.0
      B(17)=CC(3)
      B(18)=QQ(3)
      DELTA=DABS(DELTA)
      DO 9401 KK=1,18
 9401 BLIB(KK,I)=B(KK)
      DELIB(I)=DELTA
      DO 9402 KK=1,9
 9402 DLIB(KK,I)=D(KK)
      N=3
      M=6
      CALL GMTRA(B,F,N,M)
C*****B IS TRANSPOSED TO F*****************************************
C*****MULTIPLY D BY B TO GIVE H*****************************************
      N=3
      M=3
      L=6
      CALL GMPRD(D,B,H,N,M,L)
C*****MULTIPLY F BY H TO GIVE T*****************************************
      N=6
      M=3
      L=6
      CALL GMPRD(F,H,T,N,M,L)
C*****TO MULTIPLY BY DELTA/2*****************************************
      DO 38 NI=1,36
   38 T(NI)=T(NI)*DELTA/2.0
C*****WE NOW HAVE ELEMENT STIFFNESS MATRIX*****************************
C*****TO PUT T INTO BODY STIFFNESS MATRIX*****************************
      K=1
      DO 10 MS=1,3
      DO 10 NS=1,2
      DO 10 KS=1,3
      DO 10 LS=1,2
      JX=NODEL(I,MS)
      JX=2*JX-2+NS
      IY=NODEL(I,KS)
      IY=2*IY-2+LS
      LOC=JX-IY+0.5*(NBW+1)
      IF(LOC.LT.1) GO TO 10
      IF(LOC.GT.NBW) GO TO 10
      AT(IY,LOC)=AT(IY,LOC)+T(K)
   10 K=K+1
    6 CONTINUE
      WRITE(4,922)
```

```
  922 FORMAT(2X,'TOTOL STIFFNESS FORMED')
C
C     TO CALCULATE INITIAL STRAIN AND PUT INTO FORCE VECTOR**************
       DO 202 I=1,NNOD2
  202 DISP(I)=0.0
      DO 201 I=1,NEL
      I1=NODEL(I,1)
      I2=NODEL(I,2)
      I3=NODEL(I,3)
      DO 943 KK=1,18
  943 B(KK)=BLIB(KK,I)
      DO 944 KK=1,9
  944 D(KK)=DLIB(KK,I)
      DELTA=DELIB(I)
      J1=2*I1
      K1=J1-1
      J2=2*I2
      K2=J2-1
      J3=2*I3
      K3=J3-1
C***** CALL SUBROUTINE FO THERMAL STRAIN**********************************
      XO=(X(I1)+X(I2)+X(I3))/3.0
      YO=(Y(I2)+Y(I1)+Y(I3))/3.0
      XO=XO/1.0E5
      YO=YO/1.0E5
      A=VEC(I)
      PARY=P(I)
      CALL DELTS(XO,YO,CREEP,TO,A,TLIM,VEL,PARY)
      WRITE(6,666) I,XO,YO,TO,A,CREEP(1)
  666 FORMAT(5X,I10,4F10.3,E10.3)
C*****PUT ELEMENT CREEP INTO CSTIN***************************************
      DO 207 NIL=1,3
  207 CSTIN(I,NIL)=CREEP(NIL)
C*****TO INCORPERATE  CREEP BY EXPRESSING AS INITIAL STRAIN ************
C*****TO MULTIPLY D BY CREEP*********************************************
      N=3
      M=3
      L=1
      CALL GMPRD(D,CREEP,W,N,M,L)
C*****TO TRANSPOSE B TO F************************************************
      N=3
      M=6
      CALL GMTRA(B,F,N,M)
C*****TO MULTIPLY F BY W*************************************************
      N=6
      M=3
      L=1
      CALL GMPRD(F,W,V,N,M,L)
      DO 831 NERG=1,6
  831 V(NERG)=V(NERG)*DELTA/2.0
C*****TO MAKE FORCE VECTOR***********************************************
      DISP(J1)=DISP(J1)+V(2)
      DISP(K1)=DISP(K1)+V(1)
      DISP(J2)=DISP(J2)+V(4)
      DISP(K2)=DISP(K2)+V(3)
      DISP(J3)=DISP(J3)+V(6)
      DISP(K3)=DISP(K3)+V(5)
  201 CONTINUE
C
C*****TO ALLOW FOR ISOSTATIC COMPENSATION*********************************
```

```
241           KCOUNT=0
242           DO 3400 I=1,NNOD
243           YI=Y(I)
244           IF(YI.LT.CATSOS) GO TO 3400
245           KCOUNT=KCOUNT+1
246           NK(KCOUNT)=I
247        3400 CONTINUE
248           DENY=2.0*981.0
249        C*****TO CALC FISOS FOR END NODES*****************************************
250           KZ=NK(1)
251           KY=NK(2)
252           AG=X(KY)-X(KZ)
253           FISOS(1)=AG/2.0*DENY
254           KZ=NK(KCOUNT)
255           KCM=KCOUNT-1
256           KY=NK(KCM)
257           AG=X(KZ)-X(KY)
258           FISOS(KCOUNT)=AG/2.0*DENY
259        C*****  TO CALCULATE FISOS FOR REST*****************************************
260           KCT=KCOUNT-1
261           DO 2401 I=2,KCT
262           IPL=I+1
263           KT=NK(IPL)
264           IMN=I-1
265           KS=NK(IMN)
266           AG=X(KT)-X(KS)
267           FISOS(I)=AG/2.0*DENY
268        2401 CONTINUE
269        C*****TO PUT FISOS INTO BODY STIFFNESS MATRIX*****************************
270           DO 3402 I=1,KCOUNT
271           JHK=2*NK(I)
272           LOC=0.5*(NBW+1)
273           FIQ=FISOS(I)
274           FIQ=DABS(FIQ)
275           AT(JHK,LOC)=AT(JHK,LCC)+FIQ
276        3402 CONTINUE
277        C*****  INTRODUCE PRESCRIBED DISPLACEMENTS*********************************
278           DO 30 II=1,ND
279           DO 31 J=1,2
280           LIK=ISP(II,J)
281           IF(LIK.EQ.0) GO TC 31
282           I=LD(II)
283           N=2*I+J-2
284           DISP(N)=PDIS(II,J)*1.0D 24
285           LOC=0.5*(NBW+1)
286           AT(N,LOC)=1.0D 24
287        31 CONTINUE
288        30 CONTINUE
289           WRITE(4,923)
290         923 FORMAT(2X,'PRESCRIBED DISPLACEMENTS INTRODUCED')
291        C
292        C*****TO SOLVE THE EQUATION   AT*DISP=DISP*******************************
293        C******* CALL SOLUTION SR (HARWELL LIBRARY)--GAUSSIAN ELIMINATION*****
294           NUM=NNOD2
295           CALL MA07BC(AT,DISP,NUM,NNOD2,NBW,PT)
296           WRITE(4,3130)
297         3130 FORMAT(2X,'EQUATION SOLVED')
298        C*****WE NOW HAVE DISPLACEMENTS*******************************************
299        C
300        C*****TO OBTAIN STRAINS AND STRESSES FROM DISPLACEMENTS*******************
```

```
C*****TO OBTAIN STRAINS FRCM DISPLACEMENTS*******************************
      DO 20 I=1,NEL
      I1=NODEL(I,1)
      I2=NODEL(I,2)
      I3=NODEL(I,3)
      DO 9403 KK=1,18
 9403 B(KK)=BLIB(KK,I)
      DO 9404 KK=1,9
 9404 D(KK)=DLIB(KK,I)
      DELTA=DELIB(I)
      J1=2*I1
      K1=J1-1
      J2=2*I2
      K2=J2-1
      J3=2*I3
      K3=J3-1
      DISEL(1)=DISP(K1)
      DISEL(2)=DISP(J1)
      DISEL(3)=DISP(K2)
      DISEL(4)=DISP(J2)
      DISEL(5)=DISP(K3)
      DISEL(6)=DISP(J3)
C*****MULT B BY DISEL TO GIVE STRAINS************************************
      N=3
      M=6
      L=1
      CALL GMPRD(B,DISEL,STRAIN,N,M,L)
C*****TO OBTAIN STRESSES FRCM STRAINS************************************
C*****TO MULT D BY STRAINS TO GET STRESS*********************************
C***** SUBTRACT INITIAL STRAIN TO GIVE ELASTIC STRAIN********************
      DO 1007 IK=1,3
 1007 STEL(IK)=STRAIN(IK)-CSTIN(I,IK)
      N=3
      M=3
      L=1
      CALL GMPRD(D,STEL,STRESS,N,M,L)
      DO 1000 IK=1,3
 1000 STRAY(I,IK)=STRESS(IK)
   20 CONTINUE
C*****WRITE RESULTS FOR FINAL STATE*************************************
      WRITE(6,199)
      DO 209 I=1,NNOD
      IJ=2*I
      IK=IJ-1
  209 WRITE(3,162) I,DISP(IK),DISP(IJ)
  162 FORMAT(10X,I10,10X,E10.3,10X,E10.3)
C
C***** TO CALCULATE THE PRINCIPAL SRESSES*********************************
      READ(5,5005) KPLCT
      DO 210 I=1,NEL
      SC1=STRAY(I,1)
      SC2=STRAY(I,2)
      SC3=STRAY(I,3)
      THET=2.0*SC3/(SC1-SC2)
      THET=DATAN(THET)
      THET=THET/2.0
      THET=57.29*THET
      IF(THET.GT.0.0) GO TC 192
      THET=THET+90.0
  192 CONTINUE
```

```
361           ALPHA=THET/57.29
362           ANZA=(SC1*(DCOS(ALPHA))**2)+
363          1 (SC2*(DSIN(ALPHA))**2)+
364          2 (SC3*(DSIN(2.0*ALPHA)))
365           ANZB=SC1+SC2-ANZA
366           ANZF=P(I)*(SC1+SC2)-CSTIN(I,1)/(1.0+P(I))*E(I)
367     C*****ADD ON HYDROSTATIC LOAD STRESSES IF REQUIRED**********************
368     C***** 4 KM OCEEAN,7 KM CRUST, REST MANTLE**********************
369           YO=(Y(NODEL(I,1))+Y(NODEL(I,2))+Y(NODEL(I,3)))/3.0
370           HPW=-4.0E5*981.0
371           HPC=-7.0E5*2.8*981.0
372           HPR=HPW+HPC+981.0*3.3*(YO+7.0E5)
373           IF(YO.GT.-7.0E5) HPR=HPW+981.0*2.8*YO
374           HPR=HPR*DENLIT
375           ANZA=ANZA+HPR
376           ANZB=ANZB+HPR
377           ANZF=ANZF+HPR
378           RS1=ANZA
379           RS2=ANZB
380           RS3=ANZF
381           RAS=DMAX1(RS1,RS2,RS3)
382           RBS=DMIN1(RS1,RS2,RS3)
383           MK=0
384           IF(RAS.EQ.RS3) MK=1
385           IF(RBS.EQ.RS3) MK=1
386           WRITE(3,164) I,ANZA,ANZB,THET,ANZF,MK
387           STRAY(I,1)=ANZA
388           STRAY(I,2)=ANZB
389           STRAY(I,3)=THET
390           STRAY(I,4)=ANZF
391         210 CONTINUE
392         164 FORMAT(13X,I5,16X,E10.3,15X,E10.3,15X,F10.4,5X,E10.3
393            1 ,I2)
394     C***** TO PLOT THE STRESSES AND DISPLACEMENTS**************************
395          5005 FORMAT(I10)
396           IF(KPLOT.EQ.0) GO TO 5010
397           READ(5,5011) XSC,XSH,YSC,YSH
398           XSC=XSC*1.0E-5
399           YSC=YSC*1.0E-5
400           XSH=XSH*1.0E5
401           YSH=YSH*1.0E5
402          5011 FORMAT(4F10.3)
403           CALL PLOTS(X,Y,NODEL,STRAY,DISP,NNOD,NEL,
404              1 XSC,XSH,YSC,YSH,KPLOT,KIK,STMAX)
405          5010 CONTINUE
406           STOP
407           END
408     C
409     C***** SUBROUTINE MTATRIX MULTIPLICATION*********************************
410           SUBROUTINE GMPRD(A,B,R,N,M,L)
411           IMPLICIT REAL*8 (A-H,O-Z)
412           DIMENSION A(1),B(1),R(1)
413           IR=0
414           IK=-M
415           DO 10 K=1,L
416           IK=IK+M
417           DO 10 J=1,N
418           IR=IR+1
419           JI=J-N
420           IB=IK
```

```
421           R(IR)=0
422           DO 10 I=1,M
423           JI=JI+N
424           IB=IB+1
425        10 R(IR)=R(IR)+A(JI)*B(IB)
426           RETURN
427           END
428     C
429     C***** SUBROUTINE MATRIX TRANSPOSE*****************************************
430           SUBROUTINE GMTRA(A,R,N,M)
431           IMPLICIT REAL*8 (A-H,O-Z)
432           DIMENSION A(1),R(1)
433           IR=0
434           DO 10 I=1,N
435           IJ=I-N
436           DO 10 J=1,M
437           IJ=IJ+N
438           IR=IR+1
439        10 R(IR)=A(IJ)
440           RETURN
441           END
442     C
443            SUBROUTINE CALCULATES TEMPERATURE AND THERMAL INITIAL STRAIN*****
444           SUBROUTINE DELTS(XO,YO,CREEP,TO,A,TLIM,VEL,PARY)
445           IMPLICIT REAL *8(A-H,O-Z)
446           DIMENSION CREEP(1)
447           PI=3.1416
448           EC=A*(1.0+PARY)
449     C*****LITH THICKNESS IS*****************************************
450           L=80.0
451           P=37.8*(L/100.0)*VEL
452     C*****TO IS*****************************************************
453           TS=1200.0
454           X=XO/L
455           YO=YO+L
456           Z=YO/L
457           Z=CABS(Z)
458           T=1-Z
459           DO 1 I=1,20
460           RI=I
461           A=(2.0/(PI*RI))*(-1.0)**(I+1)
462           C=DSIN(RI*PI*Z)
463           B=(P/2.0-(P*P/4.0+RI*RI*PI*PI)**0.5)*X
464           B=DEXP(B)
465           A=A*B*C
466           T=T+A
467        1 CONTINUE
468           TO=T*TS
469     C*****  IF(XO.GT.1200.0) TO=1200.0
470           TST=TLIM-TO
471           IF(TST.LT.0.0) TST=0.0
472           CREEP(1)=-EC*TST
473           CREEP(2)=-EC*TST
474           CREEP(3)=0.0
475           A=A/T
476           RETURN
477           END
478     C
479     C***** SUBROUTINE PLOTS PRINCIPAL STRESSES*****************************
480           SUBROUTINE PLOTS(X,Y,NODEL,STRAY,DISP,NNOD,NEL,
```

```
      1 XSC,XSH,YSC,YSH,KPLOT,KIK,STMAX)
        IMPLICIT REAL *8(A-H,O-Z)
        DIMENSION
      1 X(1),Y(1),NODEL(540,3),STRAY(540,4)
      2 ,DISP(1)
        CALL PLTXMX(40.0)
        DO 501 I=1,NEL
        X1=X(NODEL(I,1))
        Y1=Y(NODEL(I,1))
        X2=X(NODEL(I,2))
        Y2=Y(NODEL(I,2))
        X3=X(NODEL(I,3))
        Y3=Y(NODEL(I,3))
        XXR=(X1+X2+X3)/3.0
        X1=(X1+XSH)*XSC
        X2=(X2+XSH)*XSC
        X3=(X3+XSH)*XSC
        Y1=(Y1+YSH)*YSC
        Y2=(Y2+YSH)*YSC
        Y3=(Y3+YSH)*YSC
        XXC=(X1+X2+X3)/3.0+0.5
        YYC=(Y1+Y2+Y3)/3.0
        IF(XXC.GE.40.0) GO TO 501
        IF(YYC.LT.0.0) GO TO 501
        TA=DCOS(STRAY(I,3)/57.29)*STRAY(I,1)/STMAX
        TB=DSIN(STRAY(I,3)/57.29)*STRAY(I,1)/STMAX
        TX=DCOS(STRAY(I,3)/57.29)*STRAY(I,2)/STMAX
        TY=DSIN(STRAY(I,3)/57.29)*STRAY(I,2)/STMAX
        XN1=XXC+TA
        XN2=XXC-TA
        YN1=YYC+TB
        YN2=YYC-TB
        XS1=XXC-TY
        XS2=XXC+TY
        YS1=YYC+TX
        YS2=YYC-TX
        CALL PENUP(XN1,YN1)
        CALL PENDN(XN2,YN2)
        CALL PENUP(XS1,YS1)
        CALL PENDN(XS2,YS2)
        CALL PENUP(XN1,YN1)
        CALL PENDN(XN2,YN2)
        CALL PENUP(XS1,YS1)
        CALL PENDN(XS2,YS2)
        TA=STRAY(I,1)
        TX=STRAY(I,2)
        IF(TA.LT.0.0) GO TO 9331
        CALL PSYMB(XN1,YN1,0.02,01,0.0,-1)
        CALL PSYMB(XN2,YN2,0.02,01,0.0,-1)
 9331 CONTINUE
        IF(TX.LT.0.0) GO TO 9332
        CALL PSYMB(XS1,YS1,0.02,01,0.0,-1)
        CALL PSYMB(XS2,YS2,0.02,01,0.0,-1)
 9332 CONTINUE
        RAD=DABS(STRAY(I,4))/STMAX
        GAP=0.0
        S4=STRAY(I,4)
        IF(S4.GE.0.0) GAP=0.03
        CALL PCIRCL(XXC,YYC,0.0,360.0,RAD,RAD,GAP,0.0)
        CALL PCIRCL(XXC,YYC,0.0,360.0,RAD,RAD,GAP,0.0)
```

```
541         501 CONTINUE
542             CALL PLTEND
543             RETURN
544             END
 OF FILE
```

APPENDIX 3

In this appendix the two programs used in Chapter 5 are described and listed. The programs execute the numerical calculations of finite difference temperature analysis used in the investigations of the solidification and cooling of the oceanic crust at the ridge crests. Program 1 carries out the thermal analysis with the latent heat of solidification distributed throughout the liquidus to solidus temperature interval while program 2 carries out the thermal analysis with the latent heat released entirely at the solidus isotherm. Both programs are written in Fortran 4 G and consist of a main program and subroutines. Half precision is used for all integer characters.

A3.1 Program 1. This program carries out finite difference temperature analysis for distributed latent heat.

Main Program. A flow diagram is given in figure A3.1 and summarizes the main steps carried out in the finite difference calculations.

Subroutine Temp. This subroutine calculates the initial temperature distribution in the oceanic lithosphere according to equation 5.2 and provides a starting temperature distribution for the finite difference calculations.

A listing of the main program and subroutine is given at the end of this section.

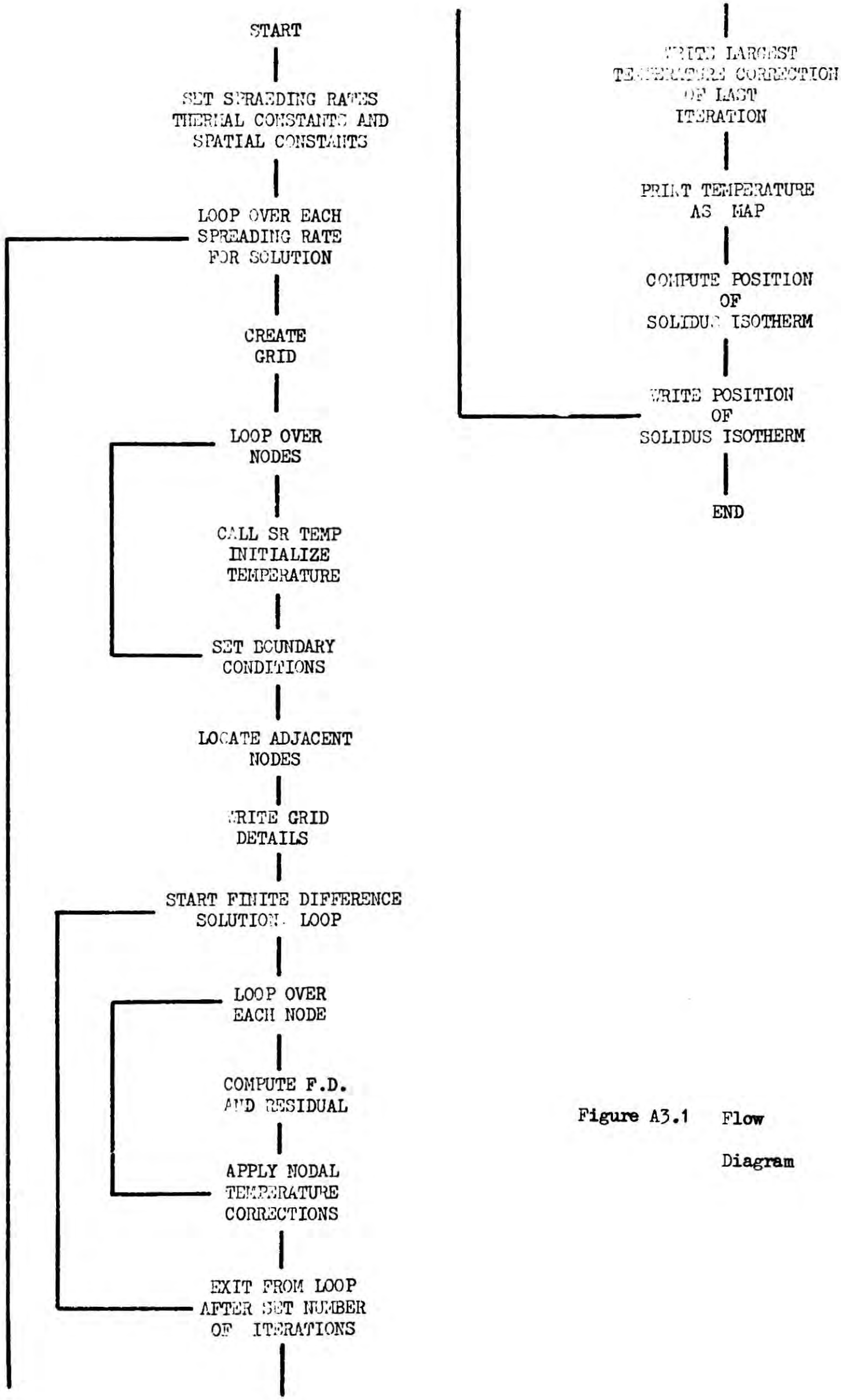

Figure A3.1 Flow Diagram

Input data

This program requires no input data. The choice of 3 spreading rates is preset in the program. Distribution of latent heat throughout the liquidus to solidus temperature interval is adjusted by alteration of the program.

Output Data

For each of the 3 half spreading rates.

1. The following information is printed; relaxation constant used in finite difference temperature corrections, half spreading rate, number of finite difference iterations, latent heat (cal/gm); liquidus to solidus temperature interval.
2. Details of the finite difference grid are printed; nodal coordinates, initial temperature, boundary conditions, and adjacent nodes. In the listed program the "write statement" has "comment cards" and does not act.
3. Write number of finite difference iterations and the maximum temperature correction of last finite difference iteration.
4. Write nodal temperatures in the form of a temperature map. The map is divided into upper and lower lithosphere to allow it to be printed on the page.
5. Position of the solidus isotherm in the crust is printed.

Preset internal parameters

1. VEL, half spreading rates.
2. DMOHO, Moho depth.
3. RELAX, relaxation constant used in finite difference corrections.

```
C*****FINITE DIFFERENCE TEMPERATURE PROGRAM FOR DISTRIBUTED LATENT*****
C*****HEAT ANALYSIS OF OCEANIC LITHOSPHERE*****************************
C***** MAIN PROGRAM*****************************************************
      IMPLICIT INTEGER*2(I-N)
      DIMENSION  X(4001),KAR(200),Y(4001),T(4001),KDJ(4,4001),
     1 ISBC(4001),FV(3)
     2 ,P(11)
C*****WRITE OUT POSITION OF PHASE BOUNDARY*****************************
C*****SUBROUTINE FOR CALCULATING INITIAL TEMPERATURE DISTRIBUTION******
C*****SET THREE HALF SPREADING RATES***********************************
      FV(1)=1.0
      FV(2)=3.0
      FV(3)=6.0
C***** SET SPATIAL AND THERMAL CONSTANTS********************************
C*****MOHO DEPTH*******************************************************
      DMOHO=5.01E5
C*****RELAXATION******************************************************
      RELAX=0.1E12
C*****GRID SCALE******************************************************
      STEP=1.0E5
      SCAX=0.5
      SCAY=0.5
      RELAX=RELAX*SCAX*SCAX
C*****NUMBER OF F.D. ITERATIONS***************************************
      NINC=1200
C*****LATENT HEAT*****************************************************
      HLAT=100.0
C*****LIQUIDUS=1125***************************************************
C*****LIQUIDUS TO SOLIDUS*********************************************
      TMD=125.0
      NNXX=61+17
      NNYY=21+7
      NNXXYY=NNXX*NNYY
C
C*****START SOLUTION FOR PARTICULAR SPREADING RATE********************
      DO 999 IPL=1,3
      VEL=FV(IPL)
      RVELO=VEL
      WRITE(6,967) RELAX,VEL,NINC,HLAT,TMD
  967 FORMAT(2E10.3,I10,2F10.3)
      BONST=0.006/(0.26*3.0)
      PONST=0.006/(0.26+HLAT/TMD)/3.0
      VEL=VEL/(60.0*60.0*24.0*365.0)
C***** TO SET UP GRID**************************************************
      XC=0.0
      K=1
      DO 1 I=1,NNXX
      YC=0.0
      DO 2 J=1,NNYY
      X(K)=XC
      Y(K)=YC
      K=K+1
      SCA=SCAY
      IF(J.GE.21) SCA=10.
      YC=YC+STEP*SCA
    2 CONTINUE
      SCA=SCAX
      IF(I.GE.61) SCA=10.
      XC=XC+STEP*SCA
    1 CONTINUE
```

```
   11 FORMAT(I10,F10.3)
C*****TO INITIALIZE TEMPERATURE IN GRID AND SPECIFY BOUNDARY CONDITIONS
      DO 5 K=1,NNXXYY
    5 ISBC(K)=0
C***** TO SET BC AND CONSTRAINTS FOR GRID**********************************
      DO 975 I=1,NNYY
      T(I)=1125.0
  975 ISBC(I)=1
      DO 976 I=2,NNXX
      J=(I-1)*NNYY+1
      K=I*NNYY
      T(J)=0.0
      ISBC(J)=1
      XF=X(K)/1.0E5
      YF=Y(K)/1.0E5
      CALL TEMP(XF,YF,TF,RVELC)
      T(K)=TF
  976 ISBC(K)=1
      DO 977 I=1,NNYY
      K=NNXXYY-NNYY+I
      XF=X(K)/1.0E5
      YF=Y(K)/1.0E5
      CALL TEMP(XF,YF,TF,RVELC)
      T(K)=TF
  977 ISBC(K)=1
C*****TO FIND ADJACENT NODES FOR GRID*********************************
      DO 7 K=1,NNXXYY
      IJ=ISBC(K)
      IF(IJ.EQ.1) GO TO 7
      KDJ(1,K)=K-1
      KDJ(2,K)=K+1
      KDJ(3,K)=K-NNYY
      KDJ(4,K)=K+NNYY
      XF=X(K)/1.0E5
      YF=Y(K)/1.0E5
      CALL TEMP(XF,YF,TF,RVELC)
      T(K)=TF
    7 CONTINUE
C***** TO WRITE GRID DETAILS*****************************************
C*****DO 1008 I=1,NNXXYY
C*****ITEMP=T(I)
C*****IX=X(I)/1.0E5
C*****IY=Y(I)/1.0E5
C*****WRITE(3,1018) I,ITEMP,IX,IY,(KDJ(J,I),J=1,4),ISBC(I)
C1008 CONTINUE
 1018 FORMAT(2X,4I6,2X,4I6,2X,I6)
C
C***** START FINITE DIFFERENCE ITERATIONS FOR TEMPERATURE SOLUTION******
      DO 100 IT=1,NINC
      CONV=0.0
      DO 20 L=1,NNXXYY
      IJ=ISBC(L)
      IF(IJ.EQ.1) GO TC 20
      IA=KDJ(1,L)
      IB=KDJ(2,L)
      IC=KDJ(3,L)
      ID=KDJ(4,L)
      TA=T(IA)
      TB=T(IB)
      TC=T(IC)
```

```
      TD=T(ID)
      TO=T(L)
      YA=Y(IA)
      YB=Y(IB)
      XC=X(IC)
      XD=X(ID)
      XO=X(L)
      YO=Y(L)
C***** COMPUTE FINITE DIFFERENCES*************************************
      GRAD2=((TA-TO)/(YA-YO)-(TO-TB)/(YO-YB))/
     1 ((YA-YB)/2.0)+
     2 ((TC-TO)/(XC-XO)-(TO-TD)/(XO-XD))/
     3 ((XC-XD)/2.0)
      GRADX=((TD-TO)/(XD-XO)+(TO-TC)/(XO-XC))/2.0
      CONST=BONST
      IF(YO.LT.DMOHO)  CONST=PONST
      TFIN=1125.0-TMO
      IF(TO.LT.TFIN) CONST=BONST
      RESID=CONST*GRAD2-VEL*GRADX
      DEL=RESID*RELAX
C***** APPLY TEMPERATURE CORECTION*************************************
      T(L)=T(L)+DEL
      IF(T(L).GT.1125.0) T(L)=1125.0
      IF(IT.LT.NINC) GO TO 20
      DEL=ABS(DEL)
      CONV=AMAX1(CONV,DEL)
   20 CONTINUE
  100 CONTINUE
C***** WRITE CONVERGENCE ACCURACY*************************************
      WRITE(6,15) IT,CONV
   15 FORMAT(2X,'NUMBER OF ITERATIONS=',I10,10X,
     1 'MAXIMUM ERROR=',F13.6)
C
C***** WRITE TEMPERATURE SOLUTION AS TEMPERATURE MAP******************
C***** TEMPERATURE MAP DIVIDED INTO UPPER AND LOWER HALVES************
   16 FORMAT(2X,I10,4X,3(F10.3,4X))
      K=1
      DO 9010 I=1,NNXX
      L=NNYY
      DO 9020 J=1,NNYY
      TP=T(K)
      KTEMP=TP
      KAR(L)=KTEMP
      K=K+1
      L=L-1
 9020 CONTINUE
      NY2=NNYY/2
      WRITE(2,9030) (KAR(IJ),IJ=NY2,NNYY)
      WRITE(1,9030) (KAR(IJ),IJ=1,NY2)
 9010 CONTINUE
 9030 FORMAT(2X,25I5)
C***** WRITE POSITION OF SOLIDUS ISOTHERM*****************************
      DO 3001 K=2,11
      DO 3000 I=2,60
      NOS=(I-1)*NNYY+K
      NM=NOS-NNYY
      NP=NOS+NNYY
      TC=T(NOS)
      IF(TC.GT.TFIN) GO TO 3000
      XPB=X(NM)+(X(NOS)-X(NM))*(T(NM)-TFIN)/(T(NM)-T(NOS))
```

```
      XPB=XPB/1.0E5
      P(K)=XPB
      GO TO 3001
 3000 CONTINUE
 3001 CONTINUE
      WRITE(7,3002) (I,P(I),I=1,11)
 3002 FORMAT(2X,11(I3,1X,F8.4))
  999 CONTINUE
      STOP
      END
C
C*****SUBROUTINE CALCULATES INITIAL TEMPERATURE**************************
      SUBROUTINE TEMP(XO,YO,TO,VEL)
      PI=3.1416
C*****LITHOSPHERS THICKNESS*************************************************
      L=80.0
      P=41.22*(L/100.0)*VEL
C***** TEMPERATURE TO********************************************************
      TS=1125.0
      YO=-YO
      X=XO/L
      YO=YO+L
      Z=YO/L
      Z=ABS(Z)
      T=1-Z
      DO 1 I=1,100
      RI=I
      A=(2.0/(PI*RI))*(-1.0)**(I+1)
      C=SIN(RI*PI*Z)
      B=(P/2.0-(P*P/4.0+RI*RI*PI*PI)**0.5)*X
      B=EXP(B)
      A=A*B*C
      T=T+A
    1 CONTINUE
      TO=T*TS
      TO=AMIN1(TS,TO)
      RETURN
      END
 OF FILE
```

4. NINC, number of finite difference iterations.
5. HLAT, latent heat (cal/gm).
6. TMD, liquidus to solidus temperature interval, (^{o}C).
7. BONST, value of $k/(\sigma\rho)$ in the mantle and solid crust.
   PONST, value of $k/((\sigma+H/(T_L-T_S))\rho)$ in molten crust.
8. STEP, SCAX, SCAY, NNXX, NNYY, parameters controlling nodal spacing in the lithosphere finite difference model.
9. TFIN, solidus temperature, (^{o}C).
10. TS, (subroutine Temp), liquidus temperature, (^{o}C).
11. L, (subroutine Temp), lithosphere thickness.
12. P, (subroutine Temp), parameter p of equation 5.2.

A3.2 Program 2. This program carries out finite difference temperature analysis with latent heat released at the solidus isotherm.

Main Program. A flow diagram is given in figure A3.2 and summarizes the main steps carried out in the finite difference calculations.

Subroutine Simq. This subroutine is used in calculating the temperature gradients at the solidification boundary. A polynomial fit is made of the temperature in the vicinity of the boundary node. The polynomial constants are then used to obtain the temperature gradients. The subroutine is adapted from the I.B.M. scientific subroutine package.

Subroutine Temp. This subroutine is identical to that of similar name in section A3.1.

A listing of the main program and subroutines is given at the end of the section.

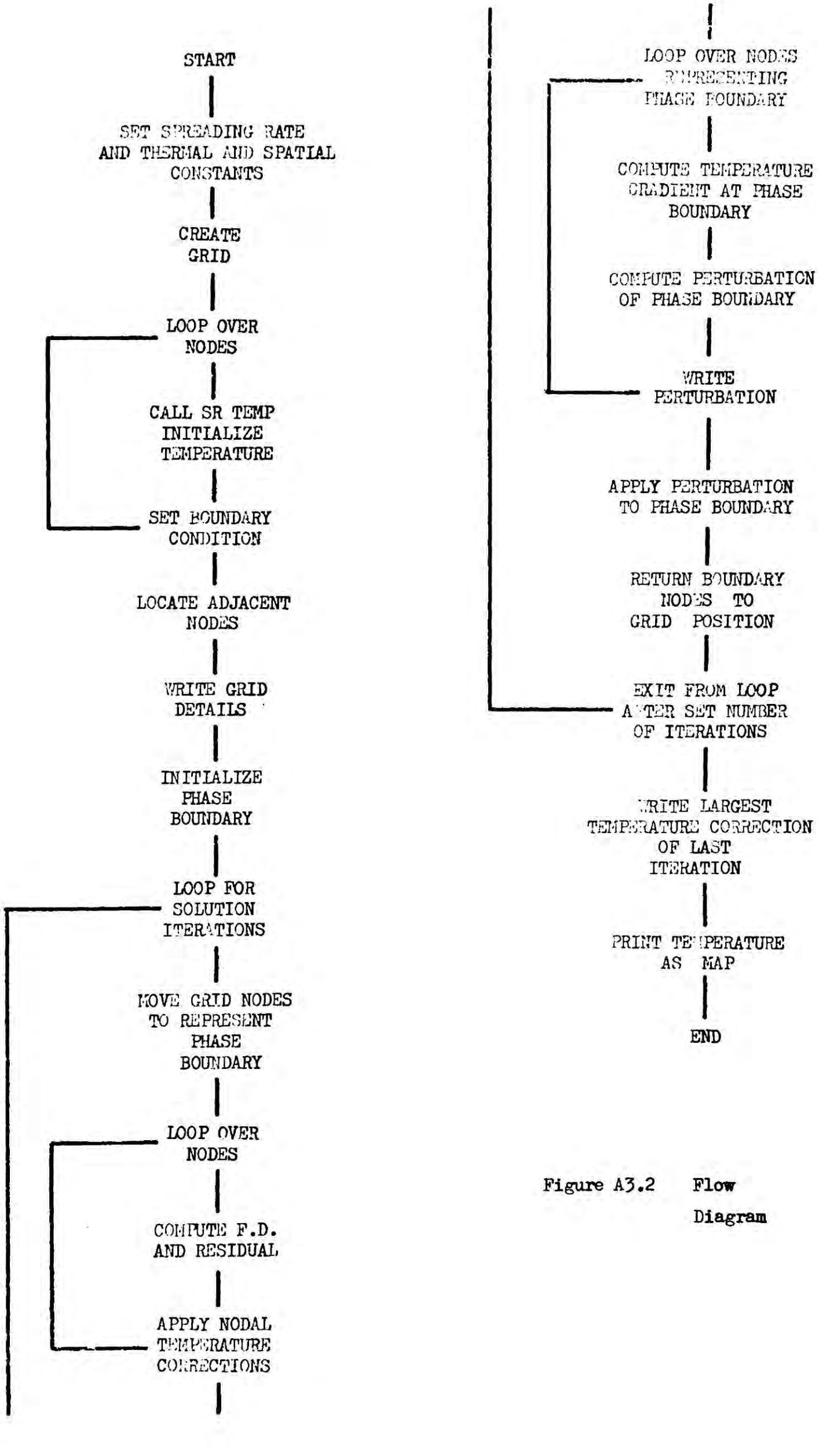

Figure A3.2 Flow Diagram

Input Data

This program requires no input data. The half spreading rate selected for the analysis must be preset in the program.

Output Data

1. The following information is printed: the value of relaxation constant used in the finite difference temperature corrections, half spreading rate, number of finite difference iterations, and latent heat (cal/gm).
2. Details of the finite difference grid are printed; nodal coordinates, initial temperature, boundary conditions, and adjacent nodes. In the listed program the "write statement" has "comment cards" and does not act.
3. For each finite difference iteration.
   (a) Maximum nodal temperature correction of iteration is printed.
   (b) Position of phase boundary and the phase boundary perturbation is printed.
4. Write nodal temperatures in the form of a temperature map. The map is divided into upper and lower lithosphere to allow it to be printed on the page.

Preset internal parameters

1. VEL, half spreading rate.
2. DMOHO, Moho depth.
3. NINC, number of finite difference iterations.
4. RELAX, relaxation constant used in finite difference corrections.

5. HLAT, latent heat.

6. CONST, value of $k/(\sigma\rho)$.

7. STEP, SCAX, SCAY, NNXX, NNYY, parameters controlling nodal spacing in the lithosphere finite difference model.

7. TVEC, temperature of solidification boundary; set equal to the solidus temperature, (^{o}C).

8. TS, (subroutine Temp), liquidus temperature, (^{o}C).

9. L, (subroutine Temp), lithosphere thickness.

10. P, (subroutine Temp), parameter p of equation 5.2.

Program Test

The two programs described in this appendix contain an internal test. An analytical lithosphere temperature solution (McKenzie, 1967) is used for the starting point of the finite difference calculations. Comparison of the analytical and finite difference solutions show very close agreement at distances greater than 30 km from the ridge axis, away from the zone of release of latent heat.

```
      C       THERMAL AND SOLIDIFICATION F.D. PROGRAM FOR OCEAN LITHOSPHERE**
      C       LATENT HEAT RELEASED AT SOLIDUS ISOTHERM IN CRUST**************
      C      MAIN PROGRAM*************************************::
             IMPLICIT INTEGER*2(I-N)
             DIMENSION  X(4001),KAR(200),Y(4001),T(4001),KDJ(4,4001),
            1 ISBC(4001),FV(3)
            2 ,ISMOL(4001),ISPB(4001),XPHB(100),XDINC(100),NPB(100),PMAT(20)
            3 ,DELXX(100),TVEC(10)
      C*****SET SPATIAL AND THERMAL CONSTANTS*********************************
      C*****RELAXATION********************************************************
             RELAX=0.05E12
      C*****SPREADING VELOCITY************************************************
             VEL=0.5
      C*****GRID SCALE********************************************************
             STEP=1.0E5
             SCAX=0.5
             SCAY=0.5
             RELAX=RELAX*SCAX*SCAX
      C*****NUMBER OF SOLUTION ITERATIONS*************************************
             NINC=500
      C*****MOHO DEPTH********************************************************
      C*****LIQUIDUS=1125*****************************************************
      C*****SOLIDUS=1000******************************************************
             DMOHO=5.01E5
             NNXX=61+17
             NNYY=21+7
             NNXXYY=NNXX*NNYY
             NPXX=DMOHO/STEP/SCAY+0.01
             RVELO=VEL
             WRITE(6,967) RELAX,VEL,NINC,HLAT
         967 FORMAT(2E10.3,I10,2F10.3)
             CONST=0.006/(0.26*3.0)
             VEL=VEL/(60.0*60.0*24.0*365.0)
      C
      C***** TO SET UP  GRID**************************************************
             XC=0.0
             K=1
             DO 1 I=1,NNXX
             YC=0.0
             DO 2 J=1,NNYY
             X(K)=XC
             Y(K)=YC
             K=K+1
             SCA=SCAY
             IF(J.GE.21) SCA=10.
             YC=YC+STEP*SCA
           2 CONTINUE
             SCA=SCAX
             IF(I.GE.61) SCA=10.
             XC=XC+STEP*SCA
           1 CONTINUE
          11 FORMAT(I10,F10.3)
             DO 5 K=1,NNXXYY
           5 ISBC(K)=0
      C***** TO SET BOUNDARY CONDITIONS FOR  GRID*****************************
      C*****INITIAL TEMPERATURES**********************************************
             DO 975 I=1,NNYY
             T(I)=1125.0
         975 ISBC(I)=1
             DO 976 I=2,NNXX
```

```
      J=(I-1)*NNYY+1
      K=I*NNYY
      T(J)=0.0
      ISBC(J)=1
      XF=X(K)/1.0E5
      YF=Y(K)/1.0E5
      CALL TEMP(XF,YF,TF,RVELC)
      T(K)=TF
  976 ISBC(K)=1
      DO 977 I=1,NNYY
      K=NNXXYY-NNYY+I
      XF=X(K)/1.0E5
      YF=Y(K)/1.0E5
      CALL TEMP(XF,YF,TF,RVELO)
      T(K)=TF
  977 ISBC(K)=1
C*****TO FIND ADJACENT NODES FOR  GRID**********************************
      DO 7 K=1,NNXXYY
      IJ=ISBC(K)
      IF(IJ.EQ.1) GO TO 7
      KDJ(1,K)=K-1
      KDJ(2,K)=K+1
      KDJ(3,K)=K-NNYY
      KDJ(4,K)=K+NNYY
      XF=X(K)/1.0E5
      YF=Y(K)/1.0E5
      CALL TEMP(XF,YF,TF,RVELO)
      T(K)=TF
    7 CONTINUE
C***** TO WRITE  GRID DETAILS*************************************************
C*****DO 1008 I=1,NNXXYY
C*****ITEMP=T(I)
C*****IX=X(I)/1.0E5
C*****IY=Y(I)/1.0E5
C*****WRITE(3,1018) I,ITEMP,IX,IY,(KDJ(J,I),J=1,4),ISBC(I)
C1008 CONTINUE
 1018 FORMAT(2X,4I6,2X,4I6,2X,I6)
C***** INITIALIZE PHASE BOUNDARY POSITION*******************************
      DO 1001 IP=1,100
 1001 XPHB(IP)=0.C
C
C***** START ITERATIONS FOR SOLUTION************************************
      DO 3500 ITPB=1,NINC
      DO 3510 I=1,NNXXYY
      ISMOL(I)=0
 3510 ISPB(I)=0
C***** TO FIND WHICH NODES ARE MOLTEN AND WHICH ARE NEAREST PHASE BOUNDA
C*****THE NODE NEAREST PHASE BOUNDARY IS MOVED FROM GRID TO REPRESENT PH
      DO 4009 J=1,11
      LC=J
      PT=XPHB(J)
      IF(PT.GE.0.0) GO TO 907
      PT=0.0
      XPHB(J)=0.0
  907 CONTINUE
      DO 4010 I=1,NNXX
      XT=X(LC)
      IF(XT.GT.PT) GO TO 4020
      ISMOL(LC)=1
      T(LC)=1000.0
```

```
      GO TO 4010
 4020 CONTINUE
C***** WE HAVE GONE PAST THE PHASE BOUNDARY*****************************
      LCA=LC-NNYY
      XTCK=X(LC)
      XTCK=ABS(XTCK-PT)
      HAFST=0.5E5/2.0
      IF(XTCK.LT.HAFST) GO TO 3045
C***** PREVIOUS NODE IS NEAREST*****************************************
      ISMOL(LCA)=0
      ISPB(LCA)=1
      NPB(J)=LCA
      T(LCA)=1000.0
      XDINC(J)=X(LCA)
      X(LCA)=PT
      GO TO 4009
C***** CURRENT NODE IS NEAREST******************************************
 3045 CONTINUE
      ISPB(LC)=1
      NPB(J)=LC
      T(LC)=1000.0
      XDINC(J)=X(LC)
      X(LC)=PT
      GO TO 4009
 4010 LC=LC+NNYY
 4009 CONTINUE
C*****WRITE(6,3580)
 3580 FORMAT(2X,'PHASE BOUNDARY FOUND')
      CONV=0.0
C
C***** START F.D. ITERATIONS HAVING FIXED PHASE BOUNDARY NODES*********
      DO 20 L=1,NNXXYY
      IJP=ISPB(L)
      IJM=ISMOL(L)
      IF(IJP.EQ.1) GO TO 220
      IF(IJM.EQ.1) GO TO 220
      IJ=ISBC(L)
      IF(IJ.EQ.1) GO TO 220
      IA=KDJ(1,L)
      IB=KDJ(2,L)
      IC=KDJ(3,L)
      ID=KDJ(4,L)
      TA=T(IA)
      TB=T(IB)
      TC=T(IC)
      TD=T(ID)
      TO=T(L)
      YA=Y(IA)
      YB=Y(IB)
      XC=X(IC)
      XD=X(ID)
      XO=X(L)
      YO=Y(L)
C***** COMPUTE FINITE DIFFERENCES***************************************
      GRAD2=((TA-TO)/(YA-YO)-(TO-TB)/(YO-YB))/
     1 ((YA-YB)/2.0)+
     2 ((TC-TO)/(XC-XO)-(TO-TD)/(XO-XD))/
     3 ((XC-XD)/2.0)
      GRADX=((TD-TO)/(XD-XO)+(TO-TC)/(XO-XC))/2.0
      RESID=CONST*GRAD2-VEL*GRADX
```

```
      DEL=RESID*RELAX
C*****APPLY TEMPERATURE PERTURBATIONS**********************************
      T(L)=T(L)+DEL
      DEL=ABS(DEL)
      CONV=AMAX1(CONV,DEL)
  220 CONTINUE
   20 CONTINUE
      WRITE(6,1002) CONV
 1002 FORMAT(F10.3)
C
C*****TO PETURBATE PHASE BOUNDARY POSITION*****************************
      DO 5700 KIM=1,NPXX
      NODE=NPB(KIM)
      KIM2=KIM+1
      NODB=NPB(KIM2)
      LK1=NODE+NNYY
      LK2=NODB+NNYY
      YDEP=Y(NODE)
C*****LATENT HEAT (MODIFIED)*******************************************
      HLAT=100.0+125.0*0.26
      IF(YDEP.LT.DMOHO) GO TO 1777
      HLAT=0.0000001
 1777 CONTINUE
      XEXB=X(NODB)-X(NODE)
      YEYB=Y(NODB)-Y(NODE)
      TAN1=-XEXB/YEYB
C*****TO SET UP MATRIX FOR CALC TEMP GRAD AT BOUNDARY******************
      PMAT(1)=1.0
      PMAT(2)=1.0
      PMAT(3)=1.0
      PMAT(4)=1.0
      PMAT(5)=X(NODE)
      PMAT(6)=X(NODB)
      PMAT(7)=X(LK1)
      PMAT(8)=X(LK2)
      PMAT(9)=Y(NODE)
      PMAT(10)=Y(NODB)
      PMAT(11)=Y(LK1)
      PMAT(12)=Y(LK2)
      PMAT(13)=X(NODE)*Y(NODE)
      PMAT(14)=X(NODB)*Y(NODB)
      PMAT(15)=X(LK1)*Y(LK1)
      PMAT(16)=X(LK2)*Y(LK2)
      TVEC(1)=1000.0
      TVEC(2)=1000.0
      TVEC(3)=T(LK1)
      TVEC(4)=T(LK2)
C*****CALC TEMP GRAD***************************************************
      XXZ=(X(NODE)+X(NODB))/2.0
      YYZ=(Y(NODE)+Y(NODB))/2.0
      NLK=4
      CALL SIMQ(PMAT,TVEC,NLK,KS3)
 1778 FORMAT(10X,I10)
      GRADY=TVEC(3)+TVEC(4)*XXZ
      GRADX=TVEC(2)+TVEC(4)*YYZ+2.0*TVEC(5)*XXZ
      PCON=HLAT*3.0/0.006
      RCON=-VEL*PCON
      GRAT=TAN1*GRADY
      RESID=RCON-GRADX-GRAT
C*****CALC PHASE BOUNDARY PERTURBATION*********************************
```

```
241         XCOR=0.5E5/2.0*RESID/(RESID+GRADX)
242         IF(RCON.GE.GRAT) XCOR=-0.5E5
243         TCCN=ABS(RCCN)
244         IF(TCON.LT.1.0E-10) XCOR=-0.5E5
245         IF(XCOR.LT.-0.5E5) XCOR=-0.5E5
246         IF(XCOR.GT.0.5E5) XCOR=0.5E5
247         DELXX(KIM2)=XCOR
248       C*****WRITE(6,1531) RCON,GRADX,GRAT,GRADY,TAN1,XCOR,KS3
249        1531 FORMAT(2X,6(E10.3,4X),I5)
250        5700 CONTINUE
251       C
252       C*****WRITE PHASE BOUNDARY POSITION*************************************
253         WRITE(6,5705) (NELT,XPHB(NELT),DELXX(NELT),NELT=1,11)
254        5705 FORMAT(2X,4(1X,I3,2X,E10.3,1X,2X,E10.3))
255       C***** TO PERTURBATE THE PHASE BOUNDARY POSITION************************
256         DO 5718 JT=1,11
257         DTT=DELXX(JT)
258         DTT=DTT*0.1
259         XPHB(JT)=XPHB(JT)+DTT
260         IF(JT.LE.2) GO TO 5719
261         XPHB(JT-1)=XPHB(JT-1)+DTT
262        5719 CONTINUE
263         IF(JT.LT.11) GO TO 5720
264         XPHB(JT)=XPHB(JT)+DTT
265        5720 CONTINUE
266       C***** PUT BACK P.B. NODE IN INITIAL GRID POSITION**********************
267         KIM=NPB(JT)
268         X(KIM)=XDINC(JT)
269        5718 CONTINUE
270        3500 CONTINUE
271       C
272         K=1
273       C*****WRITE TEMP SOLUTION AS TEMP MAP***********************************
274       C*****TEMP FIELD DIVIDED INTO TWO SECTIONS******************************
275         DO 9010 I=1,NNXX
276         L=NNYY
277         DO 9020 J=1,NNYY
278         TP=T(K)
279         KTEMP=TP
280         KAR(L)=KTEMP
281         K=K+1
282         L=L-1
283        9020 CONTINUE
284         NY2=NNYY/2
285         WRITE(2,9030) (KAR(IJ),IJ=NY2,NNYY)
286         WRITE(1,9030) (KAR(IJ),IJ=1,NY2)
287        9010 CONTINUE
288        9030 FORMAT(2X,25I5)
289         STOP
290         END
291       C
292       C***** SUBRCUTINE SOLVES SIMULTANEOUS EQUATIONS**************************
293       C*****TAKEN FROM IMB SSP
294         SUBROUTINE SIMQ(A,B,N,KS)
295         IMPLICIT INTEGER *2(I-N)
296         DIMENSION A(1),B(1)
297         TOL=0.0
298         KS=0
299         JJ=-N
300         DO 65 J=1,N
```

```
101           JY=J+1
102           JJ=JJ+N+1
103           BIGA=0
104           IT=JJ-J
105           DO 30 I=J,N
106           IJ=IT+I
107           IF(ABS(BIGA)-ABS(A(IJ))) 20,30,30
108        20 BIGA=A(IJ)
109           IMAX=I
110        30 CONTINUE
111           IF(ABS(BIGA)-TOL) 35,35,40
112        35 KS=1
113           RETURN
114        40 I1=J+N*(J-2)
115           IT=IMAX-J
116           DO 50 K=J,N
117           I1=I1+N
118           I2=I1+IT
119           SAVE=A(I1)
120           A(I1)=A(I2)
121           A(I2)=SAVE
122        50 A(I1)=A(I1)/BIGA
123           SAVE=B(IMAX)
124           B(IMAX)=B(J)
125           B(J)=SAVE/BIGA
126           DO 65 IX=JY,N
127           IXJ=IQS+IX
128           IT=J-IX
129           DO 60 JX=JY,N
130           IXJX=N*(JX-1)+IX
131           JJX=IXJX+IT
132        60 A(IXJX)=A(IXJX)-(A(IXJ)*A(JJX))
133        65 B(IX)=B(IX)-(B(J)*A(IXJ))
134        70 NY=N-1
135           IT=N*N
136           DO 80 J=1,NY
137           IA=IT-J
138           IB=N-J
139           IC=N
140           DO 80 K=1,J
141           B(IB)=B(IB)-A(IA)*B(IC)
142           IA=IA-N
143        80 IC=IC-1
144           RETURN
145           END
146     C
147     C***** SUBROUTINE CALC. INITIAL LITHOSPHERE TEMPERATURES*****************
148           SUBROUTINE TEMP(XO,YO,TO,VEL)
149           PI=3.1416
150     C*****LIHOSPHERE THICKNESS*************************************************
151           L=80.0
152           P=41.22*(L/100.0)*VEL
153     C***** TEMPERATURE TO******************************************************
154           TS=1125.0
155           YO=-YO
156           X=XO/L
157           YO=YO+L
158           Z=YO/L
159           Z=ABS(Z)
160           T=1-Z
```

```
361             DO 1 I=1,50
362             RI=I
363             A=(2.0/(PI*RI))*(-1.0)**(I+1)
364             C=SIN(RI*PI*Z)
365             B=(P/2.0-(P*P/4.0+RI*RI*PI*PI)**0.5)*X
366             B=EXP(B)
367             A=A*B*C
368             T=T+A
369           1 CONTINUE
370             TO=T*TS
371             RETURN
372             END
373       C
 OF FILE
```

APPENDIX 4

The program described in this appendix executes the numerical calculations of finite element elastic stress analysis which are used in Chapter 6 and formulated in Chapter 2. The program is written in Fortran 4 G and consists of the main program and 5 subroutines. Double precision is used for all real characters.

Main Program. A flow diagram of the main program is shown in figure A4.1 and summarized the main steps in carrying out the finite difference calculation.

Subroutine Plots. This subroutine plots the principal stresses, the finite element grid and the numerical values of deviatoric stress and failure marker. It is not the same subroutine as the ones of similar names in appendices 1 and 2.

Subroutine Fail. This subroutine tests for failure of each element using the Murrell-Griffiths theory of brittle fracture (described in Chapter 6). Failure is signified by a positive value of the parameter C returned by the subroutine.

Subroutine Matsol. This subroutine solves the equilibrium equation of finite element, $[K]\{\delta\} = \{F\}$ for displacement $\{\delta\}$ where $[K]$ is the stiffness matrix and $\{F\}$ is the total force vector. The Gauss-Seidel solution method is used.

Subroutine GMPRD and GMTRA. These subroutines are identical to those of similar names in appendix 1.

A listing of the main program and the subroutines is given at the end of the appendix.

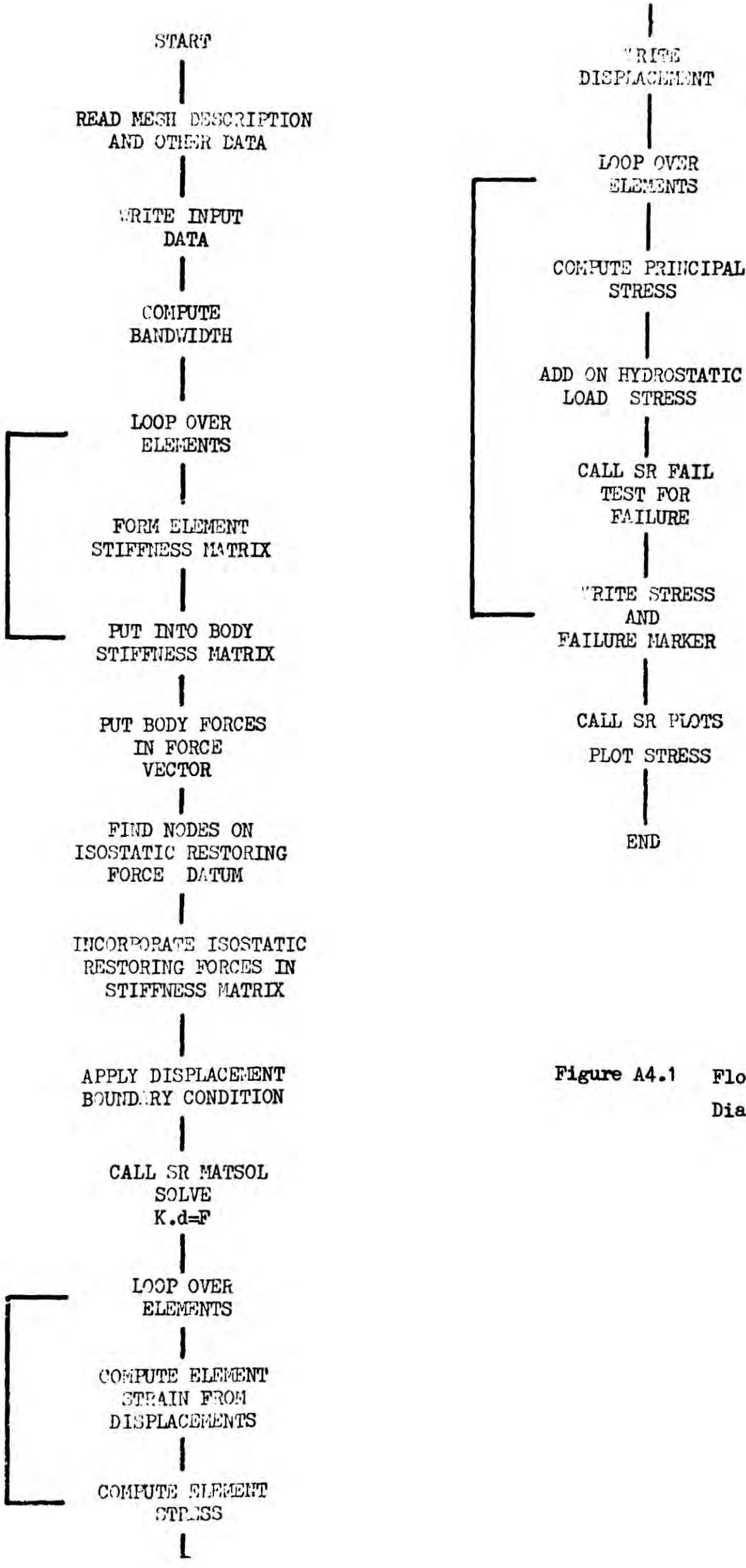

Figure A4.1 **Flow Diagram**

Program Input

The program input defines the geometry, physical constants and boundary conditions of the region under investigation together with information controlling the output form.

1. NNOD,NEL,STMAX,DENLIT (2I10,E10.3,F10.3 device 5)

   NNOD, number of nodes of finite element grid

   NEL, number of elements of finite element grid.

   STMAX, stress plot scaling factor (dynes/cm^2/inch)

   DEV, controls option which allows stresses produced by finite element analysis to have hydrostatic load stress superimposed on them. If DEV = 0 is not used; if DEV = 1 hydrostatic stresses are added on.

2. For all nodes

   K,X(K),Y(K) (I10,2F10.3 device 5)

   K, node number

   X(K),Y(K), X and Y coordinate of node (cm)

3. For all elements

   K,(NODEL(K,J),J=1,3),E(K),P(K),ND(K) (4I10,E10.3,2F10.3 device 5)

   K, element number

   NODEL(K,1,2,3), number of 3 nodes specifying element.

   E(K), element Young's modulus.

   P(K), element Poisson's ratio.

   DN(K), element density.

4. NBC (I10 device 5)

   NBC, number of specified forces.

5. I,DISP(2*I-1),DISP(2*I) (I10,2E10.3 device 5)

   I, node number

   DISP(2*I-1),DISP(2*I), X and Y components of nodal force vector

6. ND (I10 device 5)

   ND, number of nodes at which displacement is specified.

7. LD(I),((ISP(I,J),PDIS(I,J),J=1,2) (I10,2(I10,F10.3) device 5)

   LD(I), node number.

   ISP(I,1),ISP(I,2), controls specification of displacement for X and Y directions. If equals 0 no displacement specification; if equals 1 displacement is specified.

   PDIS(I,1),PDIS(I,2), X and Y components of specified displacements.

8. KPLOT (I10 device 5)

   KPLOT controls stress plot output.

   KPLOT = 0 no plot

   KPLOT = 1 plots principal stresses, numerical values of deviatoric stress and failure marker, and finite element grid.

9. XSC,XSH,YSC,YSH (4F10.3 device 5)

   XSC X coordinate scale (cm/inch)

   XSH X coordinate scale (cm)

   YSC Y coordinate scale (cm/inch)

   YSH Y coordinate shift (cm)

Program Output

1. All input data specifying grid, boundary conditions and physical constants are printed.
2. Information is printed giving the accuracy of solution of the finite element equilibrium equation by the Gauss-Seidel method. The maximum displacement change for the last Gauss-Seidel iteration is printed.
3. Final nodal displacements are printed.
4. Final element principal stresses are printed.

Additional facilities exist to plot element principal stresses (with or without additional hydrostatic load stresses), the numerical values of the deviatoric stress and failure marker, and the finite element grid.

Preset internal parameters

1. DATSOS, the datum at which isostatic restoring forces are to be applied at.
2. HPW, hydrostatic load stress of the ocean.
3. HPC, hydrostatic load stress of the crust.
3. N, (subroutine Matsol), number of Gauss-Seidel iterations.
4. T, (subroutine Fail), value of tensile strength.

Program Test

A test of the finite element elastic stress analysis program has been made against an analytical solution for the deformation of an hollow cylinder of visco-elastic material, enclosed in

an elastic ring, and subject to applied internal pressure. The analytical solution and the finite element representation of the cylinder have already been described in appendix 1. In figure A 4.2 values of radial and tangential stress calculated by finite element elastic stress analysis are compared with the analytical solution, and good accuracy is shown to be achieved by the numerical solution.

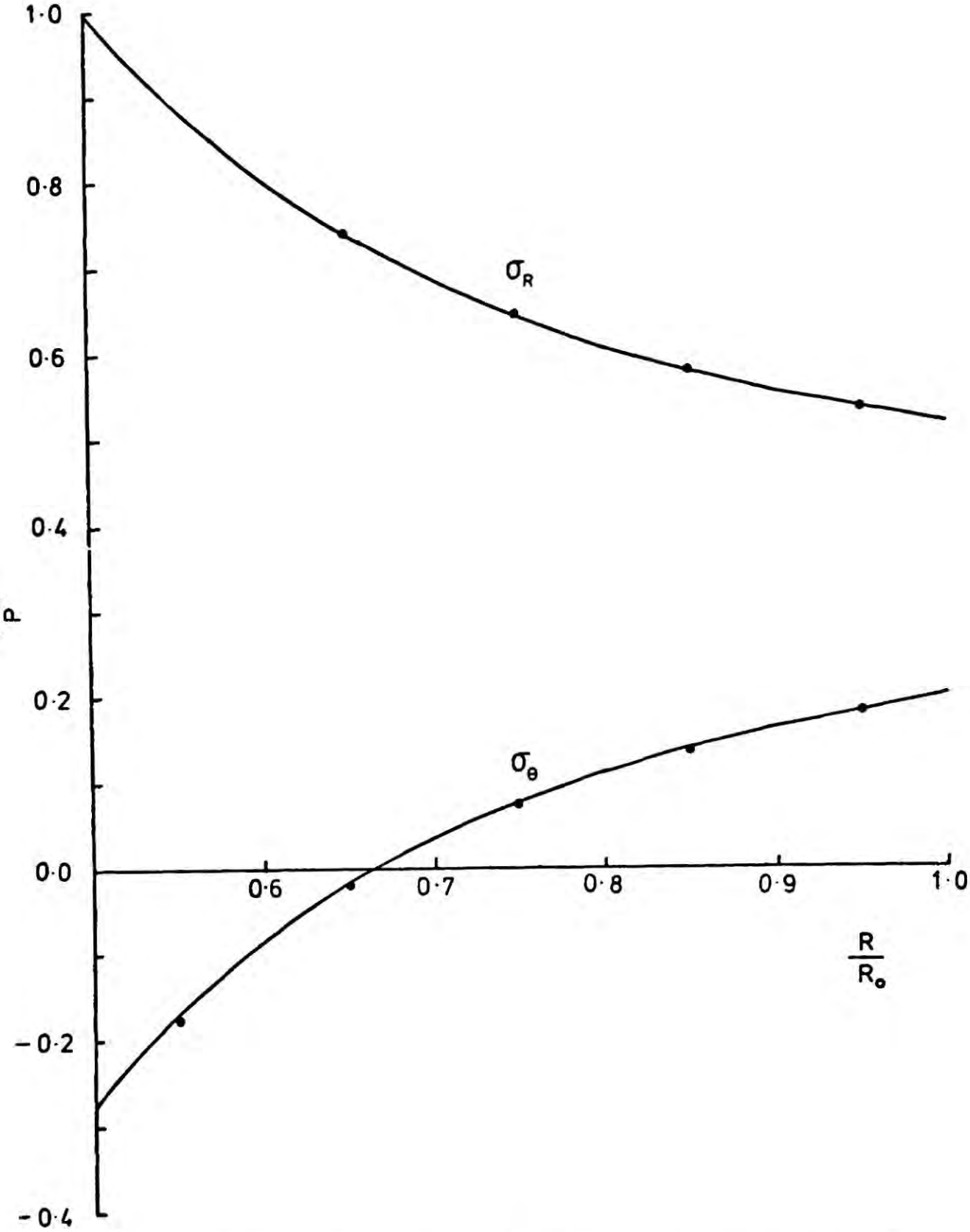

Figure A4.2. Radial and tangential stress as a function of radius. Analytical solutions are given by curves, while dots are values predicted by elastic finite element analysis.

```
C*****ELASTIC FINITE ELEMENT PROGRAM*****
C***** MAIN PROGRAM*****
      IMPLICIT REAL *8 (A-H,O-Z)
C*****DIMENSION STATEMENTS*****
      DIMENSION
     1 X(180),Y(180),NODEL(288,3),E(288),P(288),DN(288),
     3 ISP(100,2),PDIS(100,2),
     6 T(36),D(9),B(18),V(6),F(18),H(18),
     7 W(3),GQ(3),CC(3),STRAY(288,4),
     8 DISEL(6),STRESS(3),STRAIN(3),STEL(3),DISP(360)
     9 ,LD(288),AT(130,40),FISOS(100),NK(100)
     1 ,DLIB(9,288),BLIB(18,288),DELIB(288)
C
C*****READ IN INPUT DATA*****
C*****READ NUMBER OF NODES AND ELEMENTS,PLOT SCALE AND STRESS MARKER*****
      READ(5,800) NNOD,NEL,STMAX,DENLIT
      NNOD2=NNOD*2
  800 FORMAT(2I10,E10.3,F10.3)
      DO 850 I=1,NNOD
  850 READ(5,801) K,X(K),Y(K)
  801 FORMAT(I10,2F10.3)
      DO 851 I=1,NEL
  851 READ(5,802) K,(NODEL(K,J),J=1,3),E(I),P(I),DN(I)
  802 FORMAT(4I10,E10.3,2F10.3)
      DO 202 I=1,NNOD2
  202 DISP(I)=0.0
      READ(5,808) NBC
      DO 853 J=1,NBC
      READ(5,805) I,DISP(2*I-1),DISP(2*I)
  805 FORMAT(I10,2E10.3)
  853 CONTINUE
C*****READ SPECIFIED DISPLACEMENTS*****
      READ(5,808) ND
  808 FORMAT(I10)
      DO 854 I=1,ND
  854 READ(5,807) LD(I),(ISP(I,J),PDIS(I,J),J=1,2)
  807 FORMAT(I10,2(I10,F10.3))
C
C*****WRITE OUT INPUT DATA*****
      WRITE(4,150) NNOD,NEL
  150 FORMAT(2X,'NUMBER OF NODES =',I4,10X,'NUMBER OF ELEMENTS =',I4)
      WRITE(6,199)
       WRITE(4,9801) DENLIT,STMAX
 9801 FORMAT(F10.3,E10.3)
  199 FORMAT('0')
      DO 100 I=1,NNOD
  100 WRITE(6,152) I,X(I),Y(I),DISP(2*I-1),DISP(2*I)
  152 FORMAT(13X,I5,24X,F10.3,12X,F10.3,2E10.3)
      WRITE(6,199)
      DO 101 I=1,NEL
  101 WRITE(6,154) I,(NODEL(I,J),J=1,3),E(I),P(I),DN(I)
  154 FORMAT(14X,I4,18X,I4,12X,I4,12X,I4,D10.3,F6.3,D10.3)
      WRITE(6,199)
      WRITE(6,199)
      WRITE(6,199)
      DO 105 I=1,ND
  105 WRITE(6,169) LD(I),((ISP(I,J),PDIS(I,J)),J=1,2)
  169 FORMAT(20X,I10,12X,I10,10X,F10.3,10X,I10,10X,F10.3)
C*****TO CALC THE PARAM NBW*****
      NBW=0
```

```
      DO 9182 I=1,NEL
      KB1=IABS(NODEL(I,1)-NODEL(I,2))
      KB2=IABS(NODEL(I,2)-NODEL(I,3))
      KB3=IABS(NODEL(I,3)-NODEL(I,1))
 9182 NBW=AMAXO(KB1,KB2,KB3,NBW)
      NBW=2*NBW+2
      NBW=2*NBW-1
      WRITE(4,9187) NBW
 9187 FORMAT(2X,'NBW=',I10)
C
C***** FORM STIFFNESS MATRIX**********************************
C*****TO FORM ELEMENT STIFNESS MATRIX**************************************
      DO 6 I=1,NEL
C*****TO SET H AND T TO ZERO*********************************************
      DO 41 LIT=1,36
   41 T(LIT)=0.0
      DO 42 LIT=1,18
   42 H(LIT)=0.0
C*****FORM D MATRIX*******************************************************
      A=E(I)*(1.0-P(I))/((1.0+P(I))*(1.0-2*P(I)))
      Q=P(I)/(1.0-P(I))
      D(1)=A
      D(2)=A*Q
      D(3)=0.0
      D(4)=A*Q
      D(5)=A
      D(6)=0.0
      D(7)=0.0
      D(8)=0.0
      D(9)=A*(1.0-Q)/2.0
C*****FORM B MATRIX*******************************************************
      I1=NODEL(I,1)
      I2=NODEL(I,2)
      I3=NODEL(I,3)
      DELTA=Y(I3)*X(I2)
     1     -Y(I2)*X(I3)
     2     -X(I1)*Y(I3)
     3     +X(I1)*Y(I2)
     4     +Y(I1)*X(I3)
     5     -Y(I1)*X(I2)
      QQ(1)=(Y(I2)-Y(I3))/DELTA
      CC(1)=(X(I3)-X(I2))/DELTA
      QQ(2)=(Y(I3)-Y(I1))/DELTA
      CC(2)=(X(I1)-X(I3))/DELTA
      QQ(3)=(Y(I1)-Y(I2))/DELTA
      CC(3)=(X(I2)-X(I1))/DELTA
      B(1)=QQ(1)
      B(2)=0.0
      B(3)=CC(1)
      B(4)=0.0
      B(5)=CC(1)
      B(6)=QQ(1)
      B(7)=QC(2)
      B(8)=0.0
      B(9)=CC(2)
      B(10)=0.0
      B(11)=CC(2)
      B(12)=QQ(2)
      B(13)=QQ(3)
      B(14)=0.0
```

```
      B(15)=CC(3)
      B(16)=0.0
      B(17)=CC(3)
      B(18)=QQ(3)
      DELTA=DABS(DELTA)
      DO 9401 KK=1,18
 9401 BLIB(KK,I)=B(KK)
      DELIB(I)=DELTA
      DO 9402 KK=1,9
 9402 DLIB(KK,I)=D(KK)
      N=3
      M=6
      CALL GMTRA(B,F,N,M)
C*****B IS TRANSPOSED TO F**************************************************
C*****MULTIPLY D BY B TO GIVE H*********************************************
      N=3
      M=3
      L=6
      CALL GMPRD(D,B,H,N,M,L)
C*****MULTIPLY F BY H TO GIVE T*********************************************
      N=6
      M=3
      L=6
      CALL GMPRD(F,H,T,N,M,L)
C*****TO MULTIPLY BY DELTA/2************************************************
      DO 38 NI=1,36
   38 T(NI)=T(NI)*DELTA/2.0
C*****WE NOW HAVE ELEMENT STIFFNESS MATRIX**********************************
C*****TO PUT T INTO BODY STIFFNESS MATRIX************************************
      K=1
      DO 10 MS=1,3
      DO 10 NS=1,2
      DO 10 KS=1,3
      DO 10 LS=1,2
      JX=NODEL(I,MS)
      JX=2*JX-2+NS
      IY=NODEL(I,KS)
      IY=2*IY-2+LS
      LOC=JX-IY+0.5*(NBW+1)
      IF(LOC.LT.1) GO TO 10
      IF(LOC.GT.NBW) GO TO 10
      AT(IY,LOC)=AT(IY,LOC)+T(K)
   10 K=K+1
    6 CONTINUE
      WRITE(4,922)
  922 FORMAT(2X,'TOTOL STIFFNESS FORMED')
C
C*****INCORPERATE BODY FORCES IN FORCE VECTOR********************************
      DO 201 I=1,NEL
      I1=NODEL(I,1)
      I2=NODEL(I,2)
      I3=NODEL(I,3)
      DO 943 KK=1,18
  943 B(KK)=BLIB(KK,I)
      DO 944 KK=1,9
  944 D(KK)=DLIB(KK,I)
      DELTA=DELIB(I)
      J1=2*I1
      K1=J1-1
      J2=2*I2
```

```
181           K2=J2-1
182           J3=2*I3
183           K3=J3-1
184           A=DELTA/6.0*DN(I)*981.0
185           DISP(J1)=DISP(J1)+A
186           DISP(J2)=DISP(J2)+A
187           DISP(J3)=DISP(J3)+A
188         201 CONTINUE
189       C
190       C*****TO ALLOW FOR ISOSTATIC COMPENSATION*********************************
191           DATSOS=0.0
192           KCOUNT=0
193           DO 3400 I=1,NNOD
194           YI=Y(I)
195           IF(YI.LT.DATSOS) GO TO 3400
196           KCOUNT=KCOUNT+1
197           NK(KCOUNT)=I
198        3400 CONTINUE
199           SOSDEN=0.0
200           DENY=SOSDEN*981.0
201       C*****TO CALC FISOS FOR END NODES*****************************************
202           KZ=NK(1)
203           KY=NK(2)
204           AG=X(KY)-X(KZ)
205           FISOS(1)=AG/2.0*DENY
206           KZ=NK(KCOUNT)
207           KCM=KCOUNT-1
208           KY=NK(KCM)
209           AG=X(KZ)-X(KY)
210           FISOS(KCOUNT)=AG/2.0*DENY
211       C***** TO CALCULATE FISOS FOR REST*****************************************
212           KCT=KCOUNT-1
213           DO 2401 I=2,KCT
214           IPL=I+1
215           KT=NK(IPL)
216           IMN=I-1
217           KS=NK(IMN)
218           AG=X(KT)-X(KS)
219           FISOS(I)=AG/2.0*DENY
220         2401 CONTINUE
221       C*****TO PUT FISOS INTO AT*************************************************
222           DO 3402 I=1,KCOUNT
223           JHK=2*NK(I)
224           LOC=0.5*(NBW+1)
225           FIQ=FISOS(I)
226           FIQ=DABS(FIQ)
227           AT(JHK,LOC)=AT(JHK,LOC)+FIQ
228        3402 CONTINUE
229       C
230       C***** INTRODUCE PRESCRIBED DISPLACEMENTS*********************************
231           DO 30 II=1,ND
232           DO 31 J=1,2
233           LIK=ISP(II,J)
234           IF(LIK.EQ.0) GO TO 31
235           I=LD(II)
236           N=2*I+J-2
237           DISP(N)=PDIS(II,J)*1.0D 24
238           LOC=0.5*(NBW+1)
239           AT(N,LOC)=1.0D 24
240         31 CONTINUE
```

```
241          30 CONTINUE
242             WRITE(4,923)
243           923 FORMAT(2X,'PRESCRIBED DISPLACEMENTS INTRODUCED')
244         C
245         C*****TO SOLVE THE EQUATION   AT*DISP=DISP*****************************
246         C*****  CALL SR MATSOL SEIDEL GAUSS SOLUTION*********************
247               CALL MATSOL(AT,DISP,NBW,NNOD2,ERROR)
248               WRITE(4,3130) ERROR
249          3130 FORMAT(2X,'EQUATION SOLVED,ERROR=',E10.3)
250         C
251         C*****WE NOW HAVE DISPLACEMENTS***************************************
252         C*****TO OBTAIN STRAINS FROM DISPLACEMENTS*****************************
253               DO 20 I=1,NEL
254               I1=NODEL(I,1)
255               I2=NODEL(I,2)
256               I3=NODEL(I,3)
257               DO 9403 KK=1,18
258          9403 B(KK)=BLIB(KK,I)
259               DO 9404 KK=1,9
260          9404 D(KK)=DLIB(KK,I)
261               DELTA=DELIB(I)
262               J1=2*I1
263               K1=J1-1
264               J2=2*I2
265               K2=J2-1
266               J3=2*I3
267               K3=J3-1
268               DISEL(1)=DISP(K1)
269               DISEL(2)=DISP(J1)
270               DISEL(3)=DISP(K2)
271               DISEL(4)=DISP(J2)
272               DISEL(5)=DISP(K3)
273               DISEL(6)=DISP(J3)
274         C*****MULT B BY DISEL TO GIVE STRAINS IN STRAIN************************
275               N=3
276               M=6
277               L=1
278               CALL GMPRD(B,DISEL,STRAIN,N,M,L)
279         C*****TO OBTAIN STRESSES FROM STRAINS**********************************
280         C*****TO MULT D BY STRAINS TO GET STRESS*******************************
281         C*****  SUBTRACT INITIAL STRAIN TO GIVE ELASTIC STRAIN*****************
282               DO 1007 IK=1,3
283          1007 STEL(IK)=STRAIN(IK)
284               N=3
285               M=3
286               L=1
287               CALL GMPRD(D,STEL,STRESS,N,M,L)
288         C*****  ADD INITIAL STRESS TO CALC STRESS*****************************
289               DO 1000 IK=1,3
290          1000 STRAY(I,IK)=STRESS(IK)
291            20 CONTINUE
292         C*****WRITE RESULTS FOR FINAL STATE************************************
293               WRITE(6,199)
294               DO 209 I=1,NNOD
295               IJ=2*I
296               IK=IJ-1
297            209 WRITE(6,162) I,DISP(IK),DISP(IJ)
298            162 FORMAT(10X,I10,10X,E10.3,10X,E10.3)
299         C
300         C*****  TO CALCULATE THE PRINCIPAL SRESSES*****************************
```

```
      DO 210 I=1,NEL
      SC1=STRAY(I,1)
      SC2=STRAY(I,2)
      SC3=STRAY(I,3)
      THET=2.0*SC3/(SC1-SC2)
      THET=DATAN(THET)
      THET=THET/2.0
      THET=57.29*THET
      IF(THET.GT.0.0) GO TO 192
      THET=THET+90.0
  192 CONTINUE
      ALPHA=THET/57.29
      ANZA=(SC1*(DCOS(ALPHA))**2)+
     1 (SC2*(DSIN(ALPHA))**2)+
     2 (SC3*(DSIN(2.0*ALPHA)))
      ANZB=SC1+SC2-ANZA
      ANZF=P(I)*(SC1+SC2)
C*****ADD ON HYDROSTATIC LOAD STRESSES IF REQUIRED**********************
      YO=(Y(NODEL(I,1))+Y(NODEL(I,2))+Y(NODEL(I,3)))/3.0
      HPW=-4.0E5*981.0
      HPC=-7.0E5*2.8*981.0
      HPR=HPW+HPC+981.0*3.3*(YO+7.0E5)
      IF(YO.GT.-7.0E5) HPR=HPW+981.0*2.8*YO
      HPR=HPR*DENLIT
      ANZA=ANZA+HPR
      ANZB=ANZB+HPR
      ANZF=ANZF+HPR
      RS1=ANZA
      RS2=ANZB
      RS3=ANZF
      RAS=DMAX1(RS1,RS2,RS3)
      RBS=DMIN1(RS1,RS2,RS3)
      MK=0
      IF(RAS.EQ.RS3) MK=1
      IF(RBS.EQ.RS3) MK=1
C*****TEST FOR FAILURE CRITERION****************************************
      CALL FAIL(ANZA,ANZB,C,N)
      DELIB(I)=C
      C=DELIB(I)
      WRITE(6,164) I,ANZA,ANZB,THET,ANZF,MK,C,N
      STRAY(I,1)=ANZA
      STRAY(I,2)=ANZB
      STRAY(I,3)=THET
      STRAY(I,4)=ANZF
  210 CONTINUE
  164 FORMAT(8X,I5,8X,F10.3,8X ,E10.3,8X ,F10.4,5X,E10.3
     1 ,I2,5X,E10.3,5X,I2)
C***** TO PLOT THE STRESSES AND DISPLACEMENTS***************************
      READ(5,5005) KPLOT
 5005 FORMAT(I10)
 5005 FORMAT(I10)
      IF(KPLOT.EQ.0) GO TO 5010
      READ(5,5011) XSC,XSH,YSC,YSH
      XSC=XSC*1.0E-5
      YSC=YSC*1.0E-5
      XSH=XSH*1.0E5
      YSH=YSH*1.0E5
 5011 FORMAT(4F10.3)
C***** CALL PLOTING SUBROUTINE*****************************************
      CALL PLOTS(X,Y,NODEL,STRAY,DISP,NNOD,NEL,
```

```
     1 XSC,XSH,YSC,YSH,KPLCT,KIK,STMAX,DELIP)
 5010 CONTINUE
      STOP
      END
C
C*****SUBROUTINE MATRIX MULTIPLICATION**********************************
      SUBROUTINE GMPRC(A,B,R,N,M,L)
      IMPLICIT REAL*8 (A-H,O-Z)
      DIMENSION A(1),B(1),R(1)
      IR=0
      IK=-M
      DO 10 K=1,L
      IK=IK+M
      DO 10 J=1,N
      IR=IR+1
      JI=J-N
      IB=IK
      R(IR)=0
      DO 10 I=1,M
      JI=JI+N
      IB=IB+1
   10 R(IR)=R(IR)+A(JI)*B(IB)
      RETURN
      END
C
C***** SUBROUTINE MATRIX TRANSPOSE
      SUBROUTINE GMTRA(A,R,N,M)
      IMPLICIT REAL*8 (A-H,O-Z)
      DIMENSION A(1),R(1)
      IR=0
      DO 10 I=1,N
      IJ=I-N
      DO 10 J=1,M
      IJ=IJ+N
      IR=IR+1
   10 R(IR)=A(IJ)
      RETURN
      END
C
C***** SUBROUTINE SOLUTION OF SIMULTANEOUS EQUATIONS BY SEIDEL-GAUSS***
      SUBROUTINE MATSOL(AT,DISP,NBW,NNOD2,ERROR)
      IMPLICIT REAL*8(A-H,O-Z)
      DIMENSION AT(130,40),DISP(1),FORCE(360)
       N=2000
      DO 1 I=1,NNOD2
      FORCE(I)=DISP(I)
    1 DISP(I)=0.0
      DO 2 I=1,N
      DO 3 J=1,NNOD2
      Z=0.0
      M=J-(NBW-1)/2
      DO 4 K=1,NBW
      IF(M.LE.0) GO TO 5
       Z=Z+AT(J,K)*DISP(M)
    5 M=M+1
    4 CONTINUE
      M=(NBW+1)/2
      Z=(FORCE(J)-Z)/AT(J,M)
      DISP(J)=DISP(J)+Z*1.8
      IF(I.LT.N) GO TO 3
```

```
421           Z=DABS(Z)
422           ERROR=DMAX1(ERROR,Z)
423         3 CONTINUE
424         2 CONTINUE
425           RETURN
426           END
427       C
428       C***** SUBROUTINE PLOTS PRINCIPAL STRESSES*********************************
429           SUBROUTINE PLOTS(X,Y,NODEL,STRAY,DISP,NNOD,NEL,
430          1 XSC,XSH,YSC,YSH,KPLOT,KIK,STMAX,DELIB)
431           IMPLICIT REAL *8(A-H,O-Z)
432           DIMENSION
433          1 X(1),Y(1),NODEL(288,3),STRAY(288,4)
434          2 ,DISP(1),DELIB(1)
435           CALL PLTXMX(80.0)
436       C***** PLOT GRID AND PRINCIPAL STRESSES*********************************
437           DO 501 I=1,NEL
438           X1=X(NODEL(I,1))
439           Y1=Y(NODEL(I,1))
440           X2=X(NODEL(I,2))
441           Y2=Y(NODEL(I,2))
442           X3=X(NODEL(I,3))
443           Y3=Y(NODEL(I,3))
444           XXR=(X1+X2+X3)/3.0
445           X1=(X1+XSH)*XSC
446           X2=(X2+XSH)*XSC
447           X3=(X3+XSH)*XSC
448           Y1=(Y1+YSH)*YSC
449           Y2=(Y2+YSH)*YSC
450           Y3=(Y3+YSH)*YSC
451           XXC=(X1+X2+X3)/3.0+0.5
452           YYC=(Y1+Y2+Y3)/3.0
453           IF(XXC.GE.40.0) GO TO 501
454           IF(YYC.LT.0.0) GO TO 501
455           TA=DCOS(STRAY(I,3)/57.29)*STRAY(I,1)/STMAX
456           TB=DSIN(STRAY(I,3)/57.29)*STRAY(I,1)/STMAX
457           TX=DCOS(STRAY(I,3)/57.29)*STRAY(I,2)/STMAX
458           TY=DSIN(STRAY(I,3)/57.29)*STRAY(I,2)/STMAX
459           XN1=XXC+TA
460           XN2=XXC-TA
461           YN1=YYC+TB
462           YN2=YYC-TB
463           XS1=XXC-TY
464           XS2=XXC+TY
465           YS1=YYC+TX
466           YS2=YYC-TX
467           CALL PENUP(XN1,YN1)
468           CALL PENDN(XN2,YN2)
469           CALL PENUP(XS1,YS1)
470           CALL PENDN(XS2,YS2)
471           TA=STRAY(I,1)
472           TX=STRAY(I,2)
473           IF(TA.LT.0.0) GO TO 9331
474           CALL PSYMB(XN1,YN1,0.02,01,0.0,-1)
475           CALL PSYMB(XN2,YN2,0.02,01,0.0,-1)
476       9331 CONTINUE
477           IF(TX.LT.0.0) GO TO 9332
478           CALL PSYMB(XS1,YS1,0.02,01,0.0,-1)
479           CALL PSYMB(XS2,YS2,0.02,01,0.0,-1)
480       9332 CONTINUE
```

```
481           RAD=DABS(STRAY(I,4))/STMAX
482           GAP=0.0
483           S4=STRAY(I,4)
484           IF(S4.GE.0.0) GAP=0.03
485           CALL PCIRCL(XXC,YYC,0.0,360.0,RAD,RAD,GAP,0.0)
486         501 CONTINUE
487       C*****PLOT GRID AND NUMERICAL VALUES OF DEV STRESS AND FAILURE INDICATC
488           DO 200 I=1,NEL
489           X1=X(NODEL(I,1))
490           Y1=Y(NODEL(I,1))
491           X2=X(NODEL(I,2))
492           Y2=Y(NODEL(I,2))
493           X3=X(NODEL(I,3))
494           Y3=Y(NODEL(I,3))
495           X1=(X1+XSH)*XSC+40.0
496           X2=(X2+XSH)*XSC+40.0
497           X3=(X3+XSH)*XSC+40.0
498           Y1=(Y1+YSH)*YSC
499           Y2=(Y2+YSH)*YSC
500           Y3=(Y3+YSH)*YSC
501           IF(X1.GE.80.0) GO TO 200
502           IF(X2.GE.80.0) GO TO 200
503           IF(X3.GE.80.0) GO TO 200
504           IF(Y1.LE.0.0) GO TO 200
505           IF(Y2.LE.0.0) GO TO 200
506           IF(Y3.LE.0.0) GO TO 200
507           CALL PENUP(X1,Y1)
508           CALL PENDN(X2,Y2)
509           CALL PENDN(X3,Y3)
510           CALL PENDN(X1,Y1)
511           XXC=(X1+X2+X3)/3.0
512           YYC=(Y1+Y2+Y3)/3.0
513           RDT=STRAY(I,1)-STRAY(I,2)
514           RDT=RDT/2.0
515           RDT=DABS(RDT)
516           RDT=RDT/1.0E9
517           XXC=XXC-0.25
518           IF(XXC.GE.80.0) GO TO 200
519           IF(YYC.LT.0.0) GO TO 200
520           CALL PNUMBR(XXC,YYC,0.07,RDT,0.0,'F2.3 *',0.0)
521           YYC=YYC-0.125
522           RDT=DELIB(I)
523           CALL PNUMBR(XXC,YYC,0.07,RDT,0.0,'F3.1 *',0.0)
524         200 CONTINUE
525           CALL PLTEND
526           RETURN
527           END
528       C***** SUBROUTINE TEST FOR ROCK FAILURE**********************************
529           SUBROUTINE FAIL(A,B,C,N)
530           IMPLICIT REAL *8(A-H,O,Z)
531           P=DMAX1(A,B)
532           R=DMIN1(A,B)
533           N=0
534           T=0.5E9
535       C***** TEST FOR FAILURE MODE*****************************************
536           C=3.0*P+R
537           IF(C.LT.0.0) GO TO 1
538       C*****TENSIONAL*****************************************************
539           X=P-T
540           N=1
```

```
541             X=X/T
542             GO TO 100
543         C*****OPEN CRACK COMPRESSINAL FALIURE************************************
544             1 CONTINUE
545             CRIT=-T*4.19
546             IF(P.LT.CRIT) GO TO 2
547             N=2
548             CS2=-(P-R)/2.0/(P+R)
549             CC=(1.0+CS2)/2.0
550             SS=(1.0-CS2)/2.0
551             C=P*CC+R*SS
552             IF(Q.LT.CRIT) GO TO 2
553             X=-(P-R)*(P-R)/8.C/(P+R)-T
554             X=X/T
555             GO TO 100
556         C*****CLOSED CRACK COMP FAILURE*******************************************
557             2 CONTINUE
558             N=3
559             ALPHA=(1.0+1.09*1.C9)**0.5/1.C9
560             BETA=4.0*(1.0+4.9)**0.5/1.09-2.0*4.19
561             X=(P+R+ALPHA*(P-R))/BETA-T
562             X=X/T
563           100 CONTINUE
564             C=X
565             RETURN
566             END
 OF FILE
```